

# IDOJÁRÁS

QUARTERLY JOURNAL  
OF THE HUNGARIAN METEOROLOGICAL SERVICE

Special Issue: Spatial interpolation techniques in climatology and meteorology  
Guest Editor: Sándor Szalai

## CONTENTS

Editorial .....	I		
<i>Tamás Szentimrey, Zita Bihari, Mónika Lakatos, and Sándor Szalai</i> : Mathematical, methodological questions concerning the spatial interpolation of climate elements .....	1	Geostatistical modeling of high resolution climate change scenario data .....	71
<i>Patriche Cristian Valeriu</i> : Aspects regarding the uncertainty of spatial statistical models of climate parameters .....	13	<i>Petr Štěpánek, Pavel Zahradníček, and Radan Huth</i> : Interpolation techniques used for data quality control and calculation of technical series: an example of a Central European daily time series .....	87
<i>Florian Hogewind and Peter Bissolli</i> : Operational maps of monthly mean temperature for WMO Region VI (Europe and Middle East) .....	31	<i>Mónika Lakatos, Tamás Szentimrey, and Zita Bihari</i> : Application of gridded daily data series for calculation of extreme temperature and precipitation indices in Hungary .....	99
<i>Jacques Célestin Moliba Bankanza</i> : Time variation of the effect of geographical factors on spatial distribution of summer precipitation over the Czech Republic .....	51	<i>Agnieszka Wypych and Zbigniew Ustrnul</i> : Spatial differentiation of the climatic water balance in Poland .....	111
<i>Ladislav Vizi, Tomáš Hlásny, Aleš Farda, Petr Štěpánek, Petr Skalák, and Zuzana Sitková</i> : News – Farewell to the Executive Editor, <i>Margit Antal</i> .....			121

\*\*\*\*\*

<http://www.met.hu/Journal-Idojaras.php>

# IDŐJÁRÁS

*Quarterly Journal of the Hungarian Meteorological Service*

*Editor-in-Chief*

**LÁSZLÓ BOZÓ**

*Executive Editor*

**MARGIT ANTAL**

## EDITORIAL BOARD

- |                                       |   |
|---------------------------------------|---|
| AMBRÓZY, P. (Budapest, Hungary)       | MIKA, J. (Budapest, Hungary)                      |
| ANTAL, E. (Budapest, Hungary)         | MERSICH, I. (Budapest, Hungary)                   |
| BARTHOLY, J. (Budapest, Hungary)      | MÖLLER, D. (Berlin, Germany)                      |
| BATCHVAROVA, E. (Sofia, Bulgaria)     | NEUWIRTH, F. (Vienna, Austria)                    |
| BRIMBLECOMBE, P. (Norwich, U.K.)      | PINTO, J. (Res. Triangle Park, NC, U.S.A.)        |
| CZELNAI, R. (Dörgicse, Hungary)       | PRÁGER, T. (Budapest, Hungary)                    |
| DUNKEL, Z. (Budapest, Hungary)        | PROBÁLD, F. (Budapest, Hungary)                   |
| FISHER, B. (Reading, U.K.)            | RADNÓTI, G. (Reading, U.K.)                       |
| GELEYN, J.-Fr. (Toulouse, France)     | S. BURÁNSZKI, M. (Budapest, Hungary)              |
| GERESDI, I. (Pécs, Hungary)           | SIVERTSEN, T.H. (Risør, Norway)                   |
| GÖTZ, G. (Budapest, Hungary)          | SZALAI, S. (Budapest, Hungary)                    |
| HASZPRA, L. (Budapest, Hungary)       | SZEIDL, L. (Budapest, Hungary)                    |
| HORÁNYI, A. (Budapest, Hungary)       | SZUNYOGH, I. (College Station, TX, U.S.A.)        |
| HORVÁTH, Á. (Siófok, Hungary)         | TAR, K. (Debrecen, Hungary)                       |
| HORVÁTH, L. (Budapest, Hungary)       | TÄNCZER, T. (Budapest, Hungary)                   |
| HUNKÁR, M. (Keszthely, Hungary)       | TOTH, Z. (Camp Springs, MD, U.S.A.)               |
| LASZLO, I. (Camp Springs, MD, U.S.A.) | VALI, G. (Laramie, WY, U.S.A.)                    |
| MAJOR, G. (Budapest, Hungary)         | VARGA-HASZONITS, Z.<br>(Mosonmagyaróvár, Hungary) |
| MATYASOVSKY, I. (Budapest, Hungary)   | WEIDINGER, T. (Budapest, Hungary)                 |
| MÉSZÁROS, E. (Veszprém, Hungary)      |   |

*Editorial Office: Gillice tér 39, H-1182 Budapest, Hungary*

*P.O. Box 39, H-1675 Budapest, Hungary*

*E-mail: bozo.l@met.hu or antal.e@met.hu*

*Fax: (36-1) 346-4809*

---

**Indexed and abstracted in Science Citation Index Expanded™ and  
Journal Citation Reports/Science Edition  
Covered in the abstract and citation database SCOPUS®**

---

*Subscription by*

*mail: IDŐJÁRÁS, P.O. Box 39, H-1675 Budapest, Hungary*

*E-mail: kenderesy.k@met.hu or antal.e@met.hu*

## *Spatial interpolation techniques in climatology and meteorology*

Interpolation plays a growing role in the meteorology and climatology. Reconstruction of meteorological fields, developed data quality control procedures, and gridded databases require interpolation methods. The increasing needs indicate two directions for development. From one side, the diverse use of interpolation demands more accurate and complex methods, and from the other side, the common everyday's application has a request of simple useable software, usually as an option of free or commercial software. To overbridge this situation, a COST Action was implemented (COST 719: The Use of Geographic Information System in Climatology and Meteorology, end date 2006). The first Conference on the Spatial Interpolation Techniques in Climatology and Meteorology was organized in the frame of this Action. The proceedings were published by the COST Office.

Since there, several international projects deal with interpolation problems, at least partly. The request was arisen for an open meeting to overview the developments in the interpolation techniques. Therefore, the Hungarian Meteorological Service organized the conference second time in 2009.

The participants of the conference agreed, that the presentations could have a possibility to be published in a special issue of the quarterly journal of the Hungarian Meteorological Service, additionally to the abstract volume distributed widely among the other scientists working on the field of interpolation methods.

Finally, eight articles were gathered, and accepted for publication, which are covering wide range of topics on methodological issue, interpolation processes in international data bases, data quality control, applied research like hydrology, gridded data bases, interpolation in climate projections. These papers give about one-fourth of the conference presentations.

We strongly believe, that similar workshops and conferences are needed to avoid the misuse of interpolation method, understand and follow the development of interpolation methods, give new ideas for further scientific developments, involve new applied areas, and show new practices. Dissemination of best practices has benefit not only for the adopting, but the donor parties as well, they are for the common use and development.

Therefore, we are extremely grateful to the Editor-in-Chief of *IDŐJÁRÁS* supporting the progress on the field of interpolation, thank to the authors of the articles for their high scientific level work, and also to the reviewers supporting the improvement of papers with their critical comments and recommendations keeping the high standards of the journal. We have to underline the hard work of the Executive Editor of the journal, the present volume could not be published without it. Therefore, we express our thanks together with the authors of the papers for that.

*Sándor Szalai*

Guest Editor

Szent István University, Gödöllő, Hungary  
szalai.sandor@mkk.szie.hu



# IDŐJÁRÁS

*Quarterly Journal of the Hungarian Meteorological Service*  
*Vol. 115, No. 1–2, January–June 2011, pp. 1–11*

## **Mathematical, methodological questions concerning the spatial interpolation of climate elements**

**Tamás Szentimrey<sup>\*</sup>, Zita Bihari, Mónika Lakatos, and Sándor Szalai**

*Hungarian Meteorological Service,  
P.O. Box 38, H-1525 Budapest, Hungary*

*<sup>\*</sup>Corresponding author; E-mail: szentimrey.t@met.hu*

*(Manuscript received in final form January 13, 2011)*

**Abstract**—The paper focuses on the basic mathematical and theoretical questions of spatial interpolation of meteorological elements. Nowadays, in meteorology the most often applied procedures for spatial interpolation are the geostatistical interpolation methods built also in GIS software. The mathematical basis of these methods is the geostatistics that is an exact but special part of the mathematical statistics. However, special meteorological spatial interpolation methods for climate elements also exist, such as Gandin optimum interpolation as well as the MISH method developed at the Hungarian Meteorological Service in the last few years. These meteorological interpolation methods are also based on the mathematical statistical theory. Therefore, the basic type of the interpolation formulas applied by the geostatistical and meteorological methods are similar. One of our intentions is to present some comparison of the various kriging formulas, such as ordinary, universal, regression, residual, detrended, etc., ones. In general, these formulas can be derived from the multiple linear regression formula by using the generalized-least-squares estimation for certain unknown parameters. But the main difference between the geostatistical and meteorological interpolation methods can be found in the amount of information used for modeling the necessary statistical parameters. In geostatistics, the usable information or the sample for modeling is only the system of predictors, which is a single realization in time, while in meteorology we have spatiotemporal data, namely the long data series which form a sample in time and space as well. The long data series is such a speciality of the meteorology that makes possible to model efficiently the statistical parameters in question.

*Key-words:* spatial interpolation, geostatistics, statistical climatology, data series, geostatistical interpolation, meteorological interpolation

## 1. Introduction

First let us consider the abstract scheme of the meteorological examinations. The initial stage is the meteorology that means the qualitative formulation of the given problem. The next stage is the mathematics in order to formulate the problem quantitatively. The third stage is to develop software on the basis of the mathematics. Finally, the last stage is again the meteorology that is the application of the developed software and evaluation of the obtained results. In the practice, however, the mathematics is sometimes neglected. Instead of adequate mathematical formulation of the meteorological problem, ready-made software are applied to solve the problem. Of course, in this case the results are not authentic either. Allow me a not word for word citation from John von Neumann: without quantitative formulation of the meteorological questions, we are not able to answer the simplest qualitative questions either.

Concerning our topic we have the following question. What kind of mathematics of spatial interpolation is adequate for meteorology? Nowadays, the geostatistical interpolation methods built in GIS software are applied in meteorology. The mathematical basis of these methods is the geostatistics that is an exact but special part of the mathematical- statistics. The speciality is connected with the assumption that the data are purely spatial. To illustrate this problem, here are some quotations from the valuable book of Noel A.C. Cressie: "Statistics for Spatial Data" (Cressie, 1991). On page 29: "The first part of this book is concerned with modeling data as a (partial) realization of a random process  $\{Z(\mathbf{s}):\mathbf{s}\in D\}$ ....". Explanation of the sentence is that the data are purely spatial data, since  $D$  is a space domain. On page 30: "It is possible to allow for spatiotemporal data by considering the variable  $Z(\mathbf{s}, t)$ , but for most of this book it will be assumed that the data are purely spatial...". Last, on page 53: "Statistically speaking, some further assumptions have to be made. Otherwise, the data represent an *incomplete* sampling of a *single* realization, making inference impossible." It means "*incomplete* sampling" in space, "*single* realization" in time.

Consequently, as we see it, the geostatistical methods can not efficiently use the meteorological data series, while the data series make possible to obtain the necessary climate information for the interpolation in meteorology.

## 2. Mathematical statistical model of spatial interpolation

In practice, many kinds of interpolation methods exist, therefore, the question is the difference between them. According to the interpolation problem, the unknown predictand  $Z(\mathbf{s}_0, t)$  is estimated by use of the known predictors  $Z(\mathbf{s}_i, t)$  ( $i=1, \dots, M$ ), where the location vectors  $\mathbf{s}$  are the elements of the given space

domain  $D$ , and  $t$  is the time. The vector form of predictors is  $\mathbf{Z}^T(t)=[Z(\mathbf{s}_1,t),\dots,Z(\mathbf{s}_M,t)]$ . The type of the adequate interpolation formula depends on the probability distribution of the meteorological element in question. In this paper only the linear or additive formula is described in detail, which is appropriate in case of normal probability distribution. However, perhaps it is worthwhile to remark that for case of a quasi lognormal distribution (e.g., precipitation sum), we deduced a mixed additive multiplicative formula which is used also in our MISH system, and it can be written in the following form,

$$\hat{Z}(\mathbf{s}_0,t)=\vartheta^{\left(\prod_{q_i:Z(\mathbf{s}_i,t)\geq\vartheta}\left(\frac{q_i\cdot Z(\mathbf{s}_i,t)}{\vartheta}\right)^{\lambda_i}\right)}\cdot\left(\sum_{q_i:Z(\mathbf{s}_i,t)\geq\vartheta}\lambda_i+\sum_{q_i:Z(\mathbf{s}_i,t)<\vartheta}\lambda_i\cdot\left(\frac{q_i\cdot Z(\mathbf{s}_i,t)}{\vartheta}\right)\right), \quad (1)$$

where the interpolation parameters are  $\vartheta>0$ ,  $q_i>0$ ,  $\lambda_i\geq 0$  ( $i=1,\dots,M$ ), and  $\sum_{i=1}^M\lambda_i=1$ .

### 2.1. Statistical parameters

In general, the interpolation formulas have some unknown interpolation parameters which are known functions of certain statistical parameters. At the linear interpolation formulas the basic statistical parameters can be divided into two groups, such as the deterministic and the stochastic parameters.

The deterministic or local parameters are the expected values  $E(Z(\mathbf{s}_i,t))$  ( $i=0,\dots,M$ ). Let  $E(\mathbf{Z}(t))$  denote the vector of expected values of predictors, i.e.,  $E(\mathbf{Z}(t))^T=[E(Z(\mathbf{s}_1,t)),\dots,E(Z(\mathbf{s}_M,t))]$ .

The stochastic parameters are the covariance or variogram values belonging to the predictand and predictors, such as

$\mathbf{c}$  : predictand-predictors covariance vector,

$\mathbf{C}$ : predictors-predictors covariance matrix,

$\boldsymbol{\gamma}$  : predictand-predictors variogram vector,

$\boldsymbol{\Gamma}$  : predictors-predictors variogram matrix.

The covariance is preferred in mathematical statistics and meteorology, while the variogram is preferred in geostatistics. Here is a quotation from the chapter "Geostatistics" of the mentioned book of Noel A.C. Cressie (Cressie, 1991, p. 30.). "The cornerstone is the variogram, a parameter that in the past has been either unknown or unfashionable among statisticians." In our opinion, the main reason of this reluctance is that the covariance is a more general statistical

parameter than the variogram. The variogram values, can be written as functions of the covariance values and it is not true inversely.

## 2.2. Linear meteorological model for expected values

At the statistical modeling of the meteorological elements we have to assume, that the expected values of the variables are changing in space and time alike. The spatial change means that the climate is different in the regions. The temporal change is the result of the possible global climate change. Consequently, in case of linear modeling of expected values, we assume that

$$E(Z(\mathbf{s}_i, t)) = \mu(t) + E(\mathbf{s}_i) \quad (i=0, \dots, M), \quad (2)$$

where  $\mu(t)$  is the temporal trend or the climate change signal and  $E(\mathbf{s})$  is the spatial trend. We emphasize, that this spatiotemporal model for expected values is different from the classic models used in geostatistics or by the multivariate statistical methods. As regards the geostatistics, there are purely spatial data assumed in general.

## 2.3. Linear regression formula

In essence, the multiple linear regression formula is the theoretical basis of the various linear interpolation methods. The multiple linear regression formula between predictand  $Z(\mathbf{s}_0, t)$  and predictors  $\mathbf{Z}(t)$  can be written as

$$\hat{Z}_{LR}(\mathbf{s}_0, t) = E(Z(\mathbf{s}_0, t)) + \mathbf{c}^T \mathbf{C}^{-1} (\mathbf{Z}(t) - E(\mathbf{Z}(t))) \quad (3)$$

and  $\hat{Z}_{LR}(\mathbf{s}_0, t)$  is the best linear estimation that minimizes the mean-square prediction error. Consequently, the linear regression formula would be the optimal linear interpolation formula concerning the mean-square prediction error. In respect of application, however, problems arise from the unknown statistical parameters  $E(Z(\mathbf{s}_0, t))(i=0, \dots, M)$  and  $\mathbf{c}$ ,  $\mathbf{C}$ . Assuming the meteorological model, Eq. (2), for the expected values, Eq. (3) can be written as

$$\hat{Z}_{LR}(\mathbf{s}_0, t) = (\mu(t) + E(\mathbf{s}_0)) + \mathbf{c}^T \mathbf{C}^{-1} (\mathbf{Z}(t) - (\mu(t)\mathbf{1} + \mathbf{E})), \quad (4)$$

where  $\mathbf{E}^T = [E(\mathbf{s}_1), \dots, E(\mathbf{s}_M)]$  and vector  $\mathbf{1}$  is identically one. As it can be seen, the main problem is the estimation of the unknown climate change signal  $\mu(t)$ , if we want to apply the optimal linear regression interpolation formula.

### 3. Geostatistical interpolation methods

The various geostatistical interpolation formulas can be obtained from the linear regression formula, Eq. (3), by the application of the generalized-least-squares estimation for the expected values. The type of kriging formulas depends on the model assumed for the expected values.

#### 3.1. Ordinary kriging formula

The ordinary kriging formula is a special case of the universal kriging formula. The assumed model for the expected values is  $E(Z(\mathbf{s}_i, t)) \equiv \mu(t)$  ( $i=0, \dots, M$ ), thus, there is no spatial trend. The generalized-least-squares estimation for  $\mu(t)$  by using only the predictors  $\mathbf{Z}(t)$  may be expressed in the form  $\hat{\mu}_{gls}(t) = (\mathbf{1}^T \mathbf{C}^{-1} \mathbf{1})^{-1} \mathbf{1}^T \mathbf{C}^{-1} \mathbf{Z}(t)$ . Substituting the estimate  $\hat{\mu}_{gls}(t)$  into the linear regression formula, Eq. (3), we obtain the ordinary kriging formula as

$$\hat{Z}_{OK}(\mathbf{s}_0, t) = \hat{\mu}_{gls}(t) + \mathbf{c}^T \mathbf{C}^{-1} (\mathbf{Z}(t) - \hat{\mu}_{gls}(t) \mathbf{1}) = \sum_{i=1}^M \lambda_i Z(\mathbf{s}_i, t), \quad (5)$$

where  $\sum_{i=1}^M \lambda_i = 1$ .

The vector of weighting factors  $\boldsymbol{\lambda}^T = [\lambda_1, \dots, \lambda_M]$  can be written in covariance form

$$\boldsymbol{\lambda}^T = \left( \mathbf{c}^T + \mathbf{1}^T \frac{(\mathbf{1} - \mathbf{1}^T \mathbf{C}^{-1} \mathbf{c})}{\mathbf{1}^T \mathbf{C}^{-1} \mathbf{1}} \right) \mathbf{C}^{-1}, \quad (6)$$

or equivalently in variogram form

$$\boldsymbol{\lambda}^T = \left( \boldsymbol{\gamma}^T + \mathbf{1}^T \frac{(\mathbf{1} - \mathbf{1}^T \boldsymbol{\Gamma}^{-1} \boldsymbol{\gamma})}{\mathbf{1}^T \boldsymbol{\Gamma}^{-1} \mathbf{1}} \right) \boldsymbol{\Gamma}^{-1}. \quad (7)$$

The unknown variogram values  $\boldsymbol{\gamma}$ ,  $\boldsymbol{\Gamma}$  preferred in geostatistics are modeled according to the Section 3.3.

#### 3.2. Universal kriging formula

The universal kriging formula is the generalized case of the ordinary kriging formula. The model assumption is that the expected values may be expressed as

$$E(Z(\mathbf{s}_i, t)) = \sum_{k=1}^K \beta_k(t) x_k(\mathbf{s}_i) \quad (i=0, \dots, M), \text{ that is in vector form}$$

$E(Z(\mathbf{s}_0, t)) = \mathbf{x}^T \boldsymbol{\beta}(t)$ ,  $E(\mathbf{Z}(t)) = \mathbf{X} \boldsymbol{\beta}(t)$ , where  $\mathbf{x}, \mathbf{X}$  are given supplementary deterministic model variables.

The generalized-least-squares estimation for coefficient vector  $\boldsymbol{\beta}(t)$ , by using only the predictors  $\mathbf{Z}(t)$ , can be written in the form  $\hat{\boldsymbol{\beta}}_{gls}(t) = (\mathbf{X}^T \mathbf{C}^{-1} \mathbf{X})^{-1} \mathbf{X}^T \mathbf{C}^{-1} \mathbf{Z}(t)$ . It is to be remarked, that in this way the spatial trend  $E(\mathbf{s})$  according to Eq. (2) is modeled also by using only the predictors  $\mathbf{Z}(t)$ . Substituting the estimates  $\mathbf{x}^T \hat{\boldsymbol{\beta}}_{gls}(t)$ ,  $\mathbf{X} \hat{\boldsymbol{\beta}}_{gls}(t)$  into the linear regression formula, Eq. (3), we obtain the universal kriging formula as

$$\hat{Z}_{UK}(\mathbf{s}_0, t) = \mathbf{x}^T \hat{\boldsymbol{\beta}}_{gls}(t) + \mathbf{c}^T \mathbf{C}^{-1} (\mathbf{Z}(t) - \mathbf{X} \hat{\boldsymbol{\beta}}_{gls}(t)) = \sum_{i=1}^M \lambda_i Z(\mathbf{s}_i, t), \quad (8)$$

where  $\boldsymbol{\lambda}^T \mathbf{X} = \mathbf{x}^T$ .

The vector of weighting factors  $\boldsymbol{\lambda}^T = [\lambda_1, \dots, \lambda_M]$  can be written in covariance form

$$\boldsymbol{\lambda}^T = \left\{ \mathbf{c} + \mathbf{X} (\mathbf{X}^T \mathbf{C}^{-1} \mathbf{X})^{-1} (\mathbf{x} - \mathbf{X}^T \mathbf{C}^{-1} \mathbf{c}) \right\}^T \mathbf{C}^{-1},$$

or equivalently in variogram form

$$\boldsymbol{\lambda}^T = \left\{ \boldsymbol{\gamma} + \mathbf{X} (\mathbf{X}^T \boldsymbol{\Gamma}^{-1} \mathbf{X})^{-1} (\mathbf{x} - \mathbf{X}^T \boldsymbol{\Gamma}^{-1} \boldsymbol{\gamma}) \right\}^T \boldsymbol{\Gamma}^{-1}.$$

The unknown variogram values  $\boldsymbol{\gamma}$ ,  $\boldsymbol{\Gamma}$  preferred in geostatistics are modeled according to Section 3.3.

### 3.3. Modeling of unknown statistical parameters in geostatistics

In geostatistics, only the predictors  $Z(\mathbf{s}_i, t) (i=1, \dots, M)$  constitute the usable information or the sample for modeling of variogram values  $\boldsymbol{\gamma}$ ,  $\boldsymbol{\Gamma}$ . It means we have only a single realization in time for modeling of the statistical parameters in question. In order to solve the problem of absence of temporal data, some assumptions about the statistical structure are made that is some simplification of the problem. For example, such assumptions are the intrinsic stationarity or second-order (weak) stationarity, semivariogram  $\gamma(Z(\mathbf{s}_i), Z(\mathbf{s}_j)) = \gamma(\mathbf{s}_i - \mathbf{s}_j)$ , etc.

## 4. Meteorological interpolation

Similarly to the geostatistical interpolation formulas, an appropriate meteorological interpolation formula can be obtained from the linear regression

formula, Eq. (3), by the application of the generalized-least-squares estimation for the expected values. The key-question is the model assumption for the expected values.

#### 4.1. Meteorological interpolation formula

The meteorological model, Eq. (2), is assumed namely  $E(Z(\mathbf{s}_i, t)) = \mu(t) + E(\mathbf{s}_i)$  ( $i=0, \dots, M$ ), where  $\mu(t)$  is the temporal trend and  $E(\mathbf{s})$  is the spatial trend. Supposing that the spatial trend  $E(\mathbf{s})$  is known, we apply the generalized-least-squares estimation for temporal trend  $\mu(t)$  by using the predictors  $\mathbf{Z}(t)$  and the spatial trend  $\mathbf{E}^T = [E(\mathbf{s}_1), \dots, E(\mathbf{s}_M)]$ . In this case, the generalized-least-squares estimate can be written in the form as  $\hat{\mu}_{gls}^E(t) = (\mathbf{1}^T \mathbf{C}^{-1} \mathbf{1})^{-1} \mathbf{1}^T \mathbf{C}^{-1} (\mathbf{Z}(t) - \mathbf{E})$ . Substituting the estimate  $\hat{\mu}_{gls}^E(t)$  into the linear regression formula, Eq. (4), rewritten from Eq. (3) according to Eq. (2), we obtain the following interpolation formula:

$$\begin{aligned} \hat{Z}_{MI}(\mathbf{s}_0, t) &= (\hat{\mu}_{gls}^E(t) + E(\mathbf{s}_0)) + \mathbf{c}^T \mathbf{C}^{-1} (\mathbf{Z}(t) - (\hat{\mu}_{gls}^E(t) \mathbf{1} + \mathbf{E})) = \\ &= E(\mathbf{s}_0) + \sum_{i=1}^M \lambda_i (Z(\mathbf{s}_i, t) - E(\mathbf{s}_i)), \end{aligned} \quad (9)$$

where  $\sum_{i=1}^M \lambda_i = 1$ .

The vector of weighting factors  $\boldsymbol{\lambda}^T = [\lambda_1, \dots, \lambda_M]$  can be written equivalently in covariance and variogram form according to Eqs. (6) and (7). The obtained interpolation formula is a detrended or residual interpolation formula that includes the spatial trend and the theoretical ordinary kriging weighting factors. However, it is not identical with the detrended or residual interpolation method, because the interpolation formula as well as the modeling methodology of the necessary statistical parameters together defines an interpolation method. For example, at the detrended interpolation methods applied in the practice, the modeling procedure for the statistical parameters is based on only the predictors  $Z(\mathbf{s}_i, t)$  ( $i=1, \dots, M$ ).

#### 4.2. Possibility for modeling of unknown statistical parameters in meteorology

According to Eq. (9), where the sum of weighting factors is equal to one, we have the following appropriate meteorological interpolation formula

$$\hat{Z}_{MI}(\mathbf{s}_0, t) = \sum_{i=1}^M \lambda_i (E(\mathbf{s}_0) - E(\mathbf{s}_i)) + \sum_{i=1}^M \lambda_i Z(\mathbf{s}_i, t), \quad (10)$$

where  $\sum_{i=1}^M \lambda_i = 1$  and the covariance form of weighting factors is defined by Eq.

(6). Consequently, the unknown statistical parameters are the spatial trend differences  $E(\mathbf{s}_0) - E(\mathbf{s}_i)$  ( $i=1, \dots, M$ ) and covariances  $\mathbf{c}, \mathbf{C}$ . In essence, these parameters are climate parameters which in fact means that we could interpolate optimally if we knew the climate. The special possibility in meteorology is to use the long meteorological data series for modeling of the climate statistical parameters in question. The data series make possible to know the climate in accordance with the fundamentals of statistical climatology!

#### 4.3. *Difference between geostatistics and meteorology in respect of spatial interpolation*

The main difference can be found in the amount of information used for modeling the statistical parameters. In geostatistics, the usable information or the sample for modeling is only the predictors  $Z(\mathbf{s}_i, t)$  ( $i=1, \dots, M$ ) which belong to a fixed instant of time, that is a single realization in time. „Statistically speaking, some further assumptions about  $Z$  have to be made. Otherwise, the data represent an *incomplete* sampling of a *single* realization, making inference impossible.” (Cressie, 1991, p. 53.). The assumptions are, e.g., intrinsic stationarity or second-order (weak) stationarity, semivariogram  $\gamma(Z(\mathbf{s}_i), Z(\mathbf{s}_j)) = \gamma(\mathbf{s}_i - \mathbf{s}_j)$ , covariogram  $\text{cov}(Z(\mathbf{s}_i), Z(\mathbf{s}_j)) = \mathbf{C}(\mathbf{s}_i - \mathbf{s}_j) = \mathbf{C}(\mathbf{0}) - \gamma(\mathbf{s}_i - \mathbf{s}_j)$ , which are some simplifications in order to solve the problem of absence of temporal data. While in meteorology, we have spatiotemporal data, namely long data series which form a sample in time and space as well make the modeling of the climate statistical parameters in question possible. If the meteorological stations  $\mathbf{S}_k$  ( $k=1, \dots, K$ ) ( $\mathbf{S} \in D$ ) have long data series, then spatial trend differences  $E(\mathbf{S}_k) - E(\mathbf{S}_l)$  ( $k, l=1, \dots, K$ ) as well as the covariances  $\text{cov}(Z(\mathbf{S}_k), Z(\mathbf{S}_l))$  ( $k, l=1, \dots, K$ ) can be estimated statistically. Consequently, these parameters are essentially known and provide much more information for modeling than the predictors  $Z(\mathbf{s}_i, t)$  ( $i=1, \dots, M$ ) only.

### 5. *Software and connection of topics*

Our method MISH (Meteorological Interpolation based on Surface Homogenized Data Basis) for the spatial interpolation of surface meteorological elements was developed (Szentimrey and Bihari, 2007a,b) according to the

mathematical background that is outlined in Section 4. This is a meteorological system not only in respect of the aim but in respect of the tools as well. It means that using all the valuable meteorological information – e.g., climate and possible background information – is required.

The new software version MISHv1.02 consists of two units that are the modeling and the interpolation systems. The interpolation system can be operated on the results of the modeling system. In the following paragraphs we summarize briefly the most important facts about these two units of the developed software.

Modeling system for climate statistical (deterministic and stochastic) parameters:

- Based on long homogenized data series and supplementary deterministic model variables. The model variables may be height, topography, distance from the sea, etc.. Neighborhood modeling, correlation model for each grid point.
- Benchmark study, cross-validation test for interpolation error or representativity.
- Modeling procedure must be executed only once before the interpolation applications!

Interpolation system:

- Additive (e.g., temperature) or multiplicative (e.g., precipitation) model and interpolation formula can be used depending on the climate elements.
- Daily, monthly values and many years' means can be interpolated.
- Few predictors are also sufficient for the interpolation and there is no problem if the greater part of daily precipitation predictors is equal to 0.
- The interpolation error or representativity is modeled too.
- Capability for application of supplementary background information (stochastic variables), e.g., satellite, radar, forecast data.
- Data series complementing that is missing value interpolation, completion for monthly or daily station data series.
- Interpolation, gridding of monthly or daily station data series for given predictand locations. In case of gridding, the predictand locations are the nodes of a relatively dense grid.

As it can be seen, modeling of the climate statistical parameters is a key issue to the interpolation of meteorological elements, and that modeling can be based on the long homogenized data series. The necessary homogenized data series can be obtained by our homogenization software MASHv3.02 (Multiple

Analysis of Series for Homogenization; *Szentimrey*, 1999, 2007). Similarly to the connection of interpolation and homogenization, in our conception the meteorological questions can not be treated separately. We present a block diagram (*Fig. 1*) to illustrate the possible connection between various important meteorological topics.

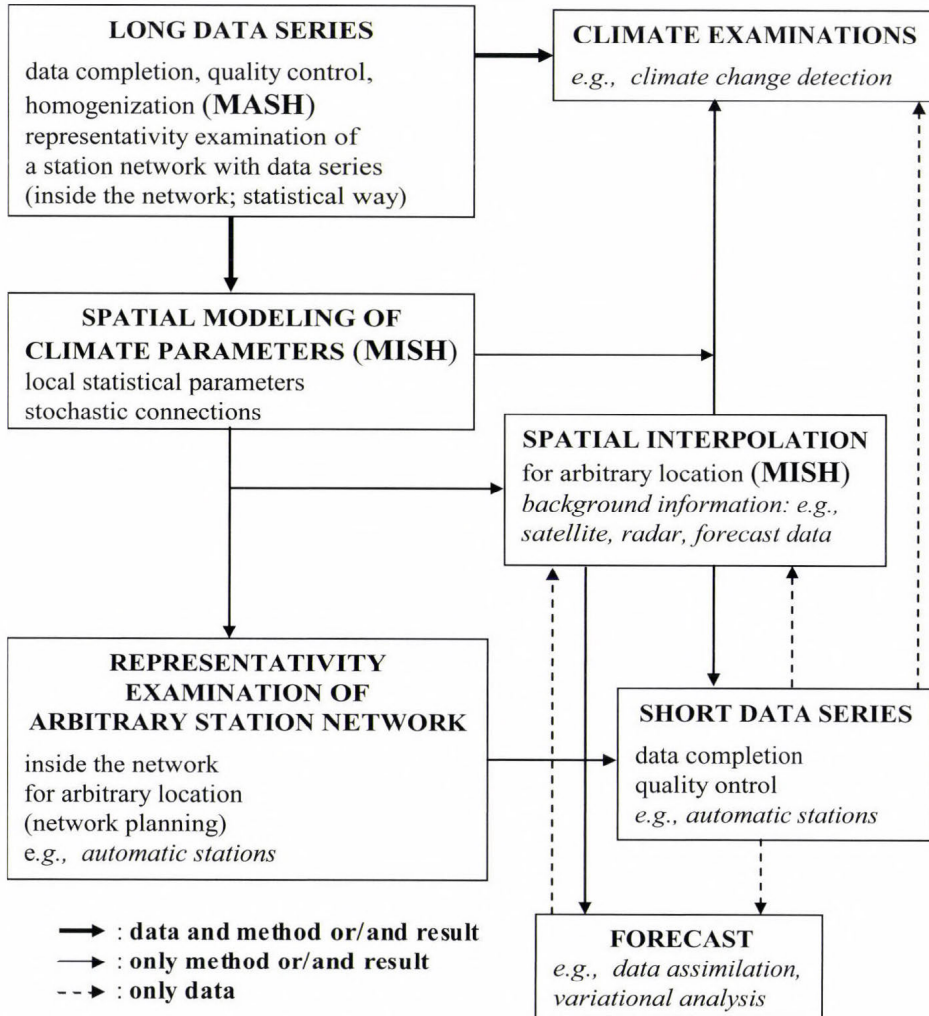


*Fig. 1.* Block diagram for the possible connections between various basic meteorological topics and systems.

## ***References***

- Cressie, N.*, 1991: *Statistics for Spatial Data*. Wiley, New York, 900 pp.
- Szentimrey, T.*, 1999: Multiple Analysis of Series for Homogenization (MASH). *Proceedings of the Second Seminar for Homogenization of Surface Climatological Data, Budapest, Hungary; WMO, WCDMP-No. 41*, 27-46.
- Szentimrey, T.*, 2007: Manual of homogenization software MASHv3.02. Országos Meteorológiai Szolgálat (Hungarian Meteorological Service), Budapest, p. 65.
- Szentimrey, T. and Bihari, Z.*, 2006: MISH (Meteorological Interpolation based on Surface Homogenized Data Basis). *COST Action 719 Final Report. The Use of GIS in Climatology and Meteorology* (eds.: Ole Einar Tveito, Martin Wegehenkel, Frans van der Wel and Hartwig Dobesch), 54-56.
- Szentimrey, T. and Bihari, Z.*, 2007a: Mathematical background of the spatial interpolation methods and the software MISH (Meteorological Interpolation based on Surface Homogenized Data Basis). *Proceedings from the Conference on Spatial Interpolation in Climatology and Meteorology*, Budapest, Hungary, 2004. *COST Action 719, COST Office*, 17-27.
- Szentimrey, T. and Bihari, Z.*, 2007b: Manual of interpolation software MISHv1.02. Országos Meteorológiai Szolgálat (Hungarian Meteorological Service), Budapest, p. 32.



# IDŐJÁRÁS

*Quarterly Journal of the Hungarian Meteorological Service  
Vol. 115, No. 1–2, January–June 2011, pp. 13–30*

## **Aspects regarding the uncertainty of spatial statistical models of climate parameters**

**Patriche Cristian Valeriu**

*Romanian Academy, Department of Iasi, Geography Group,  
8 Carol I, 700505, Iasi, Romania; E-mail: pvcristi@yahoo.com*

*(Manuscript received in final form April 26, 2010)*

**Abstract**—Any transformation of a discrete variable into a continuous one is subject to uncertainty. Consequently, the identification and assessment of errors is essential for avoiding misinterpretations of models describing the spatial distribution of climatic parameters. Our study attempts to identify the main sources of errors affecting the statistical spatial models of climatic parameters and to assess their impact on the accuracy of these models. In particular, we focus on georeference errors, the representativeness of the stations network and the related extrapolation problem, the outliers problem, error propagation from simple to complex variables, the problems aroused by heterogeneous regions.

*Key-words:* uncertainty, spatial statistical models, climate parameters, georeference errors, stations network representativeness, extrapolation, outliers, heterogeneous regions, error propagation

### **1. Introduction**

Our study derives from previous attempts to model the spatial distribution of various climate parameters, which were based, in most cases, on small samples of meteorological stations/rain gauges (Patriche, 2007; Patriche et al., 2008). Therefore, our conclusions are applied especially to outputs achieved from such samples, knowing that the degree of uncertainty rises significantly as the sample size used for statistical modeling decreases.

There are many potential sources of uncertainty, which may be grouped into two broad categories:

- **Errors from data pre-processing stage (data quality)**
  - Data recording errors / data series gaps;
  - Instrumental errors;
  - Changes in measurements standards;

- Change in the location of the station/ changes in land use around the station.
  - **Errors from data processing stage**
    - Georeference errors;
    - Errors derived from the spatial representativeness of the stations network;
    - Errors induced by the presence of outliers;
    - Errors derived from the heterogeneity of the region;
    - Statistical errors;
    - Cumulated errors from computation of complex parameters (error propagation).
- Our study focuses on the errors from the data processing stage.

## *2. Georeference errors*

Although simple, the georeference stage is very important. Georeference errors refer to errors of the  $x$ ,  $y$ ,  $z$  coordinates. Misplacements of stations/rain gauges points on the map may induce significant errors, especially in highly fragmented terrain, when predictors' values are extracted from raster layers or when local interpolators, such as kriging, are used for spatial modeling. The former will lead to wrong predictors' values and, therefore, inaccurate regression models, while the latter will generate locally displaced climatic fields.

The correlation between the stations/rain gauges altitudes and the respective DEM (Digital Elevation Model) altitudes may be used for identifying possible georeference errors or errors in recording the stations/rain gauges altitudes. The correlation should be very good, although not perfect for several reasons: the DEM generalizes the altitude information according to its resolution; the stations/rain gauges latitude and longitude values are generally given in degrees and minutes. Following up the latter issue, if we suppose that the seconds are rounded up or down to the closest minute, it actually means that we may have a coordinate error of up to 30 seconds, meaning about 900 m for latitude and 600 m for longitude, for middle latitudes. These errors double if no coordinate rounding was performed and the seconds were just disregarded.

In the example shown in *Fig. 1*, extracted from a study attempting to model the spatial distribution of mean annual precipitations in Vrancea County, Romania (*Patriche et al.*, 2008), we notice one point (Groapa Tufei) situated outside the correlation cloud indicating a possible georeference error. The recorded altitude for this rain gauge is 125 m, while the DEM altitude for this particular location is 355 m. We can see how far the 125 m altitude isoline is, along which the rain gauge should be located. There are two possible explanations for this error: either the horizontal coordinates of Groapa Tufei are wrong, or the recorded altitude is incorrect. Let us now see the potential

negative impact of such a georeference error on spatial statistical models of precipitations. If the real altitude of Groapa Tufei is 125 m, so the recorded altitude is correct, but the horizontal coordinates are wrong, then this point may be used for regression analysis, provided that neither DEM altitude values nor other derived predictors' values are used for models computation. In a geostatistical approach (ordinary kriging, residual kriging, etc.) it is not advisable to include such misplaced points, because they will misplace, in their turn, the precipitation values. Still, if the value of a misplaced point is similar to those of the neighbouring points, as it is in our case, the error induced by the georeference error may be small enough, and the respective point may be kept.

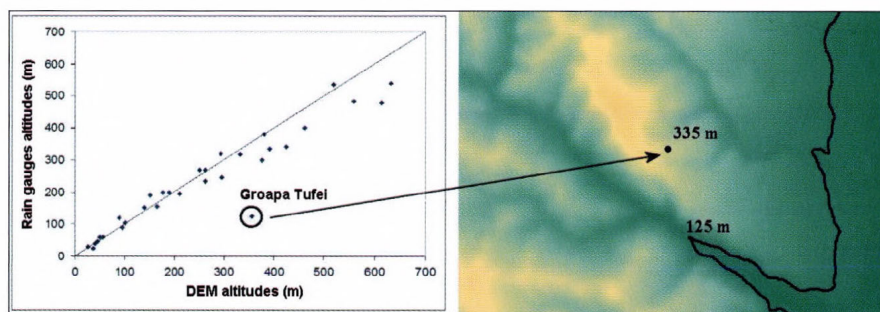


Fig. 1. Revealing two georeference errors for a sample of rain gauges situated in Vrancea County, Romania (Patriche et al., 2008).

### ***3. Spatial representativeness of the stations network and the extrapolation problem***

The spatial representativeness of the meteorological stations/rain gauges network is an important issue which needs to be addressed in a preliminary stage, as it constitutes a potential source of errors. Theoretically, the spatial distribution of the meteorological network should be well-balanced, in order to grasp all the meteorological and climatological aspects of a territory. However, in most cases, the spatial representativeness of the stations network is more or less inappropriate, due to both its feeble density and its biased location, mainly in valley bottoms.

The representativeness of the meteorological network in relation with the potential predictors may be visualized and evaluated by comparing the predictors' histograms with the histograms of the same predictors, which are based on the predictors' values associated to the meteorological stations / rain gauges.

An example is given in Fig. 2 for the altitudinal representativeness for a sample of meteorological stations situated in eastern Romania. In an ideal situation, the curves of the cumulated histograms, derived from the DEM and the stations' altitudes, should overlap. However, we notice the shortage of

stations between 300 m and 350 m of altitude. Also, we observe the lack of stations at lower altitudes (<59 m) and especially at higher altitudes, where the highest meteorological station is situated at 391 m of altitude, while the terrain altitudes go as high as 1071 m. As a consequence, we are forced to extrapolate the altitude-based regression models in these areas. As the extrapolation may induce errors, we need to give a special attention to these areas and to consider carefully the reliability of the estimated values.

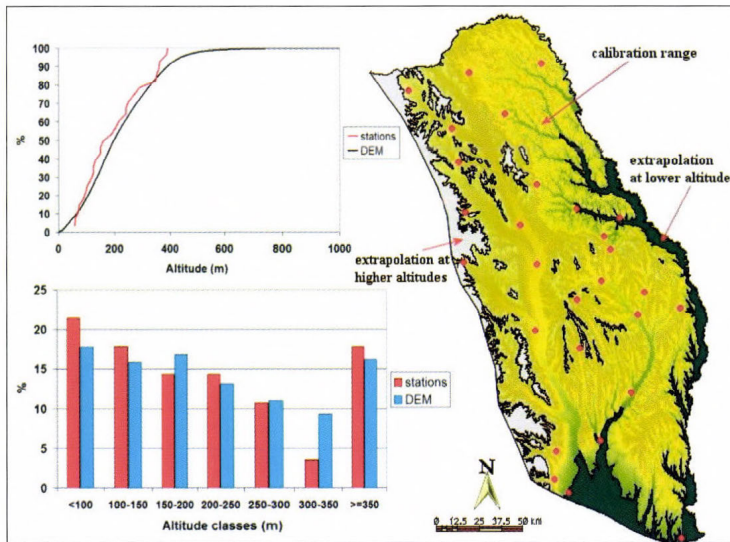


Fig. 2. Assessment of spatial representativeness of stations network by comparing frequencies of predictors' values for station points and for the whole region. Example from eastern Romania (Moldavia) for altitude representativeness for a sample of 28 stations.

Fig. 3 shows an example in which the extrapolation of the regression model should be avoided (Patriche et al., 2008). The mean annual precipitation – altitude regression model, elaborated for Vrancea County (Romania), was based on a sample of 34 rain gauges. The westernmost mountainous part of the region is uncovered by rain gauges, meaning that we must extrapolate our regression model there, if we want to estimate the mean annual precipitation values for this part as well. Performing the extrapolation up to 1770 m of altitude, we estimate precipitation values of up to 1463 mm. Such estimated values are, in our opinion, unrealistic. If the extrapolation is unreliable, then we should confine ourselves with the calibration area of our model. Taking into account that the highest rain gauge altitude is 540 m, we recommend that the study region should not extend over 700 m (Fig. 3, black line). Therefore, the entire westernmost part of our region should be excluded from the final map because of extrapolation uncertainty.

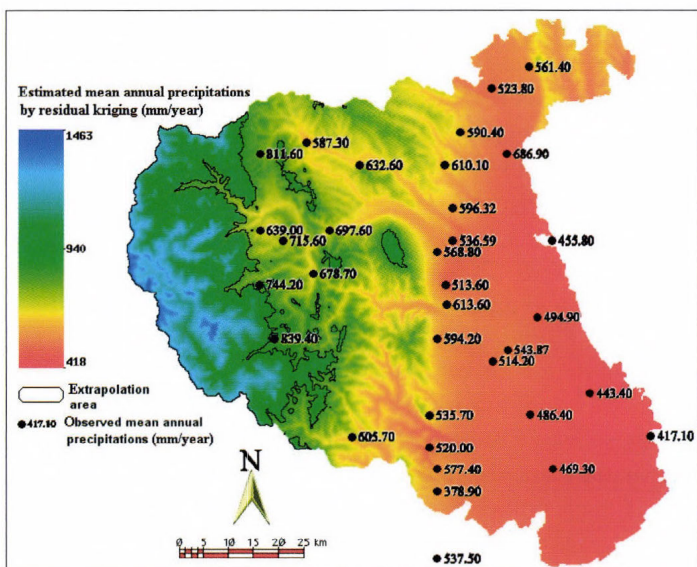


Fig. 3. Avoiding extrapolation. An example from Vrancea County (Romania) for mean annual precipitations.

#### 4. The outliers' problem

An outlier is a point value showing a significant deviation from the statistical model (therefore, marked by a high residual value), corresponding to points (meteorological stations, rain gauges) which mark spatial anomalies for the analyzed parameter's distribution (e.g., foehnization areas, areas of orographic enhancement of precipitations, temperature inversion areas, etc.). Such a "rebel" value may be also an error value, and this possibility must be checked out. If no error is identified then we should proceed to the assessment of the degree in which this value is altering the statistical models, mainly regression models. This is happening in the case of the regression analysis, because it is used mainly as a global interpolation method, and the regression itself is incapable to render spatial anomalies. If such spatial anomalies exist, then the integration within the statistical model of values describing these anomalies may significantly alter the regression equations, which, therefore, become unreliable.

From the viewpoint of their influence over the regression models, we may distinguish two types of outliers:

- Outliers showing high residuals but with similar values of the real residuals and deleted residuals (also known as jackknife error and computed without taking into account the anomaly point). Because such outliers do not modify significantly the regression models, they can be included in the analysis.

- Outliers showing high residuals but with significant differences between the values of the real residuals and those of the deleted residuals. Such outliers modify the regression model and must be, therefore, taken into consideration if the induced modifications are proved to be significant.

There are many statistical procedures aimed towards the identification of outliers. Good syntheses of these procedures are provided by *Maimon and Rokach (2005)*, and *Wilcox (2002)*.

Our approach is a simple one. In order to identify the outliers, we should first inspect the configuration of the correlation cloud between the dependent variable and the predictor, or between the real and predicted values in the case of multiple predictors, looking for points situated significantly outside the cloud. If such points exist, we should further inspect the magnitude of their residual values and see if they are located outside the  $\pm 2.5$  RMSE (root mean square error) interval. If such points exist, we should then test their influence on the regression models. The most common way to do this is to perform a cross-validation, the analysis of the differences between the actual residual values and the deleted residuals (jackknife error). If these differences are important, then the exclusion of the respective points significantly changes the regression model, which is, therefore, unstable. Next, we should actually see these changes by elaborating the models with and without the outliers and finally decide whether to keep or eliminate the respective points.

*Fig. 4* shows the correlation between the mean annual precipitation and the altitude for a sample of 28 meteorological stations situated in eastern Romania (Moldavia). The chart indicates at least 2 suspect points situated outside the correlation cloud, one with a lower precipitation value than expected for the respective altitude (Cotnari station), another with significantly higher precipitation amounts than expected (Barnova station). These deviations are related to local terrain conditions influencing the pluviometry. Cotnari station is situated in a foehnization area of western air masses descending the eastern slopes of Dealul Mare – Harlau Hill. Here, the real mean annual precipitation value is 121.3 mm lower than the value predicted by the altitude regression model using all stations. On the contrary, Barnova station is situated in an area of orographic enhancement of precipitations caused by the presence of a high energy slope (Iasi Cuesta) facing the more humid western air masses and by the shape of the Barnova-Voinesti depression, which causes the convergence of the western air masses. Another factor is related to the location of Barnova station within a well-forested area. Being the only station from our sample situated within forested areas, it is impossible for us to assess the relative importance of these factors and to state which of them, the local topography or the presence of the forest, is more responsible for the high precipitation values recorded at this location. The real mean annual precipitation value at Barnova station is 172.7 mm higher than the predicted value.

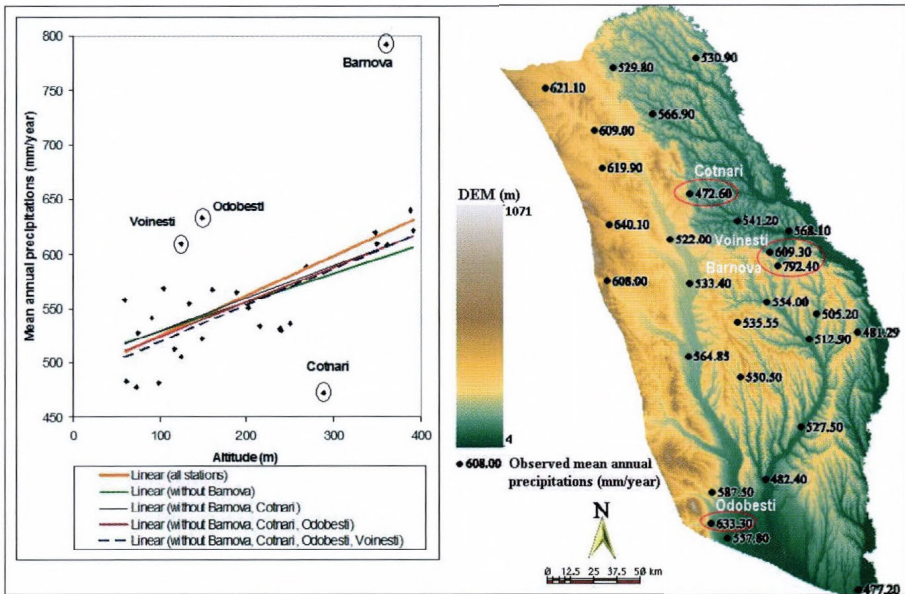


Fig. 4. Correlation chart between altitude and mean annual precipitations for a sample of 28 meteorological stations situated in eastern Romania (Moldavia), indicating the presence of four possible outliers.

If the visual inspection of the correlation charts gives us a first guess on the presence of possible outliers, other methods provide more insight. Our next step is to inspect the magnitude of the residuals. Generally, if some value goes out the interval limited by  $\pm 2.5$  RMSE (equivalent with the standard deviation of the residuals for large samples), then it is possible that this value is an outlier. From Fig. 5c (left), we notice that the residue from Barnova station goes beyond the  $+2.5$  RMSE, while the residue from Cotnari station is very close to the  $-2.5$  RMSE limit. If we eliminate only Barnova station, we find that the residual value at Cotnari goes also beyond the specified limit. Thus, the conclusion is that both stations must be excluded to ensure stability for the regression model. But if we exclude these two stations and rebuild our regression model, we shall find that yet another station (Odobesti) displays residues greater than the  $+2.5$  RMSE limit. Furthermore, if we chose to eliminate Odobesti station, we obtain another high residual value for Voinești station, situated in the same area of orographic enhancement of precipitations as Barnova station, only at a lower altitude.

So far we have established that we have some poor estimated points in our sample, displaying high residual values. Thus, we are certain that we have some points acting like the first type of outliers (referring to the above classification). The problem now is to decide whether it is necessary to eliminate them from the regression model that is, if this elimination would significantly improve the model.

To answer this question, one must test the influence of these outliers on the regression models and find out whether or not we are dealing with outliers of type two.

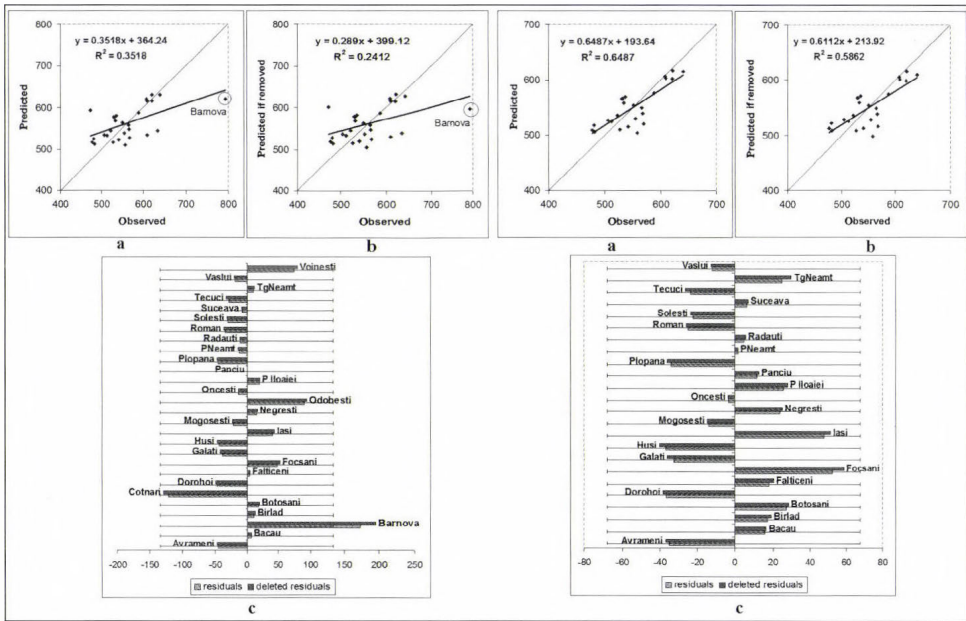


Fig. 5. Correlation between observed and predicted mean annual precipitation (a), cross-validation (b), and comparison of residuals vs. deleted residuals with bars showing the  $\pm 2.5$  RMSE (c), using all stations (left) and without four possible outliers (right).

One way to establish the answer is to perform cross-validation, that is, to compare the observed values with the predicted values obtained by successive elimination of the sample points. If the regression models are stable, one should find that the cross-validation charts are similar to the correlation charts between the observed and predicted values. In our case, we may notice that the differences between the observed vs. predicted correlations and the cross-validation correlations decrease as the outliers are removed from the models, from about 11%, in the case of all stations model, to about 6%, in the case of the regression model obtained by removing all of the four possible outliers (Fig. 5a,b). The slight difference is hampering us so far to state that the removal of the 4 stations significantly improves the regression models.

The comparison between the observed vs. predicted values and the cross-validation charts tells us only something about the stability of the regression models. In order to investigate the influence of particular values, we may find it useful to compare the regression residuals with those obtained by eliminating the suspect point (deleted residuals, jackknife error). If the suspect point is not

an outlier, then the magnitude of the residues should be very similar. In our case, we notice that the difference between the actual and deleted residuals is the greatest in the case of Barnova (22.5 mm), which means that its exclusion from the model significantly changes the altitude – precipitation relationship (*Fig. 5c*). The next greatest difference can be found in the case of Cotnari station (7.8 mm). Even if this is not such an important difference, keeping Cotnari station without Barnova station generates an even poorer regression model than the one using all stations. This is due to the fact, that these two points, one above, the other below the regression line, have opposite effects, balancing the regression line to the extent that if one point is removed, the other will “attract” the line towards it. This means that if we chose to eliminate Barnova station, we must eliminate Cotnari station as well.

If we construct our model without these two stations and analyze the residuals, we find that yet 2 other stations display high residuals, going beyond the +2.5 RMSE: Odobesti and Voinesti stations, the latter being situated within the same area of orographic enhancement of precipitations as Barnova station. However, the difference between the actual and deleted residuals is not very significant. The elimination of all these 4 stations leads to a regression model, where no more points display residuals outside the  $\pm 2.5$  RMSE interval (*Fig. 5c*, right).

*Table 1* shows how significant is the influence of the 4 outliers on the regression models. We notice, that the regression quality parameters (correlation coefficients, standard error of estimate) improve by excluding these outliers. However, one should bear in mind that even if there is an overall improvement of the regression models excluding the outliers, these models will still perform poor in the case of the outliers themselves. It is necessary for us to assess if the altitude – precipitation relationship is significantly changing. As we stated before, the regression model without Barnova only is not reliable due to the “attraction” effect of the Cotnari station, and we can clearly see that this model is the most different from the others, showing the highest intercept and the lower pluviometric vertical gradient (regression coefficient). The other models display quite similar parameters: intercepts ranging from 485.6 mm to 498.9 mm and gradients from 30.1 mm/100 m to 36.2 mm/100 m.

*Table 1.* Comparison of the regression models using and excluding the outliers

Regression model	Intercept	Regression coefficient	R <sup>2</sup>	Standard error of estimates
All stations	489.21	0.362	0.352	54.472
Without Barnova	501.82	0.265	0.321	41.678
Without Barnova, Cotnari	498.90	0.301	0.450	36.190
Without Barnova, Cotnari, Odobesti	492.72	0.315	0.547	31.697
Barnova, Cotnari, Odobesti, Voinesti	485.64	0.335	0.649	27.626

From *Fig. 6* we may see that 31% of the station sample displays the lowest residuals under the 2nd model (without Barnova and Cotnari stations). A similar percent (30%) is found for the 4th model (without all of the 4 outliers).

To sum up, our conclusion is that in the particular case of our sample, the elimination of the identified 4 outliers improves the regression model even though the differences among the various models are not very important.

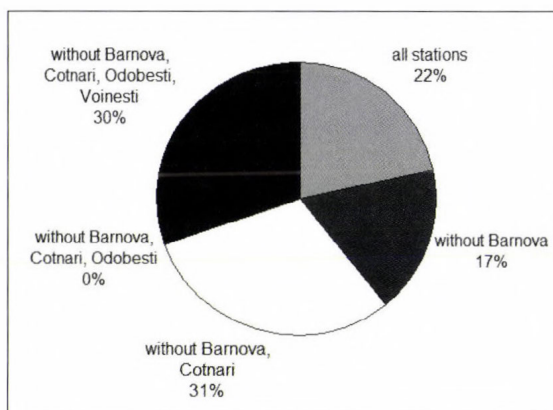


*Fig. 6.* The optimum altitude regression model (lowest values of actual residuals minus deleted residuals) for each station.

The problem is that we can not just exclude some real values from the analysis, because then we would obtain an incomplete image of the spatial distribution of the analyzed climatic parameter.

Some of the possible solutions could be:

- data transformation (logarithms);
- derivation of new predictors to account for spatial anomalies;
- application of robust regression methods (*Wilcox, 2002*);
- application of regression as a local interpolator (e.g., geographically weighted regression method);
- application of residual kriging.

A common solution is to derive one or more predictors (*Lhotellier and Patriche, 2007*) capable to explain the anomaly associated to the outlier point (e.g., the west-east aspect component combined with terrain local altitudinal range could theoretically explain the precipitations anomaly identified at Cotnari, Barnova, and Voinești stations from the previous example). Practically, we are often hampered in our analysis by the poor spatial representativeness of the stations network, especially when we have to work with small stations samples, which is, in most cases, unable to fully account for all terrain aspects relevant for the spatial distribution of the analyzed climatic parameter.

The application of residual kriging is also a common approach (*Lhotellier, 2005; Dobesch et al., 2007; Hengl, 2007; Silva et al., 2007*). Thus, what regression is unable to explain (the residuals), is interpolated using ordinary kriging, then the spatial trend, derived by regression, is added to the spatial anomalies, resulting in the final spatial model of the climate parameter. The output of this approach is still influenced by the quality of the regression model. If the model is significantly influenced by the outliers, then we can not attempt to interpret the predictors-predictand relations.

An alternative solution could be the elaboration of the regression model without the values identified as outliers, the spatialization of the residuals by ordinary kriging, including the residuals associated with the anomaly points, followed by the addition of the spatial trend with the interpolated residuals so as to obtain the final spatialization. We notice, that this is a residual kriging approach, which eliminates the outliers during the regression stage, if these belong to the type two mentioned above, but includes the residuals from these points during the kriging interpolation stage (*Fig. 7*).

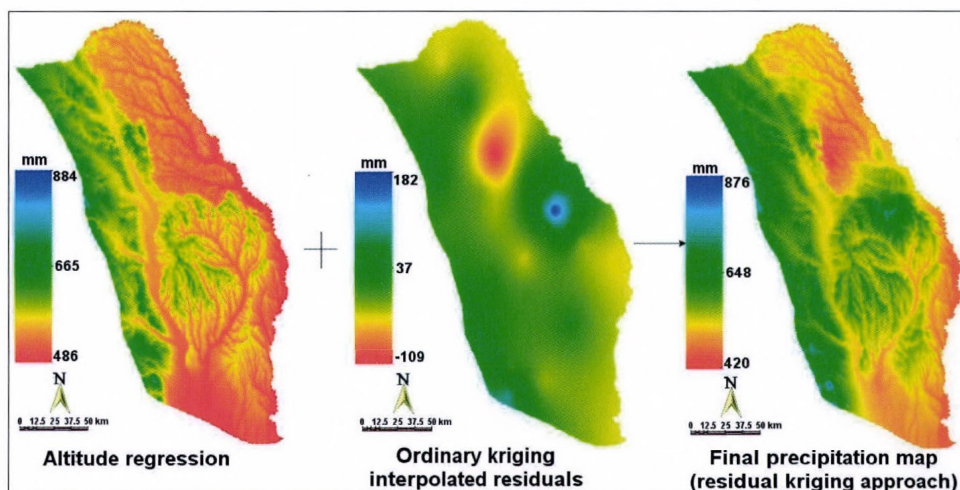


*Fig. 7.* Mapping the optimum solution: residual kriging approach leaving out the outliers during the regression stage, but taking the outliers' residuals into account during the kriging stage.

A better approach consists in the application of regression as local interpolator (e.g., geographically weighted regression, *Fotheringham et al., 2002*), taking into account the spatial anomalies (*Engen-Skaugen and Tveito, 2007; Maracchi et al., 2007*). The local regression can be further included into a residual kriging approach in order to improve the quality of the output. The main drawback to this approach is the need of a sufficiently large stations sample in order to be capable to derive local regression models.

Let us now see a situation, in which the outliers may indicate possible data errors or different recording intervals. The example is extracted from a study attempting to model the spatial distribution of mean annual precipitations in Vrancea County (Romania) on the basis of 34 rain gauges (*Patriche et al., 2008*).

*Figs. 8 and 9* show 2 points situated significantly outside the altitude – precipitation correlation cloud, namely Pufesti (686.9 mm) and Slobozia Bradului (378.9 mm), therefore, indicating the presence of two possible outliers. In the case of Pufesti rain gauge, the mean annual precipitation regime is characterized by a secondary maximum in August. Taking into account, that all other rain gauges display a single maximum in June, we are inclined to believe that either the August data is incorrect or the Pufesti data represent a shorter time frame, corresponding to a more humid period. On the other hand, the mean annual value recorded at Slobozia Bradului rain gauge is obviously too small for the climatic conditions of our region. Because the monthly values display a normal annual distribution, we are inclined to believe, as before, that the data correspond to a shorter time frame from a drier period.

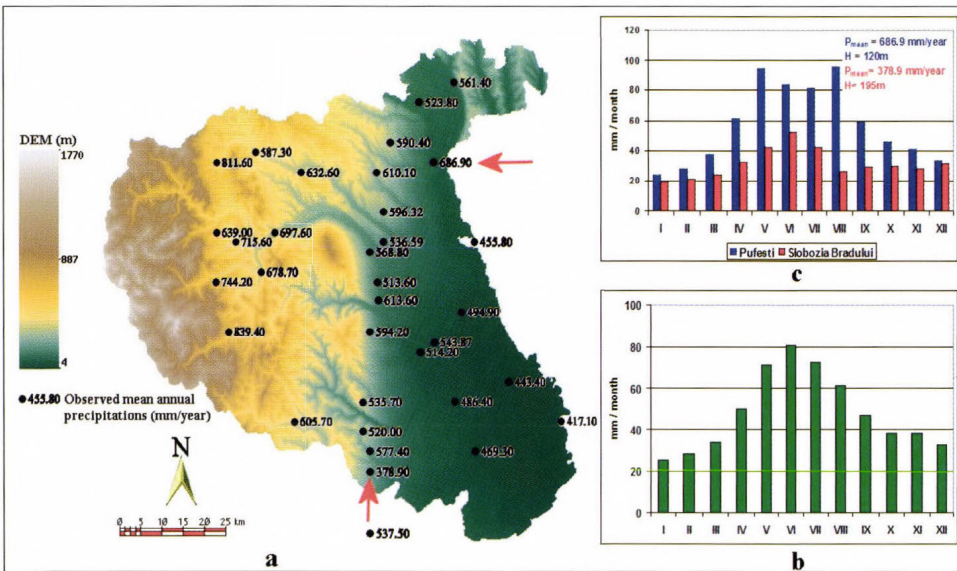


*Fig. 8.* Observed mean annual precipitations in Vrancea County, Romania (a), mean annual precipitation regime for all stations (b), and for the two suspect points (c).

From *Fig. 9b*, we notice that even though these two points are associated with the highest residuals, the difference between the actual and deleted residuals (jackknife error) is small, meaning that their removal from analysis does not significantly change the altitude regression model. This is happening because the points are situated on opposite sides as compared to the regression

line (Fig. 9a) and, therefore, they have opposite effects, balancing the regression line. Their removal increases the correlation coefficient but does not significantly change the direction of the regression line, meaning that the regression equations are very similar with or without these points. This can also be grasped, if one notices that the altitude – precipitation correlation coefficient (0.66) is quite similar with the cross-validation correlation coefficient (0.62), meaning that the one by one removal of all sample points does not significantly change the altitude – precipitation relationship (Fig. 9c).

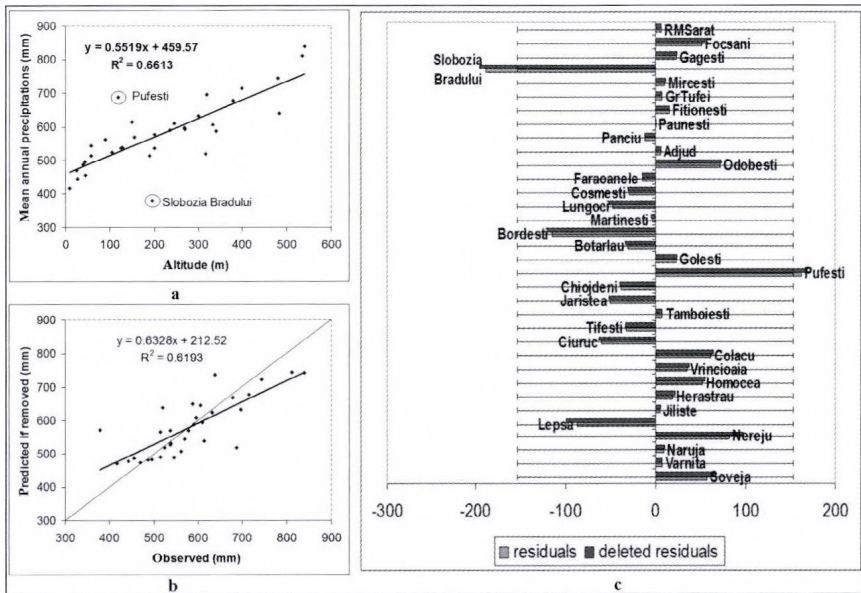


Fig. 9. The altitude – mean annual precipitation relationship (a) and the comparison between actual and deleted residuals (c) showing the presence of two possible outliers. Cross-validation of the altitude model using all stations (b).

Let us see the effects on other predictors. We must mention that, apart from altitude, we also used latitude and longitude as predictors, and at first we obtained a good regression model using both altitude and latitude. Looking further into details, we noticed that the latitude – precipitation correlation is a false correlation, induced by the presence of the two outliers (Fig. 10), one with a higher precipitation value situated in the northern part of our region (Pufesti), the other one with a lower precipitation value situated in the south (Slobozia Bradului). If one eliminates these two points, the latitudinal correlation is no longer statistically significant.

For this reason and because of our intention of using also kriging for spatialization, in which case the great residual values of the two suspect points would be represented on the map, we decided to eliminate them from analysis.

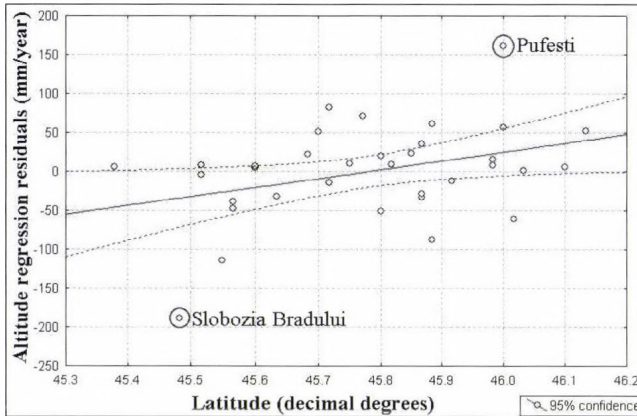


Fig. 10. An unwanted effect of outliers: false precipitation – latitude correlation.

### 5. Error propagation

Statistically based spatial models are usually computed for elementary variables, such as temperature or precipitations. In order to describe the climate of a region, we also need to compute complex variables, derived from the elementary ones, such as the de Martonne index, potential and real evapotranspiration, etc.

Spatial models of complex variables may be achieved either by computing the complex variable at stations' locations and then interpolating the results or by integrating the spatial models of the elementary variables in order to obtain the complex one. Using the first approach, we are able to quickly compute the errors as well. In this case, we cannot speak of error propagation. Still, in our opinion, this approach is conceptually less appropriate, because the computation of the complex variable is deterministic, according to a physical model. For instance, computing the potential evapotranspiration according to Penman-Monteith approach involves the computation of the net shortwave radiation, which depends on terrain slopes and expositions and on land use. If one computes this parameter at stations' locations and then interpolates the results, neither of these control factors will be taken into account.

The second approach, namely the integration of elementary variables, each of them displaying certain errors, has the disadvantage of inducing invariably in the propagation of these errors to the derived, complex variable. Knowing these errors is important for the assessment of the accuracy of the derived variable's spatial distribution.

A simple example is presented in *Table 2*. The example refers to the derivation of the de Martonne aridity index, for the territory of Moldavia (eastern Romania), on the basis of the mean annual temperatures and precipitations statistically modeled by regression. The mean annual temperature

model uses altitude and latitude as predictors, the computed standard error of estimate is  $\pm 0.215^{\circ}\text{C}$ , meaning that the real temperature differs from the estimated one with  $\pm 0.215^{\circ}\text{C}$  in about 68% of the cases. If we consider, for exemplification, an estimated mean annual temperature of  $10^{\circ}\text{C}$ , then the real temperature will most probably be found within the interval of  $9.8\text{--}10.2^{\circ}\text{C}$ . On the other hand, the mean annual precipitation model uses altitude as predictor and has a standard error of estimate of  $\pm 54.472\text{ mm/year}$ , which means that, for an estimated value of  $500\text{ mm}$ , the real precipitation values will most probably lie within the interval of  $445\text{--}554\text{ mm/year}$ . Considering the two estimated temperature ( $10^{\circ}\text{C}$ ) and precipitation ( $500\text{ mm/year}$ ) values, it results an aridity index of 25. Taking into account the possible errors for the estimated input parameters, it results that the real value of the aridity index will be most likely found between 22 and 28.

Table 2. Exemplification of error propagation

Statistical parameters		Mean annual precipitation	Mean annual temperature	Aridity index
		<i>Real values</i>		
Exemplification values		500	10	25
Mean		561.95	8.90	29.21
Standard deviation		66.395	0.734	3.136
Standard error		54.472	0.215	–
Confidence interval	Lower limit	445.528	9.785	22.039
	Upper limit	554.472	10.215	28.025
	Range	108.944	0.431	5.986
		<i>Standardized values</i>		
Standardized standard error		0.820	0.294	–
Confidence interval	Lower limit	–1.754	1.206	–2.287
	Upper limit	–0.113	1.793	–0.378
	Range	1.641	0.587	1.909

We are, however, unable to compare these confidence intervals, because the 3 parameters are expressed in different measurement units. One solution is to compute the regression models using the standardized values of the input parameters. We find that the size of the confidence intervals is 1.641 for mean annual precipitation and 0.587 for mean annual temperature. The resulting aridity index distribution for the stations sample is characterized by a mean value of 29.21 and a standard deviation of 3.136. Therefore, the lower limit of the confidence interval (22) corresponds to a standardized value of  $-2.287$  and the upper limit (28) corresponds to a standardized value of  $-0.378$ , resulting a range of 1.909. This value is greater than the ones of the input parameters, indicating the propagation and enhancement of the errors, from the elementary variables to the derived, complex variables.

## 6. Homogeneous vs. heterogeneous regions

Another issue we address in our study is that of heterogeneous regions. Generally, the greater a region, the more heterogeneous it is. A certain level of heterogeneity is necessary for the spatialization of climate parameters. For instance, within a small region, in which the altitudinal range does not exceed, for example, 100–200 m, the spatial variation of the climate fields may be too feeble for us to correctly infer the spatial variation rules. On the other hand, within a large region, the climatic heterogeneity may be too high for a single statistical model to explain it.

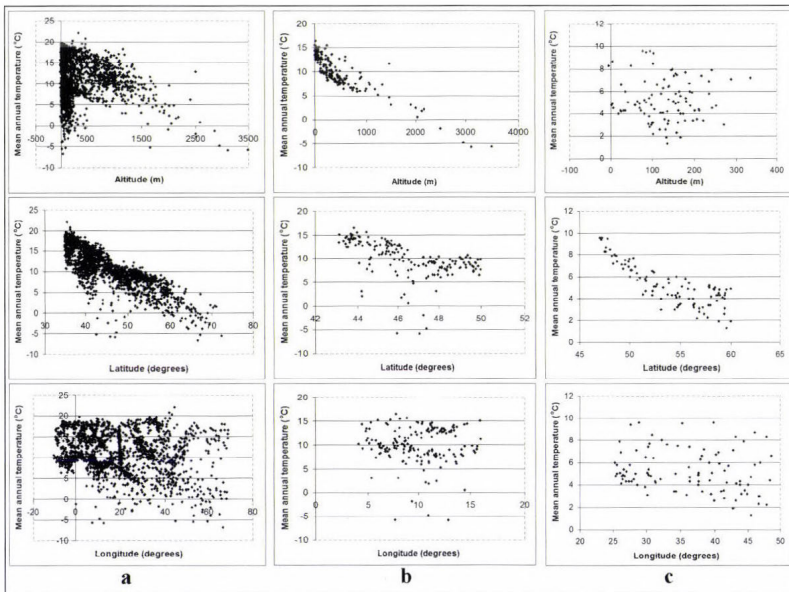


Fig. 11. Changes of the relationships between the mean annual temperatures and the altitude, latitude, and longitude for Europe (a) and for two different subregions: the Alps (b) and the Russian Plain (c). Source of data: *FAO*, 2003.

An example is shown in *Fig. 11* for the relationship between the mean annual temperature (*FAO*, 2003) and 3 predictors: altitude, latitude, and longitude. At continental scale, the territory of Europe is very heterogeneous. We may notice, that the altitude – temperature relationship changes from one region to another to such an extent that a single regression equation for the whole European territory cannot be constructed. A region like the Alps displays a very good altitude – temperature correlation, while the temperature variation within the flat relief of the Russian Plain is statistically independent of the altitude, as temperature inversions are frequent. Here, the latitude comes forward to explain a good part of the temperature spatial distribution.

In such situations, when we deal with large heterogeneous regions, it becomes necessary to divide it into smaller, more homogeneous sub-regions, for which the predictors-predictand relationships do not change. A possible approach could consist in the examination of regression parameters and residuals as we extend or reduce the area of our region and establish the sub-regions limits according to the most stable regression model (maximum correlation, minimum residuals). Another possible approach could be the application of regression as a local interpolator.

## ***7. Conclusions***

When applying statistical methods for deriving digital spatial models of climatic variables, one must take great care in identifying and assessing the sources of uncertainty, especially in the case of small stations samples. There are many such sources of different nature, which can easily mislead us towards wrong unrealistic conclusions. Consequently, a good knowledge of data quality, statistical methods, and, needless to say, climatology is imperative for the achievement of sound results. Although simple, the georeference stage is very important. The misplacement of one or more meteorological stations on the map may generate an unwanted chain of errors, because the predictors' values are automatically drawn from the raster maps in GIS environment. The representativeness of the stations network is another important issue, which needs to be analyzed in a preliminary stage of climate parameters spatialization. Theoretically, the spatial distribution of the stations network should be in agreement with terrain complexity, so as to be able to account for all climatic aspects. The extrapolation problem is tightly related to this issue. Unfortunately, in most cases, the stations network is biased, therefore, not sufficiently representative for the terrain. The extrapolation of the spatial models is correct as far as the predictors-predictand relationships do not significantly change outside the calibration area. The outliers problem, meaning the problem of values evading a certain spatial variation rule, is another aspect we analyzed in our study. This is another aspect of the representativeness of the stations network in respect to predictors, which needs to be preliminary addressed in order to minimize the potential errors. Statistical modeling is generally performed on simple, elementary variables, such as temperature or precipitation. For a more thorough investigation of a region's climate, we need to dispose of complex variables, derived from the elementary ones, such as the de Martonne aridity index, potential evapotranspiration, etc. The integration of elementary variables, each having its own statistical errors, into complex variables leads to error propagation. Knowing these errors is very important in order to assess the accuracy of the modeled spatial distribution of the complex variable. Another issue we address in our study is that of the heterogeneous regions. Generally, the greater a region, the

more heterogeneous it is. A certain level of heterogeneity is necessary for the spatialization of climate parameters. On the other hand, within a large region, the climatic heterogeneity may be too high for a single statistical model to explain it. In such a situation, it becomes necessary to divide our large region into smaller, more homogeneous sub-regions, for which the predictors-predictand relationships do not change.

**Acknowledgment** — This study was carried out with support from project POSDRU/89/1.5/S/49944, coordinated by “Alexandru Ioan Cuza” University of Iași (Romania).

## References

- Dobesch, H., Dumolard, P., and Dyras, I. (eds.), 2007: *Spatial Interpolation for Climate Data. The Use of GIS in Climatology and Meteorology*. Geographical Information Systems Series, ISTE, London and Newport Beach.
- Engen-Skaugen, T., and Tveito, O.E., 2007: Spatially distributed temperature lapse rate in Fennoscandia, in COST Action 719: *Proceedings from the Conference on Spatial Interpolation in Climatology and Meteorology* (eds.: Szalai, S., Bihari, Z., Szentimrey, T., Lakatos, M.), Budapest, 25-29 October 2004. Luxembourg: Office for Official Publications of the European Communities, EUR 22596, 93-100.
- FAO, 2003: *FAOCLIM-2. World-wide agroclimatic database v.2.02*, FAO/SDRN.
- Fotheringham, S., Brunson, C., and Charlton, M., 2002: *Geographically Weighted Regression. The Analysis of Spatially Varying Relationships*. Wiley.
- Hengl, T., 2007: *A Practical Guide to Geostatistical Mapping of Environmental Variables*. JRC Scientific and Technical Research series. Office for Official Publications of the European Communities, Luxembourg, EUR 22904 EN.
- Lhotellier, R., 2005: *Spatialisation des températures en zone de montagne alpine*, thèse de doctorat, SEIGAD, IGA, Univ. J. Fourier, Grenoble, France.
- Lhotellier, R., and Patriche, C.V., 2007: Dérivation des paramètres topographiques et influence sur la spatialisation statistique de la température. *Actes du XXème Colloque de l'Association Internationale de Climatologie*, 3-8 septembre 2007, Carthage, Tunisie, 357-362.
- Maimon, O.Z., Rokach, L. (eds.), 2005: *Data Mining and Knowledge Discovery Handbook*, Chapter 7. Outlier detection, Ben-Gal, I. Springer.
- Maracchi, G., Ferrari, R., Magno, R., Bottai, L., Crisci, A., and Genesio, L., 2007: Agrometeorological GIS products through meteorological data spatialization, in COST Action 719: *Proceedings from the Conference on Spatial Interpolation in Climatology and Meteorology* (eds.: Szalai, S., Bihari, Z., Szentimrey, T., Lakatos, M.), Budapest, 25-29 October 2004. Luxembourg: Office for Official Publications of the European Communities, 2007, EUR 22596, 9-16.
- Patriche, C.V., 2007: About the influence of space scale on the spatialisation of meteo-climatic variables. *Geographia Technica*, no. 1, Cluj University Press, 70-76.
- Patriche, C.V., Șfică, L., and Roșca, B., 2008: About the problem of digital precipitations mapping using (geo)statistical methods in GIS. *Geographia Technica*, no. 1, Cluj University Press, 82-91.
- Silva, Á.,P., Sousa, A.J., and Espirito Santo, F., 2007: Mean air temperature estimation in mainland Portugal: test and comparison of spatial interpolation methods in Geographical Information Systems, in COST Action 719: *Proceedings from the Conference on Spatial Interpolation in Climatology and Meteorology* (eds.: Szalai, S., Bihari, Z., Szentimrey, T., Lakatos, M.), Budapest, 25-29 October 2004. Luxembourg: Office for Official Publications of the European Communities, EUR 22596, 37-44.
- Wilcox, R., 2002: *Applying Contemporary Statistical Techniques*. Academic Press.

# IDŐJÁRÁS

*Quarterly Journal of the Hungarian Meteorological Service*  
Vol. 115, No. 1–2, January–June 2011, pp. 31–49

## Operational maps of monthly mean temperature for WMO Region VI (Europe and Middle East)

Florian Hogewind<sup>1</sup> and Peter Bissolli<sup>2</sup>

<sup>1</sup>*Karlsruhe Institute of Technology,  
Institute of Geography and Geoecology,  
Reinhard-Baumeister-Platz 1, 76128 Karlsruhe, Germany  
E-mail: Florian.Hogewind@kit.edu*

<sup>2</sup>*German Meteorological Service, Offenbach,  
Frankfurter Straße 135, 63067 Offenbach, Germany  
E-mail: Peter.Bissolli@dwd.de*

*(Manuscript received in final form October 30, 2010)*

**Abstract**—A spatial interpolation method for the construction of operational climate maps for the WMO RA VI Region (Europe and Middle East) is presented on the example of monthly mean temperature. The method is suitable for an in situ data base with relatively low data coverage in a relatively large and climatically heterogeneous area, and considers the classical geographical parameters latitude, longitude, and altitude by multi-dimensional linear regression, but improved by continentality, using a new continentality index. A comparison of several interpolation methods reveals that radial basis functions (subtype multiquadratic) seems to be the most appropriate approach. Separate regressions for land and sea areas further improve the results.

*Key-words:* spatial interpolation, multi-dimensional linear regression, climate maps, RA VI, Europe

### ***1. Introduction***

Climate monitoring requires an operational analysis of the variability of climatic quantities in space and time. For this purpose, operational maps, generated for regular time intervals (days, months, seasons, years) are very useful to see at a glance the spatial variability of climate elements and its change with time. Such maps are often used by national meteorological and hydrological services as a basis for climate reviews and interpretation of outstanding features of climate variability. Maps are available for various spatial areas from the catchment scale to the whole globe.

For some recent years, the German Meteorological Service (Deutscher Wetterdienst, DWD) develops methods for generating such operational maps. These methods are not exactly the same for all climate elements due to various databases, their special nature of variability, and the data availability. Some are based on satellite data (e.g., cloud and radiation parameters), others are based only on in situ data, because in that cases the in situ data have a relatively good quality compared to satellite data (e.g., temperature, precipitation, sunshine duration, snow depth). Examples of these maps can be seen on the DWD website ([www.dwd.de/rcc-cm](http://www.dwd.de/rcc-cm), [www.dwd.de/snowclim](http://www.dwd.de/snowclim), [www.dwd.de/satklim](http://www.dwd.de/satklim)).

On the other hand, it is desirable to use consistently the same method for each climate element to achieve consistent maps, at least the same basic principle of a method. Our present strategy is to develop a basic approach which is at least applicable for most of the in situ data. The process of map generation is still under further development.

Usually, maps are a result of gridding or spatial interpolation of point data into the area. Nowadays, a large variety of mathematical and geostatistical methods for spatial interpolation is available. However, in practice, it has turned out that pure mathematics and geostatistics are necessary, but not sufficient for construction of climate monitoring maps; instead it has been found that the consideration of geographical conditions and climate processes can much improve the results. Nevertheless, the impact of such additional parameters and processes depends highly on the extent and topography of the area of interest, and also on data density. Therefore, the choice of the gridding method depends on the selected area, and the selected climate element as well.

This paper refers specifically to spatial interpolation of monthly mean temperature and its anomalies from the reference period 1961–1990 in a relatively large area, the WMO (World Meteorological Organization) Region VI (covering nearly the whole Europe and the Middle East). The next chapter describes this area and the motivation for the choice of this area. After a short review of previous literature, the data and the succeeding steps of the method applied in this paper are described and compared with a number of alternatives. Results of the comparison and the mapping are presented in Section 6, followed by some conclusions in Section 7.

The main goal of this paper is to propose a method of spatial interpolation of monthly temperature data in WMO Region VI which is suitable for an operational generation of monthly climate monitoring maps. However, it is intended that this approach is applicable to other climate elements as well to receive maps of various elements which are consistent to each other as far as possible, at least for in situ data. Other data sources, like satellite data which already have a large spatial coverage certainly require a different approach.

## 2. The WMO Region VI and the Regional Climate Centre (RCC) network

Recently, a new network of so-called Regional Climate Centres (RCCs) has been established under the auspices of the World Meteorological Organization (WMO) ([http://www.wmo.int/pages/prog/dra/eur/RAVI\\_RCC\\_Network.php](http://www.wmo.int/pages/prog/dra/eur/RAVI_RCC_Network.php)). The term “regional” refers to the six WMO Regions which cover roughly (but not exactly) the various continents and the surrounding sea areas on the globe.

Nearly the whole of Europe (except the easternmost parts of European Russia from 50°E to the Ural) belongs to the WMO Region VI (often referenced as “RA VI”, indicating the Regional Association of the WMO in Region VI). Beside Europe, this region also covers parts of the Middle East which belong geographically to Asia, and also large sea areas, namely large parts of the northern and central North Atlantic, the Norwegian Sea, the European part of the Arctic, and the whole Mediterranean. The RA VI area is displayed in *Fig. 1*.

The border of the Region VI (Europe and Middle East) is not rectangular, because it is defined by the borders of single countries, which means largely by political conditions. Over European Russia, the eastern border runs along the 50°E meridian. In the south and west, the border crosses the Mediterranean Sea and the Atlantic Ocean to the Davis Strait and the Baffin Bay between Greenland and Canada.

Thus, that Region covers quite a large and climatically very heterogeneous area, spanning a wide range of latitude, longitude, and altitude and strong contrasts between land and sea climates.

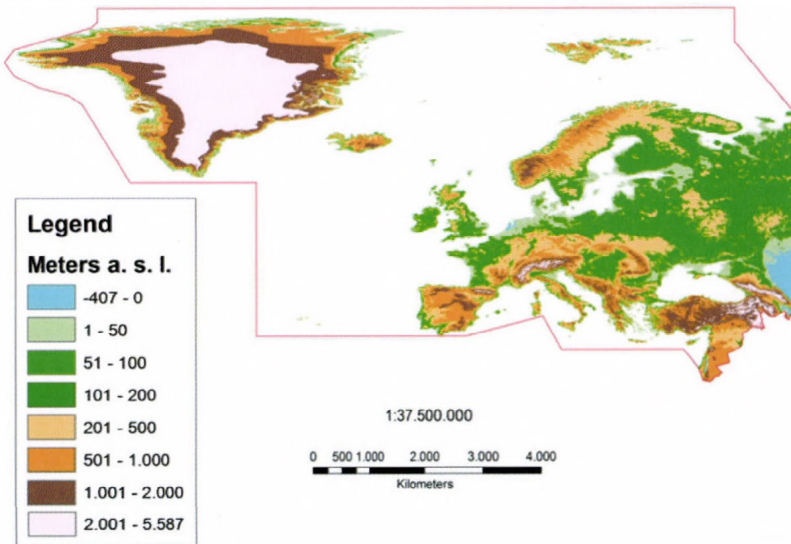


*Fig. 1.* Map of the Region VI with the height above sea level. The kilometer bar refers to Central Europe.

In RA VI, presently three RCCs (so-called nodes of the RCC network) are already preliminarily established and are operating in a pilot phase since June 2009: one RCC node on climate data, one on climate monitoring, and one on long-range forecasting. The DWD has taken over the lead function of the RCC node on climate monitoring in RA VI, within a consortium consisting of some more members (national meteorological and hydrological services) of RA VI. To fulfill this function, the generation of climate maps for various climate elements in RA VI is a very important task.

### 3. Previous approaches

A large number of papers dealing with spatial interpolation of climate data have already been published. Basic information about spatial interpolation methods can be found in various books, especially for the widely used kriging technique, which was very popular already in the 1990s (e.g., *Lang*, 1995; *Stein*, 1999). In the 2000s, geographical information systems (GIS) came more and more into operation for climate mapping. Commercial GIS software has made it technically very easy to apply spatial interpolation methods on any geographically defined data points. In 2001, the COST Action 719 was launched (COST= European Cooperation on Science and Technology, an intergovernmental framework for research coordination in Europe, supported by the European Union). The goal of COST 719 was to review and assess the use of GIS for spatial interpolation in meteorology and climatology. The Action had been finished in 2006, resulting in an overview of spatial interpolation methods and their application in climatology by GIS software (*Thornes*, 2005; *Tveito et al.*, 2008) and many related papers (e.g., *Ustrnul* and *Czekierda*, 2005; *Dobesch et al.*, 2007).

Until now, there are several more recent papers. Various methods are applied to national data, some also to larger areas, e.g., the Alps, some to global data, but in coarse resolutions. Many investigators used ordinary or residual kriging techniques for monthly, seasonal, or annual data, e.g., *Bjornsson et al.* (2007) for temperature in Iceland, *Ustrnul* and *Czekierda* (2005) for temperature in Poland, *Dolinar* (2006) for sunshine duration in Slovenia, *Perčec Tadić* (2010) for climate normal values of various elements (including temperature) for Croatia, *Alsamamra et al.* (2009) for solar radiation in southern Spain. Others just used multiple regression techniques, but in a dense station network and with many geographical predictors, e.g., *Hiebl et al.* (2009) for monthly temperature in the Alps or *Claps et al.* (2008) for monthly temperature in Italy. Non-linear instead of linear statistical relationships between terrain variables as predictors and climate variables lead to an improvement at least for special variables like, e.g., fog frequency as shown by *Vicente-Serrano et al.* (2010) for northeast Spain. In some cases, circulation types were used as predictor, e.g., the well-

known “Grosswetterlagen” catalogue from *Hess and Brezowsky (1952)* for the temperature in Poland (*Ustrnul, 2006*). Other authors included remote sensing data for statistical temperature modeling (e.g., *Cristóbal et al., 2008* for northeast Spain).

In contrast, there have been very few attempts to look for a method which is specifically appropriate for an area like RA VI. Recently, *Haylock et al. (2008)* presented a new European high-resolution gridded data set of daily precipitation and surface temperature for the period 1950–2006 on four spatial resolutions (the so-called E-OBS data set). Although this data set is widely known and used, the authors themselves pointed to limitations of their gridded data due to inhomogeneities and interpolation uncertainties (*Hofstra et al., 2009*). *Hofstra et al. (2008)* also compared several interpolation methods for various variables in some parts of Europe and found that the main controlling factor on the skill of interpolation is rather the density of the station network than the interpolation method. Only recently, another investigation used the spatial variability from past observations of a denser network to improve the interpolation skill, in this case applied to precipitation in the complex terrain of Switzerland (*Schiemann et al., 2010*).

Monthly, seasonal, and annual maps are frequently used for operational climate monitoring activities. The monitoring of the WMO RA VI Regional Climate Centre on Climate Monitoring (WMO RAVI RCC-CM) can be found on the web: <http://www.dwd.de/rcc-cm>, including links to national maps of many national meteorological and hydrological services. For global climate monitoring, monthly temperature maps are displayed, e.g., on the website of the National Oceanic and Atmospheric Administration (NOAA) in the USA: <http://www.ncdc.noaa.gov/climate-monitoring/index.php#global-icon>.

#### **4. Data and data quality**

Since the goal is to generate monthly maps for RA VI in the operational environment of DWD, it is essential to use monthly in situ data which are available at DWD soon after the end of month, but, nevertheless, of good quality. National data sets exist for each country in RA VI. Mainly they are under the responsibility of the public national and hydrological services. Due to this national responsibility of the data, each country has its own data policy, and in most cases there are restrictions in data distribution beyond the national services. For this reason, only a limited number of all existing data can be used in the DWD environment. However, there are some data which are distributed internationally and regularly via the Global Telecommunication System (GTS) of the WMO. Two important data sets in this case are the SYNOP and CLIMAT data. SYNOP data are data from synoptical stations, distributed several times a day (often hourly), containing also the air temperature at two meters height over

ground. They are mainly intended for usage in weather forecasting. CLIMAT data are distributed only monthly and the number of stations is much smaller than for SYNOP, but the selection of CLIMAT stations was done for usage of climate analyses. Monthly mean temperature is one of the climate elements which are reported in the CLIMAT bulletin. DWD has taken over the task to check the quality of the CLIMAT data each month in various steps. The quality check consists of two steps: a quick automatical check soon after data arrival and a more thoroughly manual check later. More details about the CLIMAT data archive and quality control method can be found on the DWD website ([www.dwd.de](http://www.dwd.de) – click on Climate and Environment – Climate Data Centers – ACD). The first step of quality check is normally done within 10 days after the end of each month. The check of SYNOP data would be more time consuming, and a complete routine quality control for SYNOP temperature data at DWD is only performed for German data, but not for the whole of the RA VI area. For this reason it was decided to use the CLIMAT data of monthly mean temperature for spatial interpolation, which means a data basis which is timely available in good data quality, but relatively poor data coverage (*Fig. 2a*). Around 800 CLIMAT stations are currently available for RA VI each month, and the area has an extension of several 1000 km in both zonal and meridional directions. This decision means to invest into an appropriate and reasonable interpolation procedure, which also takes the diverse topography of RA VI into account.

CLIMAT stations are available only for the land areas, but not for the sea. However, there exist weather reports from ships which are summarized into a  $2.5^{\circ} \times 2.5^{\circ}$  latitude-longitude grid and are archived at DWD. Altogether, around 130 sea grid points are used for each month. Although the grid points are uniformly distributed over the area, the underlying ship reports are not equally distributed. The best data coverage can be found along the main shipping routes such as between Europe and the eastern coast of the USA or Brasilia, and the main route to the Mediterranean Sea, but in other areas ship data are quite rare (*Fig. 2b*). Thus, the quality of ship data is strongly dependent on ship observation coverage. They are most reliable along the main shipping routes where a large number of ship observations during the whole month are considered for gridding, but quite poor in those regions where only very few ship observations are available, e.g., over the Arctic Sea. Long-term averages for the 1961–1990 reference data (CLIMAT and ship data, as far as data available) are also quality controlled and included in the DWD archive, and anomalies (monthly means minus long-term averages) are computed each month as well.

For using the topography in the interpolation procedure, grid data for altitude are needed. Data for the height above sea level are taken from the GTOPO30 altitude raster from the U.S. Geological Survey ([www.usgs.gov](http://www.usgs.gov)). The data are available in a spatial resolution of 30 seconds of degree in latitude and longitude (it means about 1 km for middle latitudes). For the operational maps, a

spatial resolution of  $0.1^\circ$  was taken; thus, the GTOPO30 data were averaged into a  $0.1^\circ$  grid.

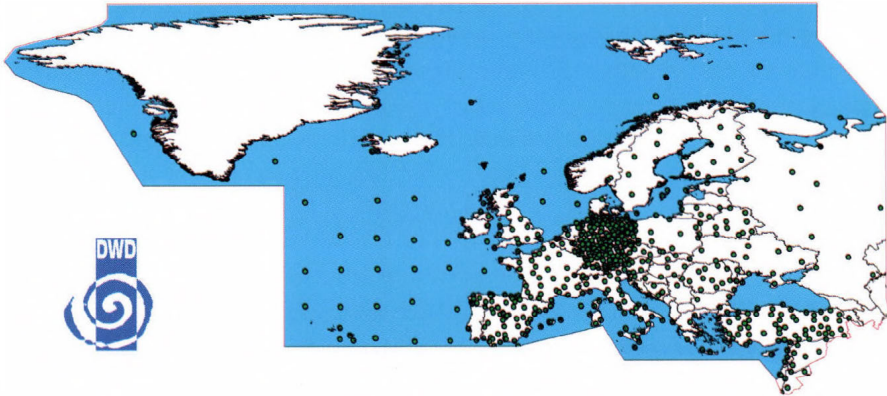


*Fig. 2a.* Spatial distribution of CLIMAT stations and ship data points available at DWD for September 2010 as an example. Ship data of the whole month are arithmetically averaged into a  $2.5^\circ \times 2.5^\circ$  grid.

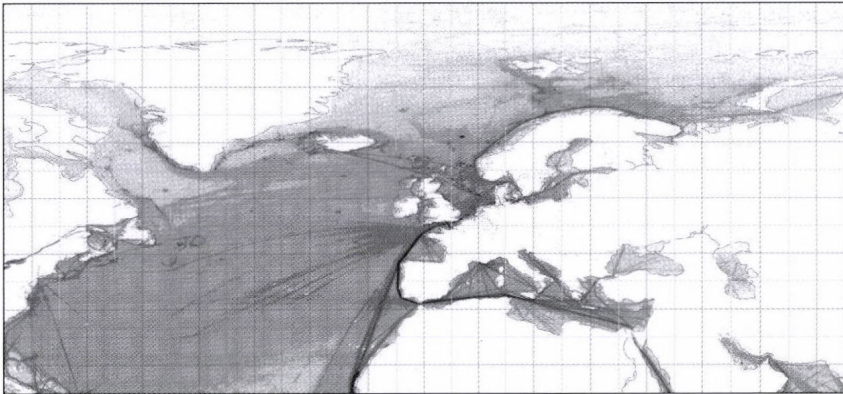


*Fig. 2b.* Ship data coverage, data from DWD (white = land area, light grey to dark grey = more travel on sea, if the color is darker, more ships travel on this route).

## 5. Methods

In principle, the spatial interpolation method for monthly averages used here consists of three steps. The first step is a multi-dimensional linear reduction of the station data, which means a multiple linear regression of latitude, longitude, altitude, and other parameters to zero level. The linear regression model is

subtracted from the original data; the results of the subtraction are often called “residuals”.

The second step is the interpolation of residuals with the method radial basis functions, using the version of the software ESRI Arc GIS 9.2 within the tool geostatistical analyst. The last step is recomputing the interpolated residuals to the original values of latitude, longitude, altitude, and other parameters. This computing is achieved by using the raster calculator of Arc GIS 9.2 within the tool spatial analyst. The three steps are described in more detail in Sections 5.1–5.6.

For the anomalies there is no reduction, just a spatial interpolation is necessary, assuming that they do not depend very strongly on geographical parameters. Spatial resolution is  $0.1^\circ$ ; this corresponds to about 10 km over Central Europe. The number of grid points in the RA VI area roughly amounts to nearly one million.

At the borders of Region VI, the problem of extrapolation appears. For this reason, the interpolation is computed for an extended area (from  $85^\circ\text{W}$  to  $70^\circ\text{E}$  and from  $20^\circ\text{N}$  to  $90^\circ\text{N}$ ), but only the Region VI itself is displayed. For this purpose, some more climate stations beyond Region VI are added to the data pool. The additional climate stations are located in the east part of the USA and Canada, the North African states, and in the part of the Middle East, which belongs to the Region II Asia.

### *5.1. General approach of multiple regression in latitude, longitude, altitude*

The assumption of the multi-dimensional reduction is that the spatial variability of monthly averaged climate is dominated by a very limited number of impact factors.

The general approach is

$$Y = a f_1(x_1, x_2, \dots, x_n) + b f_2(x_1, x_2, \dots, x_n) + \dots + k, \quad (1)$$

where  $Y$  is a climate state variable like temperature,  $x_1, x_2, \dots$  are impact factors like latitude etc.,  $f_1(), f_2(), \dots$  are functions of impact factors, which are not necessarily linear, and  $a, b, \dots, k$  are constant values.

This approach is used to find the dominating impacts,  $x_1, x_2$ , and the functions of impacts,  $f_1(), f_2()$ , for each  $Y$ . The functions of the impact factors must be linearly independent from each other. Then, a linear regression can be computed.

### *5.2. Multiple linear regression in latitude, longitude, altitude*

We start with latitude, longitude, and altitude as predictors. These factors are reasonable because of the following reasons: latitude characterizes the climate due to the solar angle, which is, by far, the most dominating factor for Region

VI. The longitude is the alternative for land-sea contrasts or continentality, which explains much of the seasonal variations. Finally, the altitude is included, because all climate state variables increase or decrease more or less with height above sea level. For monthly mean temperature, this factor is generally weak within Region VI compared to latitude and longitude but not negligible, especially in mountainous areas. The amount of variation of temperature as function of altitude varies largely from month to month, depending on season and the prevailing weather type during the month. In most cases, monthly mean temperature decreases with altitude, but in winter months, when inversion weather types are prevailing, a slight increase with altitude can also happen. For this reason, the regression model is fitted for each month separately.

The linear approach in this special case yields:

$$Y = a \cdot \text{latitude} + b \cdot \text{longitude} + c \cdot \text{altitude} + k. \quad (2)$$

This is a specialization of the general approach Eq. (1). The three predictors (latitude, longitude, and altitude) represent the three spatial dimensions which are obviously orthogonal and, therefore, independent from each other. The coordinates are mostly well known for each station, thus, these predictors are mostly easily available. The fitting of the multi-linear regression has been done using the method of least squares (see, e.g., *Mosteller and Tukey, 1977*).

### 5.3. Continentality impact

For improving the approach, the longitude is replaced by a suitable continentality index. The continentality is a function of latitude and the annual temperature amplitude, which is calculated by the difference of the long-term means (1961–1990) of the maximum temperature in summer (June to August) and that of the minimum temperature in winter (from December to February). That calculation of the annual temperature amplitude is only an approximation for simplifying the computation, but does not reflect exactly the real annual amplitude. For example, March, which belongs to spring, is sometimes the coldest month in the year because of the drifting ice in bays near Finland in the Baltic Sea. In the literature, there are various versions of continentality indices (see, e.g., *Bliithgen, 1980*). Many equations show that the continentality for Europe can be described by a function of latitude and the annual temperature amplitude. One example is the approach by *Iwanow (1959)*. *Hogewind (Hogewind, 2010)* modified this index to obtain a better suitability for the Region VI:

$$k = 260 \cdot \frac{\text{annual amplitude}}{\text{latitude } \varphi}, \quad \text{Iwanow (1959) and}$$

$$k = \frac{110 \cdot \text{annual amplitude}}{(\text{latitude } \varphi + 6)}, \quad \text{Hogewind (2010).}$$

This modification results in four classes in the range of the index: between 0 and 25 (highly maritime), from 26 to 50 (maritime), from 51 to 75 (continental), and from 76 to 100 (highly continental) over Region VI and its surroundings, and a threshold of around 50 between prevailing maritime and prevailing continental areas (Fig. 3).

Taking the continentality into account, the modified regression approach reads:

$$Y = a \cdot \text{latitude} + b \cdot \text{altitude} + c \cdot \text{annual amplitude} + d \cdot \text{continentality} + k. \quad (3)$$

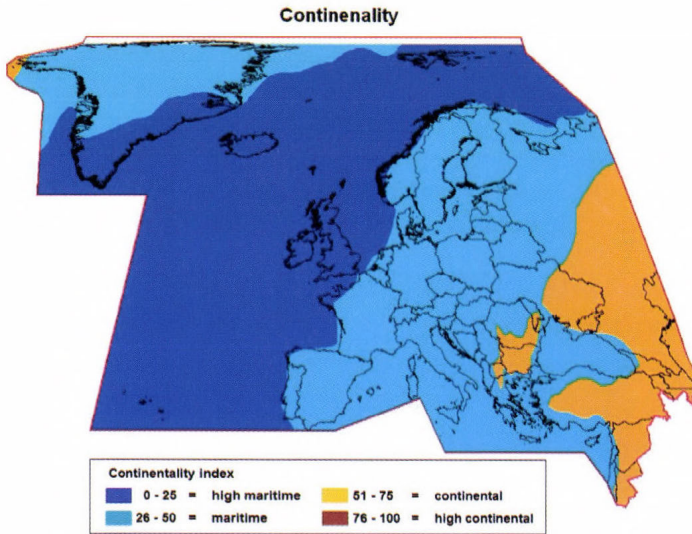


Fig. 3. Continenality (Hogewind, 2010).

This is now a non-linear approach in the explanatory variables, because continentality is a non-linear function of latitude, but the multiple regression is still linear, because a non-linear data transformation has been done (Wilks, 2006).

To get the residuals ( $T_{red}$ , the part of variability which is not explained by the regression model), the linear regression is subtracted from the original monthly mean temperature value for each station:

$$T_{red} = T_m - (a \cdot \text{latitude}) - (b \cdot \text{altitude}) - (c \cdot \text{annual amplitude}) - (d \cdot \text{continentality}) - k. \quad (4)$$

The considered parameters are now latitude, altitude, annual amplitude, and the newly created continentality index.

#### 5.4. Interpolation of residuals

The reduced climate state variable, also known as residual (here  $T_{red}$ ) is given for each measurement station and has to be interpolated into the area. The main question is now: which is the best suitable interpolation method?

The used software ArcGIS 9.2 Geostatistical Analyst offers a number of methods: inverse distance weighted, global polynomial interpolation, local polynomial interpolation, radial basis function, kriging, cokriging, and subtypes for each. From these methods a number of alternative approaches, which seem reasonable, are taken and applied to the computed residuals.

All these methods are described in the literature. An overview can be found in *Tveito et al.* (2008) including the mathematical background, the implementation in GIS software, and further references. The method “radial basis functions”, which has been used for the final construction of maps in this paper, is described in the next section.

#### 5.5. Radial basis functions

A radial basis function (RBF) is a real-valued function whose value depends only on the distance from the origin, so that  $\Phi(x) = \Phi(\|x\|)$ , or, alternatively, on the distance from some other point  $c$ , called a center, so that  $\Phi(x,c) = \Phi(\|x-c\|)$ . Any function  $\varphi$  that satisfies the property  $\Phi(x) = \Phi(\|x\|)$  is a radial function. The norm is usually the Euclidean distance, although other distance functions are also possible. For example, by using the Lukaszzyk-Karmowski metric, for some radial functions it is possible to avoid problems with ill conditioning of the matrix solved to determine coefficients  $\omega_i$  (see below), since the  $\|x\|$  is always greater than zero.

Sums of radial basis functions are typically used to approximate given functions. This approximation process can also be interpreted as a simple kind of neural network.

The radial basis functions type used in this paper is multiquadratic ( $r = \|x - c_i\|$ ):

$$\varphi(r) = \sqrt{r^2 + \beta^2} \quad \text{for some } \beta > 0. \quad (5)$$

Radial basis functions are typically used to build up function approximations of the form:

$$y(x) = \sum_{i=1}^N \omega_i \Phi(\|x - c_i\|), \quad (6)$$

where the approximating function  $y(x)$  is represented as a sum of  $N$  radial basis functions, each associated with a different center  $c_i$ , and weighted by an appropriate coefficient  $\omega_i$ . The weights  $\omega_i$  can be estimated using the matrix methods of linear least squares, because the approximating function is linear in the weights.

Approximation schemes of this kind have been particularly used in time series prediction and control of non-linear systems exhibiting sufficiently simple chaotic behavior, and 3D reconstruction in computer graphics (Lukaszyk, 2004; Buhmann, 2003).

Eq. (6) can also be interpreted as a rather simple single-layer type of an artificial neural network, called a radial basis function network, with the radial basis functions taking the role of the activation functions of the network. It can be shown that any continuous functions on a compact interval can in principle be interpolated with arbitrary accuracy by a sum of this form, if a sufficiently large number of radial basis functions is used.

The approximant  $y(x)$  is differentiable with respect to the weights  $\omega_i$ . The weights could thus be learned using any of the standard iterative methods for neural networks.

There is a lot of literature about radial basis functions for further reading (e.g., Baxter, 1992; Beatson et al., 2000; Bors, 2001; Buhmann, 2003; Wei, 1998).

### 5.6. Recomputing interpolated residuals

For recomputing the interpolated residuals to original data, the same regression equation, Eq. (4), as for reduction is used (Section 5.3). The difference is that this time the computing is not carried out for stations, but for the interpolated grid for the Region VI

$$T = T_{red} + (a \cdot \text{latitude}) + (b \cdot \text{altitude}) + (c \cdot \text{annual amplitude}) + (d \cdot \text{continentality}) + k. \quad (7)$$

Therefore, gridded data for latitude, altitude, annual temperature amplitude, and continentality are needed. Latitude is just a linear interpolation in meridional direction. For altitude, the grid GTOPO30 from U.S. Geological Survey is used with a recalculated resolution in  $0.1^\circ$ . The annual amplitude is interpolated by the interpolation method radial basis functions from station data, and finally, the continentality is computed from latitude and annual amplitude for each grid point (see Section 5.3).

### 5.7. Cross validation and root mean square error (RMSE)

To assess the quality of the spatial interpolation, a cross validation of the residuals has been carried out. This means that the spatial interpolation has been

repeated after omitting one of the residual station values, and this has been done for each station value. Then, for all station points the difference between the residual station value and the corresponding interpolated value at this point has been computed. Finally, the root mean square error (RMSE) has been computed over the differences for all points, and then for each month and each of various interpolation methods, among them radial basis functions, several kriging approaches, and inverse distance weighted interpolation. Therefore, the RMSE is a quantity for estimating the mean interpolation error. However, it has to be kept in mind that the RMSE only can represent the information at the station points, but not for the whole area, and therefore, it does not exactly give the real mean interpolation error. Nevertheless, the estimate should be near to reality if the stations are representative for the area. As most stations are located in Central Europe, where the interpolation error is expected to be lower than in other more data sparse regions, the real mean interpolation error should be greater than the RMSE, which means that the RMSE can only give a minimum estimation. However, as the data base is the same for each method and each month (except for a few stations missing from month to month), the RMSE is a comparable measure of skill for each interpolation method.

## 6. Results

### 6.1. Results of the multiple regression

For the first approach (Eq. (2)), the three predictors (latitude, longitude, and altitude) explain a large part of the variance, generally over 70% for monthly mean temperature in Region VI for all months (*Table 1*).

*Table 1.* Explained variance in % for each of the predictors in Eqs. (2) and (3), for all months of the 1991–2000 average. Other periods have similar results

Month	Latitude	Longitude	Altitude	Annual amplitude	Continental	Lat+lon+alt (Eq. (2))	Lat+alt+amp+cont (Eq. (3))
Jan	60.98	5.36	3.90	50.78	10.30	70.29	93.83
Feb	66.21	4.85	2.52	43.93	6.13	73.74	93.44
Mar	74.32	2.60	1.17	30.75	1.42	80.07	91.33
Apr	83.92	0.68	0.23	13.73	0.76	89.08	90.72
May	85.02	0.00	0.09	3.36	7.50	90.12	89.02
Jun	80.85	0.54	0.42	0.00	18.63	88.04	88.93
Jul	79.83	0.31	0.86	0.25	23.21	85.74	90.03
Aug	83.78	0.01	0.55	0.12	17.56	88.56	91.33
Sep	88.20	0.84	0.04	5.96	5.17	92.54	93.82
Oct	86.28	2.39	0.64	16.47	0.33	91.73	94.94
Nov	75.07	5.86	2.91	35.66	2.74	83.81	95.89
Dec	65.77	6.95	3.98	47.29	8.08	75.72	95.07

The largest part is explained by latitude, especially in the warmer half year, due to the large variability of temperature as function of the solar angle. The explained part of variance in Eq. (3), using the predictors latitude, altitude, annual amplitude, and continentality, is considerably larger, especially during the colder months (from November to March) compared to Eq. (2), over 90%, due to the high impact of the annual amplitude particularly in winter, which has a high spatial variability within Europe. In the warmer half year, there is practically no or only a slight improvement concerning the explained variance by Eq. (3) compared to Eq. (2). However, the explained variance by Eq. (3) is within a range between 89 and 96% (rounded) for each month.

### 6.2. Results of the spatial interpolation

Results of the comparison between the various interpolation methods are shown in Fig. 4. For some of the interpolation methods and subtypes, unwanted interpolation islands appear (so-called bulls eyes), in particular for inverse distance weighting, global and local polynomial interpolation. Some kriging and cokriging subtypes are not exact at the station points and smooth too much. The interpolation method cokriging needs a second variable with the same resolution as the climate variable. This cannot be an impact variable, because this has already been removed by reduction. Some methods, especially cokriging, need quite a high computing time depending on spatial resolution, and thus, they are not convenient for operational use.

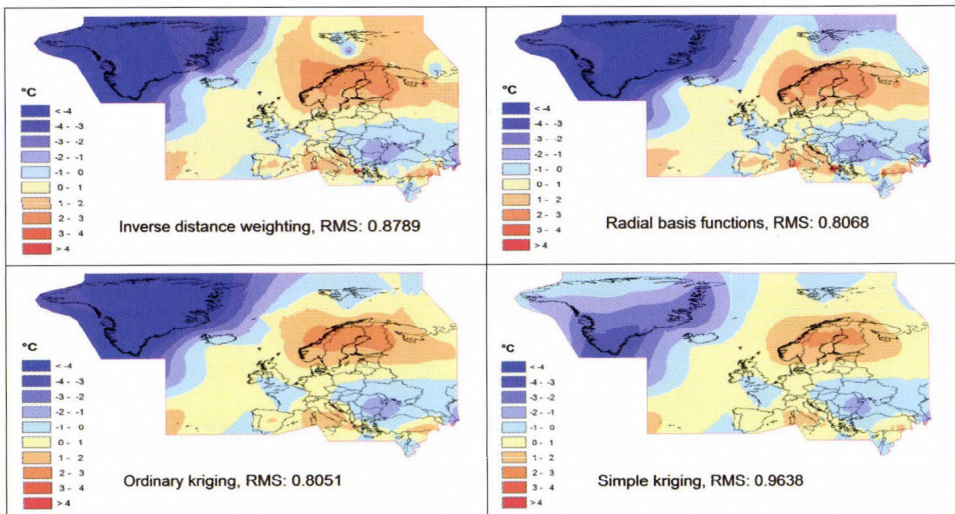


Fig. 4. Interpolated residuals (after subtracting the linear regression model) of annual temperature normal values of the period 1961–1990 using the following interpolation methods: inverse distance weighted (upper left), radial basis functions (upper right), ordinary kriging (lower left), simple kriging (lower right). RMS errors given for each method in K refer to the residuals.

*Fig. 4* also shows the root mean square errors (RMSE) for various interpolation methods. The highest RMS errors of these show the interpolation methods simple kriging (*Fig. 4*, lower right) and inverse distance weighted (upper left). For inverse distance weighted, obvious interpolation islands can be clearly seen. Simple kriging amplifies point-to-point differences too much. The other two methods (ordinary kriging, *Fig. 4*, lower left, and radial basis functions, upper right), although basically different from each other, produce more or less the same results. The difference between these two interpolation methods is the longer computing time and the more difficult calibration of ordinary kriging because of every individual interpolation for the climate variable and period. As a result of this comparison of the different methods, the radial basis functions method with the subtype multiquadratic appears as the most suitable method for meeting our demands on operational map generation. The main advantages are exactness at data points (values at the data points are not changed after interpolation, except due to different altitudes and locations of the stations compared to the grid points), no smoothing, but no unrealistic interpolation islands either. The exactness at data points is also good to detect suspicious data on the map. The RMS error for the selected method is one of the lowest, the results are similar to ordinary kriging, but the computing is faster than kriging. Kriging, on the other hand, offers more possibilities of error assessment, but they are more difficult to interpret as they are not comparable with error assessments of other methods. Generally, the choice of the interpolation method matters only in data sparse areas. Otherwise, it is more important, when the regression error is higher or the data quality is worse.

The results of the described process need a further development which is described by *Hogewind* (2010). The different thermal conditions between land and sea require a separate regression over land and sea with separate regression coefficients for land and sea, but each applied to the whole RA VI area (*Fig. 5*). To consider coastal effects, the climate stations near the coast are used for both computing processes for overlapping land-sea areas. Furthermore, the data pool is increased by including the stations from the European Climate Assessment Dataset (ECA&D, [www.knmi.nl](http://www.knmi.nl)). To study the space-time variability, the procedure has also been carried out for 10-year subperiods of the period 1951–2000. Examples of recomputed temperature fields for land and sea are shown in *Figs. 6a* and *6b* (for recomputation, a land-sea mask was used). These fields are overlaid to one complete map for the whole Region VI like a puzzle (*Fig. 7*). The effect of the thermal contrast between land and sea can be seen in various places, e.g., for Turkey.

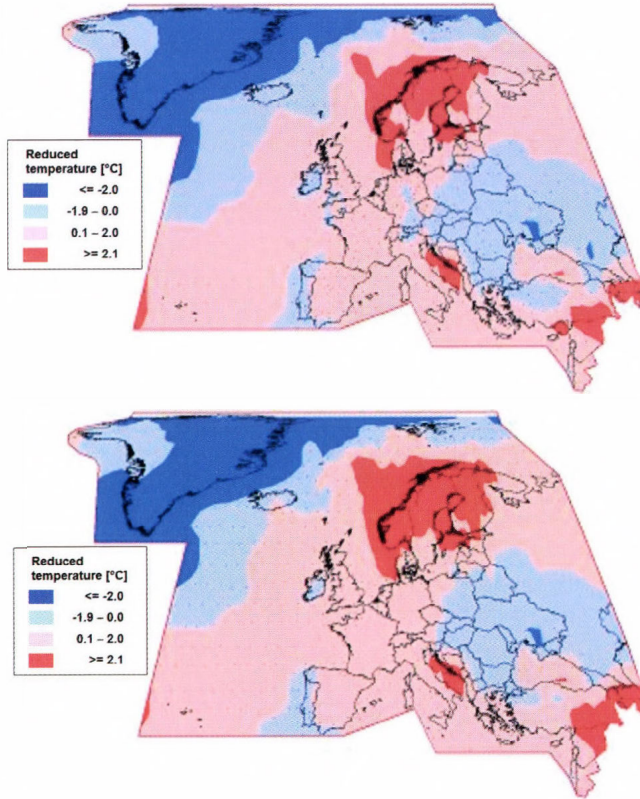


Fig. 5. Reduced temperature (residuals) over land (upper) and sea (lower) in September for the period of 1991–2000. Separate regression coefficients for land and sea are used, but applied to the whole RA VI area.

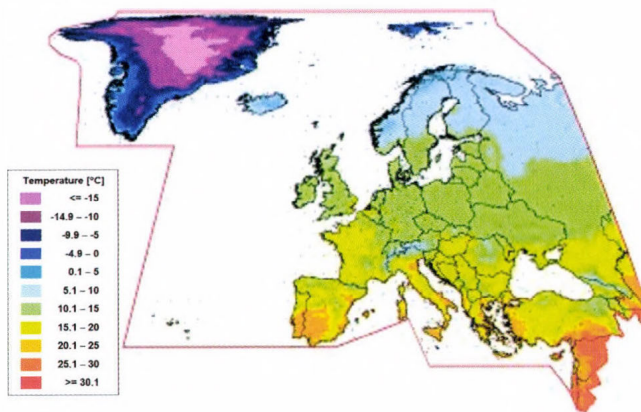


Fig. 6a. Recomputed temperature over land in September for the period of 1991–2000. White areas are excluded by using a land-sea mask.

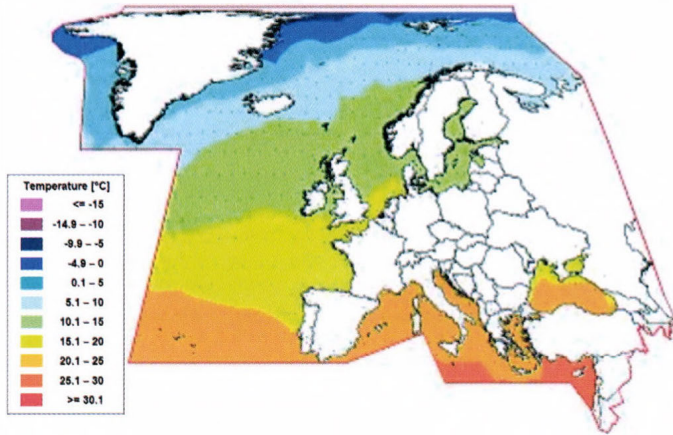


Fig. 6b. Recomputed temperature over sea in September for the period of 1991–2000. White areas are excluded by using a land-sea mask.

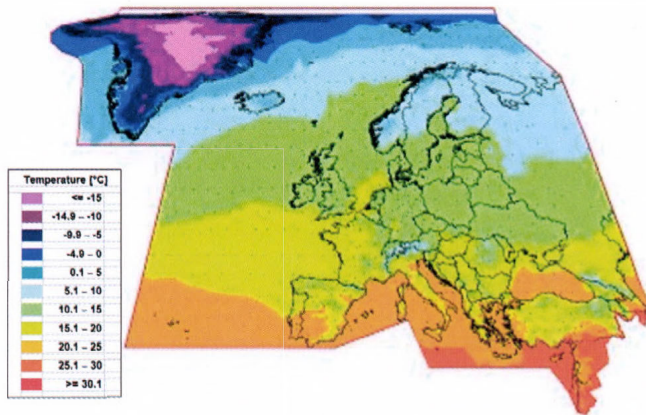


Fig. 7. Recomputed temperature in September for the period of 1991–2000 for the whole RA VI Region (consisting of separate calculations over land and sea as in Fig. 6).

## 7. Conclusions

The newly created continentality index (*Hogewind*, 2010) improves the regression model in comparison to longitude. The separate land-sea regressions improve the regression model, too. Nevertheless, the most important parameter for Region VI is still the latitude because of the strong influence of the angle of solar radiation. Residuals up to 2 K (RMSE 0.9 K) do not change, due to small scale effects. Radial basis functions turned out to be the most suitable

interpolation method at the moment, at least for operational map production of monthly mean temperature in WMO Region VI. The method is exact, has a relatively low RMSE, can be realized very easily by using GIS software, and the interpolation can be computed in reasonable time. Probably the most promising effort to improve the results further is to enlarge and improve the data base and the regression model. Another challenge will be the application of this method to daily instead of monthly data.

**Acknowledgments**—First of all, we thank our colleagues of the district office of the DWD in Hamburg to prepare the CLIMAT data and data over the sea area, especially *C. Lefebvre* and *J. Busche*. Our technician *V. Zins* at DWD was very helpful in providing some of the figures.

We also thank the Hungarian Meteorological Service for the possibility of realizing this publication, and the language corrector of IDŐJÁRÁS for improvements of wording.

## References

- Alsamamra, H., Ruiz-Arias, J.A., Pozo-Vázquez, D., Tovar-Pescador, J.*, 2009: A comparative study of ordinary and residual Kriging techniques for mapping global solar radiation over southern Spain. *Agr. Forest. Meteorol.* 149, 1343-1357.
- Baxter, B.J.C.*, 1992: The interpolation theory of radial basis functions. Cambridge University.
- Beatson, R.K., Light, W.A., Billings, S.*, 2000: Fast solution of the radial basis function interpolation equations: Domain decomposition methods. *Society for Industrial and Applied Mathematics* 22, 1717-1740.
- Bjornsson, H., Jonsson, T., Gylfadottir, S.S., Olason, E.O.*, 2007: Mapping the annual cycle of temperature in Iceland. *Meteorol. Z.* 16, 45-56.
- Blüthgen, J.*, 1980: *Allgemeine Klimageographie*. 3. new revised edition. De Gruyter, Berlin (in German).
- Bors, A.G.*, 2001: Introduction of the Radial Basis Function (RBF) Network. Online Symposium for Electronics Engineers.
- Buhmann, M.D.*, 2003: *Radial Basis Functions: Theory and Implementations*. Cambridge University Press.
- Claps, P., Giordano, P., Laguardia, G.*, 2008: Spatial distribution of the average air temperatures in Italy: quantitative analysis. *J. Hydrolog. Eng.* 13, 242-249.
- Cristóbal, J., Ninyerola, M., Pons, X.*, 2008: Modelling air temperature through a combination of remote sensing and GIS data. *J. Geophys. Res.* 113, D13106.
- Dobesch, H., Dumolard, P., Dyras, I.*, 2007: Spatial interpolation for climate data. The use of GIS in climatology and meteorology. *Geographical Information Systems Series*. ISTE, London.
- Dolinar, M.*, 2006: Spatial interpolation of sunshine duration in Slovenia. *Meteorol. Appl.* 13, 375-384.
- Haylock, M.R., Hofstra, N., Klein Tank, A.M.G., Klok, E.J., Jones, P.D., New, M.*, 2008: A European daily high-resolution gridded data set of surface temperature and precipitation for 1950-2006. *J. Geophys. Res.* 113, D20119.
- Hess, P., Brezowsky, H.*, 1952: Katalog der Grosswetterlagen Europas. *Ber. Deutscher Wetterdienst in US Zone*, Nr. 33.
- Hiebl, J., Auer, I., Böhm, R., Schöner, W., Maugeri, M., Lentini, G., Spinoni, J., Brunetti, M., Nanni, T., Perčec Tadić, M., Bihari, Z., Dolinar, M., Müller-Westermeier, G.*, 2009: A high-resolution 1961-1990 monthly temperature climatology for the greater Alpine region. *Meteorol. Z.* 18, 507-530.
- Hofstra, N., Haylock, M., New, M., Jones, P.D.*, 2009: Testing E-OBS European high-resolution gridded data set of daily precipitation and surface temperature. *J. Geophys. Res.* 114, D21101.
- Hofstra, N., Haylock, M., New, M., Jones, P., Frei, C.*, 2008: Comparison of six methods for the interpolation of daily European climate data. *J. Geophys. Res.* 113, D21110.

- Hogewind, F., 2010: Raum-zeitliche Analyse der Klimavariabilität anhand von hochaufgelösten interpolierten Klimakarten am Beispiel von Europa und dem Nahen Osten (Region VI der Weltorganisation für Meteorologie). Preliminary results (in German, to be published in PhD thesis, University of Mainz, Germany).
- Iwanow, N.N., 1959: Belts of continentality on the globe. (Izvest. Wsejoj. Geogr. Obschtsch. 91, 410-423 (in Russian). Cited in *Blüthgen* (1980), p. 590 (in German).
- Lang, C., 1995: *Kriging Interpolation*. Department of Computer Science, Cornell University.
- Lukaszuk, S., 2004: A new concept of probability metric and its applications in approximation of scattered data sets. *Computational Mechanics* 33, 299-304.
- Mosteller, F., Tukey, J.W., 1977: *Data Analysis and Regression – a second course in statistics*. Addison-Wesley, Reading MA, ISBN 020104854X.
- Perčec Tadić, M., 2010: Gridded Croatian climatology for 1961-1990. *Theor. Appl. Climatol.* 102, 87-103.
- Schiemann, R., Liniger, M.A., Frei, C., 2010: Reduced space optimal interpolation of daily rain gauge precipitation in Switzerland. *J. Geophys. Res.* 115, D14109.
- Stein, M. L., 1999: Interpolation of spatial data: Some theory for kriging. In *Springer Series in Statistics*. New York, Berlin; Springer.
- Thornes, J.E., 2005: Special Issue on the use of GIS in Climatology and Meteorology. *Meteorol. Appl.* 12, i-iii.
- Tveito, O.E., Wegenhenke, M., van der Wel, F., Dobesch, H., 2008: The use of geographic information systems in climatology and meteorology. *Office for Official Publications of the European Communities*, 245 pp.
- Ustrnul, Z., 2006: Spatial differentiation of air temperature in Poland using circulation types and GIS. *Int. J. Climatol.* 26, 1529-1546.
- Ustrnul, Z. and Czekierda, D., 2005: Application of GIS for the development of climatological air temperature maps: an example from Poland. *Meteorol. Appl.* 12, 43-50.
- Vicente-Serrano, S.M., López-Moreno, J.I., Vega-Rodríguez, M.I., Beguería, S., Cuadrat, J.M., 2010: Comparison of regression techniques for mapping fog frequency: application to the Aragón region (northeast Spain). *Int. J. Climatol.* 30, 935-945.
- Wei, G.-Q., 1998: Three-dimensional reconstruction by radial basis function networks: Shape from shading and stereo vision. Munich, Dissertation.
- Wilks, D.S., 2006: *Statistical Methods in the Atmospheric Sciences*. 2. Ed. Elsevier, Academic Press.



# IDŐJÁRÁS

*Quarterly Journal of the Hungarian Meteorological Service  
Vol. 115, No. 1–2, January–June 2011, pp. 51–70*

## **Time variation of the effect of geographical factors on spatial distribution of summer precipitation over the Czech Republic**

**Jacques Célestin Moliba Bankanza**

*Institute of Atmospheric Physics,  
Boční II 1401, 141 31 Prague, Czech Republic; E-mail: moliba@ufa.cas.cz*

*(Manuscript received in final form March 26, 2011)*

**Abstract**—This study deals with modeling of spatial distribution of summer (JJA) precipitation over the Czech Republic. The aim is to analyze the time variation of the relationships between geographical factors and precipitation during summer. Various candidates geographical predictors are evaluated in the stepwise regression models for summer precipitation, namely: (1) a set of omnidirectional parameters of the elevation that characterize an area of  $3 \times 3$  km around meteorological stations, (2) various cross products calculated on the basis of geographical coordinates and elevation or topographic parameters, (3) slope and four facets of slope aspect characterizing the orographic regimes in the Czech Republic, (4) land cover parameters describing an area of  $10 \times 10$  km around meteorological stations, and (5) geographical coordinates. The orographic parameters are derived from the 1 km resolution digital elevation model (DEM); the land cover parameters are derived from the 1 km resolution CORINE (COoRdination of INformation on the Environment) land cover data. Daily precipitation data for the period 1971–2003 have been used. The precipitations were collected from 203 stations throughout the country. Stepwise regression models of summer precipitation are generated for each year, and each overlapping decade from 1971 to 2003. To ensure the stability of the regression equations and comparability of regression models in time, similar suitable and stable independent variables in time should be selected. Therefore, orthogonally rotated principal component analysis (PCA) and frequency of significant predictors entering models are used to select them. Multivariate regression precipitation models are generated using definitive (PCA or stepwise based) selected predictors. Ten independent geographical variables have been selected as the most important predictors for precipitation regression models. They consist of latitude, longitude, slope aspect of the grid westward from the central grid, slope aspect of the grid northward from the central grid, slope of the grid northeastward from the central grid, slope of the grid eastward from the central grid, slope of the grid northward from the central grid, maximum value of elevation (percentile 95%) of northwestern grid from the central grid, minimum value of elevation (percentile 5%) of the central grid, and vegetation. The relationships between these significant predictors and precipitation are stable in time. No significant trend in regression coefficients has been found during 1971–2003.

*Key-words:* multivariate regression, precipitation models, summer precipitation, geographic influence, environmental variables, temporal variability, Czech Republic

## ***1. Introduction***

Precipitation is a climatic variable that has a high spatial and temporal variability. Its spatial distribution is influenced by various factors such as terrain height, slope, etc. For mapping purposes, it is practical to estimate the effect of such factors on precipitation distribution. Spatial modeling is a suitable tool that allows to explore the relationship between the target variable and predictors, and to get continuous information on precipitation over a targeted area. Many studies have been undertaken recently to assess and model the relationship between the climatic variables, and independent factors. Several geographical variables, including land cover (*Joly et al.*, 2003), proximity to the water bodies (*Weisse and Bois*, 2001; *Vicente-Serrano et al.*, 2003; *Marquinez et al.*, 2003; *Daly et al.* 2002), atmospheric circulation (*Johnson and Hanson*, 1995; *Basher and Zheng*, 1998; *Courault and Monestiez*, 1999), and topography (*Johnson and Hanson*, 1995; *Goodale et al.*, 1998; *Daly et al.*, 2002) have been frequently used as relevant independent variables to model spatial patterns of precipitation. The latter has a significant influence on spatial variability of precipitation (*Joly et al.*, 2003; *Weisse and Bois*, 2001, etc.). Therefore, numbers of these studies have been focused on modeling the influence of topographic features on the spatial variability of climate variables (*Prudhomme and Reed*, 1999; *Johnson and Hanson*, 1995; *Drogue et al.*, 2002; *Weisse and Bois*, 2001; *Diodatto*, 2005, etc.).

According to its geographical position in Central Europe, the Czech Republic is subject to both oceanic and continental influences. Topographically, the inner part of the country is dominated by lowlands and surrounded by highlands. Such topographic feature contributes to modifying airflow over the country and can induce a strong convective precipitation, especially in the mountains (Moravsko-slezské Beskydy, Jeseníky, Krkonoš, Jizerské hory, and Krušné hory). Extreme precipitation events are more frequent and intense over these highlands due, among other factors, to the influence of exposition to airflow (*Kakos*, 2001).

In this study, the relationships between geographical factors and summer precipitation are examined through a stepwise regression model. Summer precipitation is analyzed instead of other seasons for several reasons. First, the annual cycle of precipitation in the Czech Republic is characterized by a tendency for maximum rainfall during summer. Therefore, summer precipitation contributes significantly on the character of the precipitation fluctuation (*Tolasz et al.*, 2007). Second, summer precipitation, usually of shorter duration and greater intensity (*Tolasz et al.*, 2007), is characterized by the high frequency of occurrence of extreme precipitation events (*Kaspar and Muller*, 2008), which

are often connected with several natural hazards including hydrological flood and soil erosion. The need of precipitation information during summer time is crucial for the risk management. Moreover, spatial models examine spatial dependence of climate variables using a single time realization of the variable, i.e., they widely use the mean values for a given period, as input. However, the performance of a model depends not only on the density of the station network and the choice of methods, but also on the temporal variability (*Hulme et al., 1997*). Therefore, the choice of the period of study can bias the results of interpolation (*Hulme et al., 1997*). The spatial variability of environmental variables is commonly a result of complex processes working at the same time and over long periods of time, rather than an effect of a single realization of a single factor (*Hengl, 2007*). Geostatistics are less powerful than the statistical climatology based on sample in time, because they are based on single realization in time (*Szentimrey and Bihari, 2007*). The temporal variability seems to be an important task in modeling spatial variation of climate variables. This aspect has received substantial attention in several studies: *Basher and Zheng* (1998) take into account seasonal behavior of precipitation (ENSO variations) for mapping precipitation patterns of a data-sparse tropical southwest Pacific Ocean region. *Brown and Comrie* (2002) created the 39-year time series of maps and datasets of winter temperature and precipitation for the southwest US by comparing 30 years (1961–1990) modeled means with 39 observed winter temperature and precipitation values. *Johnson and Hanson* (1995) modeled the relative contribution of topographical and meteorological variability to regional precipitation variability. In order to improve interpolation of spatially generated weather data, *Baigorria et al.* (2007) analyzed changes in spatial correlations and compared spatial correlation on daily and monthly basis. Therefore, using seasonal rainfall amounts, temporal analysis is needed to find and determine: (1) how the relationships between independent variables and precipitation vary within years and decades; (2) how the model is affected by temporal changes. The aims of this study are: (1) to model spatial pattern of summer (JJA) precipitation in the Czech Republic at year and ten-year time steps from 1971 to 2003 using geographical variables *as independent variables*; (2) to analyze the time variation of the relationships between geographic variables, and the summer precipitation during 1971–2003.

## 2. Datasets

### *Digital Elevation Models (DEM)*

DEM with the resolutions of 100 m and 1 km have been used. The fine spatial resolution of topographic and elevation variables have been retained in this study, because large-scale topographic features at a resolution of 1–15 km yield

a high correlation with precipitation (Daly *et al.*, 1994; Daly, 2006). The 100 m DEM resolution data have been used to calculate the following smoothed elevation parameters: (1) the upper (percentile 95%) and (2) lower (percentile 5%) percentiles of elevation for a grid of 1 km resolution, and (3) mean elevation for each grid with  $1 \times 1$  km resolution. On the other hand, slope, and slope aspect are obtained directly from the 1 km resolution DEM data.

### *Land cover data*

Land cover data are obtained from the CORINE (COoRdinate INformation on the Environment) land cover dataset. These data are available in the following link: <http://www.dataservice.eea.europa.eu/dataservice>. They describe the land cover units in Europe. According to the CORINE land cover classification, four main types of landscape characterizing the Czech Republic were identified, and used as candidate geographical independent variables. They are related to vegetation, agricultural area, water bodies, and artificial areas.

### *Precipitation data*

Daily precipitation data for the period 1971–2003 have been used. The dataset consists of 203 stations distributed over the whole country (Fig. 1). Meteorological stations are unevenly distributed across these different land cover units and topographic patterns. Most of them are distributed across urban (towns, small cities, villages) and agricultural areas. Only few stations are located in vegetation-covered areas. Considering ground elevation, about 80% of meteorological stations are located below 600 m. Only 12% of them are located above 600 m on the highlands or mountainous regions that have a significant influence on precipitation distribution (Table 1). The lack of observation in forested and mountainous areas shows how much it is important to model the relationships between rainfall, and elevation and/or other geographical variables.

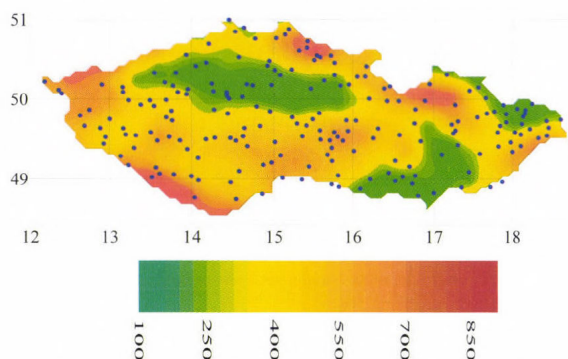


*Fig. 1.* Spatial distribution of meteorological stations with regard to DEM data (in m). Dots represent geographic position of meteorological stations.

Table 1. Elevation of meteorological stations

Elevation (m)	Number of stations	% of total area
< 200	12	6
200–400	85	42
400–600	82	40
> 600	24	12

In order to perform time variation analysis (see Section 4), two subsets of summer precipitation series are derived from the summer precipitation dataset: (I) yearly summer precipitation amounts and (II) the overlapping decade precipitation mean, with a shift of one year from 1971–1980 to 1994–2003. The lengths of both subsets of summer precipitation series are 33 and 24, respectively.

### 3. Methods: model development

#### 3.1. Independent variables

Spatial fields of precipitation are correlated with many environmental or geographic factors especially elevation and geographic coordinates. In this study, 54 candidate independent variables, which can explain spatial variability in the climate data, have been evaluated, and then selected (Table 2). A large number of geographical variables are evaluated, because none is a priori the most important. They are related to:

- Omnidirectional variables describing elevation (27 variables), topographic features (slope and slope aspect: 13 variables). Those morphotopographic variables represent the values from the grids omnidirectionally oriented around central grids. The central grids can be defined as grids in which stations are located. Eight directions around the central grid have been defined as: (1) north, (2) east, (3) south, (4) west, (5) north-east, (6) south-east, (7) south-west, and (8) northwest.
- Cross products involving (eight variables): (a) geographical coordinates and elevation variables (maximum: percentile 95%, minimum: percentile 5%, and average elevation to north and east) and (b) geographical coordinates and topographic features (slope). Cross products were calculated (as indicated in Table 2) to obtain west-east or south-north gradient of elevation and topography (Brown and Comrie, 2002; Vicente-Serrano *et al.*, 2003).
- Land cover parameters were selected from a grid data with spatial resolution of 1 km resolution. An area of 10×10 km around meteorological stations was delimited and four indexes (Iwat, Iveg, Iagr, Iurb) characterizing the main units of landscapes (water bodies,

vegetation cover, agricultural area, and urban and artificial area) in this area were calculated. Indexes are calculated as a ratio (%) of the area covered by land cover units to the total area (grid) of 10 × 10 km resolution.

- Geographic coordinates: latitude (Lat) and longitude (Long).

*Table 2.* Candidate independent variables for stepwise regression models. They are related to the Elevation variables, topographic variables (slope and slope aspect), cross products involving geographical position and morpho-topographic variables (elevation and topographic variables), geographical coordinates, and land use or cover variables. Abbreviations Emax, Emin, Eavg are related to maximum, minimum, and average elevation. Slope is related to slope values in %, while Oreg abbreviates slope aspect. The numbers after letters indicate orientation of grid from which slope or elevation values have been taken out, inside a bound of 3 × 3 km around the central grid. Central grid is defined as a grid in which meteorological stations are located. For elevation and slope eight directions have been defined (see section 3.1), while for slope aspect 4 have been taken into account (1 for east, 2 for west, 3 for north, and 4 for south). Abbreviations ending with “-grad” are related to cross product involving longitude (with number 1 on the end of letters) or latitude (with number 2 on the end of letters) and elevation variables (Egrad, Exgrad, Engrad) or slope (Sgrad). Iagr, Iveg, Iurb, and Iwat abbreviate four Indexes of landscape units (agriculture, vegetation, urban area, water bodies)

Candidate independent variables	Abbreviations	Candidate independent variables	Abbreviations
Central grid average elevation	Eavg0	Central grid slope values	Slope0
Central grid minimum elevation (percentile 5%)	Emin0	Slope in the north	Slope1
Central grid maximum elevation (percentile 95%)	Emax0	Slope in the east grid	Slope2
Average elevation in the north from the central grid	Eavg1	Slope in the south	Slope3
Minimum elevation (percentile 5%) in the north	Emin1	Slope in the west	Slope4
Maximum elevation (percentile 95%) in the north	Emax1	Slope in the north-east	Slope5
Average elevation in the east from the central grid	Eavg2	Slope in the south-east	Slope6
Minimum elevation (percentile 5%) in the east	Emin2	Slope in the south-west	Slope7
Maximum elevation (percentile 95%) in the east	Emax2	Slope in the north-west	Slope8
Average elevation in the south from the central grid	Eavg3	Slope facet east	Oreg1
Minimum elevation (percentile 5%) in the south	Emin3	Slope facet west	Oreg2
Maximum elevation (percentile 95%) in the south	Emax3	Slope facet north	Oreg3
Average elevation in the west from the central grid	Eavg4	Slope facet south	Oreg4
Minimum elevation (percentile 5%) in the west	Emin4	Cross product Long × average elevation	Egrad1
Maximum elevation (percentile 95%) in the west	Emax4	Cross product Lat × average elevation	Egrad2
Average elevation in the north-east from the central grid	Eavg5	Cross product Long × slope	Sgrad1
Minimum elevation (percentile 5%) in the north-east	Emin5	Cross product Lat × slope	Sgrad2
Maximum elevation (percentile 95%) in the north-east	Emax5	Cross product Long × 95% percentile of elevation	Exgrad1
Average elevation in the south-east from the central grid	Eavg6	Cross product Long × 5% percentile of elevation	Engrad1
Minimum elevation (percentile 5%) in the south-east	Emin6	Cross product Lat × 95% percentile of elevation	Exgrad2
Maximum elevation (percentile 95%) in the south-east	Emax6	Cross product Lat × 5% percentile of elevation	Engrad2
Average elevation in the south-west from the central grid	Eavg7	Index for the ratio of Agricultural area	Iagr
Minimum elevation (percentile 5%) in the south-west	Emin7	Index for the ratio of the Vegetation covered area	Iveg
Maximum elevation (percentile 95%) in the south-west	Emax7	Index for the ratio of Urban area	Iurb
Average elevation in the north-west from the central grid	Eavg8	Index for the ratio of the Water bodies	Iwat
Minimum elevation (percentile 5%) in the north-west	Emin8	Longitude	Long
Maximum elevation (percentile 95%) in the north-west	Emax8	Latitude	Lat

### 3.2. Selection of suitable predictors for regression model and temporal analysis

Analysis of time variation of relationship between precipitation and geographical factors mentioned in *Table 2* was the objective of this study. Relationships are analyzed through regression models that are performed at various time steps. In order to assure stability of the regression equations and comparability of models in time, it was necessary to select similar suitable and stable independent variables. Selection of suitable independent variables was based on two approaches: stepwise-based approach (STW), and principal component analysis (PCA)-based approach, both for yearly-based precipitation models (STW I/PCA I) and overlapping decade-based precipitation models (STW II/PCA II).

#### 3.2.1. Stepwise regression based models (STW)

Stepwise selection of suitable predictors has been made in two steps. At the first step, the significant candidate independent variables have been selected for each model at various time steps. At the second step, only the most frequently selected significant predictors have been taken into account.

- (a) It is important to remind that the set of geographical variables used as predictors (*Table 2*), particularly topographic and elevation parameters, are collinear. The choice of suitable predictors from this set has a significant influence on the behavior of models. Hence, forward stepwise linear regression was used to model summer precipitation as function of the collinear geographical factors at time steps of annual (STW I) and overlapping decades (STW II) from 1971–2003. All predictors mentioned in *Table 2* are used. A p-value of 0.05 has been used to force out of the model any non-significant effects, and to select significant, and non-collinear independent variables. Stepwise regression has been used in many studies (*Ninyerola et al.*, 2000, 2007; *Marquinez et al.*, 2003; *Vicente-Serrano et al.*, 2007) as an accurate method in examining relations between precipitation and collinear independent variables.
- (b) On the second step, the most frequently selected significant predictors by both STW I and STW II-based models was considered. A threshold frequency value of 20–40% was defined to select them. Geographical variables of which frequency value does not reach at least 20% are considered as improper for temporal analysis, and are discarded; while independent variables exceeding the defined threshold are retained. If the retained variables are collinear, the operation is repeated (using a higher threshold value, i.e., 30–40%) until no co-linearity is found among them. Using this procedure, six predictors have been retained for both STW I and STW II-based precipitation models (see *Table 3* and *Figs. 2* and *3*). For the STW I-based models, the selection was ended at the first step, where frequency of significant independent variables exceeded 30%. However, for the STW II-based models, 11

collinear predictors have been selected at the first step (Fig. 3a). The operation was repeated for the 11 predictors to select a final series of six non-collinear predictors exceeding 40% (Fig. 3b).

Table 3. Definitive selected independent variables for all models

I. Year by year time series			II. Moving long-term precipitation mean		
Models					
STW I	PCA-A I	PCA-B I	STW II	PCA-A II	PCA-B II
Slope2	PCI	Emin0	Slope2	PCI	Emin0
Slope5	PCII	Slope1	Slope5	PCII	Slope1
Emax8	PCIII	Vegetation	Emin8	PCIII	Vegetation
Lon	Lon	Lon	Lon	Lon	Lon
Lat	Lat	Lat	Lat	Lat	Lat
Oreg2	Oreg2	Oreg2	Oreg2	Oreg2	Oreg2
–	–	–	–	Oreg3	Oreg3

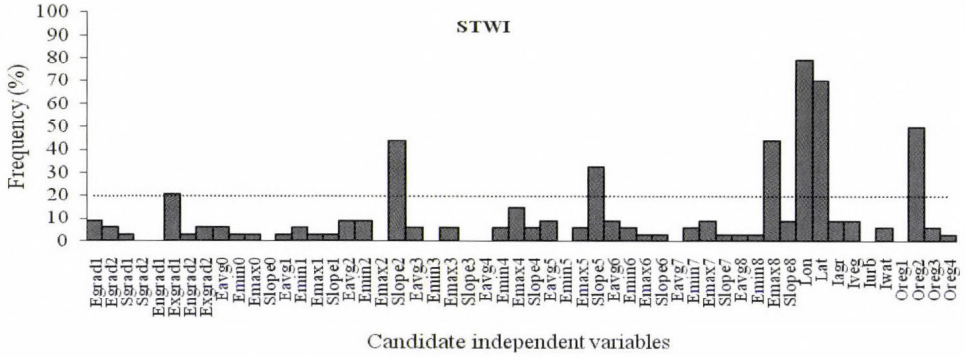


Fig. 2. Frequency of significant variables entering models for STWI-based models.

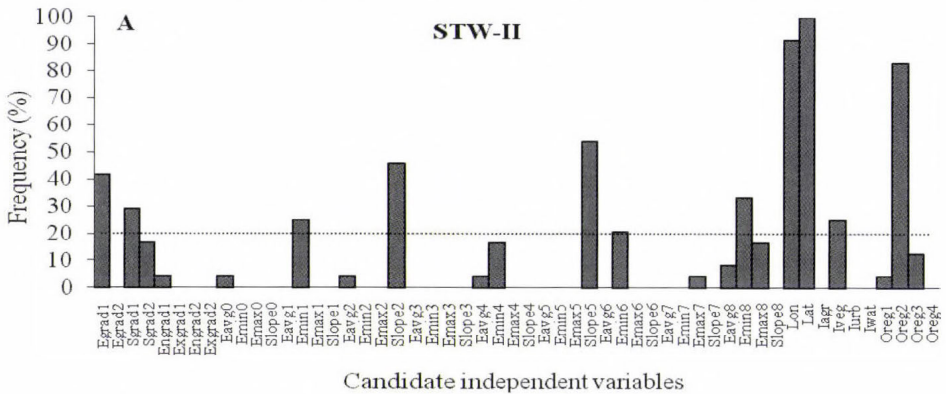


Fig. 3a. Frequency of significant independent variables for STW II-based models. Dotted line represents the threshold value for selecting more frequent predictors. First step (A) of selection.

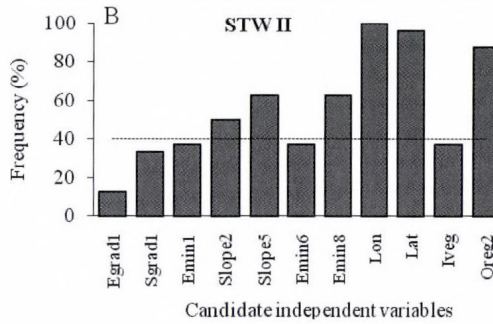


Fig. 3b. Frequency of significant independent variables for STW II-based models. Dotted line represents the threshold value for selecting more frequent predictors. Second step (B) of selection.

### 3.2.2. PCA – based models (PCA)

Principal component analysis (PCA) has been used to eliminate random variability in independent factors, and to generate stable models in time. The sets of independent variables have been checked for correlation before performing PCA. Eight independent variables, which were less correlated or uncorrelated with other independent variables, were discarded for the PCA. They were: geographical coordinates (longitude and latitude), two units of land cover (urban area and water bodies), and four orographic facets (slope aspect). PCA was performed for the remaining 46 variables. The number of principal components (PCs) to retain for rotation was given using screen test. Three PCs have been retained. They are related to: (1) characteristics of elevation, (2) topographic features, (3) land use and land cover parameters: agricultural and vegetation covers. The three PCs explain about 90.3% of total variability. Morpho-topographic variables that have the highest loadings with those retained PCs were then selected. For the further regression models, both PCs scores (three variables), and independent variables (three morpho-topographic variables), that were selected assuming highest loading, were considered as candidate independent variables. These candidate predictors selected using PCA were recombined with the 8 discarded variables before performing PCA. Then the stepwise regression has been performed to select significant and noncollinear variables. The frequencies of variables (Fig. 4) have been analyzed (considered as in Section 3.2.1.b). The frequent variables have been considered as stable and, therefore, suitable for multivariate regression model. This approach helped to avoid the problem encountered during interpretation of the PCs that involve independent uncorrelated variables. The final selected independent variables are shown in Table 3. Using this approach, six significant independent variables were selected for yearly-based precipitation models (PCA I) and seven independent

variables were selected for decade-based precipitation models (PCA II) (see Table 3). PCs scores (PCA-A) or selected variables assuming the highest loadings (PCA-B) have been used to compare their effect on the models. Table 3 shows important geographical variables that influence significantly the spatial patterns of precipitation in the Czech Republic. All approaches selected the geographical coordinates (including continentality) and the westward slope aspect.

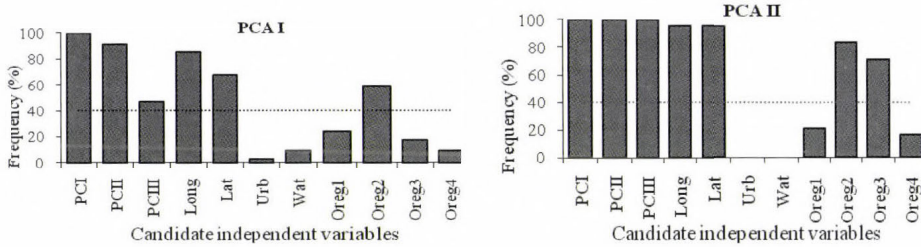


Fig. 4. Frequency of significant variables entering models for PCA I and II-based models. Dotted lines represent the threshold value for selecting more frequent predictors.

### 3.3. Regression models and trend detection

Once stable significant variables were selected, multivariate regression precipitation models were then performed using them as predictors. The multiple regression relationship is obtained through the following equations:

$$\begin{cases} P_{est}(t_1) = b_0 + b_1(x_1) + \dots + b_n(x_n) \\ P_{est}(t_2) = b_0 + b_1(x_1) + \dots + b_n(x_n) \\ \dots \\ P_{est}(t_n) = b_0 + b_1(x_1) + \dots + b_n(x_n) \end{cases}, \quad (1)$$

where  $b_{1-n}$  is the multiple regression coefficient adjusted for each retained independent variable  $x_n$ ;  $P_{est}$  represents the predicted rainfall, and  $t_{1-n}$  is the time step (i.e., year or decade).

In order to carry out temporal analysis of the relationship between significant geographical factors and precipitation, time series of regression coefficients from each time resolution and approaches-based models were built. The linear trend in those series was estimated using a least-squares regression. The significance of trends was determined using the confidence interval (CI) given by the following equation:

$$CI = t \pm \frac{2.042 \cdot \sigma_e}{\sqrt{n} \cdot \sqrt{\sigma_x^2}}, \quad (2)$$

where  $t$  is the trend value,  $n$  is the length of the time series of the regression coefficients,  $\sigma e$  is the standard deviation of the residuals, and  $\sigma x$  is the standard deviation of the independent variable.

## 4. Results

### 4.1. Model performance

Several standard statistical measures of models performance and accuracy were calculated. The goodness of fit of the model and the proportion of the variation of summer precipitation explained by the model are measured by the coefficient determination ( $R^2$ ). The magnitude and sign of errors of the regression model are given by mean absolute error (MAE) and root mean square error (RMSE).

The time variation of the coefficients of determination for all approaches and time resolution-based precipitation models is displayed in Fig. 5. The magnitude of errors is measured by the rootmeansquare error (Fig. 6) and mean absolute error (Fig. 7).

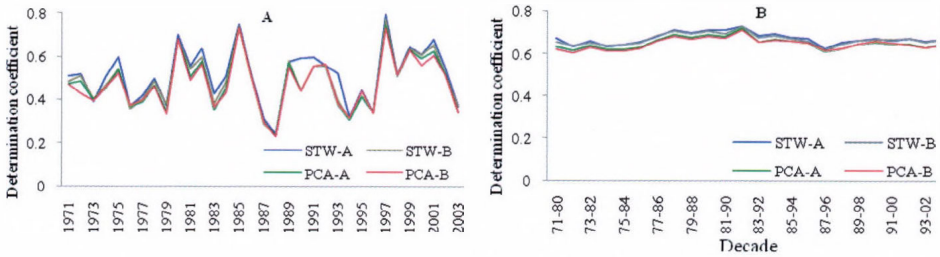


Fig. 5. Time variation of determination coefficients of STW and PCA-based models for year (A) and decade (B) time resolution.

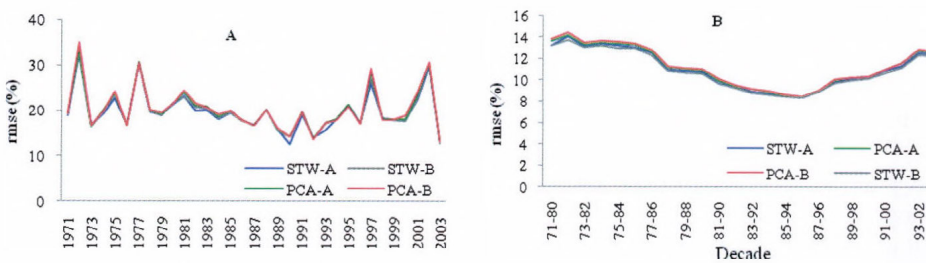


Fig. 6. Time variation of the root-mean-square errors of STW and PCA-based models for year (A) and decade (B) time resolution.

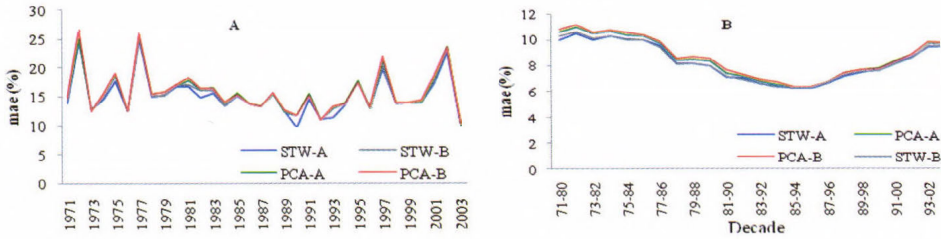


Fig. 7. Time variation of the mean absolute errors of STW and PCA-based models for year (A) and decade (B) time resolution.

The coefficients of determination and errors for model based on different approaches vary consistently in time, whereas their time variations are inconsistent for time resolution-based models. In fact, the STW-based models are more efficient than PCA-based models. Nevertheless, the difference between both approaches-based models is minor. Model accuracy varies widely among models generated at various time resolutions. Models based on long-term time resolution are more accurate and explain more variation than those based on shorter time resolution. An important variability in summer precipitation ( $> 0.61$  for both approaches-based models) is consistently captured by ten-year models for both PCA and STW-based approaches. The magnitude of errors (RMSE, MAE) does not reach 15% (37 mm) of summer precipitation for ten-year models. On the contrary, terrain influences did not always account for an important variability of summer precipitation for the annual precipitation models. The coefficients of determination of these models describe an important inter-annual variability; they vary from 0.23 (1988) to 0.7 (1997). Similarly, the magnitude of errors is fluctuant. The larger (35% – 86 mm) and the smaller RMS errors (13% – 32 mm) have occurred in 1972 and 2003, respectively. Unlike other years, where model errors are inversely proportional to the explained variance, both variance explained and error yielded by the models are large in 1997 and 2002.

Several models were unable to capture more than 50% of variability in precipitation and to generate small error. Considering that a good precipitation model must capture at least 50% of precipitation variability (Ninyerola *et al.*, 2000) and yield very small prediction error, we can conclude that numbers of these models failed. The temporal variability of summer precipitation combined with the ability of the set of predictors to capture variation in data can explain it. Fig. 8 displays the relationships between rainfall departure (from the long-term precipitation average) and coefficient of determination. It reveals that the stronger the negative rainfall anomalies for a given year, the smaller the variation explained in precipitation data. Indeed, the coefficients of determination fall under 0.5 or rarely (once) overtake this value during dry years. Therefore, additional predictors (different from the used set of predictors) or additional analysis on removing temporal variability were needed to improve models. If it is necessary

to add other auxiliary variables, then it should be important to consider that not only geographical factors but also other factors such as atmospheric circulation affect the spatial distribution of precipitation. However, their mechanisms are more complex and not easy to evaluate their statistical relationships.

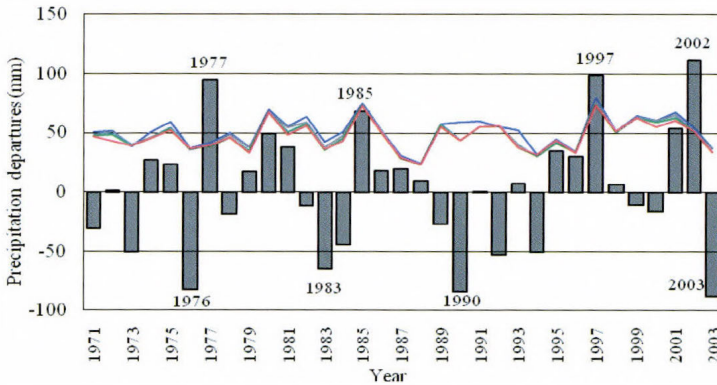


Fig. 8. Comparison of determination coefficients (color lines) with precipitation departures (histogram).

#### 4.2. Time variation of effect of significant geographical factors

The relationships between summer precipitation and geographic variables, selected using STW approach and PCA, have been examined through regression model. Resulting coefficients of regression for each approach and time resolution-based model are plotted in Figs. 9–12. Six independent variables have been selected using STW approach: slopes of grids eastward and northeastward from the locations, maximum elevation northwestward from locations, geographic coordinates (longitude and latitude), and slope aspect westward.

At the annual time resolution, spatial patterns of summer precipitation show an increase of precipitation with a growing value of elevation and slope aspect. However, they show an increase and a decrease of precipitation to increasing latitude, longitude, and slope. Considering the inter-annual variability of the relationships between precipitation and each significant geographical variable, it can be pointed out in some extreme cases of strong relationships. They are found between precipitation and elevation (emax8), latitude, slope (slope5), and slope aspect (oreg2), respectively, during 1980, 2002, 1997, and 1972. The precipitation models based on STW approach reveal that the spatial pattern of precipitation during the heavy precipitation events of 1997 and 2002 were strongly related to the slope northeastward and latitude, respectively. The fields of intense precipitation during such years have a significant influence on the spatial pattern of precipitation across the whole country. For example, the

decrease of precipitation with an increasing longitude during 1997 is mainly due to the fields of intense precipitation in the northeastern part of the country. Spatial patterns of summer precipitation and precipitation amount fluctuate in time according to different factors such as atmospheric conditions.

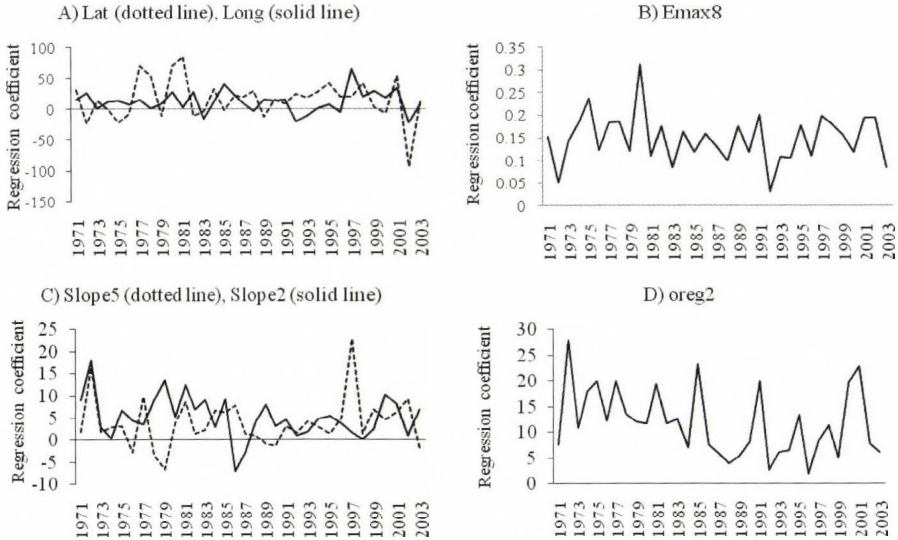


Fig. 9. Time variation of the regression coefficients of significant predictors (as indicated in A, B, C, D) for STW I-based models.

During the whole period under study, the precipitations have had a positive relationship with elevation variables. The well-known effect of elevation on the spatial pattern of summer precipitation, which is related to an increase of precipitation with growing elevation, is observed along the entire period. The highlands are seemingly rainier during summer than lowlands all over the country. However, during some years (1976, 1986, 2003, etc.) spatial pattern of precipitation is characterized by a decrease of rainfall with a growing value of slope (slope2, slope5). Thus, if multiple factors of mountain regions are taken into account, their relationships with precipitation become more complex than a simple increase with growing elevation. During the period 1971–2003, the precipitations increased strongly in 1980 and slightly in 1992 with maximum elevation northwestward from the locations. The slope orientated eastward from the locations has influenced considerably the summer precipitation during 1972.

For the decade-based models, minimum elevation northwestward (Emin8) has been selected as predictor instead of Emax8. Unlike the yearly-based models, no geographical variable was related to any decreases of summer precipitation. Although the effect of minimum elevation (Emin8) on precipitation is less variable in time, the influences of the topographic and geographical position

fluctuate largely in time. The variation of the effect of topographic features (slope5, slope2, and oreg2) shows two peaks at the beginning and at the end of the period under study. The influence falls in the middle of this study period (i.e., during 1981–1997). This can be related to drought that occurred in the Czech Republic in this period (Kaspar and Muller, 2008).

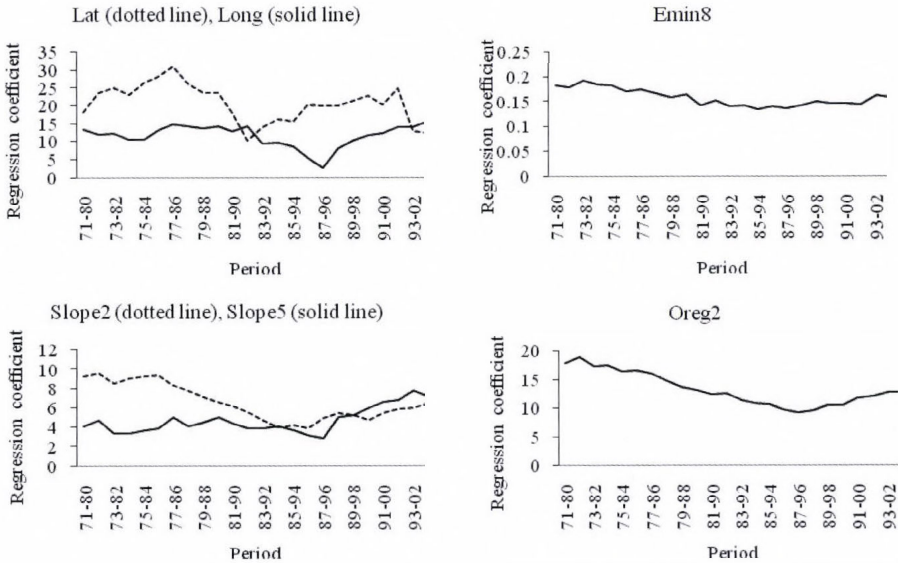


Fig. 10. Time variation of the regression coefficients of the significant predictors for STW II-based models.

Time variation of the relationships between spatial patterns of summer precipitation and significant geographical variables selected using PCA-based approach has been also analyzed (Figs. 11 and 12). New variables were selected using the loading of the components: slope northward from the locations (Slope1), vegetation (Veg), and minimum elevation at the locations. An additional geographical variable was specifically selected for the ten-year models: slope aspect oriented northward. These additional predictors influence the spatial patterns of precipitation as well. They are related to the increase of precipitation, except the vegetation during some years (1984, 1992, and 2002). A strong relationship with precipitation is observed during 1972 for slope2 and in 1995, 2002 for the vegetation.

The PCA-based models show an increase of summer precipitation for the two PCs scores during the period considered by this study (Figs. 11 and 12). In particular, spatial patterns of summer precipitation in 1972 and 1980 have been related to PC1 and PC2, respectively. Similarly to STW-based models, PCA-based models reveal that spatial distribution of precipitation during the summer

of 1997 is related to topographic features and geographical coordinates, while spatial distribution of summer precipitation in 2002 is influenced by urban effect, elevation, and especially latitude.

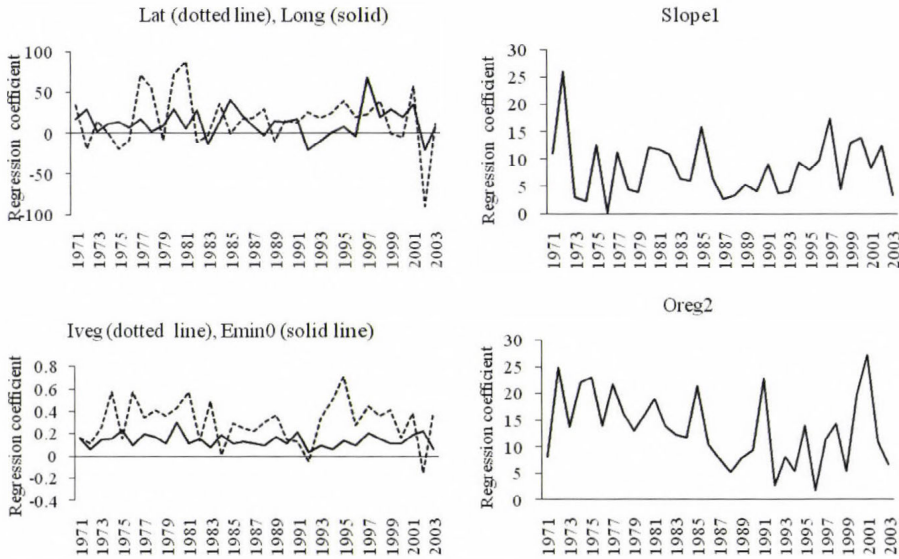


Fig. 11. Time variation of the regression coefficients of the significant predictors for PCA I-based models.

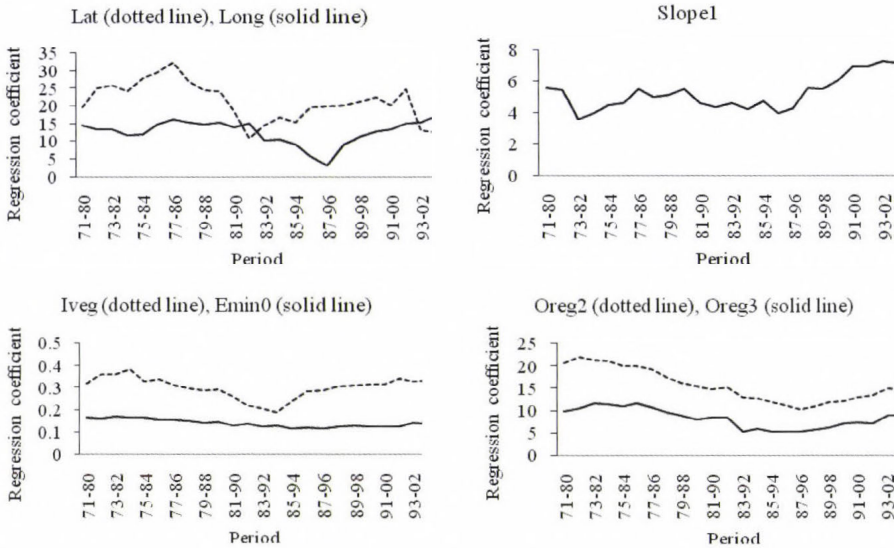


Fig. 12. Time variation of the regression coefficients of the significant predictors for PCA II-based models.

The extremeness of precipitation during the summer of 1997, especially during the two heavy precipitation episodes in July, is associated with the atmospheric advection of moist air stream (Rezacova et al., 2005). Meteorological features were specifically characterized by an intensive influx of moisture into Central Europe and intensive upward motions in the precipitation area. Finally, the regression coefficients of precipitation models reveal that topographic feature and geographic coordinates have stronger influence on spatial distribution of summer precipitation over the Czech Republic than other geographical factors.

#### 4.3. Trends in coefficients of regression of significant predictors

The trends in regression coefficients for the yearly-based models during the period 1971–2003 are displayed in Fig. 13 (a,b,c). It is obvious that the trends in regression coefficients are negative for almost all selected independent variables. The only exception concerns the slope of grids northeastward from the locations, which has positive trend. The magnitude of the trends is higher for latitude and west slope (reaching  $-0.37 \text{ yr}^{-1}$  and  $-0.23 \text{ yr}^{-1}$ ) than for other independent variables, especially elevation, vegetation, and longitude. The sign and magnitude of trends are similar for the same predictors independently selected from different model-based approaches. The positive and negative trends detected are insignificant. Therefore, the relationships between the spatial patterns of summer precipitation and geographical variables, during the relatively short period considered in this study, are stable in time.

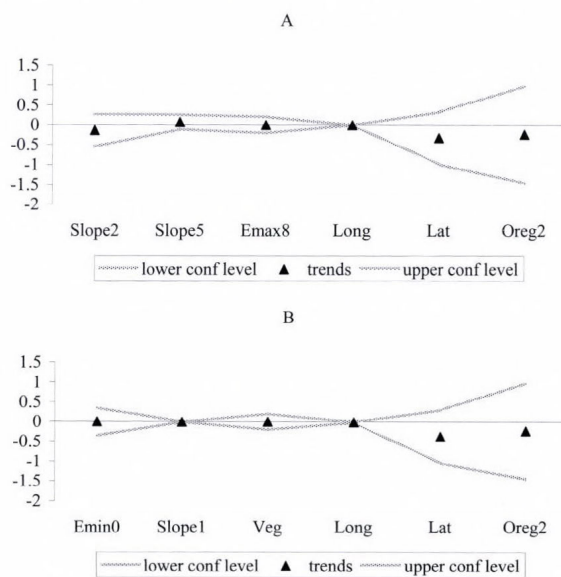


Fig. 13a,b. Trends in coefficient of regression estimated by STW-based (A) and PCA-B (B) precipitation models. Models are generated at the annual time step.

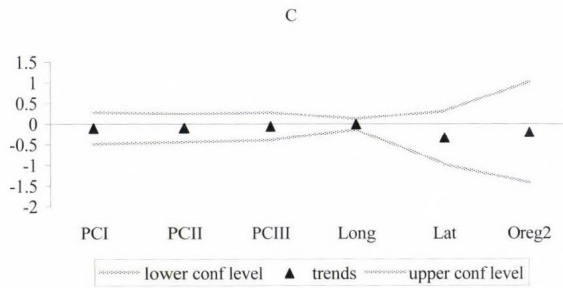


Fig. 13c. Trends in coefficient of regression estimated by PCA A-based precipitation models. Models are generated at the annual time step.

## 5. Conclusions

Relationships between geographical variables (land cover, geographical positions, morpho-topographical features) and rainfall spatial pattern were analyzed in this study using regression models. Stepwise regression and rotated PCA identified several significant geographical variables: slope2, slope5, emax8, emin0, vegetation, oreg3, oreg2, and geographical coordinates. Geographical coordinates (including continentality) and slope orientation westward are the most significant predictors for modeling the spatial distribution of summer precipitation over the Czech Republic. Except the minimum elevation (Emin0), all important topographical factors correspond to the outside grids at the distance of 1 km from the location. Therefore, the terrain characteristics had more significant influence when a larger area than a station location is taken into account for selecting independent variables. Similarly, the models working with independent variables selected from stations are slightly inaccurate in comparison with models working with independent geographical variables describing a large area around the location. Furthermore, PCA and STW-based approaches for selecting significant geographical variables to model spatial patterns of precipitation over the Czech Republic are consistent. Nevertheless, PCA-based models seem to be less powerful than STW-based models. They yield a small explained variance and a large prediction error. In the same way, models based on a one-year time resolution are notably less powerful than models based on long-term time resolution.

The time variation of explained variance indicated that precipitation variability has an influence on the variance accounted by models and on its performance. Thus, smaller explained variance is accounted by models during dry years. A temporal analysis of regression coefficients from ten-year precipitation models showed positive relationships between precipitation and geographical factors. Spatial patterns of averaged summer precipitation at a decade time resolution are modeled as increasing with continentality, morpho-topographic

features, and latitude. On the other side, at the smaller time-resolution, negative relationships were found, especially between precipitation and topographical features, vegetation, and geographical positions. The spatial pattern of precipitation during the summer of 2002, for example, is strongly related to decreasing latitude.

Trend analysis of regression coefficients revealed that relationships between summer precipitation patterns and morpho-topographical features, land cover, and geographical positions are stable in time. No significant trend in the model parameters (effect of geographical factors) has been found during 1971–2003. Model parameters are stable in time. Therefore, spatial prediction of precipitation based on single realization in time (i.e., long term average) is not biased by the length of the sample period.

Spatial precipitation patterns vary in time according to the effect of geographical factors, as well as performance of models. The models failed to capture the relationships between the precipitation patterns and the geographical factors during dry years, namely 1987 and 1988. These years have been dominated by intensive drought (Kaspar and Muller, 2008). Precipitation patterns during these years could be well modeled using other auxiliary independent variables such as the dominant mode of atmospheric circulation that are linked with both spatial and temporal variability of precipitation. Although this was not the aim of this analysis, the conclusions of this study show the necessity to investigate further on the relationships between precipitation pattern and atmospheric circulation.

## References

- Baigorria, G.A., Jone, J.W. and O'Brien, J.J., 2007: Understanding rainfall spatial variability in southeast USA at different timescales. *Int. J. Climatol.* 27, 749-760.
- Basher, R.E., Zheng, X., 1998: Mapping rainfall fields and their ENSO variation in data-sparse tropical south-west Pacific Ocean region. *Int. J. Climatol.* 18, 237-251.
- Brown, D.P., Comrie, A.C., 2002: Spatial modeling of winter temperature and precipitation in Arizona and New Mexico, USA. *Clim. Res.* 22, 115-128.
- Courault, D., Monestiez, P., 1999: Spatial interpolation of air temperature according to atmospheric circulation patterns in southeast France. *Int. J. Climatol.* 19, 365-378.
- Daly, C., 2006: Guidelines for assessing the suitability of spatial climate data sets. *Int. J. Climatol.* 26, 707-721.
- Daly, C., Neilson, R.P., Philip, D.L., 1994: A statistical-topographic model for mapping climatological precipitation in mountainous terrain. *J. Appl. Meteorol.* 33, 140-158.
- Daly, C., Gibson, W.P., Taylor, G.H., Johnson, G.L., Pasteris, P., 2002: A knowledge-based approach to the statistical mapping of climate. *Clim. Res.* 22, 99-113.
- Diodatto, N., 2005: The influence of topographic co-variables on the spatial variability of precipitation over small regions of complex terrain. *Int. J. Climatol.* 25, 351-363.
- Drogue, G., Humbert, J., Deraisme, J., Mahr, N., Freslon, N., 2002: A statistical – topographic model using an omnidirectional parametrization of the relief for mapping orographic rainfall. *Int. J. Climatol.* 22, 599-613.
- Goodale, C.L., Aber, J.D., Ollinger, S.V., 1998: Mapping monthly precipitation, temperature, and solar radiation for Ireland with polynomial regression and a digital elevation model. *Clim. Res.* 10, 35-49.

- Hengl, T., 2007: A practical guide to geostatistical mapping of environmental variables. *JRC Scientific and Technical Report* - European Communities, Luxembourg, 143 pp.
- Hulme, M., New, M., 1997: Dependence of large-scale precipitation climatologies on temporal and spatial sampling. *J. Climate* 10, 1099-1113.
- Johnson, G.L., Hanson, C.L., 1995: Topographic and Atmospheric influences on precipitation variability over a mountainous watershed. *J. Appl. Meteorol.* 34, 68-87.
- Joly, D., Nilsen, L., Fury, R., Elvebakk, A., and Brossard, T., 2003: Temperature interpolation at a large scale: test on a small area in Svalbard. *Int. J. Climatol.* 23, 1637-1654.
- Kakos, V., 2001: Maximum precipitation in the Czech Republic in terms of synoptic meteorology (in Czech). In *Sbornik přednášek ze semináře výsledkům grantového projektu VaV/510/97*, 46-60.
- Kaspar, M., Muller, M., 2008: Selection of historic heavy large-scale rainfall events in the Czech Republic. *Nat. Hazards Earth Syst. Sci.* 8, 1359-1367.
- Marquinez, J., Lastra, J., Garcia, P., 2003: Estimation models for precipitation in mountainous regions: the use of GIS and multivariate analysis. *J. Hydrol.* 270, 1-11.
- Ninyerola, M., Pons, X., Roure, J.M., 2000: A methodological approach of climatological modelling of air temperature and precipitation through GIS techniques. *Int. J. Climatol.* 20, 1823-1841.
- Ninyerola, M., Pons, X., Roure, J.M., 2007: Objective air temperature mapping for Iberian Peninsula using spatial interpolation and GIS. *Int. J. Climatol.* 27, 1231-1242.
- Prudhomme, C., Reed, D.C., 1999: Mapping extreme rainfall in mountainous region using geostatistical techniques: a case study in Scotland. *Int. J. Climatol.* 19, 1337-1356.
- Rezacova, D., Kaspar, M., Muller, M., Sokol, Z., Kakos, V., Hanslian, D., Pesice, P., 2005: A comparison of the flood precipitation episode in August 2002 with historic extreme precipitation events on the Czech territory. *Atmos. Res.* 77, 354-366.
- Szentimrey, T., Bihari, Z., 2007: Mathematical background of the spatial interpolation methods and the software MISH (Meteorological Interpolation based on Surface Homogenized Data Basis). In *Proceedings from the Conference on Spatial Interpolation in Climatology and Meteorology*, Budapest, Hungary, 2004. COST Action 719, COST Office, 2007, 17-27.
- Tolasz, R. et al. (eds.), 2007: *Climate Atlas of Czechia*. Czech Hydrometeorological Institute, Prague, Hardback ISBN 978-80-86690-1.
- Vicente-Serrano, S.M., Saz, M.A., Cuadrat, J.M., 2003: Comparative analysis of interpolation methods in the middle Ebro valley (Spain): application to annual precipitation and temperature. *Clim. Res.* 24, 161-180.
- Weisse, A.K., Bois, P., 2001: Topographic effects on statistical characteristics of heavy rainfall and mapping in the French Alps. *J. Appl. Meteorol.* 40, 720-740.

# IDŐJÁRÁS

*Quarterly Journal of the Hungarian Meteorological Service*  
Vol. 115, No. 1–2, January–June 2011, pp. 71–85

## Geostatistical modeling of high resolution climate change scenario data

Ladislav Vizi<sup>1</sup>, Tomáš Hlásny<sup>2,3\*</sup>, Aleš Farda<sup>4</sup>, Petr Štěpánek<sup>4</sup>,  
Petr Skalák<sup>4</sup>, and Zuzana Sitková<sup>2</sup>

<sup>1</sup>*Technical University Košice, Faculty of BERG,  
Park Komenského 19, Košice 04200, Slovakia; E-mail: ladislav.vizi@tuke.sk*

<sup>2</sup>*National Forest Centre – Forest Research Institute,  
T. G. Masaryka 22, Zvolen – 96001, Slovakia  
E-mail: sitkova@nlcsk.org*

<sup>3</sup>*Czech University of Life Sciences, Faculty of Forestry and Environment,  
Kamýcká 1176, Praha 6 – Suchbátka 165 21, Czech Republic*

<sup>4</sup>*Czech Hydrometeorological Institute,  
Na Šabatce 17, 14306, Prague, Czech Republic  
E-mails: ales.farda@chmi.cz; skalak@chmi.cz; stepanek@chmi.cz*

*\*Corresponding author; E-mail: hlasny@nlcsk.org*

*(Manuscript received in final form November 22, 2010)*

**Abstract**—Air temperature and precipitation data organized within a 10×10 km grid covering the whole of Slovakia were subject to analysis. The source data are produced by the ALADIN Climate/CZ regional climatic model. The output of the global climatic model ARPEGE-Climat (Meteo-France) provided the driving data for the regional model. The IPCC A1B scenario provides the information on the future development of greenhouse gas emissions. Such scenario was developed within the 6th Framework Programme project CECILIA (Central and Eastern Europe Climate Change Impacts and Vulnerability Assessment).

Geostatistical prediction of annual mean air temperature and precipitation data was carried out for the reference (1961–1990) and distant future (2071–2100) climates. The experimental data were non-stationary and significantly correlated with elevation. Therefore, we used non-stationary multivariate geostatistical techniques allowing for the integration of such information. In particular, we used kriging of residuals, universal kriging with external drift, and external drift kriging in the scope of IRF- $k$  (intrinsic random functions of order  $k$ ). Prediction based on linear regression of elevation data was used as a complementary technique. Accuracy assessment was based upon the mean square errors produced by cross-validation in case of kriging-based predictions and upon the mean square residual in case of linear regression-based prediction.

We found that all kriging-based techniques outperformed the linear regression-based approach, yielding mean square error lower by 53–75%. External drift kriging in the scope of IRF- $k$  produced slightly better results for most of the climate variables analyzed. The poorest results were achieved in the case of annual mean air temperature for the period 1961–1990, where the variogram of residuals was very erratic.

External drift kriging-based techniques were found to be very efficient for interpolating annual mean air temperature and annual precipitation data organized in regular grids. Accuracy assessment indicated that the three predictors used yielded almost identical results for a single variable, while significant differences in mean square error were observed in a between-variables comparison.

*Key-words:* mean annual air temperature, annual precipitation totals, ALADIN regional climatic model, external drift kriging, non-stationary modeling, Slovakia

## ***1. Introduction***

Maps of various climate elements produced by spatial interpolation of point-distributed data are frequently used to improve understanding of climate's spatio-temporal variability as well as for various studies of climate impacts on society and ecosystems (*Haines et al.*, 2006; *Trnka et al.*, 2004; *Hlásny and Turčáni*, 2009).

Recent availability of large amounts of climate data produced by global and regional climate models (GCMs/RCMs) has drawn attention to the need for optimizing the spatial interpolation of such data (e.g., *Haylock et al.*, 2008). The data are primarily organized in regular grids with spacing depending on the respective GCM/RCM. However, follow-up studies on agriculture, forestry, air pollution, and other areas often ask for seamless information on climate rather than point-distributed data. Therefore, the search for optimal interpolation techniques is a timely task (*Mulugeta*, 1996; *Dobesch et al.*, 2007). A growing number of recent works comparing interpolation techniques and identifying optimal data- or region-specific methods is testimony to this issue's importance (*Goovaerts*, 2000a; *Haberland*, 2007).

In addition to the frequently used non-model-based techniques (not using a variogram, such as inverse distance weighting or spline interpolation, e.g., *Hancock and Hutchinson*, 2006), there exists a range of geostatistical techniques allowing for specific improvements of spatial interpolation, mainly by integrating heterogeneous data (*Isaak and Srivastava*, 1989). In this paper, we demonstrate the use of several external drift kriging-based techniques (EDK, hereinafter) (*Matheron*, 1973) for interpolating high resolution climate change scenario data. These techniques allow for flexible integration of point-distributed climatic data with correlated grid-distributed predictor variables, such as elevation and solar insolation.

An early paper on EDK's use for predicting air temperature and precipitation in Scotland was published by *Hudson and Wackernagel* (1994). Later, EDK's ability to integrate heterogeneous data prompted many other

climatology studies. *Carera-Hernandez and Gaskins (2007)* found that the use of elevation as a secondary variable improves the prediction, even if the correlation is low. The influence of such other terrain-related parameters as relief slope and aspect was investigated by *Attore et al. (2007)*, who found that universal kriging with external drift performed the best for 17 out of 21 climatic variables analyzed. *Goovaerts (2000a)* tested the efficiency of several approaches to spatial interpolation of rainfall data (linear regression, ordinary cokriging, kriging with external drift, simple kriging with local means) and stressed the benefits of incorporating the elevation data. That author found that the latter two named techniques yield slightly better results than did the others.

The purpose of this paper is to analyze the climatic data produced by the ALADIN-Climate/CZ regional climate model (*Farda et al., 2010*) for the whole of Slovakia in  $10 \times 10$  km spatial resolution. Maps of mean annual air temperature (hereinafter just air temperature) and mean annual precipitation totals (hereinafter just precipitation) for the reference (1961–1990) and distant future (2071–2100) climates were to be produced. In particular, we focused on:

- (1) describing and preprocessing the data,
- (2) using several EDK-based techniques and a linear regression-based approach for spatial prediction of air temperature and precipitation data for the reference and distant future climates, and
- (3) assessing the accuracy of the maps produced and discussing the results.

## 2. Data

The reference and future climate data were originally calculated using the GCM ARPEGE–Climat V4 (*Déqué, 2007*) in an experiment performed by CNRM/Météo-France. Because of rather coarse resolution of the GCM (~50 km over Central Europe), the RCM ALADIN-Climate/CZ (*Farda et al., 2010*) was used for additional downscaling of the GCM data. The IPCC A1B emission scenario was adopted to provide information on future development of greenhouse gas emissions. The data were developed as part of the CECILIA (Central and Eastern Europe Climate Change Impacts and Vulnerability Assessment, [www.cecilia-eu.org](http://www.cecilia-eu.org)) project under the European Union's 6th Framework Programme. The RCM covers Central Europe with a resolution of 10 km. Such resolution allows for better representation of the driving physical processes (e.g., more accurate resolution of geographical features and thus, various interactions with the surface), thus, leading to better description of local climate and positively affecting the quality of the simulations.

The data used in this study comprise a subset of ALADIN's entire integration domain covering the Slovak Republic. The 10 km resolution grid, with rotation  $6^\circ$  azimuth, is extended beyond the country's borderline by

approximately one grid point in order to reduce interpolation errors in the edge locations (*Fig. 1*). In total, 644 grid points are used for the analysis. Source data statistics are given in *Table 1*.



*Fig. 1.* Spatial arrangement of 10×10 km grid of the ALADIN-Climate/CZ regional climate model in Slovakia.

*Table 1.* Source data statistics. Abbreviations: N – number of observations, Min – minimum, Max – maximum, Avg – average, Med – median, SD – standard deviation, IQR – inter-quartile range, Skew – skewness, Kurt – kurtosis. Variables: T – mean annual air temperature for the given period, P – mean annual precipitation totals for the given period

Variable	N	Min	Max	Avg	Med	SD	IQR	Skew	Kurt
T 1961–1990	644	0.6	10.7	7.3	7.4	2.0	3.1	−0.32	−0.42
T 2071–2100	644	5.2	13.4	10.7	10.8	1.8	3.2	−0.40	−0.90
P 1961–1990	644	416.5	1206.7	697.3	675.6	145.1	207.8	0.83	0.12
P 2071–2100	644	472.5	1175.0	671.3	629.7	154.5	214.9	0.94	0.05

Elevation of the study area is used as a supportive variable (*Fig. 1*). It is organized in a 180 m resolution grid, which is more than 55 times denser than the ALADIN grid.

### 3. Methods

The climate data used are clearly non-stationary, as they have a global elevation-controlled trend in the south-north direction. Therefore, we describe here the concepts for multivariate non-stationary geostatistical modeling that are used. All steps of the geostatistical analysis were carried out in the ISATIS v.9 environment (*Geovariances, Centre de Géostatistique in Fontainebleau*). For regression modeling, STATISTICA v.7 (*StatSoft, Inc., 2004*) was used.

### 3.1. Stationary spatial models

Stationarity of spatial data, i.e., the presence of a stable mean for an analyzed variable, is the simplest and most frequently documented case of geostatistical analysis. This allows for straightforward modeling of the variogram, which measures the spatial correlation of the studied variable, as well as for an optimal estimation using kriging. In a stationary case, where drift  $m(\mathbf{x})$  is a constant, the variogram  $\gamma$  for distance  $\mathbf{h}$  is estimated as:

$$2\gamma_Z(\mathbf{h}) = E[Z(\mathbf{x}+\mathbf{h}) - Z(\mathbf{x})]^2. \quad (1)$$

For a regionalized variable, as one realization of a random function, the variogram is estimated by forming the average dissimilarities for all  $N(\mathbf{h})$  pairs of data  $z(\mathbf{x}_\alpha)$  and  $z(\mathbf{x}_\alpha + \mathbf{h})$  available at sample points  $\mathbf{x}_\alpha$  that are linked by the vector  $\mathbf{h} = \mathbf{x}_\alpha - \mathbf{x}_\beta$  (Hudson and Wackernagel, 1994):

$$2\gamma_Z(\mathbf{h}) = \frac{1}{N(\mathbf{h})} \sum_{\alpha=1}^{N(\mathbf{h})} (z(\mathbf{x}_\alpha) - z(\mathbf{x}_\beta))^2. \quad (2)$$

Usually, we observe that the average dissimilarities between the couples of values increase when  $\mathbf{h}$  is increased, up to a value of the variable autocorrelation (range of influence). Beyond this value, the dissimilarities become more or less constant around an upper asymptote (sill of the variogram) that is approximately equal to the data variance.

### 3.2. Non-stationary spatial models

In a non-stationary case, there is a definite trend in the data, being a gradient in a given direction (Hayet et al., 2000). The non-stationary approach to spatial modeling considers the phenomenon under study as a sum of two terms:

$$Z(\mathbf{x}) = Y(\mathbf{x}) + m(\mathbf{x}), \quad (3)$$

where  $Y(\mathbf{x})$  describes the local variation of  $Z(\mathbf{x})$ , and it is assumed to be stationary with constant mean. The term  $m(\mathbf{x})$  describes a large-scale variation of  $Z(\mathbf{x})$  (drift). It is assumed that the drift can be represented by a polynomial of order  $L$ :

$$m(\mathbf{x}) = \sum_{l=0}^L a_l f_l(\mathbf{x}), \quad (4)$$

where  $a_l$  are unknown coefficients of known functions  $f_l(\mathbf{x})$  of the spatial coordinates. Note that for  $L=1$ , Eq. (4) reduces to a constant term,  $a_0$ , which

indicates no trend in the spatial coordinates. The term  $Y(\mathbf{x})$  in Eq. (3) represents the residual, i.e., the amount of variability remaining after the drift has been removed. The residuals have a stationary covariance (variogram) function between any pairs of random variables  $\{Y(\mathbf{x}), Y(\mathbf{x}+\mathbf{h})\}$ . The drift is essentially the mean value of the variable as a function of the location at which the variable is measured. In a non-stationary case, we can rewrite Eq. (1) as follows:

$$\begin{aligned}
 2\gamma_Z(\mathbf{h}) &= E[Z(\mathbf{x}+\mathbf{h}) - Z(\mathbf{x})]^2 \\
 &= E[Y(\mathbf{x}+\mathbf{h}) + m(\mathbf{x}+\mathbf{h}) - Y(\mathbf{x}) - m(\mathbf{x})]^2 \\
 &= E[Y(\mathbf{x}+\mathbf{h}) - Y(\mathbf{x})]^2 - [m(\mathbf{x}+\mathbf{h}) - m(\mathbf{x})]^2 \\
 &= 2\gamma_Y(\mathbf{h}) - [m(\mathbf{x}+\mathbf{h}) - m(\mathbf{x})]^2,
 \end{aligned} \tag{5}$$

where the trend values  $m(\mathbf{x})$  and  $m(\mathbf{x}+\mathbf{h})$  are unknown. The second term on the right side of Eq. (5) provides the drift estimate in a particular direction. The most straightforward approach to non-stationary modeling is based on computation of a residual variogram  $2\gamma_Y(\mathbf{h})$ . A proper use of this technique is documented by *Dowd* (1984) and *Goovaerts* (2000b), who suggested several ways for coping with certain shortcomings of this technique, as discussed, for example, by *Hayet et al.* (2000).

Another approach to non-stationary modeling used in this paper is the method of increments based on the theory of intrinsic random function of order  $k$  (IRF- $k$ ) (*Matheron*, 1973). It defines a linear combination of  $Z$  data that filters out the drift component  $m(\mathbf{x})$ . In a stationary case, the first order difference, or increment  $[Z(\mathbf{x}+\mathbf{h}) - Z(\mathbf{x})]$ , filters out the constant drift  $m$ . In a non-stationary case, higher order differentiation is required to filter out the higher orders of the polynomial drift. This approach leads to a so-called generalized covariance model  $K(\mathbf{h})$  instead of a variogram  $\gamma(\mathbf{h})$ . The most widely used models for generalized covariances are polynomial in form (*Matheron*, 1973):

$$K(\mathbf{h}) = a_0 + \sum_{k=0}^K (-1)^{k+1} a_{k+1} |\mathbf{h}|^{2k+1}. \tag{6}$$

More information on this technique can be found in *Dowd* (1984) or *Chiles and Delfiner* (1999).

### 3.2.1. Case of external drift(s)

In case of a non-stationary spatial model, we consider the trend  $m(\mathbf{x})$  of the variable  $Z(\mathbf{x})$  to be a function of spatial coordinates. For some applications, exhaustive data for one or more regionalized variables  $s_j(\mathbf{x})$  may be available

in the studied domain (representing, e.g., elevation). If such data are available, it is worthwhile to use them as additional constraints to the interpolation.

If we assume that  $Z(\mathbf{x})$  is on average equal to  $s_j(\mathbf{x})$  up to linear way and with coefficients  $a_0$  and  $b_1$ , then:

$$E[Z(\mathbf{x})]=m(\mathbf{x})=a_0 + \sum_{j=1}^J b_j s_j(\mathbf{x}). \quad (7)$$

Because variables  $s_j(\mathbf{x})$  are exhaustively available, they reflect the average shape of  $Z(\mathbf{x})$ , where just the scaling is different (Hudson and Wackernagel, 1994).

### 3.3. Interpolation techniques

In this study, we include several techniques under the term external drift kriging. Their common feature is that the elevation acts as an external drift correlated with the primary climatic variables. In addition, a linear regression of the elevation data was used to predict the climate data.

**Residual kriging**, known also as regression kriging (Odeh et al., 1994) or kriging after detrending (Goovaerts, 2000b), predicts the residuals at all nodes of the interpolated grid  $\mathbf{x}_0$ ,  $Y^*(\mathbf{x}_0)$ . Residual kriging uses the drift  $m^*(\mathbf{x})$  calculated by a polynomial of a selected degree by the least squares method. Residuals  $Y(\mathbf{x}_\alpha)$  are calculated as the differences between  $Z(\mathbf{x}_\alpha)$  and  $m^*(\mathbf{x}_\alpha)$  at all sample points. Using the variogram of residuals, the kriging system for weights  $\omega(\mathbf{x}_\alpha)$ ,  $\alpha=1, \dots, n$  includes  $n+1$  linear equations:

$$\begin{cases} \sum_{\beta=1}^n \omega(\mathbf{x}_\beta) \gamma_Y(\mathbf{x}_\alpha, \mathbf{x}_\beta) + \lambda_0 = \gamma_Y(\mathbf{x}_0, \mathbf{x}_\alpha) & \text{for } \alpha=1, \dots, n, \\ \sum_{\alpha=1}^n \omega(\mathbf{x}_\alpha) = 1. \end{cases} \quad (8)$$

The residual kriging estimator is a linear combination of available  $n$  data  $y(\mathbf{x}_\alpha)$  for only  $n$  random variables  $Z(\mathbf{x}_\alpha)$ :

$$y^*(\mathbf{x}_0) = \sum_{\alpha=1}^n \omega(\mathbf{x}_\alpha) y(\mathbf{x}_\alpha). \quad (9)$$

Finally, the estimated drift, Eq. (4) and kriged residuals, Eq. (9) are added together.

**Universal kriging** provides an unbiased estimation, which considers drift  $m(\mathbf{x})$  as a continuous and regular function (Eq. (4)), usually restricted to polynomials up to the order of 2. It uses a model representing both local and global variability of the variable in space. It determines the underlying variogram of  $Y(\mathbf{x})$  and estimates the degree of drift. We modeled the drift by Eq. (4), including elevation as the external drift. The simultaneous system of equations for the universal kriging estimator, considering both internal and external drift, is as follows:

$$\left\{ \begin{array}{l} \sum_{\beta=1}^n \omega(\mathbf{x}_\beta) \gamma_Z(\mathbf{x}_\alpha, \mathbf{x}_\beta) + \lambda_0 + \sum_{l=1}^L \lambda_l f_l(\mathbf{x}_\alpha) + \sum_{j=1}^J \lambda_j s_j(\mathbf{x}_\alpha) = \gamma_Z(\mathbf{x}_0, \mathbf{x}_\alpha) \\ \quad \text{for } \alpha=1, \dots, n, \\ \sum_{\alpha=1}^n \omega(\mathbf{x}_\alpha) = 1, \\ \sum_{\alpha=1}^n \omega(\mathbf{x}_\alpha) s_j(\mathbf{x}_\alpha) = s(\mathbf{x}_0) \quad \text{for } j=1, \dots, J, \\ \sum_{\alpha=1}^n \omega(\mathbf{x}_\alpha) f_l(\mathbf{x}_\alpha) = f_l(\mathbf{x}_0) \quad \text{for } l=1, \dots, L. \end{array} \right. \quad (10)$$

**The kriging system for IRF- $k$**  is similar to the universal kriging system, Eq. (10). The only difference is that it uses the generalized covariance model  $K(\mathbf{h})$  (Eq. (6)) instead of the variogram  $\gamma(\mathbf{h})$  (Eq. (2)). More details about IRF- $k$  can be found in *Dowd (1984)* or *Chiles and Delfiner (1999)*.

### 3.4. Linear regression-based estimation

The generally recognized relationship between the climate variables addressed and elevation allows for a simple prediction of climate data at all positions for which elevation data are available. There exists a set of collocated climate  $z(\mathbf{x}_\alpha)$  and elevation  $s(\mathbf{x}_\alpha)$  data  $[z(\mathbf{x}_\alpha), s(\mathbf{x}_\alpha)]$ ;  $\alpha=1, \dots, n$ , where  $n$  is the number of observations. The prediction  $z^*(\mathbf{x}_0)$  is based on a linear relationship:

$$z^*(\mathbf{x}_0) = a_0^* + b_1^* s(\mathbf{x}_0), \quad (11)$$

where coefficients  $a_0^*$  and  $b_1^*$  are estimated from the collocated climate and elevation data. A major shortcoming of this type of prediction is that the climate data at a particular grid node are derived only from the collocated elevation, regardless of the surrounding observed climate data (*Goovaerts, 2000a*).

### 3.5. Accuracy assessment

Two techniques were used to assess the accuracy of the maps produced and the performance of the predictors used. A cross-validation procedure was used in case of geostatistical predictions (Isaaks and Srivastava, 1989; Clark, 1986). The technique temporarily removes one observation at a time from the data set and “re-estimates” this value from the remaining data using a given predictor. Such procedure produces couples of values, the differences between which yield cross-validation residuals. The main criterion for assessing accuracy is mean square error (MSE), which measures the average squared difference between the observed  $z(\mathbf{x}_\alpha)$  and predicted  $z^*(\mathbf{x}_\alpha)$  values:

$$\text{MSE} = \frac{1}{n} \sum_{\alpha=1}^n [z(\mathbf{x}_\alpha) - z^*(\mathbf{x}_\alpha)]^2, \quad (12)$$

where  $n$  is the number of observations.

Correlation coefficients of observed versus predicted values, normality of residuals distribution, mean value of residuals (criterion that the mean is approaching zero), and degree of randomness of spatial distribution of residuals can also be used.

Another approach was used in the case of linear regression-based prediction. The MSE was computed as the average square residual value for the linear model fitted using all observations:

$$\text{MSE} = \frac{1}{n} \sum_{\alpha=1}^n [z(\mathbf{x}_\alpha) - (a_0^* + b_1^* s(\mathbf{x}_\alpha))]^2. \quad (13)$$

## 4. Results

### 4.1. Drift identification

To identify an optimal global trend, the polynomials of order one (linear) and two (quadratic) plus one external drift (elevation) were tested by the cross-validation procedure for the lowest mean square error. Other criteria, such as mean of residuals approaching zero, minimal variance, normal distribution, and well-structured directional experimental variograms, were used as well. We found that the linear drift along the  $x$  and  $y$  coordinates (internal drift), together with the elevation (external drift),

$$m^*(\mathbf{x}) = a_0 + a_1 x + a_2 y + b_1 s(\mathbf{x}), \quad (14)$$

performed the best for all climate variables.

#### 4.2. Kriging-based predictions

To perform the residuals kriging, we used the trend functions described above to filter out the residuals  $y(\mathbf{x}_\alpha)$  from the regionalized variable  $z(\mathbf{x}_\alpha)$ , then estimated the residual variogram models  $\gamma_Y(\mathbf{h})$  for all the climate variables analyzed (Fig. 2). Estimation of the variogram model for the variable T 1961–1990 was problematic, because there were erratic directional experimental variograms without clear spatial structure. Therefore, an omnidirectional model was fitted to the experimental variogram values in this case. The variogram’s origin was estimated from the directional variogram constructed in the azimuth  $6^\circ$  that rises from the variogram’s value at about  $0.1 (\text{°C})^2$ . Directional experimental variograms are presented in Fig. 2 to demonstrate that no anisotropy can be modeled in this case.

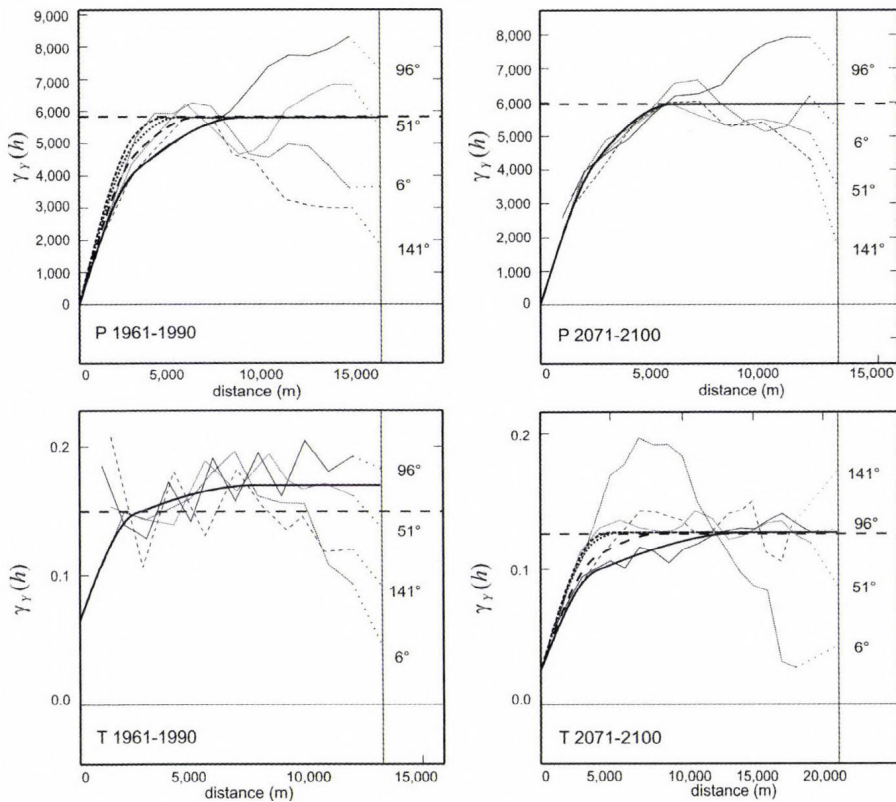


Fig. 2. Directional experimental residual variograms (thin lines) and respective variogram models (thick lines). The numbers on the right side indicate the angles at which the variograms were calculated. Abbreviations: P 1961–1990 – mean precipitation totals during the period 1961–1990, P 2071–2100 – mean precipitation totals during the period 2071–2100, T 1961–1990 – mean annual air temperature during the period 1961–1990, T 2071–2100 – mean annual air temperature during the period 2071–2100.

The estimation of kriging weights  $\omega(\mathbf{x}_\alpha)$  was based on Eq. (8). Estimation of residuals  $y^*(\mathbf{x}_0)$  was based on the linear combination of available data according to Eq. (9). Finally, the kriged residuals were summed with the trend model according to Eq. (3).

In case of universal kriging, the trend component is directly included into the kriging system according to Eq. (10) for the drift estimation (Eq. (14)). The final estimation was performed directly using the raw variable  $Z(\mathbf{x})$ .

In case of IRF- $k$ , the automatic fitting procedure of the ISATIS environment was used to determine both the degree  $k$  of the drift and the generalized covariance. For all variables, the degree of the drift was 1 (linear in  $X$  and  $Y$  directions) plus the external drift represented by the elevation. The generalized covariance of order 1 (similar to the linear model of the variogram) without nugget effect was used for all climate variables.

For interpolation neighborhood definition (Isaaks and Srivastava, 1989), we used a so-called unique neighborhood, i.e., all available data were used to estimate a value at a particular grid node. We also tested several designs for a moving neighborhood, such as a first ring neighborhood (4 adjacent samples), second ring neighborhood (16 adjacent samples), and third ring neighborhood (36 adjacent samples). The cross-validation tests indicated that the unique neighborhood was performing the best for all climate variables. In addition, the use of moving neighborhoods resulted in “radial” artefacts in the maps produced, due to the resolution of the estimated grid which is more than 55 times higher than that of the ALADIN grid.

The maps of both variables for both time slices produced by EDK in the scope of IRF- $k$  can be seen in Fig. 3. We can see that the elevation pattern is much stronger in the case of temperature than in that of precipitation data due to the different correlation of climate variables with elevation (Table 2).

### 4.3. Linear regression-based prediction

Linear regression-based prediction was used to provide the reference value for assessing the accuracy of the kriging-based techniques. Regression parameters from elevation and the respective climatic variables are based on all 644 observed values (Table 2). Mean square error was calculated using Eq. (13).

### 4.4. Accuracy assessment

Accuracy assessment was based on comparison of the MSE yielded by kriging-based predictions (Table 3) with that from the linear regression-based prediction (Table 2) (Goovaerts, 2000a). The latter technique provided the MSE reference value for evaluating the performance of kriging techniques. Proportional values of MSE are illustrated in Fig. 4. Such an approach allows for evaluating the performance of respective predictors for a single variable as well as for between-variable comparison. The results are discussed below.

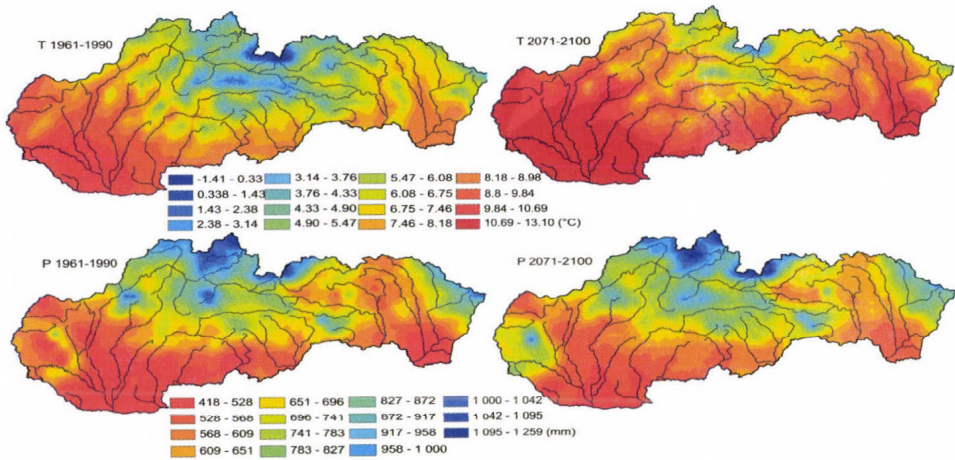


Fig. 3. Maps of mean annual air temperature and mean annual precipitation totals for the reference (1961–1990) and distant future (2071–2100) climates produced using external drift kriging in the scope of IRF- $k$ .

Table 2. Linear regression parameters between elevation (X) and respective climatic variables (Y). Abbreviations:  $a_0^*$  – intercept,  $b_1^*$  – slope, R – correlation coefficient,  $R^2$  – coefficient of determination, MSE – mean square error

X	Y	$a_0^*$	$b_1^*$	R	$R^2$	MSE
Elevation	P 1961–1990	526.86	0.39180	0.75	0.563	9141
Elevation	P 2071–2100	488.27	0.42060	0.76	0.578	10123
Elevation	T 1961–1990	10.26	-0.00688	-0.95	0.903	0.394
Elevation	T 2071–2100	13.34	-0.00606	-0.94	0.887	0.359

Table 3. Results of the cross-validation based accuracy assessment. Abbreviations: KR – residuals kriging, UK – universal kriging with external drift, IRF- $k$  – external drift kriging in the scope of IRF- $k$ , R – correlation coefficient between observed and predicted values,  $R^2$  – coefficient of determination, MSE – mean square error of prediction, AVG – average value of residuals

Variable	Interpolator	R	$R^2$	MSE	AVG
T 1961–1990	KR	0.978	0.956	0.17457	0.000286
T 1961–1990	UK	0.978	0.957	0.17165	0.000286
T 1961–1990	IRF- $k$	0.976	0.953	0.184628	0.000410
T 2071–2100	KR	0.990	0.981	0.056014	-0.000449
T 2071–2100	UK	0.991	0.981	0.055269	-0.000327
T 2071–2100	IRF- $k$	0.990	0.981	0.054161	-0.000306
P 1961–1990	KR	0.954	0.909	1588.9	-0.1220
P 1961–1990	UK	0.954	0.910	1564.6	-0.0280
P 1961–1990	IRF- $k$	0.955	0.912	1536.9	-0.0099
P 2071–2100	KR	0.939	0.881	2329.5	-0.0180
P 2071–2100	UK	0.940	0.884	2273.9	0.0470
P 2071–2100	IRF- $k$	0.943	0.889	2163.9	0.0660

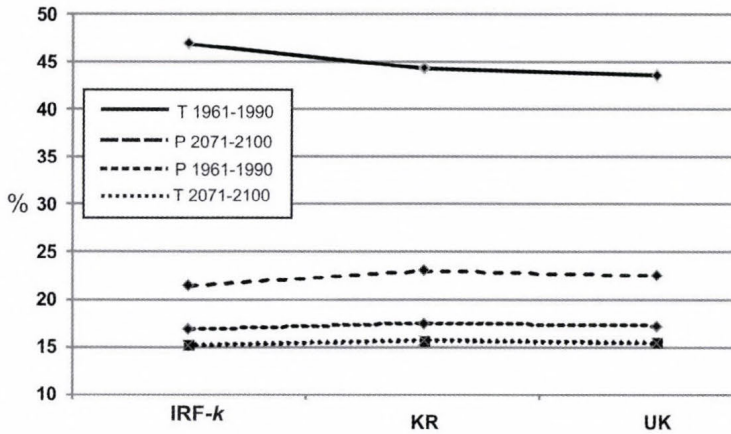


Fig. 4. Results of accuracy assessment for predictions produced by three interpolation techniques for mean annual air temperature and mean annual precipitation totals for the periods 1961–1990 and 2071–2100. The figures indicate the proportions of the MSE (mean square error) yield by cross-validation in the case of EDK-based techniques to MSE yield using the linear regression approach.

### 5. Conclusions and discussion

We performed a series of analyses of high resolution RCM data covering Slovakia. Both air temperature and precipitation data are well correlated with elevation (*Table 2*), and thus, we focused on the integration of that variable into the interpolation. Such supportive variable is presumed to reduce the amount of uncertainty in the maps produced. We used three external drift kriging-based techniques: residuals kriging, universal kriging with external drift, and external drift kriging in the scope of IRF-*k*. We described in details the particular steps of the geostatistical analysis to allow for a deeper understanding of those techniques used.

All kriging-based techniques produced comparable results for a single climate variable. The reason for this evidently lies in the high correlation of climate data with elevation, which covers the impact of different interpolation algorithms. In the cases of the variables T 2071–2100, P 1961–1990, and P 2071–2100, EDK in the scope of IRF-*k* yields slightly better results than do the remaining kriging-based techniques. This can reflect the benefit of using an automatized procedure in generalized covariance calculation for regularly distributed data in comparison to manual variogram fitting (the case of residuals kriging). The poorest results were reached in the case of the variable T 1961–1990, where the residuals were very erratic, and thus, they influenced the shape of the respective variograms (*Fig. 2*). This applies also for the remaining techniques, because drift parameters remain more or less stable.

Subsequently, we tested the ratio of mean square errors produced by kriging-based techniques to those from linear regression-based estimation. All kriging techniques significantly outperformed the linear regression-based estimation, which yields a mean square error 15–47% higher (depending on the variable). This means that, despite high correlation between climate data and elevation, information about the configuration of the surrounding data significantly improved the estimation. The accuracy assessment indicated that the three predictors used yielded almost identical results for a single variable, while significant differences in mean square error were observed by between-variables comparison.

Geostatistical techniques, in general, require a certain extent of user intervention and cannot be fully automatized. In any case, large amounts of climate data produced by various instruments require at least a semi-automatized approach when producing series of climate maps for various time slices. External drift kriging in the scope of IRF- $k$  is a candidate technique for this. It yielded slightly better results than did the remaining EDK-based techniques for three out of four variables analyzed, and the underlying generalized covariance may be calculated automatically (see implementation in the ISATIS environment used in this paper). By contrast, residuals kriging requires a series of user interventions, which were not, however, compensated by improved accuracy of the prediction.

**Acknowledgements**—This research was conducted as part of the 6th Framework Programme project CECILIA (Central and Eastern Europe Climate Change Impacts and Vulnerability Assessment), and within projects of the Ministry of Agriculture of the Czech Republic, No. QH91097 “Analysis of the climate change impacts on the distribution and voltinism of *Ips typographus* in spruce forests of the Czech Republic as underlying information for their sustainable management”, and the Scientific Grant Agency of the Ministry of Education of the Slovak Republic, VEGA 1/0222/08 “Application of geostatistical tools for multivariate analysis and data integration of regionalized variables”.

## References

- Attore, F., Alfo, M., De Sanctis, M., Francesconi, F., Bruno, F., 2007: Comparison of interpolation methods for mapping climatic and bioclimatic variables at regional scale. *Int. J. Climatol.* 27, 1825-1843.
- Carrea-Hernandez, J.J., Gaskin, S.J., 2007: Spatio temporal analysis of daily precipitation and temperature in the Basin of Mexico. *J. Hydrol.* 336, 231-249.
- Chiles, J.P., Delfiner, R., 1999: *Geostatistics – Modeling Spatial Uncertainty*. Oxford University Press.
- Clark, I., 1986: The art of cross validation in geostatistical applications. In *19th Application of Computers and Operational Research in the Mineral Industry* (ed.: V. Ramani), 211-220.
- Déqué, M., 2007: Frequency of precipitation and temperature extremes over France in an anthropogenic scenario: model results and statistical correction according to observed values. *Global Planet. Change* 57, 16-26.
- Dobesch, H., Dumolard, P., Dyras, I. (eds.), 2007: *Spatial Interpolation for Climate Data: The Use of GIS in Climatology and Meteorology*. *Geographical Information Systems Series*. Wiley-ISTE, New York.

- Dowd, P.A., 1984: *MINE5260: Non-Stationarity. MSc notes in Mineral Resources and Environmental Geostatistics*. Dpt. of Mining and Mineral Engineering, University of Leeds, United Kingdom.
- Farda A., Déqué, M., Somot S., Horányi A., Spiridonov V., Tóth. H., 2010: Model ALADIN as a Regional Climate Model for Central and Eastern Europe. *Studia Geophysica et Geodaetica, Journal of the Czech Academy of Sciences* 54, 313-332.
- Geovariances: ISATIS v.9, Centre de Géostatistique in Fontainebleau.
- Goovaerts, P., 2000a: Geostatistical approaches for incorporating elevation into the spatial interpolation of rainfall. *J. Hydrol.* 228, 113-129.
- Goovaerts, P., 2000b: Using elevation to aid the geostatistical mapping of rainfall erosivity. *Catena* 34, 227-242.
- Haberland, U., 2007: Geostatistical interpolation of hourly precipitation from rain gauges and radar for a large-scale extreme rainfall event. *J. Hydrol.* 332, 144-157.
- Haines, A., Kovats, R. S., Campbell-Lendrum, D., Corvalan, C., 2006: Climate change and human health: impacts, vulnerability, and mitigation. *Public Health* 367, 2101-9.
- Hancock, P.A., Hutchinson, M.F., 2006: Spatial interpolation of large climate data sets using bivariate thin plate smoothing splines. *Environ.Modell. Softw.* 21, 1684-1694.
- Hayet, Ch., Galli, A., Ravenne, C., Tesson, M., de Marsily, G., 2000: Estimating the Depth of Stratigraphic Units from Marine Seismic Profiles Using Nonstationary Geostatistics. *Nat. Resour. Res.* 9, 77-95.
- Haylock, M.R., Hofstra, N., Klein Tank, A.M.G., Klok, E.J., Jones, P.D., New, M., 2008: A European daily high-resolution gridded data set of surface temperature and precipitation for 1950–2006. *J. Geophys. Res.* 113, D20119.
- Hlásny, T., Turčáni, M., 2009: Insect pests as climate change driven disturbances in forest ecosystems. In *Bioclimatology and Natural Hazards* (eds.: K. Štřelcová, C. Mátyás, A. Kleidon, M. Lapin, F. Matejka, M. Blaženec, J. Škvarenina, J. Holécý). Springer, Netherlands, 165–178.
- Hudson, G., Wackernagel, H., 1994: Mapping temperature using kriging with external drift: Theory and example from Scotland. *Int. J. Climatol.* 14, 77-91.
- Isaaks, H. E., Srivastava, R. M., 1989: *Introduction to Applied Geostatistics*. Oxford University Press, New York.
- Matheron, G., 1973: The intrinsic random function and their applications. *Adv. Appl. Probab.* 5, 439-469.
- Mulugeta, G., 1996: Manual and automated interpolation of climatic and geomorphic statistical surfaces: An evaluation. *Annals of the Association of American Geographers* 86, 324-342.
- Odeh, I., McBratney, A., Chittleborough, D., 1994: Spatial prediction of soil properties from land-form attributes derived from a digital elevation model. *Geoderma* 63, 197-214.
- StatSoft, Inc., (2004). STATISTICA Cz (Software system for statistical analyses), Version 7. [www.StatSoft.Cz](http://www.StatSoft.Cz)
- Trnka, M., Dubrovský, M., Semerádova, D., Žalud, Z., 2004: Projections of uncertainties in climate change scenarios into expected winter wheat yields. *Theor. Appl. Climatol.* 77, 229-249.



# IDŐJÁRÁS

*Quarterly Journal of the Hungarian Meteorological Service*  
Vol. 115, No. 1–2, January–June 2011, pp. 87–98

## **Interpolation techniques used for data quality control and calculation of technical series: an example of a Central European daily time series**

**Petr Štěpánek<sup>1\*</sup>, Pavel Zahradníček<sup>1</sup>, and Radan Huth<sup>2</sup>**

<sup>1</sup>*Czech Hydrometeorological Institute,  
Regional office Brno, Kroftova 43, 61667, Brno, Czech Republic*

<sup>2</sup>*Institute of Atmospheric Physics, Academy of Sciences of the Czech Republic,  
Boční II 1401, 14131 Praha 4, Czech Republic*

*\*Corresponding author; E-mail: petr.stepanek@chmi.cz*

*(Manuscript received in final form August 27, 2010)*

**Abstract**—For various studies, it is necessary to work with a sufficiently long series of daily data that is processed in the same way for the whole area. National meteorological services have their own tools for data quality control; data are usually available non-homogenized (with respect to artificial changes in the series due to relocations, change of observers, etc.). In the case of areas across borders of individual countries, researchers from both sides of a frontier can obtain quite different results depending upon the data they use. This was one of the reasons for processing stations from the area along borders of four countries in the Central European region within the international CECILIA project (Central and Eastern Europe Climate Change Impact and Vulnerability Assessment, project of EC No. 037005). For the processing of the series, quality control has been carried out, gaps have been filled and, in the end, a series at a new position (grid points of RCM output) were calculated. An interpolation technique which is able to deal with all these tasks is described in this work and then applied to a series of various meteorological elements in Central Europe.

*Key-words:* data quality control, filling missing values, interpolation techniques, climatological time series

### **1. Introduction**

During validation of regional climate model (RCM) outputs, its values are compared with the values of observations. Whereas the observations are located in the station network, which is irregular in its nature, the dynamical model (GCM, RCM) outputs are provided on a regular grid (statistical downscaling

procedures can yield output either at stations or grid points, depending on what they were trained on). Dynamical models thus provide area-aggregated, rather than point-specific data, which makes a direct comparison between station data and gridded model output less straightforward, especially for variables with a short correlation distance, such as precipitation (e.g., *Skelly and Henderson-Sellers, 1996*). Therefore, validation has the potential to be truer to dynamical models if the observations are transformed from stations to a grid. This was one of the reasons that such a task was carried out within the CECILIA project.

For the development and calibration of statistical downscaling methods, and for the use of outputs from dynamical as well as statistical downscaling in climate change impact studies, a common observed dataset needed to be created. It was decided that the common dataset would extend over the area along the boundaries of the Czech Republic, Austria, Slovakia, and Hungary (this region is hereinafter called the CECILIA Central European domain). The main intention was to cover the majority of the impact target areas in Central Europe. Another deciding factor in this decision was that it would be easier to obtain meteorological data from meteorological services for only relatively small parts of the countries than for their large parts or even whole countries.

To achieve such a goal, it was necessary to prepare observation data in a way that they would be homogeneous, free of erroneous values, and they gaps would be filled. Ideally, they should also be available in the location of the used model output. For this reason, two versions of the dataset were created, one located at the stations, the other located on the grid of the regional climate model, in this case ALADIN-Climate/CZ (details about the model can be found, e.g., in *Farda et al., 2007*). To create series at given locations, interpolation methods, which are described further in this paper, have been used. The techniques for data quality control, carried out upon the data prior to any further processing, and for filling the missing values in the station series are, in principal, identical to that used for the calculation of series at a new position, mentioned above. For this reason, the quality control is described in this paper as well.

## ***2. Central European dataset, data preparation***

The area of interest covered by the dataset can be seen in *Figs. 1* and *2*. It includes:

- in the Czech Republic: the southern and southeastern part, consisting of the regions of České Budějovice, the Highlands (Vysočina), South Moravia, Zlín, and minor southern parts of Central Bohemia;
- in Austria: the federal states of Lower Austria, Upper Austria, Vienna, and Burgenland;
- in Slovakia: the western part, consisting of the regions of Bratislava, Trnava, Nitra, Trenčín, and Banská Bystrica;

- in Hungary: the regions of Győr-Moson-Sopron and Komárom-Esztergom.

The Central European area covers the following impact target areas (processed in the CECILIA project): agriculture – Lower Austria (AT), southern Moravia (CZ), the Danube lowlands (SK), and the northwestern part of Hungary (HU); forestry – southern central Slovakia (SK); hydrology – the Dyje and upper Vltava catchments (CZ), the Hron catchment (SK).

The dataset itself consists of daily data for the period of 1961–2000. Variables available in the dataset are given in *Table 1*. Potential evapotranspiration is not included, since there are several ways it can be calculated and it can also be derived from the available elements by individual users.

*Table 1.* Meteorological elements available in the common dataset

<b>Abbreviation</b>	<b>Description</b>	<b>Unit</b>
TMI	Maximum temperature	°C
TMA	Minimum temperature	°C
H	Relative humidity	%
SRA	Precipitation	mm
SSV	Sunshine duration	h

The following comments on the variables selected and not selected should be made:

- Daily mean temperature was not included because of regional differences in its calculation and a change in the practice of its calculation in Austria in the early 1970s, which could induce an inhomogeneity in the time series and inconsistency along the state boundaries.
- Relative humidity, and not another measure of atmospheric moisture unaffected by daily temperature cycle, such as specific humidity, was selected, because some of the impact models require only relative humidity as their input.
- Wind speed and direction were not subjected to gridding and the creation of technical series because of the necessity of working separately with the two wind components, which would cause considerable complications, making the resultant technical series doubtful and unreliable.
- Solar radiation can easily be approximated from the sunshine duration data. Solar radiation was not included among the final products, since meteorological services apply different approaches for its calculation (e.g., the Angström formula or regression models based on altitudes).

Even incomplete time series were allowed into the database. The data were prepared and provided by the following partners: the Czech Hydrometeorological Institute (CHMI) for the Czech Republic, the Forest Research Institute (NFC) for Slovakia (40 stations), the University of Natural Resources and

Applied Life Sciences (BOKU) for Austria (30 stations), and the Hungarian Meteorological Service (OMSZ) for Hungary. The data policy of some of the involved meteorological services does not allow the distribution of raw station data. This was another reason for creating technical series from the station data available, which were distributed among the project participants. Technical series of two kinds were constructed: (i) gridded datasets covering the area where station data are available; this was regarded as a primary dataset; (ii) station technical series, which have the advantage of better homogeneity and completeness over the raw data.

In the CECILIA Central European domain, about 150 climatological stations are available – see *Fig. 1*, in comparison with 832 grid points of the ALADIN-CLIMATE/CZ RCM – see *Fig. 2*. The number of stations available in the individual countries and meteorological elements are given in *Table 2*.

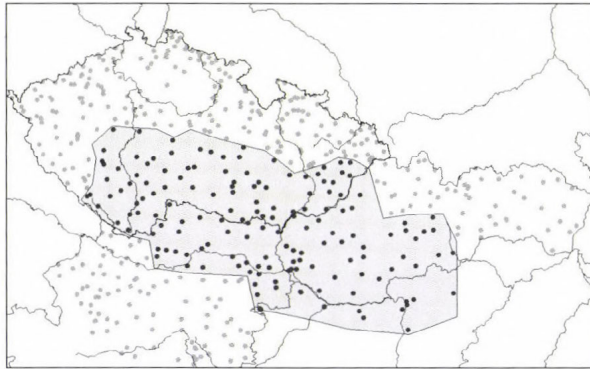


*Fig. 1.* CECILIA Central European domain (shaded area) with available climatological stations (dark/light dots for stations inside/outside the domain).

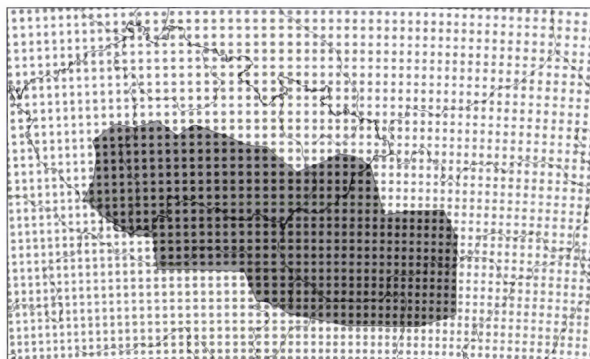


*Fig. 2.* Grid points of ALADIN-CLIMATE/CZ (dark/light dots) available within/outside the CECILIA Central European domain (shaded area).

Table 2. Number of stations, available per individual country (AT – Austria, CZ – Czech Republic, SK – Slovakia, HU – Hungary) and meteorological element (see Table 1 for explanatory notes)

Country	Element				
	TMA	TMI	SRA	SSV	H
AT	33	33	35	11	30
CZ	90	90	90	68	91
SK	39	39	39	39	40
HU	11	11	11	6	11
Total	173	173	175	124	172

### 3. Data quality control

Before the station technical series and gridded dataset were calculated, raw station data had been subjected to thorough quality control using AnClim and ProClimDB softwares (Štěpánek, 2007; more details can be found in the documentation of the softwares at [www.climahom.eu](http://www.climahom.eu)). Tools available in the softwares were designed so that they could be used for the automated finding of errors in datasets. The outliers were found by a combination of several methods: the percentage of neighbor stations which are significantly ( $p=0.05$ ) different from the base station (found from standardized differences between neighbors and base station, the limit value is more than 75%); the difference of the base station value and the median calculated from values of neighbors standardized to the base station altitude (using linear regression) divided by standard deviation of the base station, expressed as CDF of normal distribution (the limit value is more than 0.95); the coefficient (multiple) of distance of the base station value above (below) the upper (lower) quartile calculated from the standardized (to the base station altitude) values of neighbor stations (the higher the value, the more similar neighbor values are compared to the base station value, the limit value is a coefficient higher than 5); the difference from the expected value (details on its calculation are given in Section 4); and the median calculated from the original values of neighbor stations divided by the standard deviation of the base station values (expressed as CDF of normal distribution, the value should be low, otherwise it indicates that the calculation of the expected value is probably wrong, the limit value is less than 0.75). The calculation was carried out for each meteorological element and individual day separately (Štěpánek *et al.*, 2009).

Table 3 shows an example of the suspicious values found. Such values were found in all the available raw datasets (Austria, Czech Republic, Slovakia, and Hungary, their numbers are given in Table 4) and were withdrawn from further processing, replaced with a code for missing value.

Table 3. Output from the ProClimDB software with an example of suspicious values found in the raw dataset (gray column) compared to values of five neighbor stations (five rightmost columns)

Element	Station				Suspected value	Expected value	Remark	Neighboring stations				
	ID	Year	Month	Day				9900	13301	9811	15900	16000
TMIN	10000				492.0		Altitude	648.0	480.0	695.0	810.0	842.0
TMIN							Distance	22.0	43.1	50.1	56.9	62.7
TMIN	10000	1961	3	18	8.0	-1.8		-2.9	-1.7	-1.5	-1.8	-2.0
TMIN	10000	1962	4	22	10.0	2.9		1.1	3.2	3.8	3.1	4.0
TMIN	10000	1962	4	23	13.0	0.9		0.1	1.3	1.8	0.6	2.8
TMIN	10000	1962	5	22	7.0	1.1		1.3	0.8	2.9	0.7	1.4
TMIN	10000	1962	7	21	13.0	8.4		7.4	8.6	9.1	8.5	9.0
TMIN	10000	1963	5	30	10.6	3.3		3.1	3.3	4.1	2.7	3.2
TMIN	10000	1964	1	5	-10.0	-18.5		-19.7	-18.4	-16.5	-16.4	-17.0
TMIN	10000	1968	4	15	5.0	-0.6		-1.3	-0.5	0.6	-1.4	-1.4
TMIN	10000	1975	4	6	9.4	4.0			4.2	2.1	2.1	2.2
TMIN	10000	1976	2	8	-1.2	-8.9			-9.0	-7.9	-6.9	-8.3

Table 4. Numbers of suspicious values (evident errors) per country and meteorological element (see Table 1 for explanatory notes)

Country	Absolute numbers					Country	Relatively per number of stations				
	Element						Element				
	TMA	TMI	SRA	SSV	H		TMA	TMI	SRA	SSV	H
AT	28	74	195	309	118	AT	0.85	2.24	5.57	28.09	3.93
CZ	36	157	489	910	498	CZ	0.40	1.74	5.43	13.38	5.47
SK	8	37	72	975	346	SK	0.21	0.95	1.85	25.00	8.65
HU	1	10	33	374	201	HU	0.09	0.91	3.00	62.33	18.27
<b>Total</b>	<b>73</b>	<b>278</b>	<b>789</b>	<b>2568</b>	<b>1163</b>	<b>Total</b>	<b>0.42</b>	<b>1.61</b>	<b>4.51</b>	<b>20.71</b>	<b>6.76</b>

The data quality checked datasets were further used in the calculation of the station technical series and the gridded dataset.

#### 4. Calculation of station technical series and gridded dataset

Several methods can be used to calculate the values of a given meteorological element at a certain geographical position (e.g., at a grid point). Inverse distance weighting is among the more simple methods, but it still gives good results, even when compared to modern geostatistical methods such as kriging, co-kriging, and universal kriging (Kliegrová *et al.*, 2007). As weights, inverse distance or correlation may be used (Isaaks and Srivastava, 1989), possibly powered to account for lower or higher spatial correlations of a given meteorological element. Applying geostatistical methods to time series is not an easy task (mainly due to the computational demands), but some attempts that combine

time and spatial analysis already exist (e.g., *Szentimrey*, 2002; *Květoň* and *Tolasz*, 2003), and such methods have recently begun to be more widely used.

As mentioned above, daily series of several meteorological elements for hundreds of locations (grid points) were to be calculated. Utilizing a GIS environment for a task such as this would be advantageous, because it provides the potential for choosing from a variety of interpolation methods. Nonetheless, current GIS environments (e.g., ArcMap, ESRI ArcView, ArcGIS) are not designed for the easy retrieval of information for time series (calculation for each time step). This is why we needed to create our own tool with enough automation to carry out the task. The software ProClimDB (*Štěpánek*, 2007) was extended for the computation. This software is freely available.

After quality control (see the previous section), the technical series of daily values at a particular grid point (station location) were calculated from up to 6 neighboring (nearest) stations within a distance of 300 km, with an allowed maximum difference in altitude of 500 m. Before applying inverse distance weighting, data at the neighbor stations were standardized relatively to the altitude of the base grid point (station location). The standardization was carried out by means of linear regression and dependence of values of a particular meteorological element on altitude for each day, individually and regionally. Each standardized value was checked to ascertain it did not differ excessively from the original value (providing CDF did not exceed 0.99; in such a case, linear regression was not regarded a good model and an original, i.e., not standardized value, was used for further calculation). In the case of precipitation, neighbors with original values equal to zero were not standardized. For the weighted average (using inverse distances as weights), the power of weights equal to 1 (all meteorological elements except precipitation) and 3 (precipitation) were applied. In the case of temperatures, standardized neighbor values outside the 20% to 80% percentile range were not considered in the calculation of final values (i.e., trimmed mean was applied).

Originally, the “raw” station data (but with suspicious values removed), i.e., series with gaps and also series not available in the whole period of 1961–2000, were used for the calculation of technical series at both stations and grid points. Even if the statistical properties of the original measured data were preserved (like moments) in calculated technical series (calculated for each day separately), some of the time series showed inhomogeneities, which could be resulted from either the inhomogeneity of the original station data or from the method of calculation: if some stations measured only for a short time, the selection of neighbors varies in time. To avoid inhomogeneities of this kind, we proceeded as follows: first, missing values were filled in original station data series; second, for station series with filled gaps, station technical series were calculated, applying standardization of neighbors to base station altitude (estimated using linear regression for the neighboring region, for each month individually), thus, all stations were extended to have values in the whole period

of 1961–2000; third, only these equally long station technical series were used for the calculation at grid points.

The altitudes applied in the calculation of grid point series were the actual altitudes, read from a 1 km resolution model of the terrain. However, for the purposes of RCM validation, it would be better to read altitudes of a smoothed terrain (e.g., low-pass filter smoothing for a square of  $20 \times 20$  km or  $10 \times 10$  km) to characterize the vicinity of a grid point, much the same as in RCMs. The same is valid for the power of weights (inverse distances). Applying the power of about 0.5 (square root) better characterizes a wider vicinity of a grid point. The goal was, however, to create technical series at a station or grid point and to preserve the statistical characteristic of the particular point. Thus, it is reasonable to say that the calculated series provide point-specific data rather than area-aggregated data. Another reason is that the area of aggregation varies among different climate models (model resolution). The technical series should be used for validation of RCMs with caution.

The settings of parameters of the technical series calculation differ among individual meteorological elements. The next section describes the best solution for each meteorological element with an example of selected stations in the Czech Republic.

### ***5. The best settings in the calculation of station technical series and gridded datasets***

The parameter settings for station technical series and the gridded dataset differ for various meteorological elements. The “ideal” setting of parameters was determined by using four base stations in the area of the Czech Republic. Because stations were chosen so they would represent different climatological conditions, both lowland and highland stations were chosen, as well as stations both at the eastern and western edge of the area so as to capture differences between the more maritime and continental weather regimes which manifest across the Czech Republic. The four selected base stations, with their neighbor stations, are displayed in *Fig. 3*, the information on the base stations is provided in *Table 5*. The parameters were tuned by comparing original and calculated values using various verification criteria.

Altogether, 11 various parameters were tested in ProClimDB individually to find the “ideal” setting for all the required meteorological elements: maximum and minimum temperature, relative humidity, precipitation, and sunshine duration. Daily values of the meteorological elements in the period of 1991–2007 were used. The changed (controlled) parameters were: transformation of input values (log, square root, etc.); standardization of neighbor station values to monthly averages (and/or standard deviations) at a base station, standardization of neighbor stations to the altitude of the base station (this case can also be

controlled by calculating regression for the whole period – monthly, or for each time step individually, to set the behavior in the case of only one station being present in a given time, and the correction coefficient for regression to control the dependence on altitude); a check whether standardized values become outliers or not; the power of weights for calculation of a new (“expected”) value; applying trimmed mean when a new value is calculated (and setting the limits in such a case).

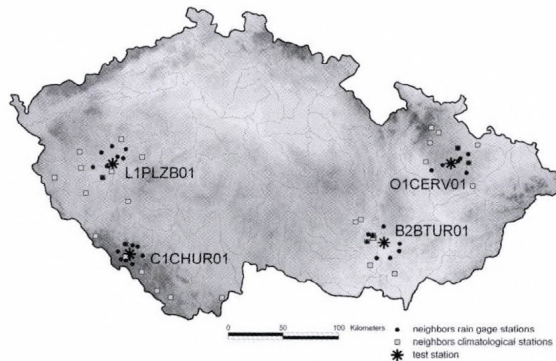


Fig. 3. Four base stations (marked with an asterisk) and their neighbors (different for precipitation and climatological stations shown in black and grey, respectively) used for the verification of calculated technical series.

Table 5. Base stations used for the verification of calculated technical series

Name	ID	Latitude	Longitude	Altitude
Brno-Tuřany	B2BTUR01	49.1597	16.6956	241.00
Plzeň-Bolevec	L1PLZB01	49.7892	13.3867	328.00
Červená	O1CERV01	49.7772	17.5419	750.00
Churáňov	C1CHUR01	49.0683	13.6131	1118.00

It was more difficult to find a solution for precipitation and relative humidity than for the other meteorological elements. Unfortunately, it seems impossible to get 100% realistic values during the calculation (e.g., non-negative relative humidity and precipitation). The unrealistic values are caused mainly by poor quality of raw station data, insufficient length of series at neighbor stations (time gaps simultaneous at several neighbor stations diminish the number of values used for regression), and a greater difference in altitudes of stations used in the regression model. These factors can be controlled to some extent. The input data were controlled for quality before calculation (see previous section). Stations allowed for the calculation can be filtered to retain only those with a certain minimum length and without longer time gaps. The third factor – the

difference in altitudes – is not easy to cope with, since we selected the nearest neighbours for the calculation, which, e.g. in the case of precipitation, seems to be the only solution (the selection of the nearest and best correlated stations is the same, while for temperatures, one could also select neighbor stations according to correlations). Problems were especially evident with the mountain station (Churáňov), since its altitude is higher than that of its neighbors and, thus, extrapolation instead of interpolation must be used.

The setting of parameters for maximum temperature, minimum temperature, relative humidity, and sunshine duration is similar to some extent. For station technical series, the neighbor station values were standardized to the base station average and standard deviation using the whole period, within each month individually (in this case we fill gaps in station measurements and this helps to avoid the introduction of inhomogeneities into the series), whereas for the gridded dataset, values were standardized to the altitude of the base station using linear regression estimated for each day individually (which is a better solution, e.g., in case of days with inversions). During the calculation, checks were done to determine that standardized values do not differ too much from the original values. For a value larger than 0.99 (CDF), the original values were used for further calculations: lower settings of 0.95 or 0.90 lead to much worse results. The power for weights (inverse distance) was taken as 1. For maximum and minimum temperature, trimmed mean was applied for calculations of the “expected” value with quantile limits of 20% and 80%. An example of the difference between the original and calculated values of the maximum temperature is shown in *Fig. 4*. It is evident, that stations in lower altitudes show a weak annual cycle of RMSE (root mean square error applied on the calculated and original values). On the contrary, the mountain station of Churáňov reaches very high values of RMSE during winter; the different behavior can be explained by the frequent occurrence of temperature inversions when the lowland stations used for the calculation have substantially different weather conditions.

For the calculation of the technical series of precipitation, a standardization to altitude for the whole period (station technical series), or applied individually for each day (gridded dataset) was again carried out. The difference from previous settings is that the power for weight was set to 3 to reflect lower spatial correlations of precipitation, and a trimmed mean is not applied. No transformation of input values (e.g., logarithms) was performed, since it gave poorer results. The average difference (bias between original and calculated values) for precipitation at Brno-Tuřany is 0.0 mm; in most months it does not exceed 0.1 mm. The highest difference occurs for June, 0.27 mm. RMSE values are highest for summer months as well. Precipitation is influenced by local effects much more than the other meteorological elements, and even at adjacent sites, there can be great differences (in some cases, a 30 to 60 mm precipitation amount is observed at two neighbor stations, while the other two stations record

no precipitation at all). For this reason, the correlation coefficient is lower, only 0.875. From the scatter plot (Fig. 5, left) we can see several outliers which influence the value of the correlation coefficient. Looking at the histogram (Fig. 5, right), we can see that 62% of values differ only negligibly.

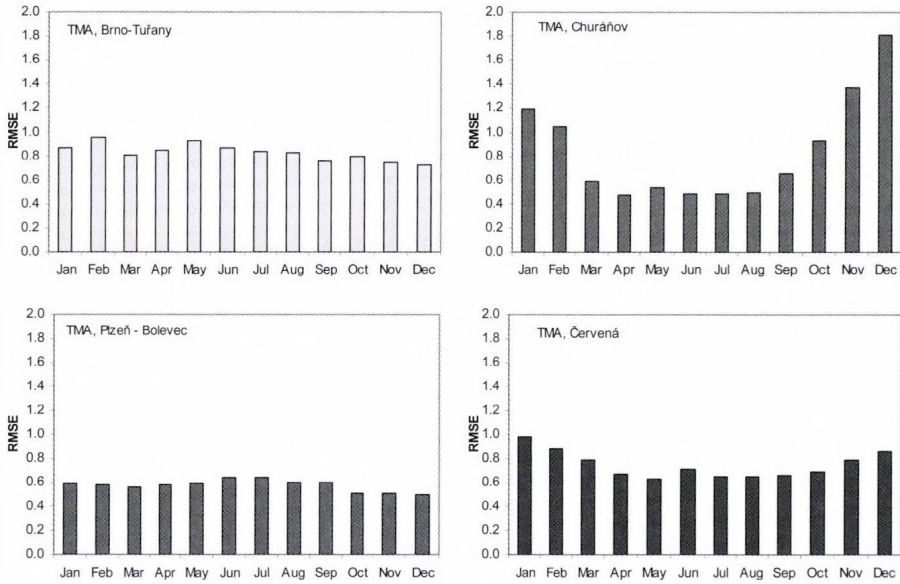


Fig. 4. RMSE (in °C) for four base (tested) stations and maximum temperature.

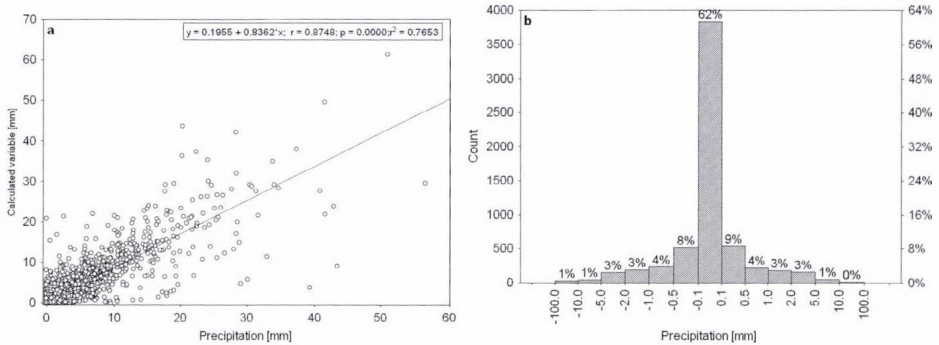


Fig. 5. Scatter plot for calculated and original values of precipitation (left) and histogram of differences between the calculated and original values (right) at station Brno-Tuřany.

More detailed information on the optimal settings found and used in the ProClimDB software is contained within the ProClimDB software documentation, which can be downloaded together with the software itself.

## 6. Summary

Interpolation techniques can solve many tasks required during data processing. In this work we have shown their application to daily data for various meteorological elements. The technique described is quite general, so that it can be applied to different tasks, such as data quality control (finding suspicious values), filling gaps in the series, or calculation of a new series for a new location. As it can be seen from the given examples of verification results, the calculated station technical series and gridded datasets do very well at reflecting the behavior of the measured values of the processed meteorological elements (maximum and minimum temperature, relative humidity, precipitation, sunshine duration), which make the series capable of being utilized for various purposes, such as a development and calibration of various methods of statistical downscaling, usage in impact studies (since the final network density is much higher than that of the original station network and is, moreover, regular), for a comparison with national datasets (border discrepancies), where available, etc.

*Acknowledgements*—The present work was supported by the European Commission under Contract 037005 (CECILIA) and the Czech Science Foundation under project 205/08/1619. The following persons are acknowledged for assistance in obtaining the original data: *Tomáš Hlásny*, Forest Research Institute, Zvolen, Slovakia; *Herbert Formeyer*, University of Environmental Sciences, Vienna, Austria, and *Monika Lakatos*, Hungarian Meteorological Service, Budapest, Hungary.

## References

- Farda, A., Štěpánek, P., Halenka, T., Skalák, P., Belda, M., 2007: Model ALADIN in climate mode forced with ERA40 reanalysis (coarse resolution experiment). *Meteorologický časopis* 10, 123–130.
- Isaaks E., Srivastava R., 1989: *An Introduction to Applied Geostatistics*. Oxford University Press, New York, 561 pp.
- Kliegrová, S., Dubrovský, M., Metelka, L., 2007: Interpolation methods of weather generator parameters. Program & Abstracts. *10th International Meeting on Statistical Climatology*, Beijing, China, August 20–24, 2007, 122–123.
- Květoň, V., Tolasz, R., 2003: *Spatial Analysis of Daily and Hourly Precipitation Amounts with Respect to Terrain*. <http://www.map.meteoswiss.ch/icam2003/468.pdf>
- Skelly, W.C., Henderson-Sellers, A., 1996: Grid box or grid point: What type of data do GCMs deliver to climate impacts researchers? *Int. J. Climatol.* 16, 1079–1086.
- Štěpánek, P., 2007: *ProClimDB – software for processing climatological datasets*. CHMI, regional office Brno. <http://www.climahom.eu/ProcData.html>.
- Štěpánek, P., Zahradníček, P., Skalák, P., 2009: Data quality control and homogenization of the air temperature and precipitation series in the Czech Republic in the period 1961–2007. *Adv. Sci. Res.* 3, 23–26.
- Szentimrey, T., 2002: *Statistical Problems Connected with the Spatial Interpolation of Climatic Time Series*. Home page: <http://www.knmi.nl/samenw/cost719/documents/Szentimrey.pdf>

# IDŐJÁRÁS

*Quarterly Journal of the Hungarian Meteorological Service*  
Vol. 115, No. 1–2, January–June 2011, pp. 99–109

## **Application of gridded daily data series for calculation of extreme temperature and precipitation indices in Hungary**

**Mónika Lakatos<sup>\*</sup>, Tamás Szentimrey, and Zita Bihari**

*Hungarian Meteorological Service,  
P.O. Box 38, H-1525 Budapest, Hungary  
E-mails: szentimrey.t@met.hu; bihari.z@met.hu*

*<sup>\*</sup>Corresponding author; E-mail: lakatos.m@met.hu*

*(Manuscript received in final form March 8, 2011)*

**Abstract**—The calculation of extreme climate indices defined by several international projects requires homogeneous time series. To this effect, long term daily extreme temperatures and daily precipitation sums were homogenized, quality controlled, and further processed by the method MASH (Multiple Analysis of Series for Homogenization). After homogenization of station observation series, a gridding procedure was performed on the daily observations by the method MISH (Meteorological Interpolation based on Surface Homogenized Data Basis). The idea behind the MISH interpolation scheme stems from the following principles: gridded data can be created (interpolated) at higher quality with respect to certain climate statistical parameters; and these parameters can be modeled by using the long climate data series. In the MISH procedure, the modeling of the statistical parameters for a given location is based on the long term homogenized monthly data of neighboring stations.

In this paper, we present the computations of extreme temperature and precipitation climate indices for the period of 1901–2009 using datasets which were processed by the above homogenization and gridding algorithms. The obtained trends of several extreme indices as well as their spatial distributions are demonstrated on graphs and maps.

*Key words:* extreme climate indices, data homogenization, data interpolation, climate of Hungary

### ***1. Introduction***

The study of climate extremes in a changing climate has come to the fore in recent years. The most common way to detect changes is the analysis of extreme climate indices, which are defined by several international projects (*Alexander et al.*, 2006). Groups, such as the World Meteorological Organization (WMO)

CCI/CLIVAR Expert team on Climate Change Detection and Indices (ETCCDI), the European Climate Assessment (ECA), and the Asia-Pacific Network (APN) have aimed to provide a framework for defining and analyzing the observed climate extremes. Climate index calculations require quality controlled, homogeneous time series, and the analysis of the results requires a consistent approach (*Wijngaard et al.*, 2003). The global and also the regional studies have focused primarily on the analysis of long term daily temperature and precipitation data (*Frich et al.*, 2002; *Haylock et al.*, 2008), as these climate variables are the most widely available ones. The majority of long data series is inhomogeneous, and often contains shifts in the mean or in the variance due to non-climatic factors, such as site-relocations, changes in instrumentation or in observing practices. Inhomogeneities can distort the true climatic signal, homogeneity testing is important for climate change studies (*van Engelen et al.*, 2008). Amongst the observation series there are good quality data as well, but sorting them out requires the execution of a homogenization procedure first (*Aguilar et al.*, 2003). Neglecting the inhomogeneous series causes a huge loss of valuable information.

Studying the spatio-temporal changes of extremes can be implemented through the analysis of observations reliable in time and space. The spatial interpolation of extreme indices is a difficult task as the distribution functions of the several derived values are unknown. However, the basic variables, such as temperature and precipitation can be gridded by the knowledge of their statistical properties, thus, higher quality gridded datasets can be constructed for further analysis. The main steps of creating the homogenized, gridded dataset for computation of extreme indices are presented in this paper. The changes of such indices for Hungary from the mid-20th century to present are illustrated and shortly analyzed on graphs and trend maps.

## **2. Data and methods**

### *2.1. Homogenization*

The computations implemented in this work are based on long term daily data in the period of 1901–2009. Daily maximum and minimum temperatures of 15 observation stations and daily precipitation sum of 58 precipitation stations were taken into account in the analysis. In the preparation phase, homogenization and quality control of the daily measurements were carried out. The homogenization of data was performed with the procedure MASH (*Szentimrey*, 1999). All the MASH options except the metadata information were used in this paper.

### *2.2. The main features of MASHv3.02*

The MASHv3.02 (*Szentimrey*, 2007) software consists of two parts.

Part 1: Quality control, missing data completion, and homogenization of monthly series:

- Relative homogeneity test procedure.
- Step by step procedure: the role of series (candidate or reference series) changes step by step in the course of the procedure.
- Additive (e.g., temperature) or multiplicative (e.g., precipitation) model can be used depending on the climate elements.
- Providing the homogeneity of the seasonal and annual series as well.
- Metadata (probable dates of break points) can be used automatically.
- Homogenization and quality control (QC) results can be evaluated on the basis of verification tables generated automatically during the procedure.

Part 2: Homogenization of daily series:

- Based on the detected monthly inhomogeneities.
- Including quality control (QC) and missing data completion for daily data. The quality control results can be evaluated by test tables generated automatically during the procedure.

The importance of homogenization is demonstrated in *Fig. 1* which show the annual number of frost days (daily minimum is below zero) for Szeged station using original and the homogenized daily minimum temperatures. Both the magnitude and the sign of the estimated linear trend are different in the two cases.

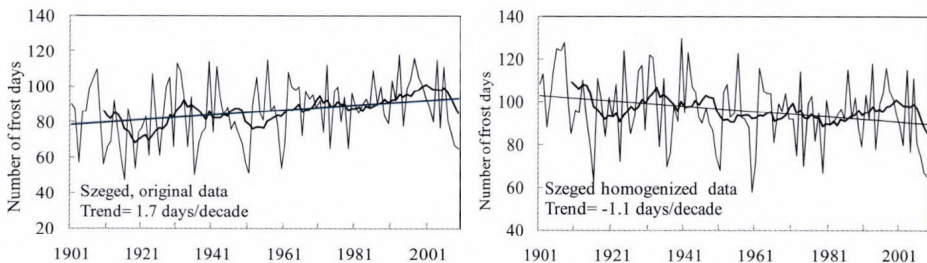


*Fig. 1.* Annual number of frost days for Szeged station with the fitted linear trend as well as the 10-year moving average in the period of 1901–2009 using the original (left) and homogenized (right) data.

### 2.3. Gridding

To obtain the high quality, good resolution dataset, a gridding procedure was performed on the homogenized daily series. According to the representativity examinations in the interpolation section, which were performed during this work, the expected interpolation errors may be accepted with using the predictor

network of 15 temperatures and 58 precipitation station data series. The MISH interpolation method is a proper choice for this purpose. The MISH procedure was developed at the Hungarian Meteorological Service especially for interpolation of meteorological data (*Szentimrey and Bihari, 2007a*). It is based on the principles that the gridded data can be derived (interpolated) at a higher quality if we know certain climate statistical parameters. For example, in the case of normal distribution the means and the covariance structure unambiguously determine the optimal interpolation formula. Long climate data series allow modeling of these statistical parameters. Thus, the modeling for a given location is based on the statistical features of the long term homogenized monthly data of neighboring stations.

#### 2.4. The main features of MISHv1.02

The software MISHv1.02 (*Szentimrey and Bihari, 2007b*) consists of two units, the modeling and the interpolation systems. The interpolation system can be operated on the output of the modeling system. The attributes of the MISHv1.02 software can be summarized as follows:

Modeling system for climate statistical parameters in space:

- Based on long homogenized data series and supplementary deterministic model variables, e.g., topography.
- Cross-validation test for interpolation error or representativity.
- Modeling procedure must be executed only once before the interpolation applications!

Interpolation system:

- Additive (e.g., temperature) or multiplicative (e.g., precipitation) model and interpolation formula can be used depending on the climate elements.
- Daily, monthly values and many years' means can be interpolated.
- Few predictors are also sufficient for the interpolation.
- The interpolation error or representativity is modeled too.
- Capability for application of supplementary background information (stochastic variables), e.g., satellite, radar, forecast data.
- Capability for gridding of data series.

Gridding system:

- Interpolation, gridding of monthly or daily station data series for given predictand locations. In case of gridding, the arbitrarily chosen predictand locations are the nodes of a relatively dense grid.

Contrary to geostatistical methods, the values of variograms must be modeled for each interpolating processes (*Szentimrey et al., 2007*). One of the

most important advantages of the MISH is that the modeling part must be executed only once before the gridding of the data on different timescales, such as daily, monthly, seasonal, or other. Additionally, different station networks can be used in the modeling and in the gridding parts. The modeling part of the MISH procedure is executed on a relative dense,  $0.5^{\circ} \times 0.5^{\circ}$  resolution grid.

In order to calculate extreme indices, the MISH gridding part was performed on homogenized daily observations for a  $0.1^{\circ} \times 0.1^{\circ}$  grid. The implementation of the MISH gridding procedure resulted in a high quality, homogenized, gridded daily maximum and minimum temperature and daily precipitation datasets with a  $\sim 10$  km spatial resolution (1104 grid points) in the period of 1901–2009 for Hungary.

### 3. Climate indices calculations on the gridded dataset

The extreme indices used in this study are based on the CECILIA (Central and Eastern Europe Climate Change Impact and Vulnerability Assessment) project definitions. In the framework of CECILIA project, numerous indices were defined (74 temperature and 55 precipitation indices) on different time scales, i.e., yearly, seasonal and monthly (Hirschi, 2008). All of them were implemented for Hungary on homogenized data for observation stations and also for gridded datasets for the whole examined long period. A few selections of the CECILIA extreme indices are presented in this work on yearly scale (Table 1).

Table 1. Extreme indices used in this study

Index	Unit
Summer days: $T_{\max} > 25^{\circ}\text{C}$	%
Hot days: $T_{\max} \geq 30^{\circ}\text{C}$	%
Frost days: $T_{\min} < 0^{\circ}\text{C}$	%
Warm nights: $T_{\min} > 20^{\circ}\text{C}$	%
Number of wet days: daily precipitation $> 1$ mm	days
Percentage of days $> 20$ mm precipitation	%
Greatest 1-day total rainfall	mm
Greatest 5-day total rainfall	mm
Simple daily intensity: precipitation sum/number of wet days	mm/day
Consecutive dry days: maximum number of consecutive days when the daily precipitation $< 1$ mm	days

The computational techniques used in the course of index calculations can lead to differences in the results. To obtain comparable results for larger regions, we have to make sure to use the same definition and algorithm. It is particularly important in the case of indices based on percentiles (Alexander and Arblaster, 2009).

With the help of homogenization, gridding, and extreme index calculation procedures, a high quality, good resolution dataset of the long-term series of indices can be generated and stored. These index datasets can form the basis of further examinations, such as trend estimation and mapping of changes.

#### **4. Graphs and maps based on homogenized gridded data**

The course of several temperature and precipitation extreme indices, from the beginning of the 20th century can be followed up in *Figs. 2–4*. Grid point averages represent the countrywide average. The increasing warm temperature extremes coincide with the warming tendencies in the region (*van Engelen, 2008*). The percentage of hot days and that of the warm nights have intensely increased since the early eighties. The presence of more warm nights is also obvious from 1901. The greatest 5-day total rainfall and the days with above 20 mm precipitation show a slight increasing in the last intense warming from eighties. The simple daily intensity index indicates that the rate of the intense rainfall events has increased in summer. The length of the longest dry spell became shorter recently, but considering the whole period, some increase is apparent.

The IPCC Fourth Assessment Report (*IPCC, 2007*) established the features of recent trends of extreme weather events from the late 20th century, in some cases typically after 1960. The trend maps in *Figs. 5–10*, which illustrate the changes of some extreme indices in Hungary, cover the time period 1961–2009 to allow the comparability with other well-known international studies like IPCC. The estimated grid point changes are depicted by linear trend fitting on the corresponding maps. The fitted linear trends were tested on station data and grid point series data as well. In extensive regions of the country, the number of frost days decreased (*Fig. 5*). White areas in *Fig. 5* represent the regions where the changes are not significant at 0.1 probability level. The obvious warming trend is indicated in the percentage of summer days (*Fig. 6*). Beside the point estimation of the slope, confidence intervals were constructed to the estimated trend at different significance levels. *Fig. 7* consists of two maps, according to the bounds of the 0.1 significance confidence interval. The lower bound illustrates the minimum change and the upper bound signifies maximum change occurred in the examined period. Maps of *Figs. 8–10* show the spatial trend of some extreme precipitation climate indices. The number of wet days decreased in Hungary, except for a small region of the country in the northeast (*Fig. 8*). The change in the greatest 1-day total rainfall varies from –15 mm to +10 mm. Regions with growing 1-day precipitation lie mainly to the East from the Danube. The daily precipitation intensity increased in summer. It means that the proportion of the heavy precipitation events in the total rainfall increases over most areas in Hungary

(Fig. 10). Regarding the past 50 years the precipitation changes were not significant in extensive regions of the country, according to the applied hypothesis testing.

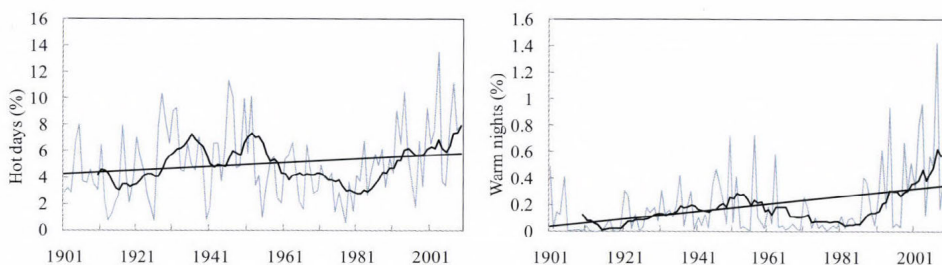


Fig. 2. Grid point average of the yearly percentage of hot days (left) and warm nights (right) with the fitted linear trend as well as the 10-year moving average in the period of 1901–2009 for Hungary.

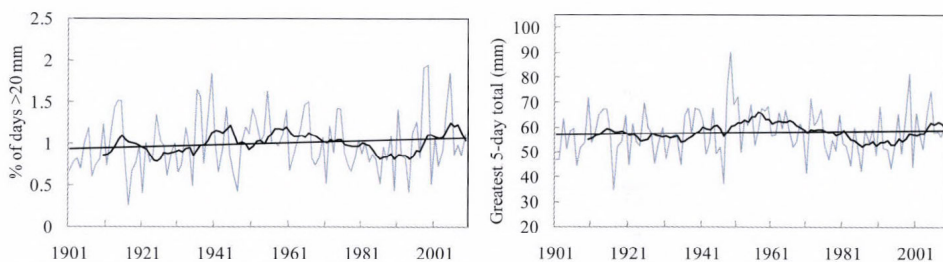


Fig. 3. Grid point average of the yearly percentage of days with above 20 mm (left) and the greatest 5-day precipitation (right) with the fitted linear trend as well as the 10-year moving average in the period of 1901–2009 for Hungary.

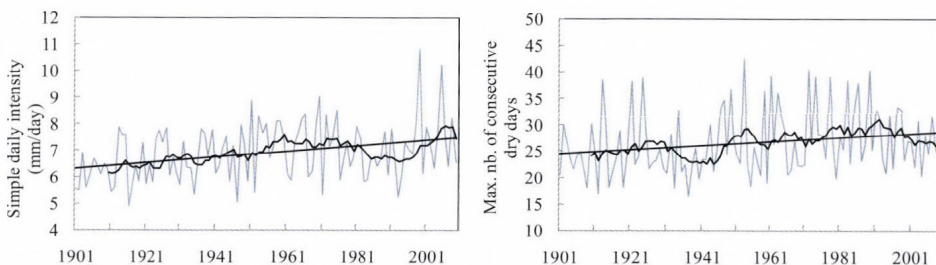


Fig. 4. Grid point average of the daily precipitation intensity index in summer (left) and the maximum number of consecutive dry days (right) with the fitted linear trend as well as the 10-year moving average in the period of 1901–2009 for Hungary.

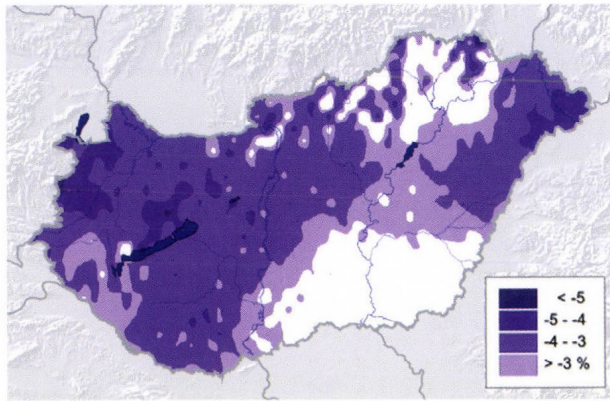


Fig. 5. Change (%) in the number of frost days in the period of 1961–2009. White color indicates no significant change on 0.1 confidence level.

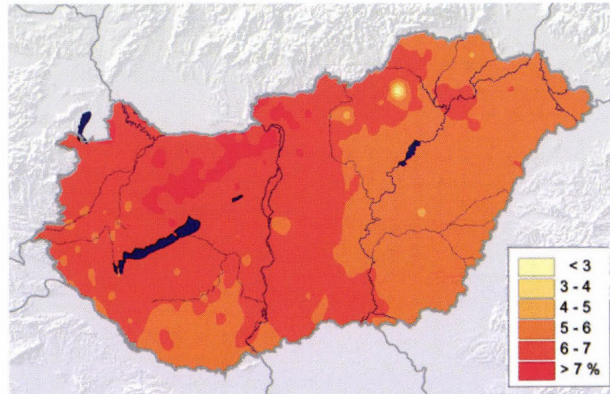


Fig. 6. Change (%) in the number of summer days in the period of 1961–2009.

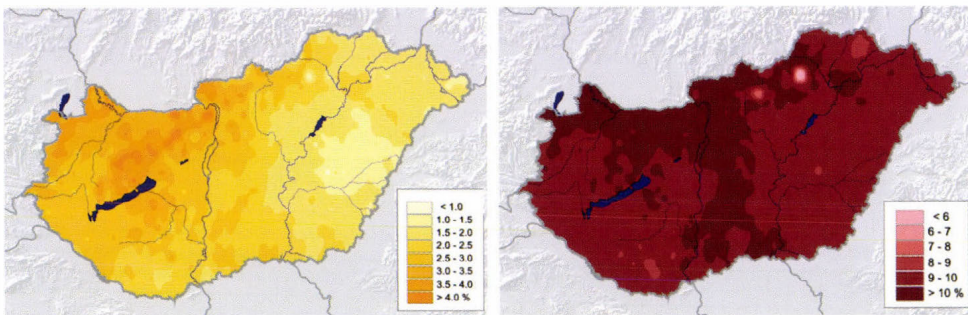


Fig. 7. Change (%) in the minimal (left) and maximal (right) number of summer days according to the 0.1 confidence interval bounds in the period of 1961–2009.

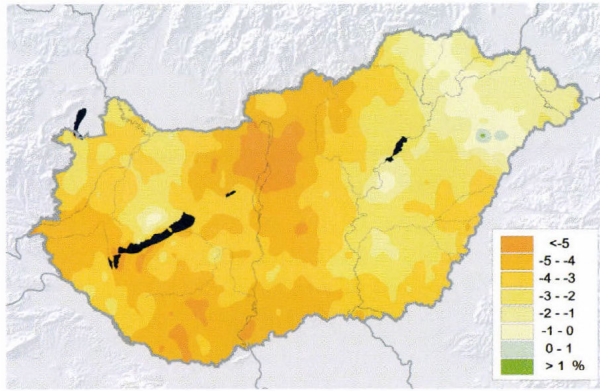


Fig. 8. Change (%) in the number of wet days in the period of 1961–2009.

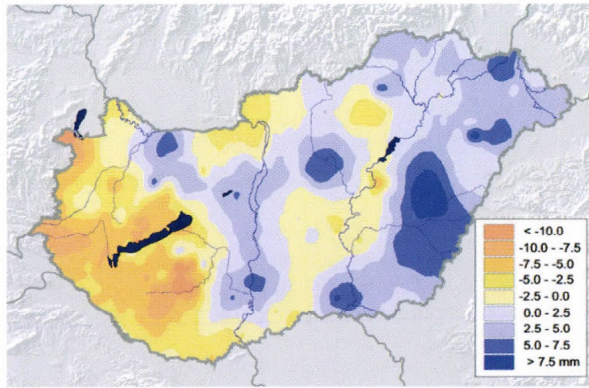


Fig. 9. Change (mm) in the greatest 1-day total rainfall in the period of 1961–2009.

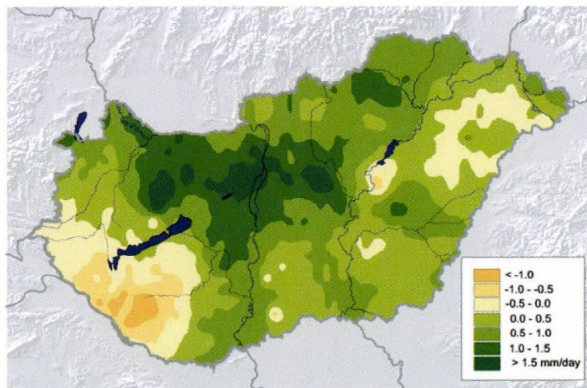


Fig. 10. Change (mm/day) in the summer simple daily precipitation intensity in the period of 1961–2009.

## 5. Conclusions

The preparation of a high quality, homogenized, and gridded daily datasets was presented in this study. Long term daily temperature extremes and precipitation data were quality controlled, homogenized, and gridded in the period of 1901–2009, in order to analyze the extreme climate indices. Instead of the interpolation of extreme indices, the gridding of the basic variables (daily maximum and minimum temperatures and daily precipitation) is recommended, as the probability distributions of the indices are unknown. Time series of the grid point averages for a few selected indices are demonstrated from 1901. The spatial distribution of changes from the mid-20th century is illustrated on trend maps.

The gridded dataset introduced in this work is updated by homogenization and interpolation on the beginning of the new calendar year regularly to serve as an 'as long as possible' time series for climate change studies. The WMO statement on the status of the global climate in 2009 (WMO, 2010) underlined that peer reviewed scientific methods for quality control, homogenization, and interpolation to constitute high-quality global climate datasets should be used in the examinations. The created datasets could be relevant contribution to the expected high quality global system of datasets.

## References

- Aguilar, E., Auer, I., Brunet, M., Peterson, T.C., and Wieringa, J., 2003: Guidelines on climate metadata and homogenization. In *WCDMP No. 53 – WMO/TD-No. 1186*.
- Alexander, L.V. and Arblaster, J.M., 2009: Assessing trends in observed and modeled climate extremes over Australia in relation to future projections. *Int. J. Climatol.* 29, 417-435.
- Alexander, L.V., Zhang, X., Peterson, T.C., Caesar, J., Gleason, B., Klein Tank, A.M.G., Haylock, M., Collins, D., Trewin, B., Rahimzadeh, F., Tagipour, A., Ambenje, P., Rupa Kumar, K., Revadekar, J., and Griffiths, G., 2006: Global observed changes in daily climate extremes of temperature and precipitation. *J. Geophys. Res.* 111, doi:10.1029/2005JD006290.
- Frich, P., Alexander, L.V., Della-Marta, P., Gleason, B., Haylock, M., Klein Tank, A.M.G., and Peterson, T., 2002: Observed coherent changes in climatic extremes during 2nd half of the 20th century. *Climate Research* 19, 193-212.
- Haylock, M.R., Hofstra, N., Klein Tank, A.M.G., Klok, E.J., Jones, P.D., and New, M., 2008: European daily high-resolution gridded dataset of surface temperature and precipitation for 1950-2006. *J. Geophys. Res.* 113, D20119, doi:10.1029/2008JD010201.
- Hirschi, M., Stepanek, P., Seneviratne, S.I., Christensen, O.B., and CECILIA WP4 members, 2008: CECILIA climate indices: Analysis of temperature extremes in Central and Eastern Europe. In *General Assembly of the European Geosciences Union (EGU)*, EGU2008-A-09640.
- IPCC, 2007: Climate Change 2007. The Scientific Basis, Contribution of Working Group I to the Fourth Assessment Report of the Intergovernmental Panel on Climate Change (IPCC). Solomon, S., D. Qin, M. Manning, Z. Chen, M. Marquis, K.B. Averyt, M. Tignor and H.L. Miller (eds.), Cambridge University Press, UK, 946 pp.
- Szentimrey, T., 1999: Multiple Analysis of Series for Homogenization (MASH). In *Proceedings of the Second Seminar for Homogenization of Surface Climatological Data*, WMO, WCDMP-No. 41, 27-46.
- Szentimrey, T., 2007: Manual of homogenization software MASHv3.02, Országos Meteorológiai Szolgálat (Hungarian Meteorological Service), Budapest, p. 61.

- Szentimrey, T. and Bihari, Z., 2007a: Mathematical background of the spatial interpolation methods and the software MISH (Meteorological Interpolation based on Surface Homogenized Data Basis). In *Proceedings from the Conference on Spatial Interpolation in Climatology and Meteorology*. Budapest, Hungary, 2004. COST Action 719, COST Office, 2007, 17-27.
- Szentimrey, T. and Bihari, Z., 2007b: Manual of interpolation software MISHv1.02. Országos Meteorológiai Szolgálat (Hungarian Meteorological Service), Budapest, p. 32.
- Szentimrey, T., Bihari, Z., Szalai, S., 2007: Comparison of geostatistical and meteorological interpolation methods (what is what?). In *Spatial Interpolation for Climate Data – The Use of GIS in Climatology and Meteorology* (eds.: Hartwig Dobesch, Pierre Dumolard and Izabela Dyras). ISTE Ltd., London, UK, 284 pp, ISBN 978-1-905209-70-5, pp. 45-56.
- van Engelen, A., Klein Tank, A., van der Schrier, G., and Klok, L., 2008: European Climate Assessment & Dataset (ECA&D) Report 2008. In *Towards an Operational System for Assessing Observed Changes in Climate Extremes*. KNMI, De Bilt, The Netherlands.
- Wijngaard, J.B., Klein Tank, A.M.G., Konnen, G.P., 2003: Homogeneity of 20th century european daily temperature and precipitation series. *Int. J. Climatol.* 23, 679-692.
- WMO, 2010: WMO statement on the status of the global climate in 2009. WMO-No. 1055.



# IDŐJÁRÁS

*Quarterly Journal of the Hungarian Meteorological Service  
Vol. 115, No. 1–2, January–June 2011, pp. 111–120*

## **Spatial differentiation of the climatic water balance in Poland**

**Agnieszka Wypych<sup>1</sup> and Zbigniew Ustrnul<sup>1,2</sup>**

<sup>1</sup>*Department of Climatology, Jagiellonian University,  
7 Gronostajowa Str., 30-387 Krakow, Poland; E-mail: agnieszka.wypych@uj.edu.pl*

<sup>2</sup>*Institute of Meteorology and Water Management,  
14 Borowego Str., 30-215 Krakow, Poland; E-mail: zbigniew.ustrnul@uj.edu.pl*

*(Manuscript received in final form October 18, 2010)*

**Abstract**—Recent developments in GIS techniques have produced a wide range of powerful methods for capturing, modeling, and displaying of climate data. The main aim of the study was to identify an optimal interpolation method to describe the spatial differentiation of the climatic water balance in Poland based on meteorological data (temperature, precipitation, solar radiation) collected at 15 weather stations from 1986 to 2006. A climatic water balance index (*CWB*) was created based on a simplified definition, where it is interpreted as the difference between the precipitation total (*P*) and potential evapotranspiration (*PE*). The latter was calculated using the so-called Turc Equation. Four different spatial interpolation methods were used: (1) inverse distance weighting (*IDW*), (2) local polynomial (*LP*), (3) radial basis function (*RBF*), and (4) ordinary kriging. A subjective visual analysis of maps, root mean square error values, and coefficients of correlation indicated that the best *CWB* interpolation methods are the radial basis function method and the ordinary kriging method. However, spatial interpolation results suggest that the problem is more complex. Calculations performed for selected points of reference suggest that local geographic factors play an important role in the shaping of *CWB*. Such results also confirm the need to perform spatial climatic water balance analysis with special attention being paid to local conditions. Further research is needed that takes into account different temporal and spatial scales and aims to test established methods in other regions in Europe.

*Key-words:* spatial analysis, GIS, interpolation methods, climatic water balance, Poland

### ***1. Introduction***

Recent developments in GIS techniques have produced a wide range of powerful methods for capturing, modeling, and displaying of climate data. Advanced data processing methods allow for detailed analysis of climate elements on different temporal and spatial scales. GIS techniques designed to

map temperature and atmospheric precipitation fields have received the most attention thus far. However, researchers are often interested not in the meteorological elements themselves but in the information that can be extracted from them in the form of various indices, which are useful in the environmental and social sciences (Tveito *et al.*, 2008).

The *CWB* is a complex index that shows a climate-based assessment of the water resources in a given area. It focuses mainly on the difference between precipitation and potential evapotranspiration. Values of the index depend on many different variables such as solar radiation, relief, land use, and urban development. Spatial distribution of the climatic water balance appears to be very important in spatial management, agriculture, and hydro-climatological modeling. Since 2007, the Drought Monitoring System for Poland has been provided by the Institute of Soil Science and Plant Cultivation – State Research Institute in Pulawy. In the system, meteorological conditions that are causing drought are evaluated by the climatic water balance expressed by the difference between the precipitation and potential evapotranspiration (by Penman formulae). Nevertheless, it has not been the subject of detailed analysis thus far. Data covering any longer period is not readily available – especially evapotranspiration data – which creates the problem of index interpretation, especially due to its reliance on spatial differentiation. Therefore, the main aim of the study was to identify an optimal interpolation method to describe the spatial differentiation of the water balance in Poland taking into account a number of scale-based variables.

## ***2. Source material and methods***

Analyses of the climatic water balance are usually developed for regions where input data, mainly air temperature and precipitation, can be readily obtained from meteorological stations. The research presented herein is based on mean monthly values of air temperature as well as monthly solar radiation and precipitation totals. The data were obtained from 61 meteorological stations (temperature and precipitation) and 23 actinometric stations (solar radiation) for the 1951–2006 and 1986–2006 time periods, respectively. Not all meteorological stations collect actinometric data, which is why data was obtained from only 15 stations and covers the period from 1986 to 2006 (*Fig. 1*).

The climatic water budget was introduced into the research literature in the middle of 20th century by *Thornthwaite* (1948). He described the budget as the balance of precipitation, potential evapotranspiration, and actual evapotranspiration, taking into account both soil moisture utilization and soil moisture recharge (*Oliver and Fairbridge*, 1987). According to *Thornthwaite* and his colleagues (*Thornthwaite and Mather*, 1957), an average climatic water budget model can be expressed using two interrelated equations:

$$P = ET + S, \quad PE = ET + D, \quad (1)$$

where  $P$  is the precipitation,  $ET$  is the evapotranspiration,  $PE$  is the potential evapotranspiration,  $S$  is the moisture surplus, and  $D$  is the moisture deficit. The first equation describes water inflow, outflow, and storage, and the second equation describes energy demands. The procedure designed by *Thornthwaite* and *Mather* (1957) to calculate climatic water balance parameters is still widely used in CWB research (e.g., *Kar* and *Verma*, 2005; *Tateishi* and *Ahn*, 1996).

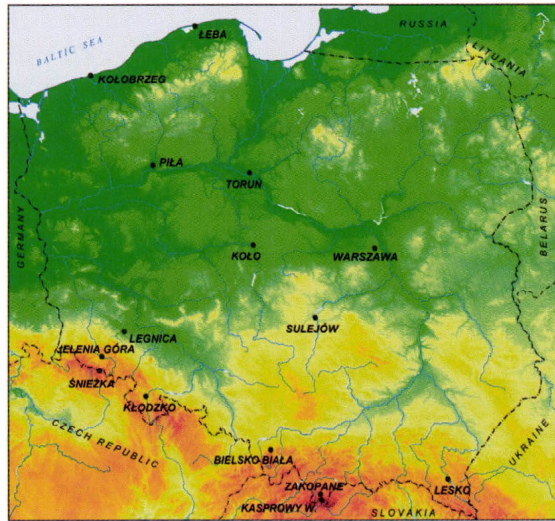


Fig. 1. Locations of the meteorological stations used in the research study.

Evapotranspiration process is the principal component of the climatic water balance, as it returns 60% to 80% of precipitation back into the atmosphere. In order to determine the value of the *CWB* index, the magnitude of evapotranspiration must be properly estimated. Owing to the difficulty of obtaining accurate field measurements, evapotranspiration is commonly computed from weather data using empirically derived formulas. A large number of more or less empirical methods have been developed over the last 50 years and are designed to estimate actual and potential evapotranspiration from different climatic variables. Some of the methods are only valid under specific climatic and agronomic conditions and cannot be applied under conditions different from those under which they were originally developed (*Allan et al.*, 2004). As a result, the *FAO Penman-Monteith Method* is now recommended as the standard method for the definition and computation of the reference evapotranspiration,  $ET_0$ . The reference evapotranspiration provides a standard to which

evapotranspiration at different periods of the year or in different regions can be compared (Allan *et al.*, 2004).

The subject of *CWB* spatial interpolation is very complex. It is, first and foremost, a subject associated with the problem of the spatial interpolation of evapotranspiration, which varies considerably with changes in the natural environment. The second complexity has to do with the availability of data. Given the complicated nature of the subject, it is no wonder that there exist many methods that attempt to model the spatial differentiation of evapotranspiration (e.g., Nováky, 2002; Xinfu *et al.*, 2002; Kar and Verma, 2005; Loheide and Gorelick, 2005; Fernandes *et al.*, 2007). Remote sensing is becoming more commonly used to address this research issue and often supplements ground-based observations (Woolhizer and Wallace, 1984; Rosema, 1990; Kalma *et al.*, 2008).

In Poland, most evapotranspiration and climatic water balance research is focused on the identification of a model that would best suit weather conditions in Poland. The following formulas were used in existing research: Turc (1961) method for potential evapotranspiration, Bac (1970) reference evaporation formulae for local index, and Penman modified to Polish conditions (Sarnaacka *et al.*, 1983). All three methods were applied to the analysis of the measurements data (Wild scale and GGI-3000 pan evaporimeter). Although the Turc method produced the largest differences between evapotranspiration totals measured *in situ* and values derived empirically (also shown by Hungarian research by Nováky, 2002), the method proved to be useful because of data availability issues. It was also selected because of other research that has shown that it is best at determining relationships with elevation (Kowanetz, 1998, 2000).

The climatic water balance index (*CWB*) was created based on a simplified definition where it is interpreted as the difference between the precipitation total (*P*) and potential evapotranspiration (*PE*). The final formula was the following:

$$CWB = P - 0.4 \frac{t}{t+15} I + 50, \quad (2)$$

where *P* is the monthly precipitation totals, *t* is the monthly average air temperature [°C], and *I* is the monthly sum of total solar radiation [ $\text{cal cm}^{-2} \text{day}^{-1}$ ].

Given the limited nature of the source data (15 data points only) and the existence of strong relationships between potential evapotranspiration and geographic factors (the same is true for *CWB*), geographic parameter regression models were used to produce grid data consisting of annual *CWB* totals (*CWB<sub>yr</sub>*) and vegetation period (April–September) *CWB* totals (*CWB<sub>veg</sub>*) at a 0.2 degree spatial resolution (latitude and longitude). The resolution was chosen as the best for regional scale studies. Moreover, the DTM resolution of 250 × 250 meters was available for calculations. Simple and multiple regression models were used, taking into account the dependence of *CWB* on elevation above sea level

( $H$ ), longitude ( $\lambda$ ), and latitude ( $\varphi$ ). The following formulas were used to perform calculations:

$$CWB = f(H) + b, \quad CWB = f(H) + f(\lambda) + f(\varphi) + b, \quad (3)$$

where  $b$  is the constant value.

Table 1 includes coefficients of correlation between geographic coordinates and  $CWB$  values on an annual as well as seasonal basis. The coefficients are very large – generally above 0.9 – and statistically meaningful at  $\alpha = 0.05$ . The coefficients of correlation tend to be somewhat larger when a multiple regression model is used. The value for the growing season is 0.95 and the value for the entire year is 0.94 (Table 1). The large size of the coefficient of correlation made it possible to use the regression method in order to calculate  $CWB$  for individual grids. The calculated values were then used in spatial analysis based on a variety of interpolation (spatialization) methods.

Table 1. Coefficients of correlation (CC) between geographic parameters ( $H$ ,  $\varphi$ ,  $\lambda$ ) and climatic water balance values ( $CWB$ ) for the growing season (April – September) and for an entire year

CC (simple)	Apr	May	Jun	Jul	Aug	Sep	Apr – Sep	Year
$H$ vs. $CWB$	0.95	0.91	0.91	0.90	0.90	0.86	0.92	0.92
CC (multiple)	Apr	May	Jun	Jul	Aug	Sep	Apr – Sep	Year
$H + \varphi + \lambda$ vs. $CWB$	0.97	0.94	0.92	0.92	0.91	0.89	0.95	0.94

There is a dearth of publications on optimal spatial  $CWB$  analysis methods, which has led to the testing of a variety of methods based on experiences with the interpolation of individual climate elements (Dobesch *et al.*, 2007; Tveito *et al.*, 2008). RMSE (root mean square error) analysis was used to assess the influence of interpolation methods on the analysis of spatial  $CWB$  differentiation. The source material available – 15 data points – was used as a source of reference. The relationship between results obtained during the spatialization process and values calculated based on field measurement data were also investigated.

### 3. Results and discussion

Four different spatial interpolation methods were used: (1) inverse distance weighting (IDW), (2) local polynomial (LP), (3) radial basis function (RBF), and (4) ordinary kriging. The first three are so-called deterministic methods. The fourth method, kriging, is used the most often and it is a geostatistical method.

Spatial interpolation was performed for different seasons and for the entire year, for Poland as a whole, using all four methods. RMSE values and coefficients of correlation as well as a subjective visual analysis of maps produced results that do not differ very much. However, the coefficient of correlation and RMSE suggest a somewhat more accurate interpolation based on RBF and kriging (Table 2).

Table 2. Validation results for different interpolation methods used in CWB calculations

Interpolation method (simple regression)	Year			Vegetation period		
	r	RMSE	$\sigma$	r	RMSE	$\sigma$
IDW	0.79	602	78	0.83	122	67
LP	0.83	683	207	0.87	186	177
RBF	0.84	641	145	0.88	147	125
Kriging	0.84	637	138	0.87	143	118
Interpolation method (multiple regression)	r	RMSE	$\sigma$	r	RMSE	$\sigma$
IDW	0.77	637	102	0.79	122	95
LP	0.83	710	196	0.75	177	174
RBF	0.84	673	144	0.86	141	131
Kriging	0.84	669	139	0.85	138	127

The CWB maps generated using the above methods can be found in Figs. 2a,b. The maps present annual CWB values as well as CWB values for the growing season (April–September). Differences between the annual spatial distribution and the growing season distribution are readily apparent. Annual CWB values range from 430 mm to 1200 mm, with maxima in the southern part of the country (mountains and uplands) and minima in the central part of the country (Figs. 2a,b). CWB fluctuates the most during the growing season (April–September), with positive values being recorded only in the mountains (up to 200 mm) and negative values (moisture deficit) across the rest of the country – as low as –230 mm in central Poland.

At the same time, Figs. 2a,b also show differences in spatial distribution resulting from the interpolation of input data using the simple regression method and the multiple regression method. Table 2 shows validation results for the interpolation methods used in the study.

The interpolation results generated for Poland as a whole may be considered good, as the differences produced by different methods are small. However, a closer look at the problem on a local scale points to a great deal of complexity. Calculation results for different locations indicate that geographic influence is a factor that does affect CWB.

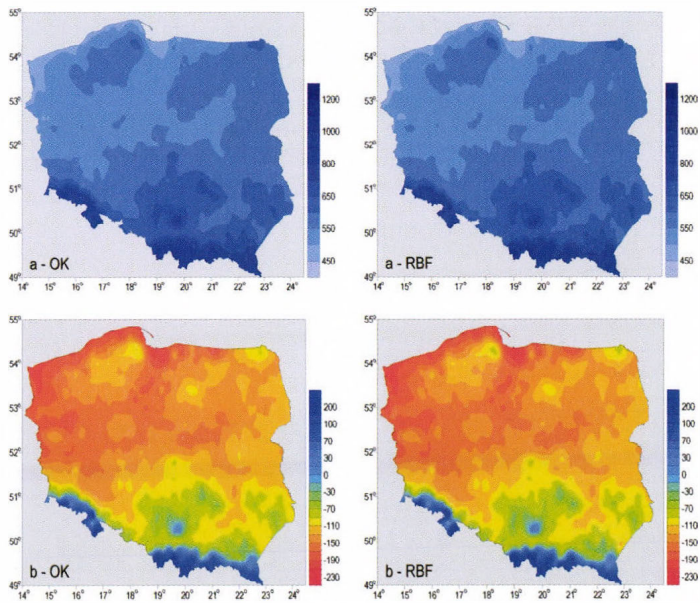


Fig. 2a. Spatial distribution of the CWB (mm) in Poland according to different interpolation methods: radial basis function (RBF) and ordinary kriging (OK) (simple regression model); a – annual values, b – vegetation period (April – September) values.

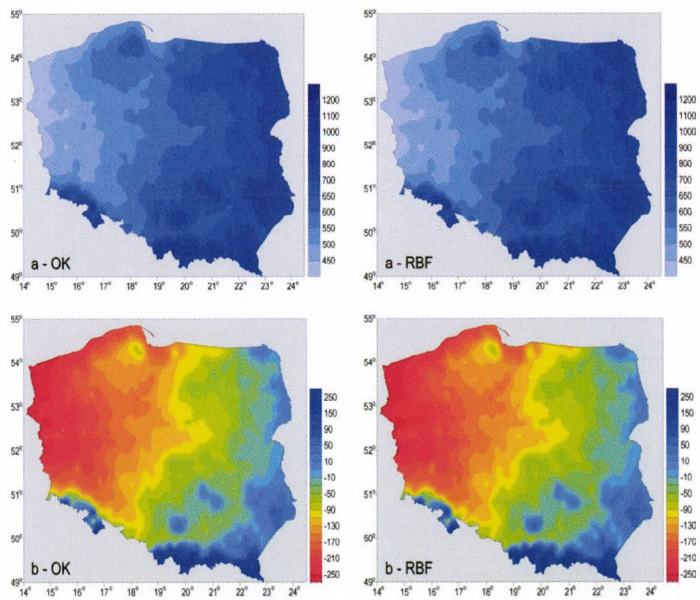


Fig. 2b. Spatial distribution of the CWB (mm) in Poland according to different interpolation methods: radial basis function (RBF) and ordinary kriging (OK) (multiple regression model); a – annual values, b – vegetation period (April – September) values.

Decidedly larger differences between values calculated based on field measurements and those produced by the model in question can be observed for the growing season. Using the simple regression model, errors exceed 100% of values calculated for the Jelenia Góra Basin and the Kłodzko Basin (Fig. 3). The multiple regression model performs the worst for coastal locations (Łeba, Kołobrzeg) and points near the eastern border of Poland – Lesko (Fig. 3). The uncertainty of the results obtained suggests that it is necessary to use supplemental descriptive variables.

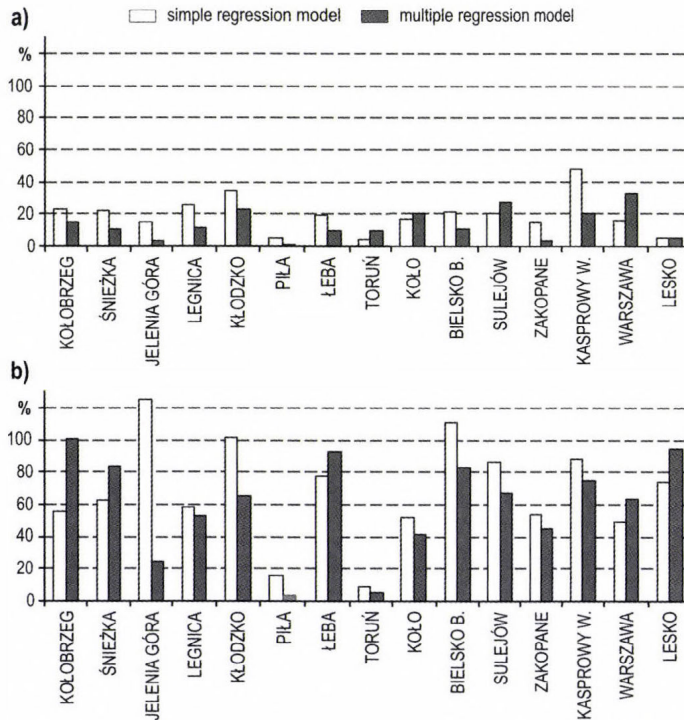


Fig. 3. Mean percent error of estimated and calculated CWB values for the meteorological stations used in the research study.

Component variables such as atmospheric precipitation and potential evapotranspiration make the climatic water balance strongly dependent on local conditions. Any analysis of data must take into account local relief and land cover (biological and soil factors). Elevation above sea level and geographic coordinates are not enough to perform an accurate spatial analysis of climatic water balance.

As elevation above sea level is a key component of spatial differentiation analysis of atmospheric precipitation (Bac-Bronowicz, 2003; Lupikasza et al.,

2007), the choice of descriptive variables is a key factor in spatial *CWB* analysis. Errors may also occur as a result of poor spatial coverage provided by weather stations as well as the interpolation and mapping techniques used. Regarding evapotranspiration estimates mapping, it is usually affected by modeling errors resulting from the derivation of *ET* values (*Climatic Atlas...*, 2001). Hence, the complexity of the evapotranspiration process demands the consideration of local conditions.

The state of current understanding of microclimate differentiation, especially that in mountain areas, suggests that other geographic variables should be taken into consideration. In order to accurately describe the spatial distribution of *CWB*, it is necessary to take into account slope, aspect, land use, and soil type – all of which determine how much solar radiation is available and, consequently, the value of the air temperature (*Ustrnul and Czekierda, 2005*). Both solar radiation and air temperature affect the degree of evapotranspiration. Furthermore, the parameters must be calculated independently for smaller regions – especially regions characterized by specific mesoclimate conditions such as those found in coastal or mountain areas.

#### ***4. Conclusions***

The spatial interpolation results presented herein, based on four different interpolation methods, prove the hypothesis that spatial differentiation analysis of the climatic water balance should take local conditions into account. The validation results are sufficient to fully assess results obtained on a national scale (Poland only), but insufficient with respect to individual geographic locations, where local differences can be quite significant.

Reducing the size of the research area appears to be a reasonable next step. A solid understanding of the causes and effects of particular component elements, such as the natural environment, on the *CWB* index should help in the process of selecting descriptive variables. Existing research suggests the use of distance from a body of water, land cover, and relief as supplemental factors. Another key factor is the selection process of the evapotranspiration (potential and/or actual) calculation method, as this appears to be the main source of possible *CWB* errors.

Given the difficult nature of the analytical process involved, the accuracy of the spatialization method is less important. The most important objectives for further research are validation of the obtained results using different evapotranspiration formulas and the optimization and testing of spatialization techniques. A few other descriptive variables should also be considered (e.g., circulation types, air masses). Further research will be designed to focus on different temporal and spatial scales as well as the validation in other areas of Europe.

## References

- Allan, R.G., Pereira, L.S., Raes, L., Smith, M., 2004: Guidelines for computing crop water requirements. *FAO Irrigation and Drainage Papers* 56, p. 328
- Bac, S., 1970: Studies on the correlation between free water surface evaporation, areal and potential evapotranspiration (in Polish). *Prace i Studia Komit. Gosp. Wodnej i Sur. PAN* 10, 287-366.
- Bac-Bronowicz, J., 2003: Methods of the visualisation of precipitation based on various observation measurement periods in GIS. In *Man and Climate in the 20th Century. Studia Geograficzne* 75, Wyd. Uniw. Wrocławskiego, Wrocław, 559-563.
- Climatic Atlas of Australia*, 2001: Evapotranspiration (ET). Bureau of Meteorology, Australia, p. 45.
- Dobesch, H., Dumolard, P., Dyras, I. (eds.), 2007: *Spatial Interpolation for Climate Data*, ISTE – Geographical Information Systems Series. London – Newport Beach, p. 284.
- Fernandes, R., Korolevych, V., Wang, S., 2007: Trends in land evapotranspiration over Canada for the period 1960–2000 based on in situ climate observations and a land surface model. *Journal of Hydrometeorology* 8, 1016-1030.
- Kalma, J.D., McVicar, T.R., McCabe, M.F., 2008: Estimating land surface evaporation: A review of methods using remotely sensed surface temperature data. *Surv. Geophys.* 29, 421-469.
- Kar, G., Verma, H.N., 2005: Climatic water balance, probable rainfall, rice crop water requirements and cold periods in AER 12.0 in India. *Agr. Water Manage.* 72, 15-32.
- Kowanetz, L., 1998: *Climatic Water Balance in Upper Vistula River Basin* (in Polish). PhD thesis, Jagiellonian University.
- Kowanetz, L., 2000: On the method of determining the climatic water balance in mountainous areas, with the example from Polish Carpathians. *Zeszyty Naukowe UJ, Prace Geograficzne* 105, 137–164.
- Loheide, S.P., Gorelick, S.M., 2005: A local-scale, high-resolution evapotranspiration mapping algorithm (ETMA) with hydroecological applications at riparian meadow restoration sites. *Remote Sens. Environ.* 98, 182-200.
- Lupikasza, E., Ustrnul, Z., Czekierda, D., 2007: The role of explanatory variables in spatial interpolation of selected climate elements. *Roczniki Geomatyki* 5, 1, 55-64.
- Nováky, B., 2002: Mapping of mean annual actual evaporation on the example of Zagyva catchment area. *Időjárás* 106, 227-238.
- Oliver, J.E., Fairbridge, R.W., 1987: *The Encyclopedia of Climatology*. Van Nostrand Reinhold Company Inc., New York, p. 986.
- Rosema, A., 1990: Comparison of Meteosat-based rainfall and evapotranspiration mapping in the Sahel region. *Int. J. Remote Sens.* 11, 2299-2309.
- Sarnacka, S., Brzeska, J., Świerczynska, H., 1983: Selected methods in distinguishing potential evapotranspiration (in Polish). *Mat. Bad. Ser. Gosp. Wodn. i Ochr. Wód, IMGW*, 1-35
- Tateishi, R., Ahn, C.H., 1996: Mapping evapotranspiration and water balance for global land, ISPRS. *Journal of Photogrammetry and Remote Sensing* 51, 4, 209-215.
- Thornthwaite, C.W., 1948: An approach. towards a rational classification of climate. *Geogr. Rev.* 38, 55-94.
- Thornthwaite, C.W., Mather, J.R., 1957: Instructions and tables for computing potential evapotranspiration and the water balance. *Publ. Climatol.* 10, 185-311.
- Turc, L., 1961: Evaluation des besoins en eau d'irrigation, évapotranspiration potentielle. *Annales Agronomiques* 12, 1, 13-49.
- Tveito, O.E., Wegehenkel, M., Wel van der, F., Dobesch, H. (eds.), 2008: The use of geographic information systems in climatology and meteorology. *Final Report COST Action 719*, COST Office, p. 246.
- Ustrnul, Z., Czekierda, D., 2005: Application of GIS for the development of climatological air temperature maps: an example from Poland. *Meteorol. Appl.* 12, 43-50.
- Woolhizer, D.A., Wallace, D.E., 1984: Mapping average daily pan evaporation. *J. Irrig. Drain. Eng.* 110, 246-250.
- Xinfa, Q., Yan, Z., Changming, L., 2002: A general model for estimating actual evaporation from non-saturated surfaces. *J. Geogr. Sci.* 12, 479-484.

# NEWS



## Farewell to the Executive Editor, Margit Antal

IDŐJÁRÁS (Weather in English) is one of the oldest meteorological journals in Europe. Since the end of the nineteenth century it has published papers on meteorology as well as other news in the Hungarian language. After the Second World War it was felt that other languages must also be used in order to make publication for foreign authors possible. However, this caused a rather chaotic situation since the language of the publication was not determined. Thus, papers of quite different quality were published in at least five languages.

At the end of the seventies and at the beginning of the eighties it became clear that papers should be accepted only in one language, namely in the world-common language of natural sciences: in English. One also believed that the manuscript reviewing procedure must be similar to that applied in leading scientific journals. The philosophy was to publish papers of Hungarian specialists and other scientists from the neighboring countries in a way that would be understandable all over the world. Further, we believed at that time, that an international forum on atmospheric science was necessary for strengthening the relationship between scientists behind and outside the iron curtain.

As the chairman of the editorial board (later the Editor-in-Chief) I needed a new board consisting of internationally well-known scientists and, also very important, a secretary for fulfilling the administration necessary. It was an obvious solution to choose for this purpose my own secretary, Ms *Margit Antal* (her married name is *Dr Antal Emánuelné*), called by everybody “*Pimpi*”, who had already proved that she is a very good person to arrange correspondence and typing not only in Hungarian, but also in English, French, and German. It turned out later that this choice was an excellent one.

I have to emphasize that *Pimpi* did not finish any course to be secretary. She began to work at the Department on Solar Radiation of the Hungarian Meteorological Service in 1963. After some years she continued similar activity at the Department on Heat and Water Balance. Her bosses were always very satisfied with her work (mostly calculations and observations), she quickly became famous because of her accuracy and precision. This was obviously the reason why the executive editor of *IDŐJÁRÁS* at that time (*J. Kakas*) used *Pimpi*’s ability to help him in editing of the journal. And, more important for myself, this motivated me to ask her to be my secretary, when I was appointed director of the research institute (Central Institute for Atmospheric Physics) of the Hungarian Meteorological Service. In the life of anyone among us there are good and bad decisions. Anyway, this was a good one for me. *Pimpi*, as secretary, helped my work in an excellent and correct way until leaving the service in 1992.

In the same year *Pimpi* became officially the technical editor of the journal. In 1996 the president of the Hungarian Meteorological Service nominated her to the post of executive editor. By this time she already knew everything concerning the editorial work. She played a decisive role in introducing the up-to-date computerized journal production, giving to *IDŐJÁRÁS* the present attractive aspect. *IDŐJÁRÁS* has been indexed and abstracted in Science Citation Index Expanded and Journal Citation Reports/Science Edition since 2007. This milestone could not be reached without her perfect editorial activity. She has executed the editorial work to the satisfaction of everybody, including members of the editorial board, authors, and readers. For acknowledging her work during decades for *IDŐJÁRÁS* and the Hungarian Meteorological Service, the Minister of the Environment Protection and Water Management rewarded her in 2006 with the medallion “Pro Meteorologia”.

Dear *Pimpi*! On the occasion of your retirement, on behalf of all the Editor-in-Chiefs with whom you worked, I want to thank you for your efforts to make this journal an international forum. I wish you further health and a long and peaceful life after almost fifty years of professional work!

*Ernő Mészáros*  
Former Editor-in-Chief  
Member of the Hungarian Academy of Sciences

## INSTRUCTIONS TO AUTHORS OF *IDŐJÁRÁS*

The purpose of the journal is to publish papers in any field of meteorology and atmosphere related scientific areas. These may be

- research papers on new results of scientific investigations,
- critical review articles summarizing the current state of art of a certain topic,
- short contributions dealing with a particular question.

Some issues contain "News" and "Book review", therefore, such contributions are also welcome. The papers must be in American English and should be checked by a native speaker if necessary.

Authors are requested to send their manuscripts to

*Editor-in Chief of IDŐJÁRÁS*  
P.O. Box 39, H-1675 Budapest, Hungary  
E-mail: [antal.e@met.hu](mailto:antal.e@met.hu)

including all illustrations. MS Word format is preferred in electronic submission. Papers will then be reviewed normally by two independent referees, who remain unidentified for the author(s). The Editor-in-Chief will inform the author(s) whether or not the paper is acceptable for publication, and what modifications, if any, are necessary.

Please, follow the order given below when typing manuscripts.

*Title page:* should consist of the title, the name(s) of the author(s), their affiliation(s) including full postal and e-mail address(es). In case of more than one author, the corresponding author must be identified.

*Abstract:* should contain the purpose, the applied data and methods as well as the basic conclusion(s) of the paper.

*Key-words:* must be included (from 5 to 10) to help to classify the topic.

*Text:* has to be typed in single spacing on an A4 size paper using 14 pt Times New Roman font if possible. Use of S.I. units are expected, and the use of negative exponent is preferred to fractional sign. Mathematical formulae are expected to be as simple as

possible and numbered in parentheses at the right margin.

All publications cited in the text should be presented in the *list of references*, arranged in alphabetical order. For an article: name(s) of author(s) in Italics, year, title of article, name of journal, volume, number (the latter two in Italics) and pages. E.g., *Nathan, K.K., 1986: A note on the relationship between photo-synthetically active radiation and cloud amount. Időjárás 90, 10-13.* For a book: name(s) of author(s), year, title of the book (all in Italics except the year), publisher and place of publication. E.g., *Junge, C.E., 1963: Air Chemistry and Radioactivity.* Academic Press, New York and London. Reference in the text should contain the name(s) of the author(s) in Italics and year of publication. E.g., in the case of one author: *Miller (1989)*; in the case of two authors: *Gamov and Cleveland (1973)*; and if there are more than two authors: *Smith et al. (1990)*. If the name of the author cannot be fitted into the text: *(Miller, 1989)*; etc. When referring papers published in the same year by the same author, letters a, b, c, etc. should follow the year of publication.

*Tables* should be marked by Arabic numbers and printed in separate sheets with their numbers and legends given below them. Avoid too lengthy or complicated tables, or tables duplicating results given in other form in the manuscript (e.g., graphs).

*Figures* should also be marked with Arabic numbers and printed in black and white or color (under special arrangement) in separate sheets with their numbers and captions given below them. JPG, TIF, GIF, BMP or PNG formats should be used for electronic artwork submission.

*Reprints:* authors receive 30 reprints free of charge. Additional reprints may be ordered at the authors' expense when sending back the proofs to the Editorial Office.

*More information* for authors is available: [antal.e@met.hu](mailto:antal.e@met.hu)

Published by the Hungarian Meteorological Service

---

Budapest, Hungary

**INDEX 26 361**

**HU ISSN 0324-6329**

# IDOJÁRÁS

QUARTERLY JOURNAL  
OF THE HUNGARIAN METEOROLOGICAL SERVICE

## CONTENTS

<i>Detlev Möller</i> : Atmospheric chemistry – Bridging the chemical air composition with the climate .....	123
<i>Beáta Szabó-Takács</i> : Numerical simulation of the cycle of aerosol particles in stratocumulus clouds with a two-dimensional kinematic model .....	147
<i>Erzsébet Enzsölné Gerencsér, Zsuzsanna Lantos, Zoltán Varga-Haszonits, and Zoltán Varga</i> : Determination of winter barley yield by the aim of multiplicative successive approximation .....	167
<i>Márton Balczó, Miklós Balogh, István Goricsán, Torsten Nagel, Jenő M. Suda, and Tamás Lajos</i> : Air quality around motorway tunnels in complex terrain – computational fluid dynamics modeling and comparison to wind tunnel data .....	179
<i>Ernő Führer, László Horváth, Anikó Jagodics, Attila Machon, and Ildikó Szabados</i> : Application of a new aridity index in Hungarian forestry practice .....	205
Book review .....	217

\*\*\*\*\*

<http://www.met.hu/Journal-Idoiaras.php>

# IDŐJÁRÁS

*Quarterly Journal of the Hungarian Meteorological Service*

*Editor-in-Chief*  
**LÁSZLÓ BOZÓ**

*Executive Editor*  
**MÁRTA T. PUSKÁS**

## EDITORIAL BOARD

- |                                       |   |
|---------------------------------------|---|
| AMBRÓZY, P. (Budapest, Hungary)       | MIKA, J. (Budapest, Hungary)                        |
| ANTAL, E. (Budapest, Hungary)         | MERSICH, I. (Budapest, Hungary)                     |
| BARTHOLY, J. (Budapest, Hungary)      | MÖLLER, D. (Berlin, Germany)                        |
| BATCHVAROVA, E. (Sofia, Bulgaria)     | NEUWIRTH, F. (Vienna, Austria)                      |
| BRIMBLECOMBE, P. (Norwich, U.K.)      | PINTO, J. (Res. Triangle Park, NC, U.S.A.)          |
| CZELNAI, R. (Dörgicse, Hungary)       | PRÁGER, T. (Budapest, Hungary)                      |
| DUNKEL, Z. (Budapest, Hungary)        | PROBÁLD, F. (Budapest, Hungary)                     |
| FISHER, B. (Reading, U.K.)            | RADNÓTI, G. (Reading, U.K.)                         |
| GELEYN, J.-Fr. (Toulouse, France)     | S. BURÁNSZKI, M. (Budapest, Hungary)                |
| GERESDI, I. (Pécs, Hungary)           | SIVERTSEN, T.H. (Risør, Norway)                     |
| GÖTZ, G. (Budapest, Hungary)          | SZALAI, S. (Budapest, Hungary)                      |
| HASZPRA, L. (Budapest, Hungary)       | SZEIDL, L. (Budapest, Hungary)                      |
| HORÁNYI, A. (Budapest, Hungary)       | SZUNYOGH, I. (College Station, TX, U.S.A.)          |
| HORVÁTH, Á. (Siófok, Hungary)         | TAR, K. (Debrecen, Hungary)                         |
| HORVÁTH, L. (Budapest, Hungary)       | TÁNCZER, T. (Budapest, Hungary)                     |
| HUNKÁR, M. (Keszthely, Hungary)       | TOTH, Z. (Camp Springs, MD, U.S.A.)                 |
| LASZLO, I. (Camp Springs, MD, U.S.A.) | VALI, G. (Laramie, WY, U.S.A.)                      |
| MAJOR, G. (Budapest, Hungary)         | VARGA-HASZONITS, Z. (Moson-<br>magyaróvár, Hungary) |
| MATYASOVSKY, I. (Budapest, Hungary)   | WEIDINGER, T. (Budapest, Hungary)                   |
| MÉSZÁROS, E. (Veszprém, Hungary)      |   |

*Editorial Office: Kitaibel P.u. 1, H-1024 Budapest, Hungary*  
*P.O. Box 38, H-1525 Budapest, Hungary*  
*E-mail: journal.idojaras@met.hu*  
*Fax: (36-1) 346-4669*

---

**Indexed and abstracted in Science Citation Index Expanded™ and  
Journal Citation Reports/Science Edition  
Covered in the abstract and citation database SCOPUS®**

---

*Subscription by*

*mail: IDŐJÁRÁS, P.O. Box 38, H-1525 Budapest, Hungary*  
*E-mail: journal.idojaras@met.hu*

# IDŐJÁRÁS

*Quarterly Journal of the Hungarian Meteorological Service*  
Vol. 115, No. 3, July–September 2011, pp. 123–145

## **Atmospheric chemistry – Bridging the chemical air composition with the climate**

**Detlev Möller**

*Chair for Atmospheric Chemistry and Air Pollution Control,  
Brandenburg Technical University, P.O. Box 10 13 44, D-03013 Cottbus, Germany  
Volmerstr. 13, D-12489 Berlin, Germany  
E-mail: moe@btu-lc.fta-berlin.de*

*(Manuscript received in final form June 14, 2011)*

**Abstract**—Studying the environment is an extremely complex issue, comprising all natural sciences and regarding the “key” compartments water, air, and soil, often defined as the climate system. Without any doubt, the atmosphere is the most important one, it is highly dynamic and globally interlinking the biosphere. Nowadays, the humans are shortly before reaching the “tipping point” between moving into the (climate) catastrophe or the sustainable development. This paper introduces a new discipline, the “chemistry of the climate system”. Atmospheric chemistry, without using this term before the 1950s, was a fundamental approach in the beginning of modern chemistry (air analysis and understanding combustion) some 200 years ago, and it is now enlarging to the interfaces (“interfacial chemistry”) with the biosphere and hence our climate system. Humans created a new dimension (the “anthroposphere”) by globally modified biogeochemical cycles. Climate control means learning from nature and creating closed man-made material cycles, first of all that of carbon. Our environmental problem is not the limited energy but creating unbalanced reservoir distributions of substances with different characteristic timescales out of steady-state conditions.

*Key words:* atmospheric chemistry, air pollution, climate, climate change, chemical climate, sustainable chemistry, human evolution, anthroposphere, biogeochemistry

### **1. Introduction**

Out of the recognized complexity of nature, the three basic sciences arose: physics, chemistry, and biology. Further progress in the understanding of natural processes created numerous sub-disciplines and cross-disciplines, termed with a variety of prefixes and combinations, often creating misunderstandings unless careful definitions are used. In order to overcome disciplinary borders, a new

super-science was established, the earth system science, to study the earth as a system, with an emphasis on observing, understanding, and predicting global environmental changes involving interactions between land, atmosphere, water, ice, biosphere, societies, technologies, and economies. Humans – by decoupling their life cycle from natural conditions – have altered “natural” biogeochemical cycles. The Russian geochemist, *Vladimir Ivanovich Vernadsky*, understood a new dimension of the biosphere called noosphere (or anthroposphere by *Paul Crutzen*) a new dimension of the biosphere, developing under the evolutionary influence of humans on natural processes (*Vernadsky*, 1926).

We will define air (or atmospheric) chemistry as the discipline dealing with the origin, distribution, transformation, and deposition of gaseous, dissolved, and solid substances in air. This chain of matter provides the atmospheric part of the biogeochemical cycles. A more general definition, but one that is appealing as a wonderful phrase, was given by the German air chemist, *Christian Junge* “Air chemistry is defined ... as the branch of atmospheric science concerned with the constituents and chemical processes of the atmosphere ...” (*Junge*, 1963). In other words, air chemistry is the science concerned with the origin and fate of the components in air. The origin of air constituents concerns all source and formation processes, the chemicals of air itself, but also emissions by natural and man-made processes into the atmosphere. The fate of air constituents includes distribution (which is the main task of meteorology), chemical conversion, phase transfers and partitioning (reservoir distribution), and deposition of species. Deposition is going on via different mechanisms from gas, particulate, and droplet phases to the earth’s ground surface, including uptake by plants, animals, and humans. Removal from the atmosphere is the input of matter to another sphere (see *Fig. 1*).

The term “atmospheric chemistry” appears to have been used for the first time in German by *Hans Cauer* in 1949 (*Cauer*, 1949). It was soon used as the label for a new discipline. The first monograph in the field of this new discipline was written by *Junge*, entitled “Air Chemistry and Radioactivity” (New York and London, 1963), soon after he had published a first long chapter entitled “Atmospheric Chemistry” in a book in 1958 (*Junge*, 1958). This clear term identifies a sub-discipline of chemistry and not meteorology or physics. The “discipline” was called “chemical meteorology” before that time. However, before the 1950s, chemical meteorology was mainly looking for the relationship between condensation nuclei, its chemical composition, and the formation of clouds and rain.

Basically, there is no need to prefix the sciences (environmental, ecological, geo-, air, hydro-, etc.). Other sciences such as geology and meteorology, for example, can be reduced to the natural sciences. It is worth noting the language roots of “geo” and “meteor”. In Greek, γῆ (ge) means earth, land, and ground (poetically γαῖα (gaia))<sup>1</sup>. In the composition of words, Greek γέα (gea), γης

---

<sup>1</sup> In Latin, the word for earth, land, and ground is “tellūs” (in sense of the celestial body) and “terra” (in sense of matter).

(ges), γην (gen), and γεω (geo) occur. Already before the year 600 B.C., the Greek word μετέωρος (metéoros) was in use, meaning “a thing in the air, altitude, or above ground”<sup>2</sup>. Until the end of the eighteenth century, μετέωρος denoted all celestial phenomena: aqueous, vaporous, solid, and light. Aristotle’s “Meteorologia” is a book on natural philosophy (in modern terms: earth science). Hence, in a more narrow (historical) sense, geosciences (geology, geography, geochemistry, geophysics, etc.) deal with the subject of the solid earth (the geosphere). Geochemistry studies the composition and alterations of the solid matter of the earth; geology is the scientific study of the origin, history, and structure of the earth; geography studies the earth and its features and the distribution of life on the earth, including human life and the effects of human activity. Geography (which is an old discipline, founded as a modern science by Humboldt) is thus the science of the earth’s surface – the physical and human landscapes, the processes that affect them, how and why they change over time, and how and why they vary spatially. In other words, geography is an interfacial science between the solid and the gaseous earth (the atmosphere); indeed some geographers consider climatology to be a sub-discipline of geography (and vice versa, some meteorologists do not include climatology in meteorology). Finally, the liquid earth (the hydrosphere) is the subject of hydrology<sup>3</sup>. It is important to note that gaseous water (vapor) in the atmosphere is not considered to be an object in hydrology, but liquid water in the atmosphere is. Logically we now can state that the science of studying the “gaseous earth” (atmosphere) is meteorology. Older (synonymous) terms for the science of the study of earth’s atmosphere are aerology and atmospherology. For example, meteorology has been defined as the physics and chemistry of the atmosphere (*Scharnow et al.*, 1965) but also reduced to just the physics of the atmosphere (*Liljequist and Cehak*, 1984). Some definitions focus meteorology on weather processes and forecasting, which surely was the beginning of that science. A satisfactory definition is “the study dealing with the phenomena of the atmosphere, including physics, chemistry, and dynamics, extending to the effects of the atmosphere on the earth’s surface and the oceans”. Hence, meteorology is more than “only” the physics and chemistry of the atmosphere. Nowadays, the term “atmospheric sciences” is also used to summarize all the sub-disciplines needed to explain atmospheric phenomena and processes. To return to chemistry, (atmospheric)

<sup>2</sup> μετεωρολογία [metéorologia] means the “science of celestial, heavenly things” but also “vague talk” and “philosophical shenanigans” (*Benselers Greek-German School Dictionary (Griechisch-Deutsches Schulwörterbuch*, Leipzig and Berlin 1911).

<sup>3</sup> In Greek ὕδωρ (idor) means originally rain water and generally water; it appears in composite words as ὕδρο (idro). This is the derivation of the prefix “hydro” (the pronunciation of Greek letter υ̅ and υ̇ is like “hy”). In Latin, water as a substance is “aqua”, but natural waters are referred to as “unda”, derived from the Greek “hy-dor” (ὑδωρ); ὕδρα (Greek), and hydra (Latin) is the many-headed water snake in Greek mythology. From Gothic “vato” and Old High German “waz-ar”, are clearly seen the roots of English “water” and German “Wasser”.

chemistry is just one of the sciences to understand the (chemical) processes in the atmosphere (see above for definition of atmospheric chemistry).

*Antoine Lavoisier*, who revolutionized the science of chemistry in the eighteenth century and replaced the mythical “phlogiston” with the term and concept of oxygen, clearly understood the importance of accurate definitions. In his words: “We cannot improve the language of any science without at the same time improving the science itself; nor can we, on the other hand, improve a science without improving the language or nomenclature” (*Lavoisier*, 1789). *Imre Lakatos* (1981) wrote “Philosophy of science without history is empty; history of science without philosophy is blind”.

## ***2. Air and atmosphere – a multiphase and multi-component system***

The typical dictionary definition of atmosphere is “the mixture of gases surrounding the earth and other planets” or “the whole mass of an aeriform fluid surrounding the earth”. The terms air and atmosphere are widely used as synonyms. The word “air” derives from Greek *ἀήρ* and Latin *aer* or *ær*. The term “atmosphere”, however, originated from the Greek *ατμός* (= vapor) and *σφαῖρα* (= sphere), and was not regularly used before the beginning of the nineteenth century. The Dutch astronomer and mathematician *Willebrord van Roijen Snell* translated the term “damphoogde” into Latin “*atmosphæra*” in 1608. *Otto von Guericke*, who invented the air pump and worked on his famous experiments concerning the physics of the air in the 1650s, used the term “*ærea sphæra*” (*Guericke*, 1672). In addition, in the nineteenth century the term “Air Ocean” was also used, in analogy to the sea.

It makes even more sense to define the atmosphere as being the reservoir (space) surrounding our (and any) planet, and air to be the mixture of substances filling the atmospheric space. With this in mind, the term air chemistry is more adequate than atmospheric chemistry. From a chemical point of view, it is possible to say that air is the substrate with which the atmosphere is filled. This is in analogy to the hydrosphere where water is the substance. Furthermore, air is an atmospheric suspension containing different gaseous, liquid (water droplets), and solid (dust particles) substances, and therefore, it provides a multiphase and multi-component chemical system. Solar radiation is the sole primary driving force in creating gradients in pressure, temperature, and concentration which result in transport, phase transfer, and chemical processes (*Fig. 1*).

The physical and chemical status of the atmosphere is called climate (see Section 4 for details). Supposing that the incoming solar radiation shows no trend over several hundred years, and accepting that natural biogenic and geogenic processes vary but also do not show trends on these time scales, it is only mankind’s influence on land use and emissions into the atmosphere that changes air chemical composition, and thus, the climate. Human activities have

an influence on natural processes (biological, such as plant growth and diversity, and physical, such as radiation budget), resulting in a cascade of consequent physical and chemical developments (feedback).

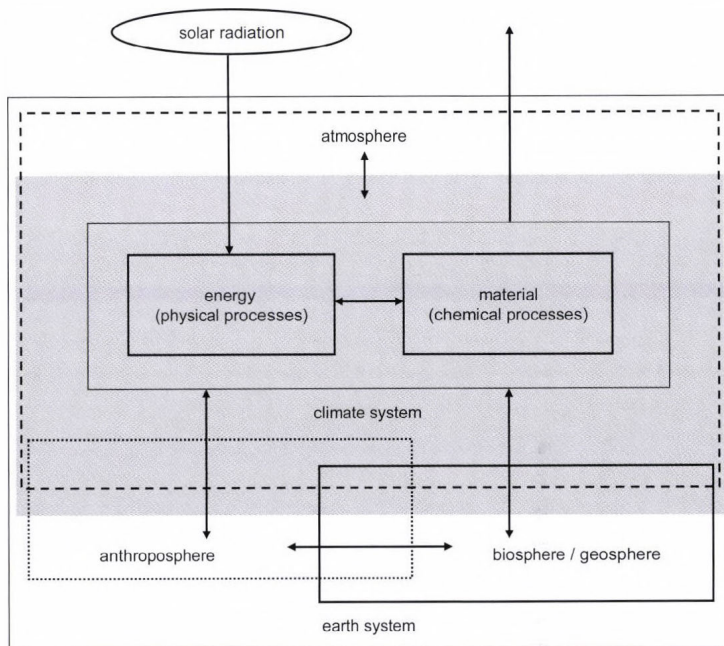


Fig. 1: Scheme of the physico-chemical interactions between the atmosphere, biosphere, and anthroposphere (the climate system).

We will initially set the climate system in a chain of subsystems:

Cosmic system → solar system → earth system → climate system →  
→ sub-systems (e.g., atmosphere).

In other words, each system to be defined lies in another “mother” system, the surrounding or environment where an exchange of energy and material is realized via the interfaces. Consequently, there are no fully closed systems in our world.

The chemical composition of air depends on the natural and man-made sources of the constituents (their distribution and source strength in time and space) as well as on the physical (e.g., radiation, temperature, humidity, wind) and chemical conditions (other trace species), which determine transportation and transformation. Thus, atmospheric chemistry is not a pure chemistry but it also includes other disciplines which are important for describing the

interactions between atmosphere and other surrounding reservoirs (biosphere, hydrosphere, etc.). Measurements of chemical and physical parameters in air will always contain a “geographical” component, i.e., the particularities of the locality. That is why the terms “chemical weather” and “chemical climate” have been introduced. For example, diurnal variation of the concentration of a substance may occur for different reasons. Therefore, general conclusions or transfer of results to other sites should be done with care. On the other hand, the basic task in atmospheric chemistry is not only to present local results of chemical composition and its variation in time, but also to find general relationships between trace species and their behavior under different conditions.

Without discussing the biological and physical processes within the climate system in any details, the chemical composition of the atmosphere and its variation in time and space, as well as its trends, are essential for an understanding of climate change. Atmospheric substances with their physical and chemical properties will have many effects in the climate system; we list the most important ones together with their impacts (there are many more impacts, parallel and synergistic effects):

- formation of cloud condensation nuclei (CCN) and subsequent cloud droplets: hydrological cycle;
- greenhouse gases (GHG): radiative interaction (warming the atmosphere);
- ozone-depleting substances (ODS): radiative interaction (increasing UV radiation penetration into the lower troposphere);
- formation of atmospheric aerosol: radiative interaction (cooling the atmosphere);
- oxidation capacity: lifetime of pollutants;
- acidity: chemical weathering;
- toxicity: poisoning the environment (affecting life functions and biodiversity);
- nutrition: bioavailability of compounds essential for life but also eutrophication.

We see that the climate system has physical and chemical components, interacting and (at least partly) determining each other. Physical quantities in the climate system show strong influences on chemical processes:

- temperature and pressure: reactions, rates, and (chemical and phase) equilibria;
- radiation (wavelength and intensity): photochemistry,
- motion: fluxes of matter (bringing substance together for chemical reactions).

Let us now turn to the atmosphere as a multiphase system. While gases and particles (from molecules via molecular clusters to nano- and micro-particles) are always present in the air, although with changing concentrations, condensed water (hydrometeors) is occasionally present in air, depending on the presence of so-called cloud condensation nuclei (CCN) and water vapor supersaturation at the site of fog and cloud formation. With the formation, transportation, and evaporation of clouds, huge amounts of atmospheric energy are transferred. This results in changing radiation transfer and thus “makes” the weather, and, on a long-term scale, the climate. Furthermore, clouds provide an effective “chemical reactor” and transport medium and cause redistribution of trace species after evaporation. When precipitating, clouds remove trace substances from the air (we term it wet deposition) to the earth’s surface. As a consequence, beside the continuous process of dry deposition, clouds may occasionally lead to large inputs of trace substances into ecosystems. The amount of condensed water in clouds and fog is very small, with around  $1 \text{ g/m}^3$  air or, in the dimensionless term, liquid water content  $1 \cdot 10^{-6}$  (identical with 1 ppb). Thus, 99.99% or more of total atmospheric water remains in the gaseous phase of an air parcel. Hydrometeors may be solid (ice crystals in different shapes and forms) or liquid (droplets ranging from a few  $\mu\text{m}$  up to some tens of  $\mu\text{m}$ ). We distinguish the phenomenon of hydrometeors into clouds, fog, and precipitation (rain, drizzle, snow, hail, etc.). This atmospheric water is always a chemical aqueous solution where the concentration of dissolved trace matter (related to the bulk quantity of water) is up to several orders of magnitude higher than in the gaseous state of air. This analytical fact is the simple explanation why collection and chemical analysis of hydrometeors began much earlier than gas-phase measurements.

Due to permanent motion, namely advection and turbulent diffusion, having stochastic characteristics on different time and spatial scales, it is extremely complicated to model chemistry and transport (so-called chemistry-transport models, CTM, which are also a basis for climate modeling) in space and time. At the earth-air interface, exchange of matter occurs, emission as well as deposition.

### ***3. Changes in air chemical composition: air pollution***

Changes in the chemical composition of air caused by humans are termed air pollution. The terms air pollution and pollutant need some comments. To start with, the term pollutant should be used only for man-made (anthropogenic) emitted substances, despite the fact that most of them are also of natural origin. Air pollution represents a deviation from a natural chemical composition of air (providing a reference level) at a given site. Depending on the residence time of the pollutant, we can characterize the scale of pollution from local via regional to global. Air pollution nowadays is a global phenomenon because long-lived pollutants can be found to be increasing at any sites of the globe. Remote air just

means that the site is located far away from the sources of emissions and, consequently, this air has lower concentrations of short-lived (reactive) substances compared with sites close to sources of pollutants. Although polluted air is human-influenced air, clean air is not synonymous with natural air. The natural atmosphere no longer exists; it was the chemical composition of air without man-made influences. However, this definition is also not exact, because humans are part of nature. In nature situations may occur, such as volcanic eruptions, sand storms and biomass burning, where the air is being “polluted” (rendered unwholesome by contaminants) or in other words, concentrations of substances of natural origin are increased. Therefore, the reference state of natural air is a climatological figure where a mean value with its variation must be considered. The term clean air is also used politically in air pollution control as a target, i.e., to make our air cleaner (or less polluted) in the sense of pollutant abatement. A clean atmosphere is a political target, it represents an air chemical composition (defined in time and scale) which should permit sustainable development. The largest difficulty, however, lies in the definition of what sustainable means. This term comprises the whole range of categories from simple scientific questions (for example, impact threshold) to political decisions (global ecomanagement) and also to philosophical questions (for example, what human life needs).

Therefore, air pollution in terms of the changing chemical composition of the atmosphere must be identified through a problem, not simply by measured concentrations. The problem lies between “dangerous” and “acceptable” climate impact, a definition that is beyond the direct role of the scientific community despite the fact that scientists have many ideas about it (*Schneider, 2006*).

Doubtless, the air of settlements and towns was extremely polluted in the past. Heavy metals have been found in Greenland ice cores dating back to the Roman Empire; thus demonstrating that metallurgical operations of immense volume took place in that era. The modern quality of air pollution, since the industrial revolution of the nineteenth century, is best characterized by a continuous worldwide increase in emissions as the era of fossil fuel combustion began. In the last 150 years, serious air pollution problems have been described, analyzed, and solved (to an extent, by end-of-pipe technologies), such as soot, dust and smoke plagues, winter and summer smog, and acid rain. The chemicals (or emitted compounds) behind these phenomena are soot, sulfur dioxide (SO<sub>2</sub>), nitrogen oxides (NO<sub>x</sub>), and volatile organic compounds (VOC) – all of them short-lived species, but because of global use of fossil fuels, the pollution problem is distributed globally. Some air pollution problems connected with long-lived compounds – now in terms of persistent compounds, such as agricultural chemicals (food chain accumulation) and halogenated organic compounds (ozone layer destruction) – have been solved by legislation banning their use. Unfortunately, some long-lived emitted compounds, the so-called greenhouse gases, have increased significantly in global mean concentration (*Table 1*).

Table 1. Increase of some climate relevant gases in air (in ppb)

Substance	1850	2008	Increase (in ppb)	Increase (in %)
Carbon dioxide CO <sub>2</sub>	285,000	383,000	98,000	34
Methane CH <sub>4</sub>	700	1700	1000	143
Nitrous oxide N <sub>2</sub> O	300	320	20	7
Ozone O <sub>3</sub>	10	20	10	100

Ozone is not among long-lived species but globally it is a secondary product from methane oxidation. CH<sub>4</sub> and N<sub>2</sub>O (mainly byproducts of agriculture) as well as CO<sub>2</sub> (a byproduct of fossil fuel combustion) are coupled with the two columns of human existence; food and energy. There is no doubt that the CO<sub>2</sub> problem can be solved only through sustainable technology change. It should be noted that these three pollutants (CO<sub>2</sub>, CH<sub>4</sub>, and N<sub>2</sub>O), even with much higher atmospheric concentrations, are harmless for life. They are in fact key substances in biogeochemical cycles, but there is also no doubt that these three substances contribute to about 90% of global warming. Besides, N<sub>2</sub>O acts as an ozone-depleting substance in the stratosphere, while CH<sub>4</sub> contributes to O<sub>3</sub> formation in the troposphere and is probably responsible for up to 80% of the global O<sub>3</sub> increase. Future air pollution control is synonymous with climate control and must be focused on CO<sub>2</sub>, CH<sub>4</sub>, and N<sub>2</sub>O.

#### 4. Climate and the climate system

The physical and chemical status of the atmosphere on a medium-range timescale (by definition 30 years) is called climate. The expression climate is currently often used in connection with climate change (a term widely popularized in recent years). Synonymously, the expression climate alteration (a more scientific term) is used. In the United Nations Framework Agreement on Climate Change, which was signed by 34 countries and was approved in New York on May 9, 1992, climate change is defined as “changes in climate, that are directly or indirectly attributable to anthropogenic activities, which change the composition of the atmosphere and which add up to the natural climatic changes observed over comparable periods of time”. This definition is circumscribed, as natural processes are included in the sense of climate change but not in the sense of climate alteration. However, it can only be observed that climate change is due to all factors. Possible anthropogenic factors having an effect on climate (and, therefore, on its alteration) are manifold and stretch from an alteration in the use of land (altered surface properties) to emissions, whereas direct energetic influences (e.g., warmth islands) are at most (first) of local importance. Thus, a climatic change is the difference between two states of climate. A state of climate is described through the static condition of the climatic system. A

climatic fluctuation can therefore be described as a periodic climatic change, independent of the respective scale of time. Climate is a function of space and time – and is continuously changing (*Schneider-Carius*, 1961).

The climate system is too complex to be clearly mathematically described. In all likelihood, this will be valid in the future as well. Our knowledge about many single processes in this system is still imperfect. Nevertheless, immense progress has been made in the past twenty years and the description of the principal processes is considered as assured (*Hansen et al.*, 2007). It is all the more surprising, that a (quasi)-linear relationship between the GMT (global mean temperature) and the cumulative CO<sub>2</sub> emission was found; on the other hand, the atmospheric CO<sub>2</sub> concentration also shows a strong linear relation with the cumulative CO<sub>2</sub> emission since about 1910 (*Möller*, 2010).

Both climate researchers and historians of climate science have conceived of climate as a stable and well defined category, but such a conception is flawed. Of particular interest becomes the impact of climate on human beings and the environment. In modern climate research, at the close of the twentieth century, the concept of climate lost its temporal stability. Instead, climate change has become a core feature of the understanding of climate and a focus of research interest. Climate has also lost its immediate association with specific geographical places and become global. Interest is now focused on the impact of human beings on climate (*Heymann*, 2009).

*Alexander von Humboldt's* often cited definition of climate shows three remarkable particularities: the relation of changes instead of a mean status (as defined later in the nineteenth century), the inclusion of the chemical status of the atmosphere (by using the terms cleanness and pollution), and the restriction on parameters affecting human organisms but also the whole biosphere:

“The term climate, taken in its most general sense, indicates all the changes in the atmosphere which sensibly affect our organs, as temperature, humidity, variations in the barometric pressure, the calm state of the air or the action of opposite winds, the amount of electric tension, the purity of the atmosphere or its admixture with more or less noxious gaseous exhalations, and, finally the degree of ordinary transparency and cleanness of the sky, which is not only important with respect to the increased radiation from the earth, the organic development of plants, and the ripening of fruits, but also with reference to its influence on the feeling and mental condition of men.” (*Humboldt*, 1850–1852)

The father of the physical definition of climate is *Julius Hann* who defined the climate as “the entirety of meteorological phenomena which describe the mean status of the atmosphere at any given point of the earth’s surface”<sup>4</sup> (*Hann*,

---

<sup>4</sup> “...Gesamtheit meteorologischer Erscheinungen, welche den mittleren Zustand der Atmosphäre an irgendeiner Stelle der Erdoberfläche charakterisieren.”

1883). He further stated that “climate is the entirety of the weathers<sup>5</sup> of a longer or shorter period as occurring on average at a given time of the year”. The aim of climatology is to establish the mean states of the atmosphere over different parts of the earth’s surface, including describing its variations (anomalies) within longer periods for the same location (*Hann*, 1883). *Hann* also introduced the term climatic element emphasizing that measurements must characterize these through numerical values. He also freed the term “climate” from the close relation to humans and plants, and related it to the time before life appeared on the earth (without using the term palaeoclimate).

*Köppen* (1906) adopted *Hann*’s definition (“mean weather at a given location”) but stated in contrast to *Hann* that it is meaningless to define a climate without focus on human beings; hence only factors (elements) influencing “organic life” should be considered. *Köppen* explicitly presents a “second definition” of climate “... as the entirety of atmospheric conditions, which make a location on earth more or less habitable for men, animals and plants” (*Köppen*, 1906). He wrote that “with the progress in knowledge new subjects will be included in the number of climatic elements when their geographical characteristics are unveiled” (*Köppen*, 1923). During the last 60 years the idea of climate has broadened in so far that, in the definition of climate, apart from the mean value, higher statistical moments are included. According to the new definition, climate describes the “statistical behavior of the atmosphere, which is characteristic for a relatively large temporal order of magnitude” (*Hantel et al.*, 1987).

For an understanding of the dynamics of climate, that is, the processes that determine the average state and variability of the atmosphere over longer periods, the meteorological definition is inadequate, as over longer periods, changes in the atmosphere are considerably affected by interdependencies of the atmosphere, the ocean, vegetation and ice masses (*Claußen*, 2006). For this reason, in climate dynamics, climate is defined by the state and the statistical behavior of the climatic system, as can be read in modern textbooks on meteorology and climate physics (e.g., *Peixoto and Oort*, 1992; *Kraus*, 2004; *Lutgens et al.*, 2009). *Claußen* (2006) distinguishes between a meteorological and a system-analytical definition. Note that it is essential to include the statistics into the idea of climate, i.e., climate means not simply the “mean weather”. It follows that

- climate is a function of space and time;
- climate cannot be described as a single unit.

---

<sup>5</sup> There is no direct English translation of German Witterung. The translation as “weather” (German Wetter) is not fully correct because Witterung denotes short-term averaged weather (a weather period).

In the history of mankind and the exploration of air and atmosphere, the concept of climate has been subject to change, but also various descriptions have existed at the same time. It is beyond the scope of this paper to address them here. Here, one can conclude that different definitions of climate are also in use. A priori, this is a contradiction, as there is only one climate system on the Earth. Obviously, this results from a pragmatic approach to the cognition and description of the climatic system by

- diverse disciplinary points of view,
- different objectives (e.g., description of subsystems), and/or
- differentiated knowledge of the system relationships.

The climate system can be described (and widely quantified through measurements) by the

- natural energy system,
- hydrologic cycle,
- carbon cycle and
- other biogeochemical cycles.

The subsystems are linked to each other through flows of energy, impulse, and matter. To the flows of matter, the transport of chemical substances and the processes of their transformation need to be added, as far as these substances, e.g., greenhouse gases or nutrients of the biosphere are directly or indirectly related to the energy budget. The definition of the climate system is not derived from superior principles, but is a pragmatic restriction of the subject to be examined by classification in subsystems and interpretation of the respective system environment. The separation of the climate system from its environment is carried out in that way, as no significant flow of matter between the system and its environment occurs on timescales relevant for examination.

In a broader sense, the climate system can be seen as an interlayer within the earth system, buffering a habitable zone from uninhabitable physical and chemical conditions in altitude (upper atmosphere) and depth (deep lithosphere); see *Fig. 2*. In a more narrow sense, the human-habitable zone is limited to the gas-solid interface (earth-surface/atmosphere) with a very small extension of a few tens of meters. The anthroposphere (or noosphere), however, is permanently expanding in space – also out of the climate system – due to the fact that humans are creating inhabited and uninhabited closed habitable systems in an uninhabitable surrounding.

In the literature, the total of climate system and anthroposphere is defined as the earth system (*Schellnhuber* and *Wenzel*, 1998; *Schellnhuber*, 1999; *Claußen*, 1998, 2001). *Hantel* (2001) presents a very pregnant definition “The

climate is not a subject-matter but a property. Its carrier is the climate system. The climate is the entirety of the properties of the climate system.”

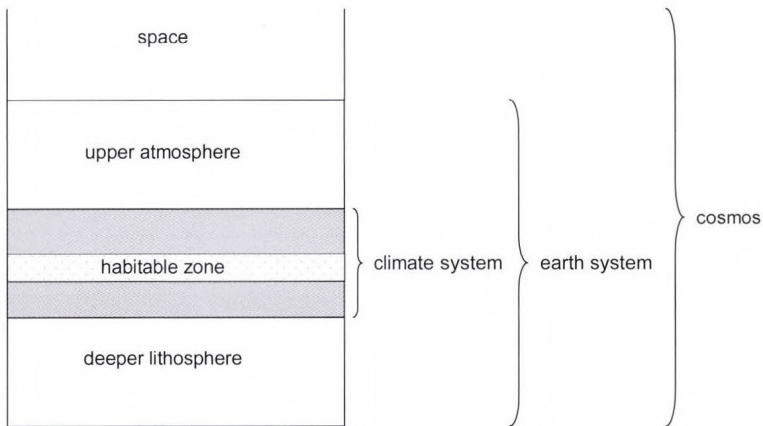


Fig. 2. Layer structure of the climate system.

According to the definition of “chemical weather” given by *Lawrence et al.* (2005), we arrive at a formal definition of chemical climate as: “The synthesis of chemical weather conditions in a given area, characterized by long-term statistics (mean values, variances, probabilities of extreme values, etc.) of the chemical substances in that area.”

Instead of “meteorological elements”, we have “chemical substances”. When – as implicitly mentioned earlier – meteorology feels responsible as a discipline for the description of the chemical state of the atmosphere, the list of “meteorological elements” can simply be expanded to accommodate all relevant chemical variables as well. So as not to raise misunderstandings, “chemical aspects” and not “chemistry” are dealt with the extension of the term climate, since climatology is not a subdiscipline of physics.

I would like to define climate in a general sense as follows:

Climate describes the mean status of the atmosphere at a given site of the earth’s surface, represented by the statistical total properties (mean values, frequencies, durations etc.) of a long enough time period.

It is understood, and, therefore, no differentiation between a meteorological and a system-related definition of climate according to *Claußen* shall be undertaken, that the atmosphere is only one part of the climatic system, and therefore, climate can only correctly be described in a physical-chemical manner taking into consideration material and energetic interdependencies with the other subsystems. Advantageously, a climatic state (i.e., the scientific, broadly mathematical description of the climate) can be defined:

A climate state is given by the whole description of the statistical status of the internal climate system.

The conclusion that the climate is permanently but slowly changing is true. Now, however, we have the likely situation of man-made abrupt climate change. An abrupt climate change occurs when the climate system is forced into transition to a new state at a rate that is determined by the climate system itself, and which is more rapid than the rate of change of the external forcing. Moreover, with this background we understand climate change better, because it means that one or more of the earth-system determining climate elements is changing by a qualitative jump. In nature there is no jump, as nature itself composes of jumps. The idea of interactive changes from quality to quantity and vice versa is a main principle of dialectics. The fact, that our subjective thinking and the objective world underlies the same laws, and therefore, cannot be contradictory in their results, but correspond, rules our complete theoretical thinking. It is an unconscious and unconditional premise. The materialism of the eighteenth century studied this premise according to its vitally metaphysical character on its content only. It limited itself to the proof that the content of all thinking and knowledge descends from sensual experience, and reconstructed the sentence: *Nihil est in intellectu, quod non fuerit in sensu*. (Nothing is in the mind, which has not been in the senses before). Dialectics as the science of the common laws of all movement was first scientifically postulated by *Friedrich Engels*. Despite the linguistic simplification, we should not forget the complexity of the system: even the most advanced mathematical models running on the biggest (and networked) computers are still unable to produce a true picture of the climate system sufficient to draw reliable conclusions. Experimental validation of the model outputs, however, is only possible after climate change – that is the dilemma! Parts of the model (or the system) can be validated with relevant experimental approaches, for example, cooling of the atmosphere by particulate matter after large volcanic eruptions.

### ***5. Chemical evolution and the role of humans***

The term evolution was used first in the field of biology at the end of the nineteenth century. In the context of biology, evolution is simply the genetic change in populations of organisms over successive generations. Evolution is widely understood as a process that results in greater quality or complexity (a process in which something passes by degrees to a different stage, especially a more advanced or mature stage). However, depending on the situation, the complexity of organisms can increase, decrease, or stay the same, and all three of these trends have been observed in biological evolution. Nowadays, the word has a number of different meanings in different fields. The term chemical evolution is not well-defined and used in different senses.

Chemical evolution is not simply the change and transformation of chemical elements, molecules, and compounds as it is often asserted – that is the nature of chemistry itself. It is essentially the process by which increasingly complex elements, molecules, and compounds develop from the simpler chemical elements that were created in the Big Bang. The chemical history of the universe began with the generation of simple chemicals in the Big Bang. Depending on the size and density of the star, the fusion reactions can end with the formation of carbon or they can continue to form all the elements up to iron.

The origin of life is a necessary precursor for biological evolution, but understanding that evolution occurred once organisms appeared and investigating how this happens do not depend on understanding exactly how life began. The current scientific consensus is that the complex biochemistry that makes up life came from simpler chemical reactions, but it is unclear how this occurred. Not much is certain about the earliest developments in life, the structure of the first living things, or the identity and nature of any last universal common ancestor or ancestral gene pool. Consequently, there is no scientific consensus on how life began, but proposals include self-replicating molecules such as RNA, and the assembly of simple cells. Astronomers have recently discovered the existence of complex organic molecules in space. Small organic molecules were found to have evolved into complex aromatic molecules over a period of several thousand years. Chemical evolution is an exciting topic of study, because it yields insight into the processes which lead to the generation of the chemical materials essential for the development of life. If the chemical evolution of organic molecules is a universal process, life is unlikely a uniquely terrestrial phenomenon, instead, it is likely to be found wherever the essential chemical ingredients occur.

In colloquial contexts, evolution usually refers to development over a long time scale, and the question is not important whether evolution tends toward more complexity. Many definitions tend to postulate or assume that complexity expresses a condition of numerous elements in a system and numerous forms of relationships among the elements. At the same time, deciding on what is complex and what is simple is relative and changes with time.

A modern understanding of evolution includes continuous development, but also leaps (catastrophes). This is referred to as “transformation of quantity into quality” (dialectic leap) and may characterize the current discussion on the impacts of climate change. However, it is hard to envisage a physical situation in which a quantifiable parameter can increase indefinitely without a critical condition occurring. Physical processes – starting with the Big Bang – created the first atoms (which form chemical elements) and physical conditions, permanently affecting the subsequent chemical and biological evolution. Compared with the Big Bang as the beginning of physical evolution, the creation of molecules and life can be referred to as the starting point of a chemical and biological evolution, respectively. Life became a geological force

with oxygenic photosynthesis and created an interactive feedback with chemical and physical evolution. After forming the geosphere and the first atmosphere in the sense of a potentially habitable system, and later the biosphere with the modern atmosphere, a habitable climate system evolved.

If water was as common in the solar system as it is implied by the facts, that would suggest that there were many environments in the solar system where the conditions were right for the development of life. What is life? For instance, *Lynn Margulis* (quoted by *Horgan*, 1997) has stated that to proceed "...from a bacterium to people is less of a step than to go from a mixture of amino acids to that bacterium". At the beginning of the seventeenth century, the ultimate origin of life was considered to be primarily a theological issue. However, it was thought possible that small creatures, such as maggots and even mice, could arise from non-living material by spontaneous generation, a theory first propounded by Aristotle. Today, there is no doubt that bacterial life is created, exists, and survives in space (*Maurette*, 2006). But, what is life? Where did we come from? These two fundamental questions remain (still) unanswered in science. The existence of humans (and all animals) depends on free oxygen in the atmosphere, and this compound is almost completely produced from oceanic cyanobacteria. Hence, the origin of life lies in the darkness of the evolution of molecules in structured systems (a chemical plant that we call a cell) to provide work-sharing synthesis via non-equilibrium electron transfer processes (in other terms, redox processes). Cells represent a dissipative structure, whose organization and stability is provided by irreversible processes running far from equilibrium. *Falkowski* and *Godfrey* (2008) state that the question posed above reflects our ignorance of basic chemistry of the electron transfers, that bring the ensemble of molecules in cells to "life".

But life created a further dimension, human intelligence, which becomes another geological force (human evolution – today approaching a critical condition which we call crisis). Human intelligence disengaged humankind from the rigorous necessities of nature and provided unlimited scope for reproduction (at least in the past). Man, in all his activities and social organizations is part of, and cannot stand in opposition to or be a detached or external observer of, the nature. However, the new dimension (or quality) of human intelligence as a result of biological evolution – without some global ecomanagement – could change the climate system in a direction not providing the internal principle of self-preservation. Mankind converts the biosphere into a noosphere. Chemical evolution is now interloped with human evolution. Changing fluxes and concentrations of chemicals in bio- (or rather noo-) geochemical cycles with a subsequent changing climate system seems to be the creation of a human-chemical evolution.

*Vernadsky* was the first to propose the idea of biogeochemical cycling (having asked: What is the impact of life on geology and chemistry of the earth?). *Vernadsky*, who had met *Suess* in 1911, popularized the term biosphere in his book *The Biosphere* (first published in Russian in 1926, not translated into

a full English version until more than 60 years later), hypothesizing that life is the geological force that shapes the earth (*Vernadsky*, 1926; 1944; 1945). *Vernadsky* first took the term “noosphere” in 1931, as a new dimension of the biosphere under the evolutionary influence of humankind (*Vernadsky*, 1944). He wrote: “The Noosphere is the last of many stages in the evolution of the biosphere in geological history” (*Vernadsky*, 1945). The biosphere became a real geological force that is changing the face of the earth, and the biosphere is changing into the noosphere. In *Vernadsky*’s interpretation, the noosphere is a new evolutionary stage of the biosphere, when human reason will provide further sustainable development both of humanity and the global environment

“In our century the biosphere has acquired an entirely new meaning; it is being revealed as a planetary phenomenon of cosmic character... In the twentieth century, man, for the first time in the history of earth, knew and embraced the whole biosphere, completed the geographic map of the planet earth, and colonized its whole surface. Mankind became a single totality in the life on earth... The noosphere is the last of many stages in the evolution of the biosphere in geological history.” (*Vernadsky*, 1945).

Today the term “anthroposphere” is also used. The idea of a close interrelation between the humans and the biosphere is topical in understanding the “earth system”, i.e., the climate change, and is used by *Schellnhuber* (1999) with the terminology “global mind” and by *Crutzen* and *Stoermer* (2000) with “anthropocene” to characterize the present epoch<sup>6</sup>.

We also may state that the climate is first a result of geophysical and chemical processes, and that evolving life adapts to these conditions. We know that oxygen is definitively a result of the photosynthesis of plants, hence it is of biological origin. Without any doubt we can state that life did change the climate – with “sense” or without –, and that feedback did influence the evolution of life. What is life or a living thing? Each living thing is composed of “lifeless” molecules, independently of its dimension and complexity, which are subject to the physical and chemical laws that are characteristic of inanimate bodies. A living thing (to avoid the definition of “life”) has certain characteristics which are common to living matter but not found in nonliving objects, such as:

- the capacity for self-replication (they grow and reproduce in forms identical in mass, shape, and internal structure),
- the ability to extract, transform, and use energy from their environment (in the form of nutrients and sunlight), and
- an organized structure, where each component unit has a specific purpose or function.

---

<sup>6</sup> *Zalasiewicz et al.* (2008) published the first proposal for the formal adoption of the Anthropocene epoch by geologists, and this adoption is now pending.

All these characteristics result in non-equilibrium with themselves and with their environment. Non-living things tend to exist in equilibrium with their surroundings. An earth-like planet, not developing life, would therefore be oxidized with aging. Only photolytic dissociation and thermal degradation would occur, depending on incoming radiation (distance from the Sun) and available thermal heat (planetary size). At a final stage, the atmosphere would be composed solely of oxides and acids. The large  $\text{CO}_2$  content would increase the atmospheric temperature. Missing free oxygen (because it is fixed in oxides, volatile and non-volatile) in the atmosphere (and subsequent ozone) would prevent a UV-absorbing layer and, therefore, allow almost all photodissociations close to the planetary surface. With time, all water would disappear due to photolytic splitting into hydrogen, which escapes into space. The oxygen from water splitting cannot accumulate until all primordial reduced atoms are oxidized. Finally, free oxygen could be possible in the case of an excess over the equivalent of atoms in reduced state. Conversely, no free oxygen would occur when the reduction equivalent exceeds that of oxygen. The planet becomes irreversibly uninhabitable, especially because of absence of water. There is no doubt that this process would occur over a long time, potentially over the planetary lifetime.

The non-living world tends to dissipate structures and, therefore, to increase entropy. However, because of its huge energy pools, the earth's internal geothermal heat and the Sun's radiation, both are likely to remain over the entire expected lifetime of the earth, provide gradients to force geochemical cycling with the irreversible direction of oxidation and acidification (*Fig. 3*).

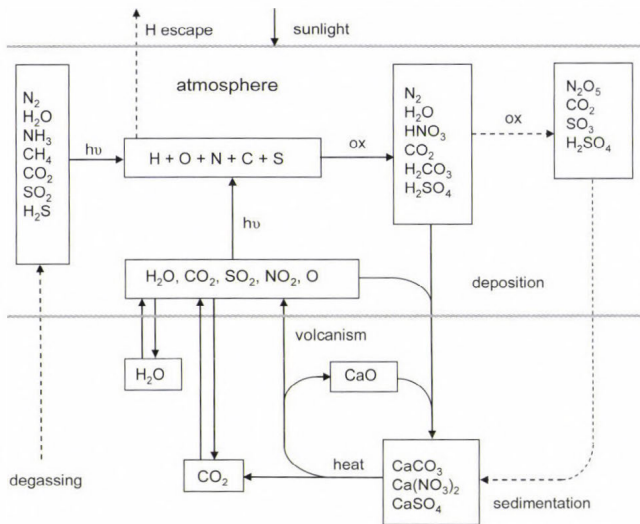


*Fig. 3.* Scheme of geochemical cycling over geological epochs.

Only the living world is able to reduce entropy by creating structures, or in other words, to move the system back from equilibrium. Indeed, the central role

of life (more exactly, autotrophic organisms) is to maintain the cycle shown in Fig. 4, starting with light-induced electrolytic water splitting, and subsequent parallel – but, important to note, in separated organs – reduction of  $\text{CO}_2$  into hydrocarbons and the oxidation of them back to  $\text{CO}_2$ . Globally, this cycle represents a dynamic equilibrium. Consequently, there are established stationary concentrations in the climate system.

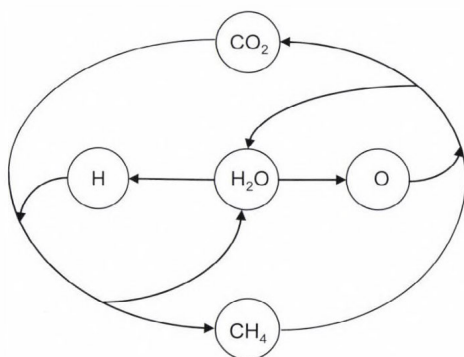


Fig. 4. Scheme of the water-carbon interlinked cycle.

Under the evolution of the earth and the climate system, we will simply understand the historical development from earliest times until the present. Theories for how the atmosphere and ocean formed must begin with an idea of how the Earth itself originated (*Kasting, 1993*). An understanding of our atmosphere and climate system is incomplete without going into the past. “The farther backward you can look the farther forward you can see.” (*Winston Churchill*).

### 6. Conclusion: toward sustainability

In recent decades, humans have become a very important force in the earth system, demonstrating that emissions and land use changes are the cause of many of our environmental issues. These emissions are responsible for the major global reorganizations of biogeochemical cycles. With humans as part of nature and the evolution of a man-made changed earth’s system, we also have to accept that we are unable to remove the present system into a preindustrial or even prehuman state, because this means disestablishing humans. The key question is which parameters of the climate system allow the existence of humans (and how many) under which specific conditions.

The chemical composition of air is now contributed by both natural and man-made sources. The chemical composition of air has been changing since the settlement of humans. In addition to the scale problem (from local to global), we

have to regard the time scale. Natural climate variations (e.g., due to ice ages) had a minimum time scale of 10.000 years. The man-made changes in our atmosphere over the last 2000 years were relatively small before the 1850s. In the past 150 years (but almost all after 1950), however, the chemical composition has changed drastically. For many atmospheric compounds anthropogenic emissions have grown to the same or even larger order of magnitude than natural ones. Because of the huge population density, the need (or consumption)<sup>7</sup> of materials and energy has drastically forced the earth's system. "The Great Acceleration is reaching criticality. Whatever unfolds, the next few decades will surely be a tipping point in the evolution of the Anthropocene" write *Steffen et al.* (2007).

The time scale of the adaptation and restoration of natural systems is much larger than the time scale of man-made stresses (or changes) to the climate system. We should not forget that "nature" cannot assess its own condition. In other words, the biosphere will accept all chemical and physical conditions, even worse (catastrophic) ones. Only humans possess the facility to evaluate the situation, accepting it or not, and coming to the conclusion of making it sustainable. But humans also do have all the facilities to turn the "chemical revolution" into a sustainable chemical evolution. That does not mean "back to nature".

Let us define a sustainable society as one that balances the environment, other life forms, and human interactions over an indefinite time period. A global sustainable chemistry first needs a paradigm change, namely the awareness that growth drives each system towards a catastrophe. The basic principle of global sustainable chemistry, however, is to transfer matter for energetic and material use only within global cycles without changing reservoir concentrations above a critical level, which is "a quantitative estimate of an exposure to one or more pollutants below which significant harmful effects on specified sensitive elements of the environment do not occur according to present knowledge" (*Nilsson and Grennfelt, 1988*).

The value in identifying current trends and viewing them in a historical light is that the results can be used to inform ongoing policy and investment decisions. The planet could not support the six to seven billion people that exist today without the commercialization of first coal, and then oil and gas. Whereas historical increases in energy consumption had been gradual, once industrialization occurred, the rate of consumption increased dramatically over a

---

<sup>7</sup> This is an interesting question: do we need all this consumption? What consumption do we need to realize a *cultural* life? Of course we move from natural (earth sciences) to a social and political dimension (life sciences) in answering these questions. But there is a huge potential to economize and save resources in answering these questions and implementing it. *Karl Marx* wrote "The philosophers have only managed to interpret the world in various ways. The point is to change it". (This is still fixed in the main hall of the central building of the Humboldt University in Berlin, Germany). However, the key point is how and in which direction we have to change the world to receive sustainability.

period of just a few generations. In fact, the rate of energy use from all sources has been growing even faster than, the world population growth. Thus, from 1970 to 1995, energy use increased at a rate of 2.5% per year (doubling in every 30 years) compared with a worldwide population growth of 1.7% per year (doubling in every 40 years). During the next 20 years, energy use is projected to increase at a rate of 4.5% per year (doubling in every 16 years) compared with a population growth rate of 1.3% per year (doubling in every 54 years). Although about 50% of all the solar energy captured by worldwide photosynthesis is used by humans, this amount is still inadequate to meet all human needs for food and other purposes (*Pimentel and Pimentel, 2007*). Hence, only the direct conversion of solar energy (heat and radiation) into electricity and chemically stored energy can overcome the future gap.

A global sustainable chemistry first needs a paradigm change, namely the awareness that growth drives each system towards a catastrophe. Sustainable chemistry, also known as green chemistry, is a chemical philosophy encouraging the design of products and processes that reduce or eliminate the use and generation of hazardous substances.

Permanent growth – as stated by politicians – will not solve life problems such as employment; this is a question of reorganizing society. In nature, many processes follow a simple law Eq. (1), which expresses that the change of a quantity  $N$  (for example population, mass, energy) is proportional to the quantity itself. In other words, exponential growth occurs when some quantity regularly increases by a fixed percentage. The proportionality coefficient  $\lambda$  characterizes the process (biology, chemistry, physics, economy, etc.) as follows:

$$\frac{dN}{dt} = \lambda N = F, \quad N(t) = N_o \exp(\lambda t). \quad (1)$$

We see that  $dN/dt$  denotes a flux  $F$ ; according to the sign, it could result in a growth (positive sign) or decline (negative sign). It is clearly seen that a negative flux will end with  $N(t)=0$  with  $t \rightarrow \infty$  when there is no permanent source (positive flux) of  $N$  to maintain a pool of this quantity. After productivity (expressed as constant annual turnover) satisfies social consumption needs, stationary conditions are then achievable, i.e.,  $\lambda$  becomes zero in Eq. (1). Naturally, the human population will (and must) tend to a constant number. This limitation process is likely to go on over the next 200 years. Another limitation must be set through per capita consumption to provide social and cultural standards. The growth, however, is going on this century. Without revolutionary technological changes, the climate becomes out of control. As stated above, the atmospheric  $\text{CO}_2$  increase must be stopped within the next few decades. There are several ways, simultaneously linked with the solution of the energy problem:

- reducing fossil fuel combustion and (drastically) replacing by solar energy (e.g., desertec conception),
- CO<sub>2</sub> capture from exhaust gases and storage (CCS technology) – likely for future reuse and cycling (CCC technology), and
- CO<sub>2</sub> capture from ambient air and recycling (or sequestration achieving a negative flux) to establish a global carbon/CO<sub>2</sub> man-made cycle.

## References

- Cauer, H., 1949: Aktuelle Probleme der atmosphärischen Chemie. In *Meteorologie und Physik der Atmosphäre* (ed.: R. Mügge). 19: *Naturforschung und Medizin in Deutschland 1936-1946*. Dietrich'sche Verlagsbuchhandlung, Wiesbaden, 277-291.
- Claußen, M., 1998: Von der Klimamodellierung zur Erdsystemmodellierung: Konzepte und erste Versuche. *Ann. der Meteorol. (Neue Folge)* 36, 119-130.
- Claußen, M., 2001: Earth system models. In *Understanding the Earth System: Compartments, Processes and Interactions* (eds.: E. Ehlers and T. Krafft). Springer-Verlag, Berlin, 145-162.
- Claußen, M., 2006: Klimaänderungen: Mögliche Ursachen in Vergangenheit und Zukunft. In: *Klimawandel - vom Menschen verursacht? 8. Symposium Mensch – Umwelt* (ed.: D. Möller). *Acta Acad. Scientiarum* (Academy of the Arts and Sciences Useful to the Public in Erfurt) 10, 217.
- Crutzen, P.J. and Stoermer, E.F., 2000: The "Anthropocene". *Glob. Change Newsletters* 41, 17-18.
- Falkowski, P.G. and Godfrey, L.V., 2008: Electrons, life and the evolution of Earth's oxygen cycle. *Philosop. Transact. Roy. Soc., Ser. B* 363, 2705-2716.
- Guericke, O. von, 1672: Neue „Magdeburgische“ Versuche über den leeren Raum. In: *Ostwald's Klassiker der exakten Naturwiss.. 59. Unveränderter Nachdruck (Drittes Buch)*. Akademische Verlagsgesellschaft (ca. 1930), Leipzig, 116.
- Hann, J. von, 1883: Handbuch der Klimatologie. In: *Bibliothek geographischer Handbücher* (ed. F. Ratzel), J. Engelhorn, Stuttgart, 764. (translated into English: *Handbook of Climatology: Part I. General Climatology*, Macmillan Company, 1903).
- Hansen, J., Sato, M., Kharecha, P., Russel, G., Lea, D.W. and Siddall, M., 2007: Climate change and trace gases. *Philos. Transact. of the Roy. Society A* 365, 1925-1954.
- Hantel, M., Kraus, H. and Schönwiese, C.-D., 1987: Climate definition. In: *Landolt-Börnstein - Group V Geophysics. Numerical Data and Functional Relationships in Science and Technology. Subvolume C1 'Climatology. Part 1' of Volume 4 'Meteorology'*. Springer-Verlag, Berlin, 5.
- Hantel, M., 2001: Klimatologie. In: *Bergmann-Schaefer Lehrbuch der Experimentalphysik, 7: Erde und Planeten* (ed. W. Raith), de Gruyter, Berlin and New York, 311-426.
- Heymann, M., 2009: Klimakonstruktionen. Von der klassischen Klimatologie zur Klimaforschung. *NTM Zeitschrift für Geschichte der Wissenschaften, Technik und Medizin* 17, 171-197.
- Horgan, J., 1997: The end of science: Facing the limits of knowledge in the twilight of the scientific age. Broadway Books, New York, 319.
- Humboldt, A.V., 1850-1852: *Cosmos: A sketch of a physical description of the universe*. Translated from German by E. C. Otté. Harper & Brothers, New York, 1. 1850: 275., 2. 1850: 367., 3. 1851: 219., 4. 1852: 234.
- Junge, C.E., 1958: Atmospheric chemistry. In: *Advances in geophysics. IV*, Acad. Press. New York, (separate volume), 108.
- Junge, C.E., 1963: Air chemistry and radioactivity. *Int. Geophys. Ser.* (ed. J. van Mieghem) 4, Academic Press, New York and London, 382.
- Kasting J.F., 1993: Earth's early atmosphere. *Science* 259, 920-926.
- Köppen, W. 1906: *Klimakunde I: Allgemeine Klimakunde*. Göschen, Leipzig, 8; 132.
- Köppen, W., 1923: *Die Klimate der Erde. Grundriß der Klimakunde*. 1. Auflage. de Gruyter, Berlin, 3; 369.
- Kraus, H., 2004: *Die Atmosphäre der Erde. Eine Einführung in die Meteorologie*. Springer-Verlag, 422.

- Lakatos, I., 1980: History of science and its rational reconstructions. In: *Scientific revolutions* (ed. J. Hacking), Oxford University Press, 107-127.
- Lavoisier, A.-L., 1789: Elements of Chemistry in a new systematic order, containing all the modern discoveries. (Transl. by R. Kerr) reprint 1965, Dover Publ. New York, 511.
- Lawrence, M.G., Hov, O., Bekmann, M., Brandt, J., Elbern, H., Eskes, H., Feichter H. and Takigawa, M., 2005: The chemical weather. *Environ. Chemist.* 2, 6-8.
- Liljequist, G.H. and Cihak, K., 1984: Allgemeine Meteorologie. Fr. Vieweg und Sohn, Braunschweig, 368.
- Lutgens, F.K., Tarbuck, E.J. and Tasa, D., 2009: The atmosphere: An introduction to meteorology. (11th edition). Prentice Hall, Toronto, 544.
- Maurette, M., 2006: Micrometeorites and the mysteries of our origins. Springer-Verlag, Berlin, 200.
- Möller, D., 2010: Chemistry of the climate system. De Gruyter, Berlin 722.
- Nilsson, J. and Grennfelt, P., eds. 1988: Critical loads for sulphur and nitrogen. *UNECE/Nordic Council workshop report*, Skokloster, Sweden. March 1988. Nordic Council of Ministers: Copenhagen.
- Peixoto, J.P. and Oort, A.H., 1992: Physics of climate. Springer, New York, 520.
- Pimentel, D. and Pimentel, M.H., 2007: Food, energy, and society. (3rd edition), CRC Press, 380.
- Scharnow, U., Berth, W. and Keller, W. 1965: Wetterkunde. VEB Verlag für Verkehrswesen, Berlin, 415.
- Schellnhuber, H.-J. and Wenzel, V., eds. 1998: Earth system analysis - integrating science for sustainability. Springer-Verlag, Berlin, 530.
- Schellnhuber, H.-J., 1999: Earth system analysis and the second Copernican Revolution. *Nature, Suppl.* 402, C19-C23.
- Schneider, St.H., 2006: Climate change: Do we know enough for policy action? *Sci. Engineer. Ethics* 12, 607-636.
- Schneider-Carius, K., 1961: Das Klima, seine Definition und Darstellung. Zwei Grundsatzfragen der Klimatologie. In: *Veröffentlichungen der Geophysik*, Institut der Universität Leipzig, 2. Serie, Bd. XVII, Heft 2, Berlin.
- Steffen, W., Crutzen, P.J. and McNeill, J.R., 2007: The Anthropocene: Are humans now overwhelming the Great Forces of Nature? *Ambio* 36, 614-621.
- Vernadski, V.I. 1926: Biosphera (in Russian). *Nautschnyi-chim.-techn.* Izdatelstvo, Leningrad 48 pp. Translated into French (*La Biosphère*, 1929), German (*Biosphäre*, 1930), and English (*The Biosphere*, 1998; a reduced version in English appeared in 1986)
- Vernadski, V.I., 1944: Some words on noosphere (in Russian). *Учену соврем. биол. (uspechi sovrem. biol.* 18, 113-120.
- Vernadsky, V.I., 1945: The biosphere and the noosphere. *Scient. Amer.* 33, 1-12.
- Zalasiewicz, J., Williams, M., Smith, A., Barry, T.L., Coe, A.L., Bown, P.R., Brenchley, P., Cantrill, D., Gale, A., Gibbard, P., Gregory, F.J., Hounslow, M.W., Kerr, A.C., Pearson, P., Knox, R., Powell, J., Waters, C., Marshall, J., Oates, M., Rawson P. and Stone, P., 2008: Are we now living in the Anthropocene? *GSA Today* 18, 4-8.



# IDŐJÁRÁS

*Quarterly Journal of the Hungarian Meteorological Service  
Vol. 115, No. 3, July–September 2011, pp. 147–165*

## **Numerical simulation of the cycle of aerosol particles in stratocumulus clouds with a two-dimensional kinematic model**

**Beáta Szabó-Takács**

*University of Pécs, Institute of Environmental Sciences  
Ifjúság u. 6, H-7624 Pécs, Hungary;  
E-mail: takacs.beata@gamma.ttk.pte.hu*

*(Manuscript received in final form October 20, 2010)*

**Abstract**—The purpose of the paper was to develop a numerical model to study the cycle of aerosol particles in stratocumulus clouds in different air mass types. A detailed microphysical scheme was incorporated into an idealized two-dimensional kinematic model to investigate the role of the aerosol particles in the formation of the water droplets, regeneration of the aerosol particles due to evaporation of the water drops, and the washout of the aerosol particles. The calculations were made with different cloud condensation nuclei (CCN) size distributions and concentrations typical for maritime, rural, and remote continental air mass types, furthermore, with two different updraft profiles. The water droplets were formed on soluble ammonium-sulfate aerosol particles. The ratio of the number concentration of the soluble and insoluble aerosol particles depended on their size. The drops grew by condensation and collision coalescence in the updraft core, but they evaporated due to the subsaturation in the downdraft region.

The model clearly simulated the regeneration of the aerosol particles. The majority of the water soluble particles were scavenged due to the water drop formation. The efficiency of the scavenging of the water insoluble particles depended on the concentration of the water soluble aerosol particles. While Brownian effect played an important role in capturing these particles, only few of them were washed out due to the phoretic- and gravitational forces. Results of the numerical simulation show that in the case of the stratocumulus clouds the number concentration of insoluble aerosol particles larger than  $0.1\ \mu\text{m}$  is hardly modified due to different scavenging mechanisms.

*Key-words:* aerosol particles, drop formation, condensational growth, collision coalescence, aerosol scavenging, aerosol regeneration

## 1. Introduction

In the 20th century the interest in the effect of the aerosol particles in the clouds has been increased. The aerosol particles play important role in the formation of the clouds. Their characteristics strongly affect both the optical properties of the clouds and precipitation formation. The impact of aerosol particles on the clouds is strongly affected by the physical and chemical attributes of the particles, which depend on the various air mass types (*Hoose et al.*, 2008; *Sassen et al.*, 1999). While the dynamical processes in general define where supersaturated environments occur in the atmosphere, the cloud attributes are determined by aerosol-cloud interaction (*Targino et al.*, 2007). This interaction includes variety of microphysical processes that affect the concentration, size distribution, and chemical composition of cloud droplets (*Gilliani et al.*, 1995). Clouds play an important role in the redistribution of aerosol particles in the atmosphere. The wet scavenging can be separated into two categories. The in-cloud scavenging refers to nucleation and interstitial scavenging. Another category is the below-cloud scavenging, when the aerosol particles are collected by hydrometeors that fall out from the cloud (*Feng*, 2007). The majority of the water-soluble particles are removed by nucleation scavenging (water drops form on the particle).

Results of numerical simulations about the effect of the size distribution and chemical composition on the albedo and the precipitation formation of the stratocumulus clouds have been published in numerous papers (*Geresdi et al.*, 2006; *Caro et al.*, 2004; *Geresdi and Rasmussen*, 2005; *Zhang et al.*, 2004; *Bott*, 2000; *Feingold et al.*, 1996; *Ackerman et al.*, 1995). In our research we have focused on the aerosol–cloud interactions that occur in stratocumulus clouds. Not only the role of the aerosol particles in the precipitation formation was investigated, but also how the water insoluble aerosol particles are washed out. We also studied the regeneration of the aerosol particles in the subsaturated regions.

These processes were investigated in stratocumulus clouds due to their relatively simple dynamics. The weak convective updrafts generate shallow, horizontally extensive cloud layers due to the overlaying drier and stable air that blocks the vertical development of the air mass. Stratocumulus clouds play an important role in climate change due to their high albedo, which causes a significant negative contribution to the overall radiative forcing.

In the present paper we discuss our results on the cycle of the aerosol particles in stratocumulus clouds under different dynamic and environmental conditions.

## 2. Model description

The microphysical processes that occur in a stratocumulus cloud were simulated in a dynamic framework of the idealized two-dimensional kinematic model developed by *Szumowski et al.* (1998) and *Morrison and Grabowski* (2007) with

2D MPDATA routine written by Smolarkiewicz (*Smolarkiewicz and Margolin, 1998*). The two-dimensional domain includes both updraft and downdraft regions. The updraft and downdraft regions were characterized with two different maximum velocities. The horizontal and vertical extensions of the domain were 2000 m and 750 m, respectively. The resolution was 20 m in horizontal direction and it was 15 m in vertical direction.

Detailed microphysical scheme was used in the research (see the details in *Geresdi, 1998; Geresdi and Rasmussen, 2005*). The size distribution of water drops and wet aerosol (haze) particles were divided into 55 bins. At the left side edge of the first bin, the particle mass was  $3.048 \times 10^{-20}$  kg with doubling the mass in the bin edges ( $m_{k+1} = 2 m_k$ ). The size distribution of the dry aerosol particles were divided into 36 bins. At the left side edge of the first bin, the particle mass was the same in the case of the dry aerosol particles and haze particles (wet aerosol particles). While the density of the aerosol particles was assumed to be size independent ( $1600 \text{ kg/m}^3$ ), the density of the haze particles depended on the molar concentration of the solution. The aerosol particles were divided into two categories: water soluble and water insoluble ones. The uncertainties about the size dependence of number concentration of water soluble ammonium-sulfate particles are large. The field observations show that number concentration of the soluble ammonium-sulfate particles comparing with the total aerosol concentration is relatively large in size range of  $0.1 \text{ }\mu\text{m}$  to  $1 \text{ }\mu\text{m}$  (*Masahiro et al., 2003; Charlson et al., 1983; Kulmala et al., 1997; Mertes et al., 2005; Svenningsson et al., 1997*). On the base of these observations the ratio of the number concentration of soluble aerosol particles and the total aerosol particle concentration was chosen to be 0.5 when the radius of the aerosol particles was less than  $0.012 \text{ }\mu\text{m}$  (in the first 10 bins), and this ratio was 0.7 in case of the larger sizes. The purpose of using external mixture was to investigate the different scavenging mechanisms. The aerosol particles contained water soluble fraction can be washed out mostly by water drop formation (nucleation scavenging). The water insoluble aerosol particles can be collected by water drops through other different scavenging mechanisms (Brownian, phoretic, and gravitational collection).

In this study the following microphysical processes were taken into consideration: (i) drop formation on water soluble aerosol particles, (ii) condensational growth/evaporation of water drops, (iii) collision - coalescence of water drops, and (iv) aerosol particles collection by water drops due to Brownian, phoretics and gravitational motion. Some theoretical studies suggest that the turbulence enhances the water drops - aerosol particles collection efficiency. However, efficient turbulent collection was found for collector drops near  $200 \text{ }\mu\text{m}$  in combination with particles with diameter of  $2\text{--}4 \text{ }\mu\text{m}$  (*Zhang and Vet, 2006*). Because in the stratocumulus clouds the drops size generally less than  $200 \text{ }\mu\text{m}$ , the effect of turbulent collision was not taken into account in this study.

The water soluble aerosol particles were transferred into the water drop category, if the relative humidity was larger then 90%. The transfer of dry aerosol particles to wet aerosol particles due to vapor diffusion starts at subsaturated condition. In the case of the small water soluble particles ( $< 0.1 \mu\text{m}$ ), this process occurred at relative humidity larger than 95%, at larger particles size the transfer occurred at 90%. If the mass of the water in a wet aerosol particle decreased to be equal to the mass of the aerosol inside, the wet aerosol particles were transferred to the dry aerosol particle category. Thirty minutes of cloud life time was simulated using 1 s time step.

The diffusional growth of these particles were calculated by using hybrid bin method. More details about this method can be found in the papers published by *Chen and Lamb (1994)* and *Geresdi and Rasmussen (2005)*. The collision – coalescence processes of water drops were calculated by using two-moments method. These moments – the concentration ( $N_k$ ) and the mixing ratio ( $M_k$ ) inside the  $k$ th bin – were approximated by the following linear equations:

$$N_k(m, t) = f_k \cdot \left( \frac{m_{k+1} - m}{m_{k+1} - m_k} \right) + \psi_k \cdot \left( \frac{m - m_k}{m_{k+1} - m_k} \right) = a_k + b_k \cdot m, \quad (1)$$

$$M_k(m, t) = m_k \cdot f_k \cdot \left( \frac{m_{k+1} - m}{m_{k+1} - m_k} \right) + m_{k+1} \cdot \psi_k \cdot \left( \frac{m - m_k}{m_{k+1} - m_k} \right) = c_k + d_k \cdot m, \quad (2)$$

where  $m_k$  and  $m_{k+1}$  are the particle mass at the bin boundaries, hereafter  $m$  is the mass of the particles. The  $f$  and  $\psi$  parameters were calculated by using the following equation:

$$M_k^j = \int_{x_k}^{x_{k+1}} m^j n_k(m, t) dx, \quad (3)$$

where  $M_k^0$  and  $M_k^1$  are the concentration ( $N_k$ ) and mixing ratio ( $M_k$ ) in the  $k$ th bin, respectively.

To calculate the kinetic collection equation of water drops, the Smoluchowski equation was used (*Tzivion et al., 1999*). The water drop – water drop collision efficiencies used in the model are based on the data published by *Hall (1980)*. The collision efficiencies for the given sizes of water drops were calculated by linear interpolation. The Brownian motion, the phoretic effect, and the gravitational collection were taken into consideration when the scavenging of the aerosol particles was simulated (*Ackerman et al., 1995; Gwen et al., 2004; Jian, 2007; Mircea et al., 2000*).

The Brownian motion affects the collision between hydrometeors and very small aerosol particles ( $r_p < 0.01 \mu\text{m}$ ). The following equation gives the number of collected aerosol particles in unit time due to Brownian motion:

$$\left. \frac{dN_p}{dt} \right|_B = 4\pi r_d D_p n_p f_p, \quad (4)$$

where  $r_d$  is the radius of the water drop,  $n_p$  is the number concentration of the aerosol particles,  $D_p$  is the diffusion coefficient for the aerosol particles,  $f_p$  is a correction factor which depends on the Reynolds and Schmidt numbers of the aerosol particles (*Pruppacher and Klett, 1997*). The motion of aerosol particles due to temperature gradients near to the drop surface is called thermophoresis. Particle motion due to the spatial vapor density gradient is called diffusio-phoresis. The sum of the thermophoretic and diffusio-phoretic forces is known as phoretic force. The following equation gives the number of collected aerosol particles in unit time due to phoretic forces:

$$\left. \frac{dN}{dt} \right|_{th+df} = \frac{4\pi r_d n_p s f_v}{\left[ \frac{L_v}{k_a T_\infty} \left( \frac{L_v}{R_v T_\infty} - 1 \right) + \frac{R_v T_\infty}{D_v e_s(T_\infty)} \right]} \left( \frac{C}{\rho_a} - \frac{L_v f_{th}}{p} \right), \quad (5)$$

where  $s, T_\infty, k_a, p, \rho_a$ , and  $D_v$  are the supersaturation, temperature, thermal conductivity, pressure, density of air, and diffusivity of vapor in the air, respectively;  $R_v$  is the gas constant for the water vapor,  $L_v$  is the evaporation heat,  $e_s$  is the saturation vapor pressure over flat water surface.  $f_v$  and  $f_{th}$  represent the ventilation coefficient and thermophoretic force, respectively (*Pruppacher and Klett, 1997*).  $C$  is the Cunningham-correction, which value depends on the Knudsen number. While in the case of evaporating drop the motion of the aerosol particles is directed toward the surface of the water drop (the right side term in Eq. (5) is larger than zero), in the case of diffusional growth the direction of the motion is opposite (the right side term in Eq. (5) is less than zero). The effect of the phoretic forces is dominant if the size of the aerosol particles is about  $0.1 \mu\text{m}$  (*Wang, 2002*). The phoretic force results in collision between the submicron aerosol particles and the water drops in the subsaturated regions where the drops evaporate. This condition is realized in the precipitation zone and at the lateral edge of the cloud.

If the radius of the aerosol particles is larger than  $1 \mu\text{m}$ , the phoretic forces hardly affect their motion. They are collected by the water drops due to the gravitational collection. The following equation gives the number of aerosol particles collected by a water drop in unit time due to gravitational force:

$$\left. \frac{dN_p}{dt} \right| = E(r_d + r_p)^2 \pi v_t(r_d) n_p, \quad (6)$$

where  $E$  is the collection efficiency,  $r_d$  and  $r_p$  are the radius of the water drop and the aerosol particles, respectively.  $v_t$  is the terminal velocity of the water drop.

### 3. Results

Formation of the water drops and washout of the aerosol particles were examined in the case of three different air mass types: maritime, rural, and remote continental. Initial size distributions of the aerosol particles (*Fig. 1*) were given by equations published by *Jaenicke* (1988). These equations are frequently used in numerical experiments (e.g., *Bott*, 2000; *Leroy et al.*, 2006; *Caro et al.*, 2004; *Mircea et al.*, 2000).

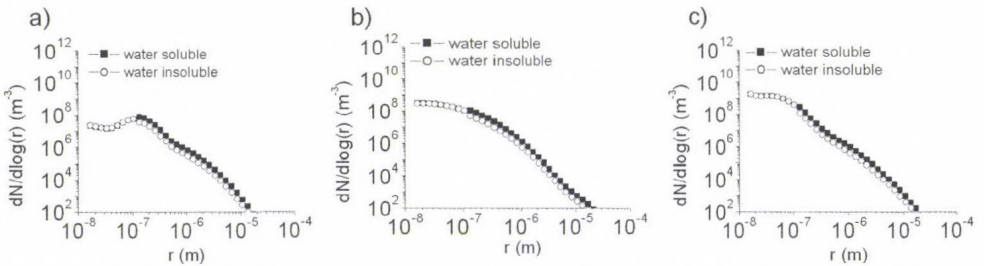


*Fig. 1.* Initial size distribution of the water soluble (square symbol) and water insoluble (circle symbol) aerosol particles in three different air mass types: (a) maritime, (b) rural, and (c) remote continental.

The spatial distribution of the supersaturation gives information about the development of the cloud. In addition, the phoretic force depends on the subsaturation (see Eq. (5)). The supersaturation is affected by the adiabatic rising of the moist air and by the formation and condensational growth of water drops (*Cohard et al.*, 1998). The supersaturation rapidly increases above the cloud base until it reaches its maximum value. Thereafter it decreases gradually, and at about 100 m above the cloud base it becomes near constant. Most of the haze particles reach their critical size in the updraft region, near to the cloud base where supersaturation is the largest. *Fig. 2* shows the simulated vertical profile of the supersaturation at 0.5 m/s and 1.2 m/s maximum updraft velocities at different aerosol concentrations.

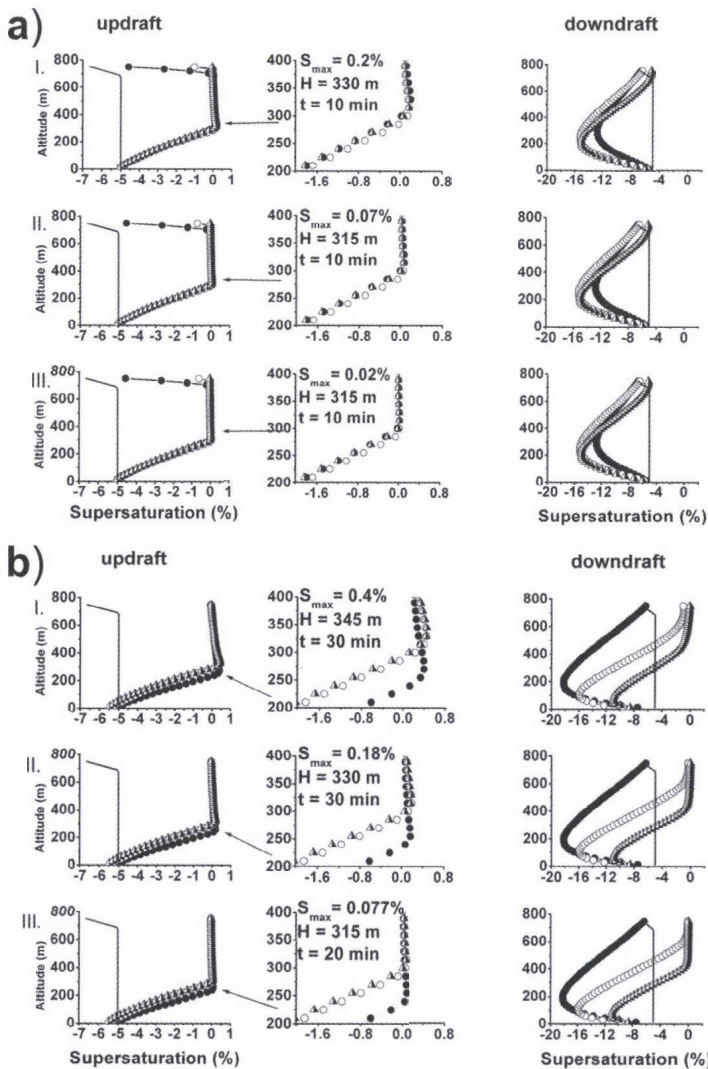


Fig. 2. Vertical profile of the supersaturation in case of maritime (I), rural (II), and remote continental (III) air masses at  $t = 10$  min (black circle),  $t = 20$  min (white cycle) and  $t = 30$  min (black and white triangle) according to initial supersaturation (solide line) at maximum updraft velocity of 0.5 m/s (a) and 1.2 m/s (b).

In case of weaker maximum updraft velocity ( $w_{max} = 0.5$  m/s), the supersaturation reached its maximum value at about 300 m above the surface, and after a small diminution it became nearly constant with increasing altitude. The largest maximum supersaturation value occurred in the case of the maritime air mass, because the low CN concentration resulted in lower concentration of droplets. Above the cloud top, the saturation suddenly decreased in all

simulation times. With increasing time, reduction rate decreased. In the downdraft region, the relative humidity decreased at lower altitude. After 30 minute of simulation time, the rate of the depletion significantly decreased. Below the cloud base, the relative humidity slightly increased due to the evaporation of falling droplets.

When the maximum updraft velocity was stronger ( $w_{max} = 1.2$  m/s) the maximum supersaturation occurred at lower altitude at the beginning (10th minute) than in the case of weaker maximum updraft. With increasing time, the position of the maximum of the supersaturation rose to higher altitude. In the downdraft core, the relative humidity depended on the adiabatic descend of the air and the evaporation of the water drops. While the warming due to adiabatic descend reduces the relative humidity, the evaporation of the water drops increases it. The decrease of the relative humidity until about the 10th minute of the simulation was the consequence of the dry adiabatic descend of the air. The appearance of water drops after the 10th minute resulted in increase of the relative humidity everywhere in the downdraft. This explains that the relative humidity was lower in the case of stronger updraft until the 10th minute of the simulation than in the case of weaker updraft. The increase of the relative humidity was the consequence of the evaporation of the water drops in the down draft core. While this process confined to near to the top of the domain in the case of weaker updraft, evaporation of the water drops occurred in an about 400 m deep layer in the case of the stronger updraft. (See the layer where the supersaturation is equal to zero in the right coloumn in *Fig. 2b*.) The effect of evaporation was the largest in the case of remote continental air mass type (IIIrd row in *Fig. 2b*). This can be explained by the fact, that the total surface area of the water drops was the largest in this case.

Some features of simulation are summarized in *Tables 1* and *2*. The domain integrated number concentration or mixing ratios ( $M$ ), furthermore, the domain and time integrated production terms ( $P$ ) were calculated by the following equation:

$$M = \sum_{i,j} M_{i,j} \rho_a \Delta x \Delta y, \quad P = \sum_{n=1}^{n_{max}} \Delta t \sum_{i,j} p_{i,j} \rho_a \Delta x \Delta y, \quad (7)$$

where  $\Delta x$  and  $\Delta y$  are the horizontal and vertical distances between the grid points, respectively,  $\rho_a$  is the density of air,  $\Delta t$  is the time step,  $n_{max}$  is the number of time steps used during the simulation;  $p_{i,j}$  is the production term calculated at the grid point  $i, j$  and  $M_{i,j}$  is the number concentration or the mixing ratio of the aerosol particles.

*Table 1* shows the time and domain integrated production term for the condensation of vapor, change of the number concentration, mixing ratio and

aerosol mass of the wet aerosol particles due to condensation, and the change of the concentration of the water drops due to the collision-coalescence.

*Table 1.* The following domain integrated production term: change of the mass of wet aerosol particles-water drops due to condensation ( $\Delta M_c$ ); transfer of the dry aerosol particles to wet aerosol particles due to the increase of the relative humidity. Number (column a), mass of water plus aerosol (column b), only aerosol mass (column c); decrease of the number of the water drops due to drop-drop collision

	$\Delta M_c$	N	$M_w$	$M_a$	$N_w$	<b>Updraft</b>
	(a)	(b)	(c)			
	(kg m <sup>-1</sup> )	(m <sup>-1</sup> )	(kg m <sup>-1</sup> )	(kg m <sup>-1</sup> )	(m <sup>-1</sup> )	m/s
Maritime	$1.31 \times 10^2$	$9.54 \times 10^{13}$	$4.80 \times 10^{-2}$	$2.40 \times 10^{-2}$	$-4.50 \times 10^{11}$	
Rural	$1.31 \times 10^2$	$4.43 \times 10^{14}$	$5.37 \times 10^{-2}$	$2.68 \times 10^{-2}$	$-4.45 \times 10^{11}$	0.5
Remote continental	$1.31 \times 10^2$	$2.02 \times 10^{15}$	$6.19 \times 10^{-2}$	$3.09 \times 10^{-2}$	$-3.81 \times 10^{11}$	
Maritime	$2.07 \times 10^2$	$9.72 \times 10^{13}$	$4.80 \times 10^{-2}$	$2.40 \times 10^{-2}$	$-1.84 \times 10^{12}$	
Rural	$2.09 \times 10^2$	$4.62 \times 10^{14}$	$5.37 \times 10^{-2}$	$2.68 \times 10^{-2}$	$-1.42 \times 10^{12}$	1.2
Remote continental	$2.11 \times 10^2$	$2.12 \times 10^{15}$	$6.21 \times 10^{-2}$	$3.10 \times 10^{-2}$	$-1.08 \times 10^{12}$	

The increase of the total water content was caused by the condensational growth of the wet aerosol particles and water drops. Both the wet aerosol particles and water drops evaporated in the subsaturated region. Similarly to the results published by *Szumowski et al. (1998)*, our results show that the water drops, that remained in the updraft core, permanently grow, and the water drops that fall out from the updraft into the outflow, remain small, or completely evaporate. This is demonstrated by the joint size distributions of the water drops and of wet aerosol particles in *Figs. 3 and 4*. The mean size of the water drops increases in the updraft core and decreases in the downdraft regions. Another important feature of the size distributions is that while they were getting narrower in the ascending air due to the condensational growth of the water drops and due to the evaporation of the wet aerosol particles which did not reach the critical size, they got wider due to the evaporation of the water drops in the downdraft. Near to the surface in the downdraft region, the size distribution should be similar to that of the initial size distribution of the aerosol particles due to the complete evaporation of the water drops. The differences can be the consequence of the following reasons: (i) some of the water soluble aerosol particles can be captured by the water drops due to different scavenging mechanisms; (ii) numerical deficiency. During the calculation, the discrete bin width limits the information about the mass of the aerosol particle inside of the drops. This uncertainty of the mass of aerosol particles inside the water drops caused fluctuations in the number concentration of the regenerated aerosol particles at the submicron size in the downdraft core. To avoid this effect, the size distribution can be smoothed by calculation of the mean value of the concentration in three neighboring bins ( $n_{k-1}, n_k, n_{k+1}$ ) (*Geresdi and Rasmussen, 2005*).

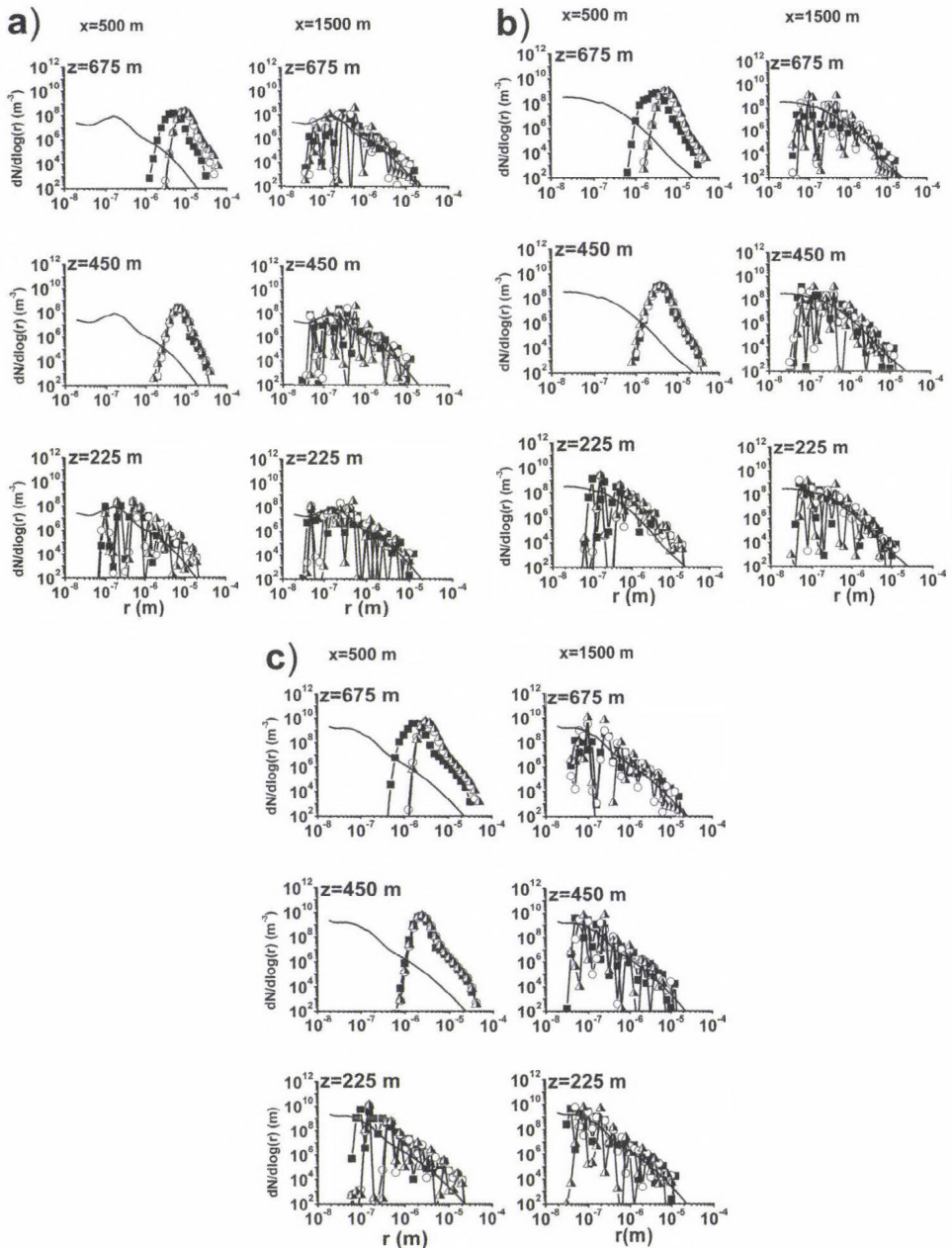


Fig. 3. The evolution of size distribution of the water drops in maritime (a), rural (b) and remote continental (c) air masses at  $t = 10$  min (black square), at  $t = 20$  min (white cycle) and at  $t = 30$  min (black and white triangle) according to initial size distribution of water soluble aerosol particles at  $0.5$  m/s maximum updraft velocity in the updraft core ( $x = 500$  m) and in the downdraft core ( $x = 1500$  m).

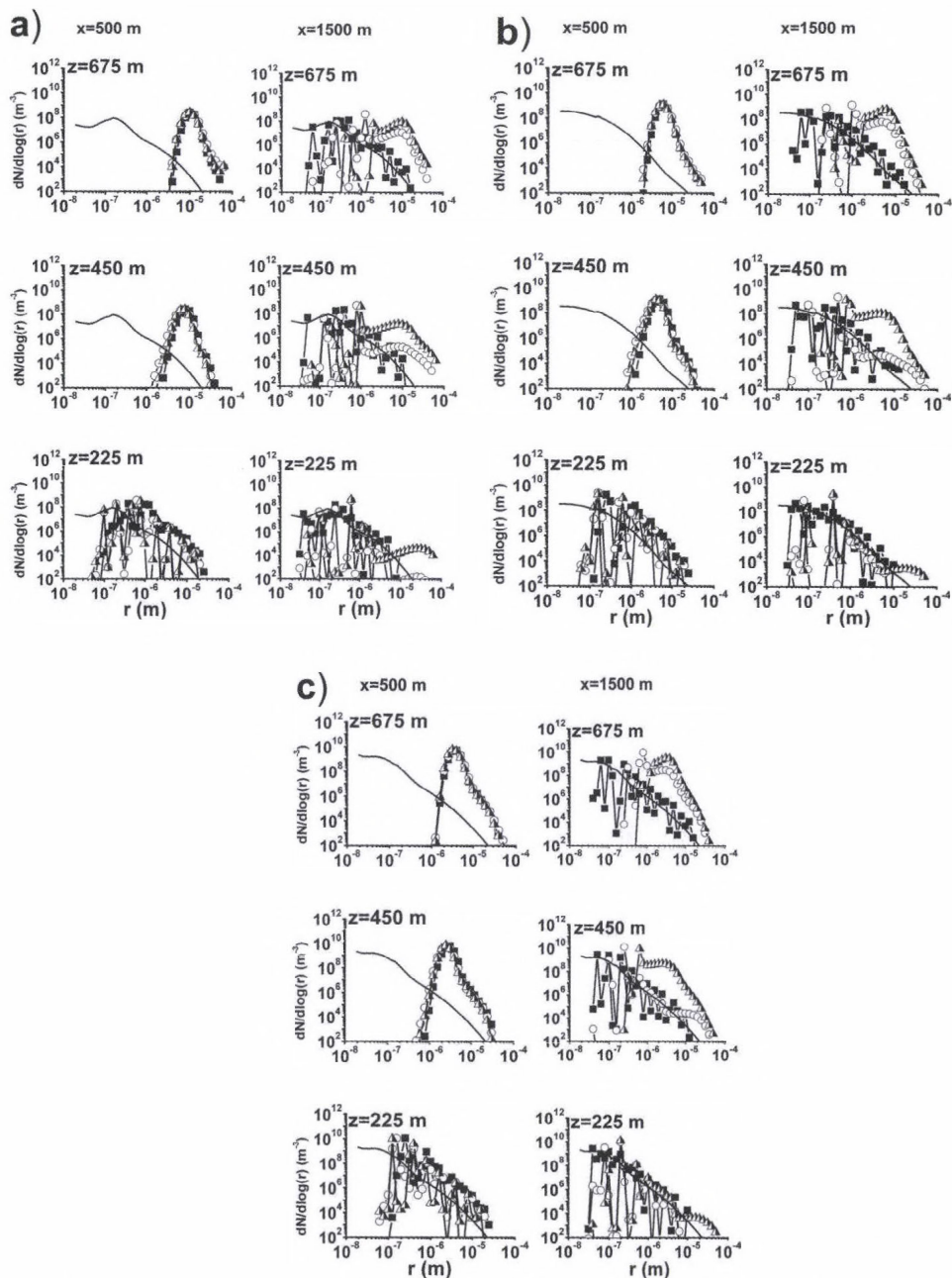


Fig. 4. The evolution of size distribution of the water drops in maritime (a), rural (b) and remote continental (c) air masses at  $t = 10$  min (black square),  $t = 20$  min (white cycle) and  $t = 30$  min (black and white triangle) according to initial size distribution of water soluble aerosol particle at maximum updraft velocity of 1.2 m/s in the updraft core ( $x = 500$  m) and in the downdraft core ( $x = 1500$  m).

The initial size distribution of the water soluble aerosol particles significantly affects the size distribution of the water drops form on them. The concentration of the water drops less than 25  $\mu\text{m}$  was the smallest in the case of maritime air mass and it was the largest in the case of remote continental one (Fig. 5).

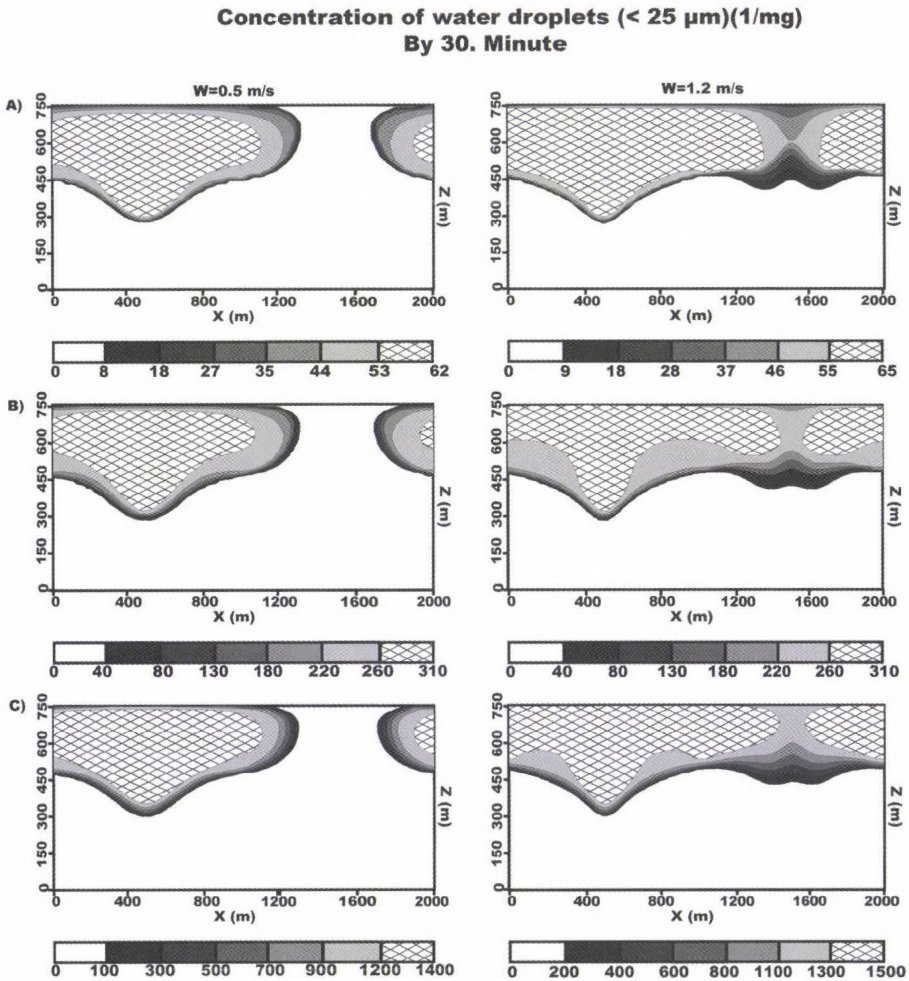


Fig. 5. The evolution of size distribution of the water drops in maritime (a), rural (b), and remote continental (c) air masses at maximum updraft velocity of 0.5 and 1.2 m/s.

Due to the small concentration of water soluble aerosol particles less water drops formed in the maritime air mass. Hence, more water vapor condensed on each of these drops. As a result, the mean mass of drops was larger in the maritime air mass than in the rural and remote continental air masses. This result was reported also by Leroy *et al.* (2006), Reisin *et al.* (1996), and Rasmussen *et*

al. (2002). As the efficiency of the collision-coalescence of the water drops strongly depends on the mean size of the drops, the concentration of the drizzle size water drops ( $r > 25 \mu\text{m}$ ) was the highest in the maritime case. The mixing ratio of these drops was ten times larger in the maritime case than in the rural air mass case (Fig. 6). The water drops were rising until their terminal velocity was equal to the vertical velocity of air and, thereafter, they began to fall down. The fall-out of the rain drops began earlier in the maritime air mass due to the larger terminal velocity of the rain drops.

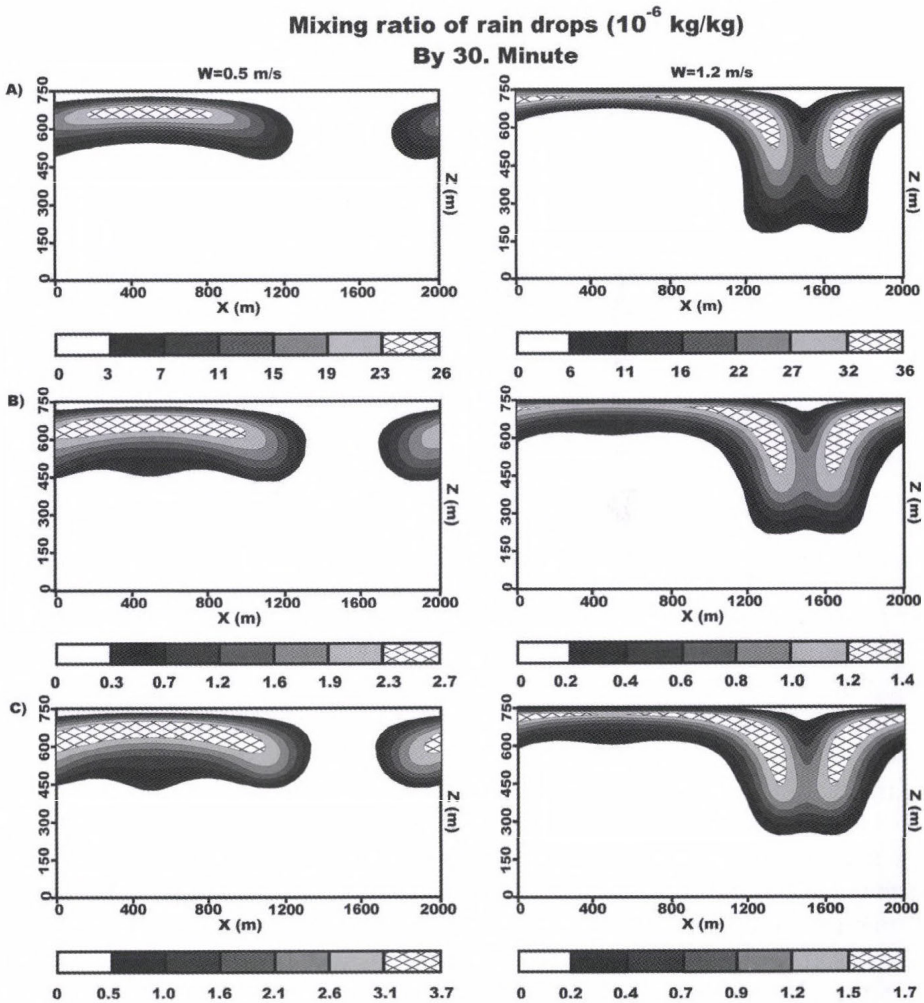


Fig. 6. Mixing ratio of the rain drops in maritime (a), rural (b), and remote continental (c) air mass types at two different maximum updraft velocities by the end of simulation. Scale is given in kg/kg.

Table 2 shows the domain and time integrated values of the production terms, that give the change of number and mass of the water soluble and water insoluble aerosol particles due to Brownian and phoretic effects.

Table 2. Domain and time integrated value of the change of concentration ( $\Delta N_s$ ) and mixing ratio ( $\Delta M_s$ ) of water soluble and insoluble ( $\Delta N_{is}$ ,  $\Delta M_{is}$ ) aerosol particles due to Brownian and phoretic collision with water drops, initial domain integrated concentration and mixing ratio of the water soluble and insoluble aerosol particles

	$\Delta N_s$ ( $m^{-1}$ )	$\Delta M_s$ ( $kg\ m^{-1}$ )	$\Delta N_{is}$ ( $m^{-1}$ )	$\Delta M_{is}$ ( $kg\ m^{-1}$ )	Updraft m/s
Maritime	$-6.09 \times 10^8$	$-3.65 \times 10^{-10}$	$-6.33 \times 10^{11}$	$-5.55 \times 10^{-6}$	0.5
Rural	$-1.22 \times 10^{10}$	$-3.26 \times 10^{-9}$	$-1.36 \times 10^{13}$	$-1.40 \times 10^{-5}$	
Remote continental	$-5.59 \times 10^{10}$	$-1.45 \times 10^{-8}$	$-1.45 \times 10^{14}$	$-6.69 \times 10^{-5}$	
Maritime	$-4.98 \times 10^8$	$-2.97 \times 10^{-10}$	$-1.35 \times 10^{12}$	$-7.87 \times 10^{-6}$	1.2
Rural	$-9.69 \times 10^9$	$-2.56 \times 10^{-9}$	$-3.03 \times 10^{13}$	$-3.27 \times 10^{-5}$	
Remote continental	$-4.48 \times 10^{10}$	$-1.16 \times 10^{-8}$	$-3.03 \times 10^{14}$	$-1.43 \times 10^{-4}$	
	$N_{s0}$ ( $m^{-1}$ )	$M_{s0}$ ( $kg\ m^{-1}$ )	$N_{is0}$ ( $m^{-1}$ )	$M_{is0}$ ( $kg\ m^{-1}$ )	
Maritime	$9.86 \times 10^{13}$	$2.40 \times 10^{-2}$	$6.60 \times 10^{13}$	$8.34 \times 10^{-3}$	0.5
Rural	$4.75 \times 10^{14}$	$2.69 \times 10^{-2}$	$4.28 \times 10^{14}$	$9.52 \times 10^{-3}$	
Remote continental	$2.19 \times 10^{15}$	$3.11 \times 10^{-2}$	$2.11 \times 10^{15}$	$1.19 \times 10^{-2}$	
Maritime	$9.86 \times 10^{13}$	$2.40 \times 10^{-2}$	$6.60 \times 10^{13}$	$8.34 \times 10^{-3}$	1.2
Rural	$4.75 \times 10^{14}$	$2.69 \times 10^{-2}$	$4.28 \times 10^{14}$	$9.52 \times 10^{-3}$	
Remote continental	$2.19 \times 10^{15}$	$3.11 \times 10^{-2}$	$2.11 \times 10^{15}$	$1.19 \times 10^{-2}$	

For the depletion rate of aerosol particle due to nucleation scavenging we got similar result to that of published by Zhang *et al.* (2004). They investigated aerosol scavenging by low-level, warm stratiform clouds and precipitation using a one-dimensional model with detailed cloud microphysics and size resolved aerosol particles and hydrometeors. By the end of the simulation, more than 90% of the water soluble aerosol particles and more than 99% of the mass of the water soluble aerosol particles were depleted due to the formation of water drops in each case. The rate of condensation increased with the strength of the updraft. Negligible fraction of water soluble particles was scavenged due to the Brownian and phoretic effects. These results also agree with that of published by Zhang *et al.* (2004). Fig. 7 shows the time integrated change of the concentration of the water insoluble aerosol particles in the case of 0.5 m/s and 1.2 m/s maximum updraft velocities by the 30th minute of the simulation. In case of smaller clouds (weaker updraft) the aerosol particles were scavenged just inside the clouds. While in case of larger clouds (stronger updraft) the drops collected the particles at the edge of clouds and in the downdraft core too. Collection was most significant in the upper divergence region. The high collection rate in the remote continental and rural air mass was the consequence of the larger total surface area of the droplets in a unit volume of the air.

Comparing the initial and final size distributions of the aerosol particles, the total number of water insoluble aerosol particles decreased by 1% and 2% in the case of maritime airmass, 3% and 7% in the case of rural airmass, and 7% and 14% in the case of remote continental airmass at maximum vertical velocities of 0.5 m/s and 1.2 m/s, respectively.

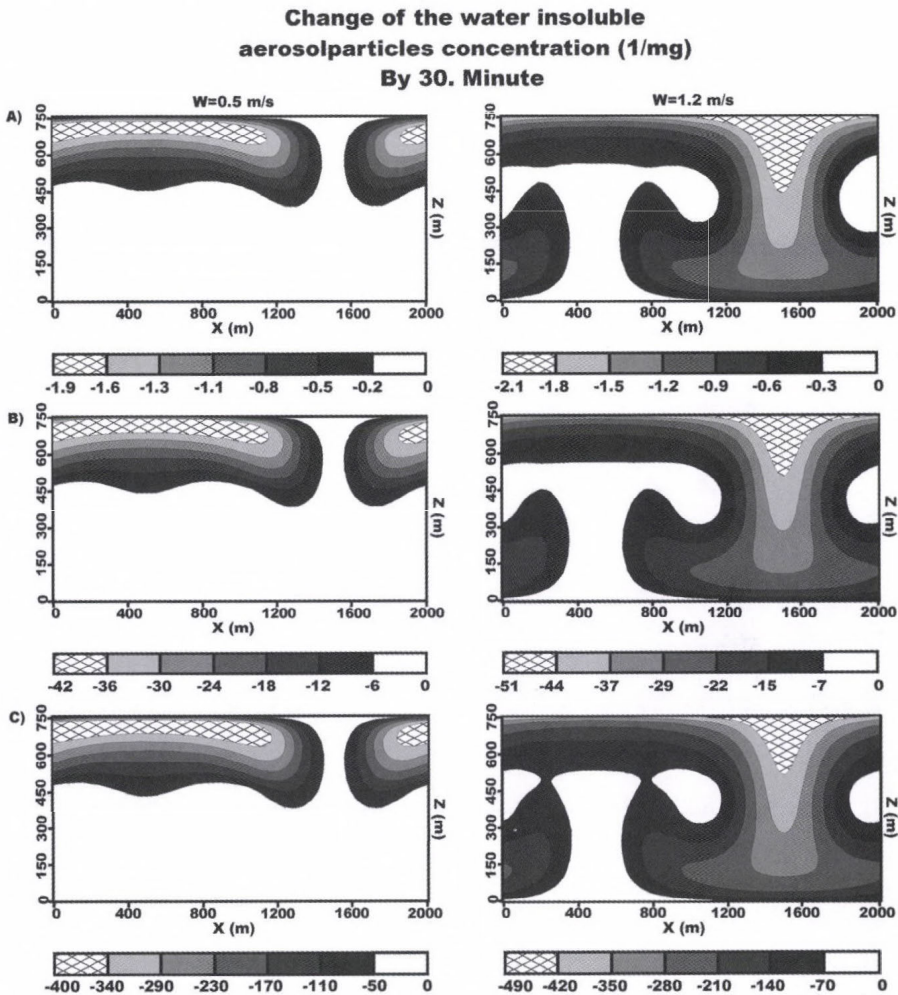


Fig. 7. Concentration of the water droplets in maritime (a), rural (b), and remote continental (c) air mass types at two different maximum updrafts velocities by the end of the simulation. Scale is given in 1/mg.

The reduction in mass of the water insoluble aerosol particles was just a few tenth percents in each case. It follows from the fact that relatively more small particles were collected than large ones. The relative efficiency of scavenging of

the aerosol particles less than  $0.1 \mu\text{m}$  means that scavenging of the water insoluble particles was mostly governed by the Brownian effect inside the cloud.

To investigate the efficiency of the scavenging in different regions of the domain, the following equation was calculated:

$$Scav_{eff} = \frac{N_0 - N_t}{N_0}, \quad (8)$$

where  $N_0$  and  $N_t$  are the number concentration of the aerosol particles at a given grid point at the beginning and the end of the simulation, respectively. *Figs. 8a* and *8b* show the efficiency of scavenging in the case of remote continental airmass, when the maximum of the updraft velocity was  $0.5 \text{ m/s}$  and  $1.2 \text{ m/s}$ , respectively.

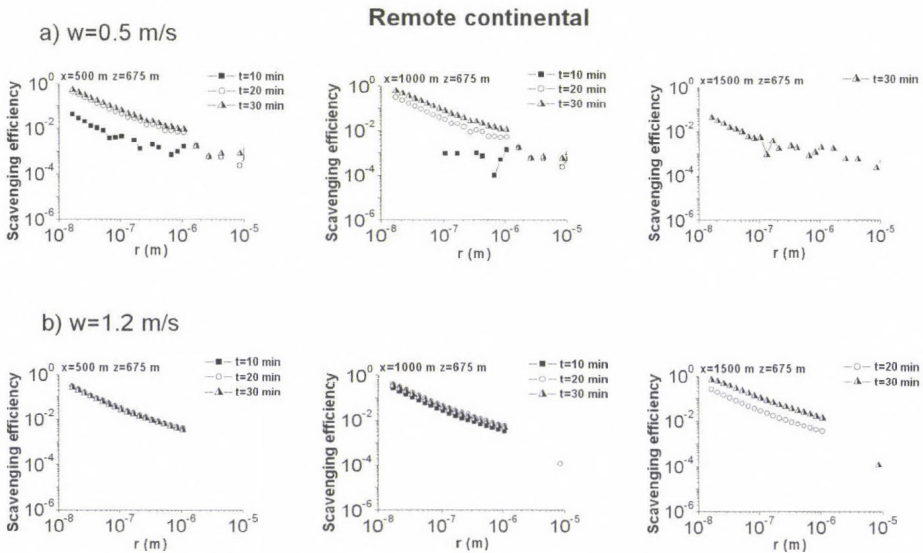


*Fig. 8.* Collection efficiency of the Brownian, phoretic, gravitational and dynamical processes at maximum updraft velocities of  $0.5 \text{ m/s}$  (a) and  $1.2 \text{ m/s}$  (b) in the remote continental airmass at three different grid points.

The three grid points represent three different regions of the domain. The left side figures in *Figs. 8a* and *8b* represent the updraft region near to the top of the cloud. Figures at  $x=1000 \text{ m}$  represent the cloud region where only horizontal flow occurs. The right side figures show the scavenging efficiency in the downdraft regions. It is clearly shown that the steepness of the curves is very similar at different grid points and at different maximum updraft velocities, as well. The difference between *Figs. 8a* and *8b* indicates that it takes longer time to reach the steady state in the case of weaker updraft. The aerosol particles less

than  $0.1\ \mu\text{m}$  were collected most efficiently by Brownian motion. The effect of Brownian motion strongly decreased above this particle size (Young, 1974). In the size range of  $0.1\ \mu\text{m}$  to  $1\ \mu\text{m}$ , only less than 1 percent of the particles were scavenged due to phoretic forces. The effect of the gravitational force was negligible. This force would have changed the concentration of the micron size particles considerably if the size of the hydrometeor had reached the value of  $100\text{--}200\ \mu\text{m}$ .

#### 4. Summary

The aim of our research was to study the cycle of aerosol particles in stratocumulus clouds using a detailed microphysical scheme in the case of maritime, rural, and remote continental air mass types and at different dynamic conditions. In this study we focused on the following processes:

##### 4.1. Drop formation and regeneration of aerosol particles

The model was able to simulate the regeneration of the water soluble aerosol particles. Neglecting the effect of numerical deficiency caused by the limits of information about the mass of the aerosol particle inside of the drops, the initial size distribution of the water soluble aerosol particles and the size distribution of the regenerated aerosol agree well.

The size distribution of the wet aerosol particles was mostly affected by the nucleation scavenging. Because the mean drop size was relatively small even in the case of maritime airmass, the collision-coalescence of the water drops hardly affected the size distribution of the regenerated aerosol particles.

##### 4.2. Scavenging of water soluble and water insoluble aerosol particles

The water soluble aerosol particles diminished more than 90% in number and more than 99% in mass during the drop formation. Only about 0.1% of the water soluble particles were collected due to Brownian and phoretic forces.

The efficiency of scavenging of water insoluble aerosol particles depended on the initial concentration of the water soluble aerosol particles and on the intensity of the updraft.

Depending on the initial concentration of aerosol particles and the intensity of the updraft, about from 1 to 14% of the insoluble aerosol particles were collected by the different scavenging processes. In the case of more intense updraft, the aerosol particles were removed most efficiently in the downdraft core. The decrease of the number concentration was most significant in the size range of  $0.01\text{--}0.1\ \mu\text{m}$  due to the Brownian motion.

The results of numerical simulation show that phoretic effects hardly affect the washout of the aerosol particles in the case of the precipitable stratocumulus.

Thus the aerosol particles which do not contain water soluble fraction and their size is between 0.1 and 1.0  $\mu\text{m}$  can have a relative long atmospheric retention time. Further research about how the other cloud types with more efficient precipitation formation can affect the washout these particles is necessary.

**Acknowledgements**—I would like to thank to *Dr. István Geresdi* for his contribution to the present work and for reviewing the manuscript, and also for using his numerical code. I also should like to thank to the anonymous reviewers for their comments and suggestions.

## References

- Ackerman, A.S., Toon, O.B., Hobbs, P.V., 1995: A model for particle microphysics, turbulent mixing, and radiative transfer in the stratocumulus-topped marine boundary layer and comparisons with measurements. *J. Atmos. Sci.* 52, 1204-1236.
- Bott, A., 2000: A numerical model of cloud-topped planetary boundary-layer: influence of the physico-chemical properties of aerosol particles on effective radius of stratiform clouds. *Atmos. Res.* 53, 15-27.
- Caro, D., Wobrock, W., Flossmann, A.I., Chaumerliac, N., 2004: A two-moment parametrization of aerosol nucleation and impaction scavenging for a warm cloud microphysics: description and results from two-dimensional simulation. *Atmos. Res.* 70, 171-208.
- Charlson, R.J., Vong, R., Hegg, D.A., 1983: The sources of sulphate in precipitation: 2. Sensitivities to chemical variables. *J. Geophys. Res.* 88, 1375-1377.
- Chen, J.P., Lamb, D., 1994: Simulation of cloud microphysical and chemical processes using multicomponent framework. Part I: Description of the microphysical model. *J. Atmos. Sci.* 51, 2613-2630.
- Cohard, J.M., Pinty, J., Bedos, C., 1998: Extending Twomey's analytical estimate of nucleated cloud droplet concentration from CCN spectra. *J. Atmos. Sci.* 55, 3348-3357.
- Feingold, G., Heymsfield, A.J., 1992: Parametrizations of condensational growth of droplets for use in general circulation models. *J. Atmos. Sci.* 49, 2325-2342.
- Feingold, G., Kreidenweis, S.M., Stevens, B., Cotton, W.R., 1996: Numerical simulations of stratocumulus processing of cloud condensation nuclei through collision-coalescence. *J. Geophys. Res.* 101, 21391-21402.
- Feng, J., 2007: A 3-mode parametrization of below-cloud scavenging of aerosols for use in atmospheric dispersion models. *Atmos. Environ.* 41, 6808-6822.
- Geresdi, I., 1998: Idealized simulation of the Colorado hailstorm case: comparison of bulk and detailed microphysics. *Atmos. Res.* 45, 237-252.
- Geresdi, I., Rasmussen, R., 2005: Freezing drizzle formation in stably stratified layer clouds. Part II: The role of giant nuclei and aerosol particle size distribution and solubility. *J. Atmos. Sci.* 62, 2037-2057.
- Geresdi, I., Mészáros, E., Molnár, A., 2006: The effect of chemical composition and size distribution of aerosol particles on droplet formation and albedo of stratocumulus clouds. *Atmos. Environ.* 40, 1845-1855.
- Gilliani, N.V., Schwartz, S.E., Leaitch, W.R., Strapp, J.W., Isaac, G.A., 1995: Field observations in continental stratiform clouds: Partitioning of cloud particles between droplets and unactivated interstitial aerosols. *J. Geophys. Res.* 100, 18687-18706.
- Gwen, A., Cederwall, R.T., 2004: Precipitation scavenging of atmospheric aerosols for emergency response applications: testing an updated model with new real-time data. *Atmos. Environ.* 38, 993-1003.
- Hall, W.D., 1980: A detailed microphysical model within a two-dimensional dynamic framework: model description and preliminary results. *J. Atmos. Sci.* 37, 2486-2507.
- Hoese, C., Lohmann, U., Bennartz, R., Croft, B., Lesins, G., 2008: Global simulation of aerosol processing in clouds. *Atmos. Chem. Phys. Discuss.* 8, 13555-13618.
- Jaenicke, R., 1988: Aerosol physics and chemistry. In *Zahlenwerte und Funktionen aus Naturwissenschaften und Technik*. (ed.: L. Boernerstein) 4b, 391-457, Springer-Verlag.

- Kulmala, M., Korhonen, P., Laaksonen, A., Charlson, R.J., 1997: A generalized reformulation of Köhler theory: Effects of soluble trace gases and slightly soluble substances. *J. Aeros. Sci.* 28, S749-S750.
- Leroy, D., Monier, M., Wobrock, W., Flossmann, I.A., 2006: A numerical study of the effect of the aerosol spectrum on the development of the ice phase and precipitation formation. *Atmos. Res.* 80, 15-45.
- Masahiro, H., Sachio, O., Naoto, M., Sadamu, Y., 2003: Activation capability of water soluble organic substances as CCN. *J. Aeros. Sci.* 34, 419-448.
- Metres, S., Galgon, D., Schwirn, K., Nowak, A., Lehmann, K., Massling, A., Wiedensohler, A., Wieprecht, W., 2005: Evolution of particle concentration and size distribution observed upwind, inside and downwind hill cap clouds at connected flow conditions during FEBUKO. *Atmos. Environ.* 39, 4233-4245.
- Mircea, M., Stefan, S., Fuzzi, S., 2000: Precipitation scavenging coefficient: influence of measured and raindrop size distributions. *Atmos. Environ.* 34, 5169-5174.
- Morrison, H., Grabowski, W.W., 2007: Comparison of bulk and bin warm-rain microphysics models using kinematic framework. *J. Atmos. Sci.* 64, 2839-2861.
- Pruppacher, H.R., Klett, J.D., 1997: *Microphysics of Clouds and Precipitation*. Kluwer Academic Publishers, Dordrecht/Boston/London.
- Rasmussen, R., Geresdi, I., Thompson, G., Manning, K., Karplus, E., 2002: Freezing drizzle formation in stably stratified layer clouds: The role of radiative cooling of cloud droplets, cloud condensation nuclei and ice initiation. *J. Atmos. Sci.* 59, 837-860.
- Reisin, T., Levin, Z., Tzivion, S., 1996: Rain production in convective clouds as simulated in an axisymmetric model with detailed microphysics. Part II: Effect of varying drops and ice initiation. *J. Atmos. Sci.* 53, 1815-1837.
- Sassen, K., Mace, G.G., Wang, Z., Poellot, M.R., Sekelsky, S.M., McIntosh, R.E., 1999: Continental stratus clouds: A case study using coordinated remote sensing and aircraft measurements. *J. Atmos. Sci.* 56, 2345-2358.
- Smolarkiewicz, K.P. and Margolin, L.G., 1998: MPDATA: A finite-difference solver for geophysical flows. *J. Comput. Phys.* 140, 459-480.
- Svenningsson, B., Hansson, H., Martinsson, B., Wiedensohler, A., Swietlicki, E., Cederfelt, S., Wendish, M., 1997: Cloud droplet nucleation scavenging in relation to the size and hygroscopic behavior of aerosol particles. *Atmos. Environ.* 31, 2463-2475.
- Szumowski, M.J., Grabowski, W.W., Ochs, H.T., 1998: Simple two-dimensional kinematic framework designed to test warm rain microphysical models. *Atmos. Res.* 45, 299-326.
- Targino, A.C., Noone, K.J., Drewnick, F., Schneider, J., Krejci, R., Olivares, G., Hings, S., Borrmann, S., 2007: Microphysical and chemical characteristics of cloud droplet residuals and interstitial particles in continental stratocumulus clouds. *Atmos. Res.* 86, 225-240.
- Tzivion, S., Reisin, T.G., Levin, Z., 1999: A numerical solution of kinetic collection equation using high spectral grid resolution: a proposed reference. *J. Comput. Phys.* 148, 527-544.
- Wang, P.K., 2002: Sharpe microdynamics of ice particle and their effect, in cirrus clouds. In: *Advances in Geophysics* (eds.: R. Dmowska, B. Saltzman) 45. Academic Press.
- Young, K.C., 1974: The role of contact nucleation in ice phase initiation in clouds. *J. Atmos. Sci.* 31, 768-776.
- Zhang, L., Michelangeli, D.V., Taylor, P.A., 2004: Numerical studies of aerosol scavenging by low-level, warm stratiform clouds and precipitation. *Atmos. Environ.* 38, 4653-4665.
- Zhang, L., Vet, R., 2006: A review of current knowledge concerning size- dependent aerosol removal. *China Particool* 4, 272-282.



# IDŐJÁRÁS

*Quarterly Journal of the Hungarian Meteorological Service  
Vol. 115, No. 3, July–September 2011, pp. 167–178*

## **Determination of winter barley yield by the aim of multiplicative successive approximation**

**Erzsébet Enzsölné Gerencsér, Zsuzsanna Lantos,  
Zoltán Varga-Haszonits, and Zoltán Varga\***

*Department of Mathematics and Physics,  
Faculty of Agricultural and Food Sciences, University of West Hungary,  
Vár 2, H-9200 Mosonmagyaróvár, Hungary  
E-mail: varzol@mtk.nyme.hu*

*\*Corresponding author*

*(Manuscript received in final form October 20, 2010)*

**Abstract**—The aim of our study was to analyze the climate-winter barley yield relationship by means of a model which took impact of successive periods into account. This approximation is a step from statistical models to dynamic models.

Study was based on data of an agroclimatological database, which contained daily values of meteorological elements during 1951–2000 measured by the Hungarian Meteorological Service and yearly county average values of winter barley yield published by Hungarian Central Statistical Office. In order to investigate the impact of meteorological factors on yield, we separated the influence of weather and technology. Impact of meteorological factors on yield was examined by regression equations during selected periods, but only time periods with significant influence on yield were taken into consideration. Applying this model, trend function was determined firstly, then relationship between trend ratio and meteorological element of first significant time period was calculated. This process was continued until the last function of meteorological impact had been determined.

Verification and validation of results were accomplished by studying of correlation between measured and calculated values and determination of frequency distribution of estimation errors.

The multiplicative successive model is suitable for estimating yields of winter barley, which grows in the cool and wet part of the year. It demonstrates how successive periods of growing season influence yield. This method is a better tool for studying the effects of climatic variability or a possible climate change than a simple statistical model.

*Key-words:* winter barley, yield, multiplicative successive model, water supply, temperature

## **1. Introduction**

Winter barley is an important fodder grain crop in Hungary. This is a mesotherm plant which prefers cold spring weather. Its temperature demand and absorption of radiation are similar to those of winter wheat, but its cold hardening is worse. Mainly, cold weather without snow seems to be unfavorable for winter barley. Length of sowing-emergence phenophase is usually longer than that of winter wheat, because of higher water demand of barley (Szakály, 1968). Peak of water demand can be observed between shooting and heading, after heading water demand decreases (Varga-Haszonits *et al.*, 2000). This plant can be harvested first (in the second half of June) among grain crops; therefore, it is less affected by summer droughts. Winter barley is mainly used as fodder and its nutrition value is higher than that of winter wheat. It usually has the third biggest harvested area, which follows the area of winter wheat and maize. This harvested area of winter barley did not increase over the last some years, but a drying tendency can change that (Varga-Haszonits *et al.*, 2000, 2006).

## **2. Material and methods**

Study was based on data of an agroclimatological database which had been built by Meteorological Group of Institute of Mathematics, Physics and Informatics of University of West Hungary. That database contains daily values of meteorological elements during 1951–2000 measured by Hungarian Meteorological Service and yearly county average values of winter barley yield published by Hungarian Central Statistical Office.

Yield of winter barley is mainly influenced by agrotechnical factors (variety, nutrient supply, plant protection) and meteorological elements. Weather is a key component, because in most cases high percentage of the variability of the yield (20%–80%) is due to the variability in weather conditions (Fageria, 1992; Porter and Semenov, 2005). Agrotechnical factors change slowly year by year in a given area, that is why these factors show trend of change (Fig. 1). Variability of meteorological elements from year to year can be significant, this is the reason of the fluctuation around the trend. In order to investigate the impact of meteorological factors on yield, we have to separate the influence of weather and technology. This can be evaluated by the method of making ratio or difference between the trend and the actual yield or by the help of simulation using different model-calculations (Andresen *et al.*, 2001; Thompson, 1962, 1969, 1975, 1986).

Fig. 1 shows that course of barley yields in the second half of the 20th century can be expressed by means of a polynomial of the third degree. Relative

position of single points to trend function indicates that variability of yield increases with rising yields. For this reason, meteorological effect is expressed by trend ratio instead of the trend anomalies. So it can be calculated as follows:

$$\frac{Y(t)}{f(t)} = f(m), \tag{1}$$

where  $Y(t)$  is actual yield in the  $t$ th year,  $f(t)$  is yield calculated by means of trend function in the  $t$ th year, and  $f(m)$  is a function of meteorological impact.

In this manner, actual yield can be expressed as follows:

$$Y(t) = f(t)f(m). \tag{2}$$

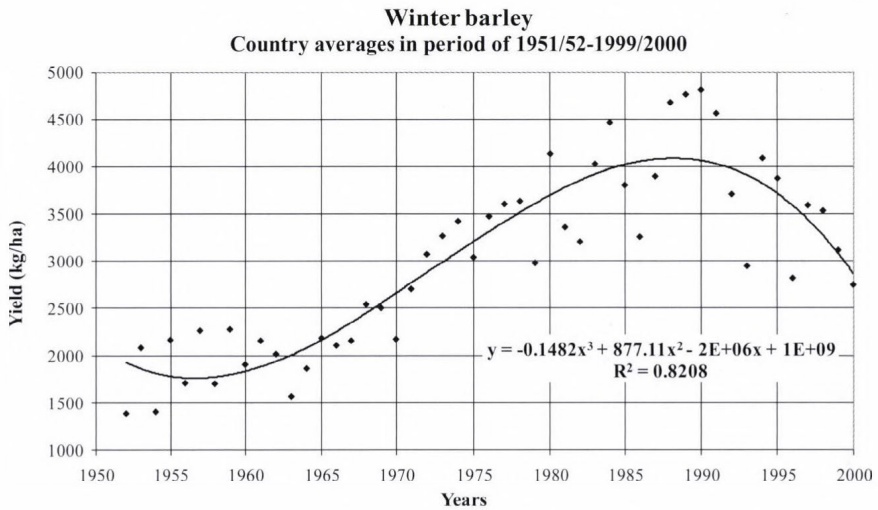


Fig. 1. Tendency of yearly variability in winter barley yield (kg/ha).

It seems to be practical to divide the growing season into different stages. These stages can be natural periods (phenological phases, intervals determined by threshold values) or calendar terms (seasons, months, ten or five days periods). Impact of meteorological factors on yield is examined by regression equations during selected periods, but only time periods with significant influence on yield are taken into consideration (Szabó and Tóth, 1989). These agrometeorologically important time periods are joined in a model based on multiplicative successive approximation. This dynamically estimating yield model makes possible to predict the crop yield before ripening (Fuqin and Tian, 1991; Panofsky and Brier, 1963; Varga-Haszonits, 1986, 1987, 1992).

Applying this model, trend function was determined firstly, then relationship between trend ratio and meteorological element ( $m_1$ ) of first significant time period was calculated. First function of meteorological impact ( $f_1(m_1)$ ) was determined this way:

$$\frac{Y(t)}{f(t)} = f_1(m_1). \quad (3)$$

Then the ratio of  $Y(t)$  actual yield and  $f(t):f_1(m_1)$  estimating function is created, and this ratio has to be correlated with  $m_2$  meteorological element of next significant time period for determining  $f_2(m_2)$  function:

$$\frac{Y(t)}{f(t)f_1(m_1)} = f_2(m_2). \quad (4)$$

This process is continued until the last function of meteorological impact has been determined. Herewith  $Y^*(t)$  estimating function is worked out, and the model can be described as follows:

$$Y^*(t) = f(t) f_1(m_1) f_2(m_2) \dots f_k(m_k), \quad (5)$$

where  $f_1(m_1)$ ,  $f_2(m_2)$ , ...,  $f_k(m_k)$  are functions of meteorological impact of significant time periods which are calculated by the aim of successive approximation.

Verification and validation of results (Mavi and Tupper, 2004) were accomplished by studying of correlation between measured and calculated values and determination of frequency distribution of errors.

Crop yield models are divided into three groups by Ritchie and Alagarswamy (2002). These are groups of statistical, mechanistic, and functional models. Statistical models are used to make large-area yield predictions. Nowadays, these models have been replaced by complex simulation models (Abbaspour et al., 1992). Mechanistic models include mathematical descriptions of plant growth and development. Functional models contain simple equations or empirical relationship to describe the plant process and its environment (Hoogenboom, 2000).

This model belongs to the first (statistical) group, because it is based on dividing agrotechnical and meteorological impact and calculating meteorological impact as trend ratio. Calculation took into consideration ten-day periods with significant thermal effects, and it was accomplished by the aim of a multiplicative successive approximation.

### 3. Results and discussion

It is practical to start from the principle that – as we mentioned earlier – yields are influenced by agrotechnical factors and meteorological elements. Four production levels were distinguished (Hoogenboom, 2000; Penning de Vries, 1962) for these impacts. Yields would be determined by meteorological impact on first production level, if water and nutrient supply are basically favorable. Following this temporary water shortage, lack of nitrogen or phosphorus and potassium deficit can be observed on second, third, or fourth production level, respectively.

First and second levels can be interpreted as unchanged levels of meteorological elements in our study. In the case of third and fourth production levels, change of the yield was thought to be caused by change of nutrient supply and procedure of plant protection. Influences exerted on yield were examined agroclimatologically, and effects of nutrient supply and plant protection were taken into account by means of trend in the case of third and fourth levels.

Yield of first two levels was essentially determined by meteorological elements. These meteorological factors can be divided into two groups: thermal (radiation and temperature) and humidity (relative humidity, precipitation, evapotranspiration, and soil moisture) factors. Water supply is influenced by humidity factors directly. That is the reason why humidity conditions of winter barley during growing season were analyzed (Fig. 2).

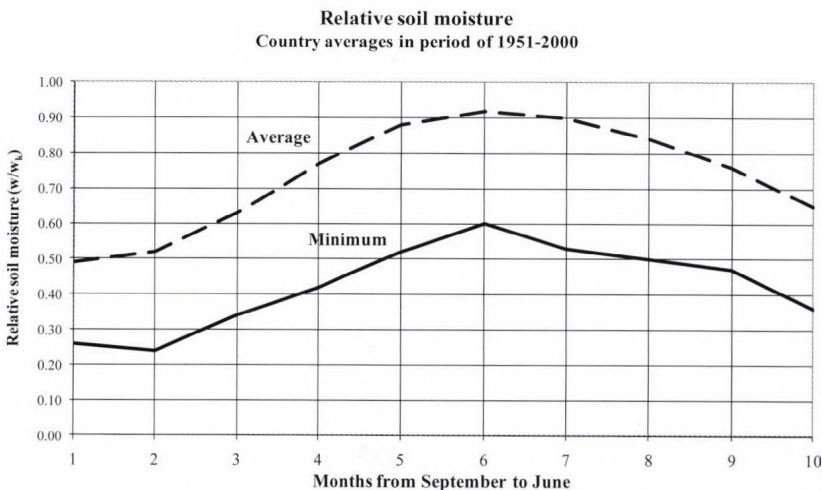


Fig. 2. Temporal changes in relative soil moisture (%) during the growing season of winter barley.

### 3.1. Water supply conditions of winter barley during growing season

Growing season of winter barley lasts from the second half of September to the second half of June. If survey is based on calendar terms, then months between September and June could be taken in account. Run of soil moisture during that period can be studied (Fig. 2). Soil moisture is expressed in the form of relative soil moisture in the first 1 meter depth of upper layer in soil:

$$w_r = \frac{w_a - WP}{FC - WP} = \frac{w}{w_k}, \quad (6)$$

where  $w_a$  is the actual soil water content (in mm),  $WP$  is the soil water content at wilting point (in mm),  $FC$  is the soil water content at field capacity (in mm),  $w$  is the available water content, and  $w_k$  is the available water capacity (in mm). All soil moisture values are related to 1 meter depth of upper layer in soil.

Lower limit of soil moisture demand of winter barley is 45% of available water according to Szalóki (1989, 1991). Soil moisture values above this threshold value are favorable for that crop. Higher limit of soil moisture demand is hard to be defined. Generally, high soil moisture values below field drained upper limit decrease air porosity causing oxygen shortage in pores and unfavorable water uptake.

Fig. 2 shows temporal changes in relative soil moisture during growing season of winter barley in Hungary (country average). It can be seen in Fig. 2, that mean values are above 45% of available water during the whole growing season. On the other hand, minimum values of relative soil moisture are below 45% between September and the middle of January and in the last month of the growing season. As we can see later, soil moisture conditions of autumn-early winter period have just a little effect on yields, and only May–June interval means a certain risk. The results were very similar in the case of other stations.

Hence, it can be presumed that water supply conditions are generally favorable for winter barley, but value of humidity factors can become critical in certain years. In this study, favorable water supply is assumed and impact of temperature on yield is analyzed.

### 3.2. Influence of temperature on yields of winter barley

Firstly, the growing season has to be divided into shorter periods. In this work a calendar term, namely ten-day period was chosen, because experience suggests that the same effect of meteorological conditions rarely extends for a longer interval, that meteorological impact of shorter periods varies, in turn, year by year.

Table 1a. Correlation coefficients of quadratic relationship between average temperature of ten-day periods and trend ratios of winter barley (from September to January)

Stations	Ten days periods in months														
	September			October			November			December			January		
	1	2	3	1	2	3	1	2	3	1	2	3	1	2	3
Győr	0.28	0.30	0.03	0.16	0.10	0.38	0.11	0.30	0.25	0.29	0.37	0.45	0.18	0.11	0.20
Szombathely	0.17	0.27	0.08	0.31	0.10	0.40	0.21	0.35	0.31	0.38	0.36	0.42	0.30	0.28	0.25
Zalaegerszeg	0.18	0.31	0.12	0.26	0.11	0.20	0.16	0.50	0.41	0.46	0.30	0.30	0.11	0.20	0.16
Kaposvár	0.15	0.29	0.23	0.15	0.36	0.18	0.00	0.57	0.33	0.18	0.20	0.18	0.13	0.22	0.25
Pápa	0.20	0.22	0.16	0.12	0.07	0.34	0.09	0.43	0.23	0.24	0.26	0.31	0.15	0.12	0.30
Tatabánya	0.17	0.26	0.19	0.13	0.09	0.24	0.31	0.39	0.24	0.39	0.29	0.34	0.14	0.14	0.22
Martonvásár	0.28	0.25	0.16	0.17	0.22	0.30	0.09	0.39	0.15	0.21	0.35	0.28	0.26	0.11	0.27
Iregszemcse	0.19	0.28	0.25	0.11	0.34	0.23	0.18	0.51	0.20	0.12	0.18	0.19	0.15	0.14	0.22
Pécs	0.20	0.20	0.11	0.06	0.35	0.05	0.25	0.55	0.33	0.13	0.26	0.25	0.23	0.30	0.15
Kecskemét	0.10	0.27	0.16	0.16	0.24	0.25	0.17	0.49	0.30	0.16	0.30	0.22	0.19	0.19	0.24
Budapest	0.20	0.28	0.21	0.10	0.19	0.23	0.07	0.32	0.28	0.39	0.34	0.34	0.18	0.22	0.26
Szolnok	0.25	0.28	0.23	0.22	0.39	0.44	0.15	0.43	0.22	0.25	0.51	0.35	0.14	0.32	0.31
Szeged	0.10	0.17	0.21	0.09	0.28	0.35	0.14	0.31	0.21	0.07	0.46	0.37	0.33	0.19	0.30
Békéscsaba	0.19	0.35	0.27	0.43	0.34	0.34	0.14	0.31	0.18	0.00	0.52	0.45	0.26	0.15	0.33
Debrecen	0.18	0.36	0.06	0.35	0.31	0.38	0.18	0.29	0.33	0.23	0.57	0.42	0.09	0.03	0.23
Nyíregyháza	0.11	0.44	0.21	0.23	0.27	0.28	0.21	0.22	0.29	0.17	0.57	0.42	0.17	0.19	0.04
Miskolc	0.06	0.31	0.10	0.13	0.14	0.48	0.26	0.03	0.19	0.36	0.47	0.37	0.15	0.16	0.04
Kompolt	0.32	0.24	0.10	0.05	0.25	0.40	0.34	0.29	0.34	0.25	0.29	0.31	0.20	0.20	0.12
Balassagyarm.	0.30	0.15	0.04	0.18	0.03	0.29	0.43	0.11	0.25	0.07	0.23	0.42	0.40	0.20	0.33

Table 1b. Correlation coefficients of quadratic relationship between average temperature of ten-day periods and trend ratios of winter barley (from February to June)

Stations	Ten days periods in months														
	February			March			April			May			June		
	1	2	3	1	2	3	1	2	3	1	2	3	1	2	3
Győr	0.39	0.36	0.15	0.15	0.21	0.08	0.12	0.30	0.32	0.25	0.32	0.34	0.48	0.25	0.25
Szombathely	0.34	0.37	0.05	0.18	0.08	0.12	0.13	0.13	0.33	0.36	0.35	0.37	0.32	0.27	0.13
Zalaegerszeg	0.42	0.43	0.15	0.22	0.13	0.23	0.13	0.06	0.37	0.18	0.29	0.21	0.26	0.19	0.13
Kaposvár	0.35	0.34	0.15	0.23	0.17	0.02	0.22	0.18	0.20	0.10	0.03	0.23	0.27	0.07	0.14
Pápa	0.35	0.36	0.01	0.02	0.06	0.14	0.23	0.18	0.28	0.18	0.31	0.45	0.39	0.28	0.21
Tatabánya	0.54	0.51	0.21	0.08	0.07	0.17	0.28	0.15	0.34	0.01	0.26	0.24	0.48	0.06	0.42
Martonvásár	0.35	0.27	0.10	0.14	0.09	0.13	0.22	0.26	0.26	0.19	0.33	0.37	0.35	0.16	0.26
Iregszemcse	0.35	0.31	0.17	0.18	0.17	0.19	0.15	0.37	0.32	0.32	0.07	0.15	0.30	0.15	0.17
Pécs	0.26	0.29	0.23	0.20	0.14	0.16	0.09	0.44	0.27	0.29	0.11	0.12	0.25	0.08	0.19
Kecskemét	0.38	0.41	0.24	0.21	0.15	0.09	0.27	0.42	0.25	0.23	0.23	0.29	0.26	0.15	0.24
Budapest	0.34	0.36	0.18	0.20	0.09	0.18	0.32	0.20	0.39	0.13	0.36	0.42	0.37	0.07	0.26
Szolnok	0.37	0.39	0.13	0.26	0.19	0.07	0.17	0.23	0.28	0.15	0.35	0.40	0.39	0.02	0.22
Szeged	0.36	0.20	0.29	0.30	0.28	0.13	0.26	0.37	0.39	0.30	0.31	0.33	0.39	0.05	0.11
Békéscsaba	0.31	0.24	0.24	0.45	0.12	0.29	0.16	0.30	0.46	0.22	0.26	0.27	0.40	0.06	0.08
Debrecen	0.41	0.37	0.11	0.37	0.07	0.23	0.10	0.31	0.48	0.20	0.29	0.28	0.37	0.05	0.18
Nyíregyháza	0.32	0.49	0.02	0.28	0.29	0.10	0.32	0.26	0.33	0.12	0.32	0.44	0.40	0.26	0.42
Miskolc	0.37	0.29	0.04	0.08	0.22	0.41	0.18	0.13	0.39	0.18	0.09	0.21	0.56	0.12	0.26
Kompolt	0.43	0.38	0.11	0.12	0.07	0.35	0.17	0.16	0.34	0.13	0.16	0.22	0.55	0.05	0.27
Balassagyarm.	0.49	0.47	0.18	0.09	0.16	0.06	0.49	0.24	0.38	0.26	0.15	0.31	0.40	0.15	0.52

Relationship between temperature and trend ratio was studied for all ten-day periods of growing season. *Table 1a* shows correlation coefficients of these relationships for September–January period and *Table 1b* demonstrates  $r$  values of January–June interval.

Temperature values of the third ten days period of October and the second ten-day period of November are in close correlation with yields as it can be seen in *Table 1a*. This is because of the relatively poor frost-tolerance of winter barley (*Varga-Haszonits et al.*, 2006). In winter, mostly the third ten-day period of December (see *Table 1a*) and the first and second ten-day periods of February (see *Table 1b*) influence barley yield. It suggests that the success of barley production is basically influenced by permanent cold weather without snow-cover. Thus, significant influence of winter temperature values on yield are demonstrated also by investigations based on data of ten-day periods. In spring (and in early summer) mainly the third ten-day period of April, the third ten days period of May and the first ten-day period of June have great influence on productivity.

Selection of the most significant periods was done separately in the case of all stations, that is why these ten-day periods of our model can differ in different places. Data of *Tables 1a* and *1b* make it possible to choose appropriate intervals which can be used in the multiplicative successive model. Selected ten-day periods can be seen in *Table 2*.

*Table 2.* Ten-day periods chosen by means of sensitivity analysis

Stations	Selected periods			
	Period 1	Period 2	Period 3	Period 4
Győr	Nov 11–Nov 30	Dec 11–Dec 20	Feb 1–Feb 20	Apr 21–Jun 10
Szombathely	Nov 11–Nov 20	Dec 11–Dec 20	Feb 1–Feb 20	Apr 21–Jun 10
Zalaegerszeg	Nov 11–Nov 20	Dec 21–Dec 31	Apr 21–Apr 30	Apr 21–Apr 30
Kaposvár	Nov 11–Nov 20	Dec 11–Dec 31	Jan 1–Feb 20	Jan 1–Feb 20
Pápa	Nov 11–Nov 20	Dec 11–Dec 31	Feb 1–Feb 20	May 11–Jun 10
Tatabánya	Nov 11–Nov 20	Dec 11–Dec 31	Apr 21–Apr 30	Jun 1–Jun 10
Martonvásár	Nov 11–Nov 20	Dec 11–Dec 31	Jan 21–Feb 20	May 11–Jun 10
Iregszemcse	Oct 11–Oct 31	Nov 11–Nov 30	Feb 1–Feb 20	Apr 11–May 31
Pécs	Nov 11–Nov 20	Dec 11–Dec 20	Feb 1–Feb 20	Apr 11–May 10
Kecskemét	Nov 11–Nov 20	Dec 11–Dec 20	Feb 1–Feb 20	Mar 1–Jun 10
Budapest	Nov 11–Nov 20	Dec 1 –Dec 20	Feb 1–Feb 20	Mar 1–Jun 10
Szolnok	Nov 11–Nov 20	Dec 11–Dec 20	Feb 1–Feb 20	Mar 1–Jun 10
Szeged	Nov 11–Nov 20	Dec 11–Dec 20	Feb 1–Feb 20	Apr 1–Jun 10
Békéscsaba	Nov 11–Nov 20	Dec 11–Dec 20	Feb 1–Feb 20	Mar 1–Jun 10
Debrecen	Nov 11–Nov 20	Dec 11–Dec 20	Feb 1–Feb 20	Mar 1–Jun 10
Nyíregyháza	Nov 11–Nov 20	Dec 11–Dec 20	Feb 1–Feb 20	Mar 1–Jun 10
Miskolc	Nov 11–Nov 20	Dec 11–Dec 20	Feb 1–Feb 20	Mar 1–Jun 10
Kompolt	Oct 21–Feb 20	Apr 21–Apr 30	Jun 1–Jun 10	Jun 1–Jun 10
Balassagyarmat	Dec 21–Dec 31	Feb 1 –Feb 20	Apr 21–Apr 30	Jun 1–Jun 10

Calculations displayed in Section 2 can be done on the base of temperature data of those intervals. *Table 3* contains our results.

*Table 3.* Correlation coefficients of estimating functions for selected periods

Station	Trend $f(t)$	Correlation coefficients of estimating function			
		Period 1	Period 2	Period 3	Period 4
		$f(t) \cdot f_1(m_1)$	$f(t)f_1(m_1)f_2(m_2)$	$f(t)f_1(m_1)f_2(m_2)f_3(m_3)$	$f(t)f_1(m_1)f_2(m_2)f_3(m_3)f_4(m_4)$
Győr	0.9139	0.9319	0.9325	0.9405	0.9514
Szombathely	0.8627	0.8889	0.8903	0.9146	0.9275
Zalaegerszeg	0.9042	0.9241	0.9276	0.9252	0.9252
Kaposvár	0.9187	0.9460	0.9479	0.9588	0.9588
Pápa	0.9173	0.9451	0.9466	0.9504	0.9706
Tatabánya	0.8575	0.8955	0.8933	0.8922	0.9092
Martonvásár	0.8958	0.9288	0.9295	0.9429	0.9568
Iregszemcse	0.9207	0.9225	0.9499	0.9580	0.9630
Pécs	0.9054	0.9378	0.9381	0.9468	0.9524
Kecskemét	0.8139	0.8807	0.8921	0.8972	0.9233
Budapest	0.8545	0.8826	0.8859	0.8865	0.9014
Szolnok	0.8961	0.9290	0.9457	0.9523	0.9538
Szeged	0.8313	0.8511	0.8852	0.8932	0.9117
Békéscsaba	0.9162	0.9201	0.9409	0.9480	0.9519
Debrecen	0.8424	0.8647	0.9099	0.9314	0.9300
Nyíregyháza	0.8138	0.8315	0.8847	0.9282	0.9281
Miskolc	0.8430	0.8437	0.8809	0.9011	0.9197
Kompolt	0.8559	0.8939	0.8947	0.9075	0.9076
Balassagyarmat	0.8641	0.8873	0.9138	0.9125	0.9304

As it can be seen in *Table 3*, we have got better and better estimating functions by the aim of multiplicative successive approximation, and correlation coefficients came closer to the value of 1. According to our results it can be stated that if ten-day periods with no significant impact are used then the accuracy of estimation will essentially diminish.

The check-up of method was done by comparison of calculated and measured values. According to our results coefficient of determination ( $r^2$  values) were higher than 0.9 at all stations. It means that correlation coefficients ( $r$  values) were close to 1. *Fig. 3* shows such a relationship.

The accuracy of estimation was checked by error of estimation – that is the difference between calculated and measured value – and then by studying the frequency of these errors. Results are indicated in *Table 4*.

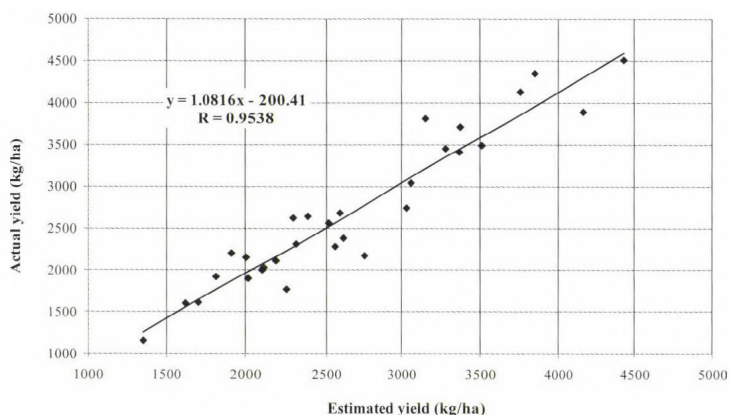


Fig. 3. Comparison of calculated and measured yield (kg/ha) values.

Table 4. Cumulative frequency of the difference between measured and calculated values

Stations	Error of estimation (%) under					
	5%	10%	15%	20%	25%	30%
Győr	47	77	87	93	93	97
Szombathely	33	77	80	90	97	97
Zalaegerszeg	27	73	83	90	97	100
Kaposvár	43	73	80	97	97	100
Pápa	37	77	97	97	97	100
Tatabánya	40	73	80	93	93	93
Martonvásár	37	77	90	93	97	100
Iregszemcse	37	73	83	93	100	100
Pécs	33	70	83	90	97	100
Kecskemét	60	70	83	90	93	93
Budapest	27	70	77	90	93	97
Szolnok	37	70	87	93	93	100
Szeged	37	70	87	87	97	97
Békéscsaba	27	73	87	90	90	100
Debrecen	20	70	90	93	97	97
Nyíregyháza	43	73	83	100	100	100
Miskolc	40	70	80	87	90	93
Kompolt	30	70	80	87	93	97
Balassagyarmat	33	77	83	87	93	97

The error of estimation was expressed in % of actual yield. As it can be seen in Table 4, our model gives acceptable results for yield estimation. When we used this method, the error of estimation was less than 5% in 30–40% of all cases and it was less than 10% in 70–80% of all cases. It means that inaccuracy of estimation remained under 10% in two third of all studied cases.

#### 4. Conclusions

Our results suggest that multiplicative successive model is suitable for estimating yields of winter barley which grows in the cool and wet part of the year in Hungary. Considering the fact that yield of cultivated plants is mainly influenced by meteorological conditions, water supply, nutrient supply and plant protection, yields can be accurately estimated if impact of agrotechnical factors (variety, nutrient supply, plant protection) is defined numerically by means of a trend function, and impact of meteorological factors is calculated as the fluctuation around trend values. This model becomes more simply if we suppose that water supply is favorable during the growing season of winter barley. Unfavorably dry spells usually occur only from July in Hungary.

Our model demonstrates how successive periods of growing season influence the yield. In this way, this method takes impact of successive periods into account, and it is a step from statistical models to dynamic models. Our results demonstrated that autumn frosts and permanent cold winter weather without snow-cover have great influence on productivity of winter barley.

This model is a better tool for studying the effects of climatic variability or a possible climate change, than a simple statistical model. The multiplicative successive model is a useful tool to estimate the effect of the possible climate change on the yield of winter barley and to determine the past of the growing season in which the changes would occur.

#### References

- Abbaspour, K.C, Hall, J.W. and Moon, D.E., 1992: A yield model for use in determining crop insurance premiums. *Agr. Forest Meteorol.* 60, 33-51.
- Andresen, J.A., Alagarwamy, G., Rotz, C.A., Ritchie, J.T. and LeBaron, A.W., 2001: Weather impacts on maize, soybean, and alfalfa production in the Great Lakes Region, 1895–1996. *Agron. J.* 93, 1059-1070.
- Fageria, N.K., 1992: *Maximizing Crop Yields*. Marcel Dekker, New York.
- Fuqin, L. and Tian, G. 1991: *Research on Remote Sensing – Meteorological Model for Wheat Yield Estimation*. 12th Asian Conference on Remote Sensing. Asian Association of Remote Sensing (AARS), Oct. 30 - Nov. 5, 1991, Singapore. (<http://www.aars.org/acrs/proceeding/ACRS1991/Papers/AGV91-4.htm>)
- Hoogenboom, G., 2000: Contribution of agrometeorology to the simulation of crop production and its applications. *Agr. Forest Meteorol.* 103, 137-157.
- Mavi, H.S. and Tupper, G.J., 2004: *Agrometeorology. Principles and Applications of Climate Studies in Agriculture*. Food Product Press, New York.
- Panofsky, H.A. and Brier, G.W., 1963: *Some Applications of Statistics to Meteorology*. The Pennsylvania State University, Pennsylvania.
- Penning de Vries, F.W.T., 1962: System analysis and models of crop growth. In *Simulation of plant growth and crop production* (eds.: F.W.T. Penning de Vries and H.H. van Laar). Simulation Monographs, Pudoc, Wageningen, 99-19.
- Porter, J.R. and Semenov, M.A., 2005: Crop responses to climatic variation. *Philos. Trans. R. Soc. Lond. B Biol. Sci.* 360(1463), 2021-2035.

- Ritchie, J.T. and Alagarwamy, G., 2002: Overview of crop models for assessment of crop production. In *Effect of Climate Change and Variability on Agricultural Production System* (eds.: O.C. Doering, III, J.C. Randolph, J. Southworth, R.A. Pfeifer). Kluwer Academic Publishers, Boston, 43-68.
- Szabó, T. and Tóth, R., 1989: Determination of significant periods influencing the productivity on the basis of meteorological factors (in Hungarian). *Növénytermelés* 38, 55-67.
- Szakály, J., 1968: Meteorological conditions of early development of rye and winter barley and temperature sums of developmental periods (in Hungarian). *Beszámolók az 1966-ban végzett tudományos kutatásokról*. 31. Országos Meteorológiai Szolgálat, Budapest, 152-162.
- Szalóki, S., 1989: Water Demand, Water Use and Irrigation Water Need of Crops (in Hungarian). In: *Manual of irrigation* (ed.: Szalai, Gy.). Mezőgazdasági Kiadó, Budapest, 100-154.
- Szalóki, S., 1991: Water and irrigation demand of plants (in Hungarian) (eds.: Lelkes, J. and Ligetvári, F.). Fólium Könyvkiadó Kft., Budapest, 21-42.
- Thompson, L.M., 1962: Evaluation of weather factors in the production of wheat. *J. Soil Water Conservation* 17, 218-230.
- Thompson, L.M., 1969: Weather and technology in the production of wheat in the United States. *J. Soil Water Conservation* 24, 219-224.
- Thompson, L.M., 1975: Weather variability, climatic change, and grain production. *Science* 188, 535-541.
- Thompson, L.M., 1986: Climatic change, weather variability, and corn production. *Agron. J.* 78, 649-653.
- Varga-Haszonits, Z., 1986: Principal-methodical basis of multiplicative crop-weather models (in Hungarian). *Beszámolók az 1983-ban végzett tudományos kutatásokról*. Országos Meteorológiai Szolgálat, Budapest, 155-164.
- Varga-Haszonits, Z., 1987: Relationship between winter wheat yield and weather determined by multiplicative model using successive approximation (in Hungarian). *Beszámolók az 1985-ben végzett tudományos kutatásokról*. Országos Meteorológiai Szolgálat, Budapest, 184-196.
- Varga-Haszonits, Z., 1992: *Complex Agroclimatological Model for Characterizing the Productivity of Winter Wheat* (in Hungarian). PhD Thesis, Hungarian Academy of Sciences, Budapest.
- Varga-Haszonits, Z., Varga, Z., Lantos, Zs., Vámos, O. and Schmidt, R., 2000: *Agroclimatological Analysis of Climatic Resources in Hungary* (in Hungarian). LÓRIPRINT, Mosonmagyaróvár.
- Varga-Haszonits, Z., Varga, Z., Lantos, Zs. and Enzsölné Gerencsér, E. 2006: *Climatic Variability and Ecosystems* (in Hungarian). Monocopy, Mosonmagyaróvár.

# IDŐJÁRÁS

*Quarterly Journal of the Hungarian Meteorological Service  
Vol. 115, No. 3, July–September 2011, pp. 179–204*

## **Air quality around motorway tunnels in complex terrain – computational fluid dynamics modeling and comparison to wind tunnel data**

**Márton Balczó<sup>1\*</sup>, Miklós Balogh<sup>1</sup>, István Goricsán<sup>1</sup>, Torsten Nagel<sup>2</sup>,  
Jenő M. Suda<sup>1</sup>, and Tamás Lajos<sup>1</sup>**

<sup>1</sup>*Theodore von Kármán Wind Tunnel Laboratory, Department of Fluid Mechanics,  
Budapest University of Technology and Economics (BME),  
Bertalan L. u. 4-6, H-1111 Budapest, Hungary  
E-mails: balczo@ara.bme.hu; baloghm@ara.bme.hu; goricsan@ara.bme.hu;  
suda@ara.bme.hu; lajos@ara.bme.hu*

<sup>2</sup>*Lohmeyer Consulting Engineers  
An der Roßweid 3, 76229, Karlsruhe, Germany  
E-mail: t.nagel@lohmeyer.de*

*\*Corresponding author*

*(Manuscript received in final form September 21, 2010)*

**Abstract**—The current paper describes numerical simulations of flow and dispersion performed in a complex suburban area of Budapest using the microscale model MISKAM and accompanying wind tunnel tests which provided reference concentration data for validation of the model results. Main pollutant sources are traffic related and include a planned motorway section of 9 km length consisting of sections running in tunnel, on ground, and on viaduct. Four different route alternatives were investigated. In the paper, first a condensed review is given about problems related to air quality around motorway tunnels in complex terrain. The effect of larger scales on microscale air quality was determined using background concentrations from monitoring station time series with removal of short-term fluctuations, for which a simple method is introduced here. The validation wind tunnel tests were carried out at several wind directions on a 1:1000 scale model containing topography, buildings, and vegetation with measurement of tracer concentrations in 50 sampling locations. In the microscale CFD simulation, flow and dispersion considering topography, vegetation, and buildings were calculated three-dimensional in a large domain using  $k-\varepsilon$  model, and advective diffusion equation was set up on a Cartesian grid treating air pollutants as non-reactive scalars. Results give more detailed information about the flow, for example local speedup above hills, slowdown in vegetation zones, separation regions are resolved well. Deviation of pollutant plume paths from the mean wind direction caused by the topography could be also observed.  $\text{NO}_x$  concentration maps showed that air quality limit exceedances occur near motorway tunnel portals in form of large surface plumes, which can only be avoided by the application of

tunnel ventilation stacks. These will exhaust polluted tunnel air in larger heights. The comparison of numerical results to the wind tunnel reference data was performed using statistic metrics (fractional bias, normal mean square error, geometric mean bias, geometric variance, correlation coefficient) showing a generally good agreement.

*Key-words:* air quality, complex terrain, tunnel portal, CFD simulation, background concentration, model validation, wind tunnel measurement

## 1. Introduction

The prediction of air quality in urban or suburban areas often requires sophisticated tools when the surrounding terrain is complex. The major pollutant sources are mostly traffic related, emitting pollutants along main road or motorway routes. Buildings and vegetation have also strong influence on the dispersion process. Additional problems can emerge due to the concentrated exhaust of polluted air from roadway tunnel portals. A short literature overview of these topics will be given in the following subsections, followed by a short description of the investigated area in the north of Budapest, which includes, besides existing main roads, a 9 km long planned motorway section with longer tunnels. Section 2 discusses the proper input data collected for the microscale numerical simulations and wind tunnel tests, which are then described in detail in Section 3. In Section 4, we give an overview of the CFD results and compare them to the wind tunnel data. Additionally, we also summarize the proposed arrangements for reducing air pollution from the tunnel portals.

### 1.1. Flow over complex terrain

Complex terrain can produce a variety of flow patterns, mainly depending on the topography, vegetation cover, and the thermal stratification (Froude number), as described in standard texts, for example in *Plate* (1982) and *Kaimal and Finnigan* (1994). Basic mechanisms are discussed by *Belcher and Hunt* (1998), and an overview of research in the last 50 years is given by *Wood* (2000).

To validate the modeling tools for complex terrain flows, numerous studies were performed. Beyond isolated and simplified 2D or 3D slopes and hills measured in wind tunnels (e.g., *Ayotte and Hughes*, 2004), the Askervein hill project (*Taylor and Teunissen*, 1987; *Walmsley and Taylor*, 1996) has gained specific importance, with an on-site measurement campaign being performed in 1982–1983, which served as reference data for dozens of wind tunnel and numerical studies. The wind tunnel method gave good agreement with the measurement reference data (see e.g., particle image velocimetry (PIV) measurements of *Rodrigues*, 2005). *Bowen* (2003) discusses aspects of physical modeling like model scale and roughness in detail. In CFD modeling, besides the Reynolds-averaged Navier-Stokes (RANS) approach using mostly  $k-\epsilon$  turbulence closure (*Kim and Patel*, 2000; *Castro et al.*, 2003), in the last decade

even more large-eddy simulation (LES) was used to model the Askervein hill flow (e.g., *Silva Lopes et al.*, 2007).

The application focus of the practical studies in this field is on wind turbine siting, heavy gas dispersion, and the determination of airport wind conditions. Several authors reported wind tunnel tests of real-world, very complex terrain. *Cermak* (1984) performed tests for different stratifications. Further studies to mention are those of *Snyder* (1990), *Liu et al.* (2001), and *McBride et al.* (2001). Numerical application examples using a RANS  $k-\epsilon$  model and comparison with on-site measurements are shown for example in *Brodeur and Masson* (2006) and *Palma et al.* (2008).

### 1.2. Tunnel related air quality problems

In roadway tunnels, a large amount of traffic pollution can be accumulated, which is removed by the pressure difference, the piston effect of moving vehicles, and the tunnel ventilation system mostly through the tunnel portal. The tunnel ventilation system for one directional tunnel of medium length consists of axial fans mounted in the tunnel pipe, which drive air into the driving direction and exhaust polluted air at the forward tunnel exit. An overview of tunnel related air quality problems is given by *Longley and Kelly* (2008) and *Bettelini et al.* (2001), the latter is also showing modeling results near a tunnel portal with a Gaussian model and CFD. *Oettl et al.* (2003) compared results from two specific portal dispersion models with on-site measurements.

Wind tunnel measurements of a tunnel portal with moving vehicles were reported by *Nadel et al.* (1994) and *Plate* (1999). They observed high concentrations near the portal and recognized the influence of traffic induced turbulence. *Contini et al.* (2003) measured flow and dispersion near tunnel portals behind a 2D hill. Tunnel emissions were released from a point source in the middle of the tunnel.

Tunnel ventilation systems are designed according to national standards like those of Switzerland (*ASTRA*, 2004). To avoid large concentrations outside the portals of longer tunnels, it is often necessary to install separate ventilation stacks which direct polluted air from the tunnel into larger heights or filter facilities which remove a part of pollutants.

### 1.3. Site description

The area of investigation covers about 8 km  $\times$  5 km. The topography has moderate slopes similar to Askervein hill, with height differences of about 200–300 m (*Fig. 1*). In the south-eastern part of the domain, outskirts of Budapest are located with 10–15 storey block buildings and a population of about 70,000. On the northern and western side, four suburban towns can be found in the complex terrain of Buda Mountains with 20,000 inhabitants. Deciduous forests cover a smaller part of the not habited areas, mainly hilltops.



Fig. 1. The investigated domain with existing main roads and planned route alternatives 1, 3, 3.1, and 6 of the M0 motorway. Route colors are black or white. Please note that the routes are partly overlapping. Circular black dots: wind tunnel sampling points (50); thin continuous black rectangles: close investigation areas of numerical simulation in the 3 junctions; thin dashed line: inhabited areas.

Major pollutant sources are traffic sources, existing main roads (national roads No. 10 and No. 11) and most importantly, a planned section of the ring motorway M0 of Budapest, consisting of three traffic junctions. Four route alternatives have been investigated: 1, 3, 3.1, and 6, all of them include several bridges and tunnels.

The planned ring motorway section connects national road No. 10 and planned motorway M10 in the northwest of Budapest with national road No. 11 in the north of Budapest. Route 1 (marked white in *Fig. 1*) is the most southern from the alternatives, and has shorter tunnels. Route 3.1 and 6 differ from route 3 only in the middle and eastern part: route 6 runs in Junction 2 longer eastwards on surface and has a shorter eastern tunnel. Route 3.1's surface section and eastern tunnel's portal in Junction 2 are shifted to the north. On the far eastern side, in Junction 1 near the national road No. 11, all routes are identical. In Junction 1 and 3, the routes cross the valleys on viaducts. In Junction 2, the routes run in deep cutting.

Rush-hour traffic on the new section is expected to reach about 2,800 vehicle h<sup>-1</sup> in the year 2018 with further growth to 4,400 vehicle h<sup>-1</sup> until 2023. The planned one-directional tunnels are up to 3.2 km long, and their original design included longitudinal ventilation using axial fans without separate ventilation stacks (see later in *Fig. 10*). As a consequence, all pollutants produced in the tunnel are supposed to leave the tunnel through the forward portal.

Due to the closeness to inhabited areas, air quality and noise impacts of the new motorway were of most concern. The availability of high-resolution pollutant concentration maps of the area is thus crucial for the decision makers to help them find the best route alternative, and also for the public<sup>1</sup> to accept the selected route.

## 2. Input data

Unlike the investigations, focusing on the dispersion phenomenon itself, at the end of environmental impact assessment studies like this, exact concentrations should be calculated as a decision basis for the authorities. Any errors in input data like background concentrations, wind statistics, or car emissions will also be reflected in the results. Thus, one has to pay specific attention to the collection of high-quality input data.

### 2.1. Background concentrations

Pollutant dispersion is a multi-scale process in both space and time. Besides the possibility of a full coupling of different scale models (nesting), a demanding task for modelers, the usual approach is to consider the effect of larger scales in the microscale dispersion model as a background concentration. The background

---

<sup>1</sup> Short reports prepared for the public about this project can be found at [www.karman-wtl.com](http://www.karman-wtl.com) (in Hungarian).

concentration might be significantly different in urban and rural areas, and can be determined in several ways: (a) by taking the output of a mesoscale / urban scale model or (b) using measurement data from urban background stations.

In *Mensink et al.* (2008), coupling of the Gaussian mesoscale dispersion model IFDM and the street canyon scale model OSPM was realized. Example of the second method can be seen in *Berkowicz* (2000), a simple urban background model developed for Copenhagen, using the urban emission inventory, rural background measurement data, and wind statistics.

When applying the second method, one has to consider the fact that urban background stations are also subject to short-term variations due to local pollution sources. Their effect should hence be removed to obtain clean background values. *Cremades* (2000) demonstrated two methods for this in a hypothetical case, while *Jones et al.* (2008) removed the effect of nearby traffic sources by comparing weekend and weekday concentrations at an urban monitoring station in London and determined the urban background values and urban non-traffic increments of  $PM_{10}$ . *Tchepel* and *Borrego* (2010) analyzed spectra of air quality monitoring data using spectral methods and found that short-term fluctuations correlate with daily variations in traffic and wind speed. Long-term variance over a 21-day period caused by long-range pollutant transport was also observed. In *Tchepel et al.* (2010), after spectral analysis of the concentration time series, short-term components above a frequency threshold were flattened using the Kolmogorov-Zurbenko filter.

In the present case, data from two background stations in Budapest were analyzed for the years 2007–2008. Pesthidegkút station is located in a suburban area, and thus, it is characteristic for Junction 2 and 3, while Gilice tér station is in an outer district of the city, which can provide background data for the semi-urban environment of Junction 1 (*Fig. 1*). Both stations are influenced by local sources with daily peaks in the morning and afternoon rush-hours (*Fig. 2*), especially for  $NO_x$ , which indicates a relatively close traffic release.

This local influence was removed by separating the baseline and short-term parts of the time series using Fourier transformation.

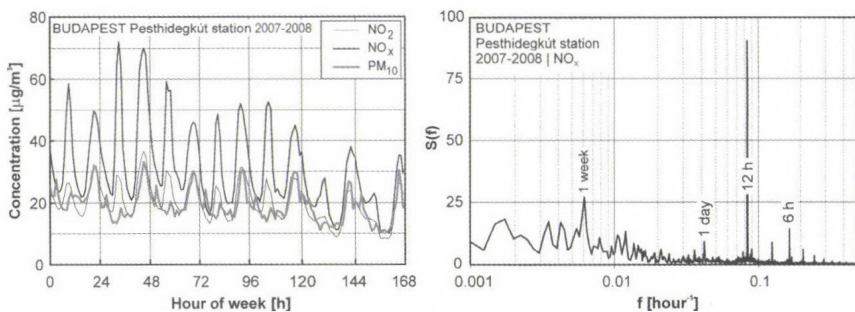


*Fig. 2.* Left: Average weekly concentrations at Pesthidegkút station in Budapest; right: spectrum of  $NO_x$  concentrations with a strong 12 h peak.

Because local traffic influence is reflected in the strong 12 h and 6 h components of the FFT spectrum (*Fig. 2*), the separation frequency was chosen as  $0.056 \text{ h}^{-1}$ , corresponding to the period of 18 h. After the separation, the average absolute value of the short-term signal was subtracted from the mean value of the original time series to obtain the annual mean background concentration without the contribution of local sources (*Table 1*).

*Table 1.* Background concentrations [ $\mu\text{g m}^{-3}$ ]

	Annual mean		Fluctuations removed	
	NO <sub>x</sub>	PM <sub>10</sub>	NO <sub>x</sub>	PM <sub>10</sub>
Budapest, Pesthidegkút <sup>a</sup>	31.5	19.2	15.8	13.2
Budapest, Gillice tér <sup>b</sup>	39.6	31.2	20.0	20.4

<sup>a</sup> Suburban background station, 47.5617°N, 18.9608°E, Junction 2 and 3

<sup>b</sup> Urban background station, 47.4298°N, 19.1812°E, Junction 1

## 2.2. Emissions

Car emissions can be determined from traffic density and the emission factors of different vehicle categories. These are again dependent from fleet composition, traffic situation, slope, and so on. In this project, fleet-average emission factors for the reference year 2006 and realization year 2018 had to be determined. The Handbook of Emission Factors – HBEFA 2.1 (*Infras*, 2004) is the emission factor database of several mid-European countries (D, A, CH, NL) based on emission factors determined for individual vehicle groups, the so-called vehicle subsegments. Vehicles of the same class, engine power, and emission category have obviously similar emission factors, which were determined by dynamometer measurements. These may vary depending on traffic situation, speed, slope, road quality, and temperature. The accumulated emission factor valid on a specific road section (urban, rural, motorway etc.) is then an average of subsegment factors weighted by the actual traffic composition, which is also included in the database. The method was validated in several studies, e.g., through emission measurements in the Gubrist tunnel by *Colberg et al.* (2005).

To apply the method in Hungary, the national vehicle database of the years 2001–2006 was analyzed, and the fleet was divided into vehicle subsegments defined in the HBEFA database. As a rough estimate, a four-year delay compared to the vehicle fleet in Germany was demonstrated for passenger cars and light duty vehicles<sup>2</sup>.

<sup>2</sup> In the meantime, the new HBEFA version 3.1 was released, supporting also vehicle fleets of Norway and Sweden. Further validation of emission factors and the new emission models applied lead in the upgrade to higher NO<sub>x</sub> and PM emission factors for passenger cars and lower ones for light and heavy-duty vehicles. These changes might increase the accuracy of the concentration predictions, however, it could not anymore considered in this paper.

The fleet-averaged emission factors for the M0 motorway with 80 km/h speed limit and  $\pm 2\%$  slope are shown in *Table 2*. The general improvement of factors over the years is due to the replacement of older vehicles with vehicles that comply with the EURO4 and newer standards. Also, non-exhaust  $PM_{10}$  emissions from abrasion and resuspension were considered, based on an on-site measurement campaign along a motorway (*Ketzel et al., 2007*).

*Table 2.* Accumulated exhaust and non-exhaust emission factors [ $g\ km^{-1}\ veh^{-1}$ ] for different vehicle categories calculated from the subsegment emission factors of the HBEFA 2.1 database and Hungarian fleet composition data. Traffic situation: motorway with 80 km/h speed limit and  $\pm 2\%$  slope

Emission factor Year	$NO_x$		$PM_{10}^a$		$PM_{10, n-e}^b$
	2006	2018	2006	2018	All years
Passenger car	0.60	0.17	0.008	0.007	0.022
Light duty vehicle	1.17	0.54	0.193	0.034	0.022
Coach	7.86	3.66	0.494	0.052	0.200
Heavy duty vehicle	5.04	2.81	0.120	0.037	0.200

<sup>a</sup> exhaust factors

<sup>b</sup> non-exhaust factors (*Ketzel et al., 2007*)

### 2.3. Wind statistics

Long-term wind statistics were only available at a station of the Hungarian Meteorological Service (HMS) about 5 km from the site in a flat area. To determine local wind statistics, which may be different from the flat terrain measurements and could show systematic mesoscale changes due to the Buda Mountains, the mesoscale diagnostic wind field model DIWIMO<sup>3</sup> was run on a 30 km  $\times$  16.3 km domain shown in *Fig. 3*. Elevation in this domain varies between 87 and 562 m above sea level.

The model generates a mass-consistent wind field based on the measured wind statistics in one point of the domain considering the topography, stratification, varying surface roughness, and surface coverage of the area. The model's parameterizations are described in detail by *Moussiopoulos et al. (1988)*.

The model uses a terrain-following mesh, in the current simulation with a horizontal grid resolution of 100 m, while in vertical direction the domain of 800 m height was divided into 26 layers of varying thickness. The lowermost layer's thickness changed between 7 and 19 m due to the stretching of the vertical grid to the terrain.

<sup>3</sup> Further description can be found at [www.stadtklima.de/EN/E\\_1tools.htm#DIWIMO](http://www.stadtklima.de/EN/E_1tools.htm#DIWIMO) and on the webpage of Lohmeyer Consulting Engineers: [www.lohmeyer.de/modelle/diwimo.htm](http://www.lohmeyer.de/modelle/diwimo.htm) (in German).

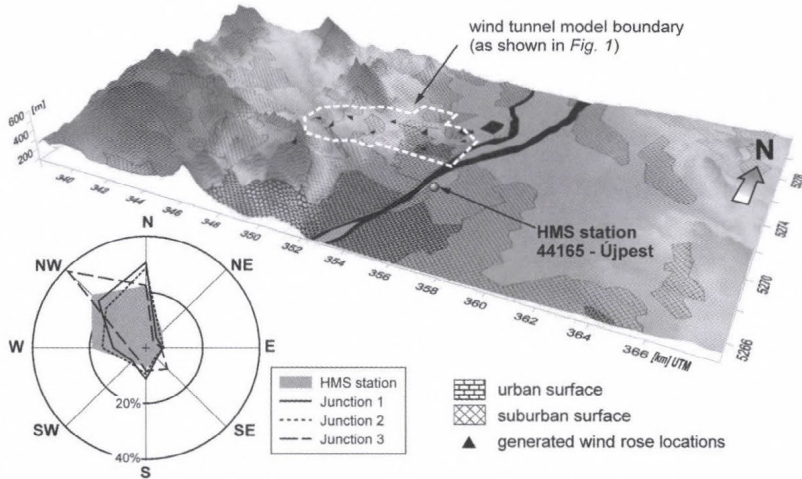


Fig. 3. Top: Domain of DIWIMO simulation with land usage patterns and generated wind rose locations. Elevation is scaled by 5. Bottom left: original wind statistics of the HMS station simplified for eight main wind directions (grey plot); mean wind roses, averaged from all calculated wind roses in the specific junction.

The model was run with 36 wind directions, and wind statistics were generated at 9 locations in the closer investigation area (3 in each traffic junction) using the known wind statistics at the location of the HMS station. These were averaged in each of the three junctions and simplified for the 8 main wind directions. The averaged wind roses can be seen as representative for the individual junctions, and can also be used as inlet boundary condition for the microscale investigation of the junctions.

In Junction 1 and 2, the wind roses show higher mean wind speed and distortions due to topographic effects towards the north (Fig. 3, bottom left). At Junction 3, influence of a NW–SE oriented valley can be clearly recognized. Based on the wind statistics, 5–7 important incident wind directions were selected at each junction for further microscale investigation, covering about 80% of the wind conditions in a year.

### 3. Microscale investigation methods

#### 3.1. MISKAM flow and dispersion simulations

In the last decade, dozens of different CFD models were developed and applied for the investigation of microscale air pollution problems, where the effect of a singular or a group of obstacles is not negligible, and thus, the solution of the full equations of motion is necessary. On behalf of the numerous publications in this topic, most of them are concentrating on built urban areas, more specifically

street canyons, only the reviews of *Vardoulakis et al.* (2003) and *Holmes and Morawska* (2006) may be cited here. Besides the models utilizing the RANS (Reynolds-averaged Navier-Stokes) approach with  $k$ - $\varepsilon$  type turbulence closures, large-eddy simulation is applied with promising results (e.g., *Xie and Castro*, 2009), however, on the price of a very high computational demand (needing multi-processor computer clusters), which is in most cases not accessible for environmental agencies and consulting engineers.

The code used in the current investigation, MISKAM gained currency in environmental assessment practice due to the relatively simple model setup and the fast code able to run on a single processor PC. The model solves the RANS equation using a  $k$ - $\varepsilon$  turbulence closure on a Cartesian grid. Buildings are represented as blockouts from the grid. Dispersion of an inert pollutant is calculated afterwards by the advection-diffusion equation using the wind field simulation results. Vegetation effects can be accounted for by additional terms in the flow and turbulence equations. Details of the MISKAM model are given in *Table 3* or in more depth in *Eichhorn* (2008).

Extensive model evaluation activities were undertaken according to *VDI* (2005) by *Eichhorn and Kniffka* (2010) and in the framework of COST Action 732<sup>4</sup> (*Goricsán et al.*, 2011) using the MUST data set. The implemented vegetation model (*Ries and Eichhorn*, 2001), which introduced additional terms in the motion and turbulence equations, was validated in *Balczó et al.* (2009) using the CODASC<sup>5</sup> wind tunnel data set.

Besides these, the model has been used in several validation and comparison studies. *Ketzel et al.* (2000) compared MISKAM data to on-site measurements, as it was also done in the Podbi-exercise (*Lohmeyer et al.*, 2002). Comparison of MISKAM simulation data to urban wind tunnel measurements can be found in *Ketzel et al.* (2002), *Sahm et al.* (2002), *Goricsán et al.* (2004), and for a simple stack-building configuration in *Olesen et al.* (2009). Several authors used MISKAM results as input for other transport and chemistry models (*Stern and Yamartino*, 2001; *Dixon and Tomlin*, 2007), or for emergency response tools (*Donnelly et al.*, 2009).

Although MISKAM is able to model the effect of stable stratification on dispersion by decreasing turbulence production in the equations of  $k$  and  $\varepsilon$ , and in general, CFD modeling of stratification and thermal induced flows is possible (see, e.g., the adaptation of CFD solvers for stratified flows in *Kristóf et al.*, 2009), in this case we limited the influence of thermal stratification to neutral conditions to preserve the compatibility of CFD results with the wind tunnel measurements.

---

<sup>4</sup> COST Action 732: Quality Assurance and Improvement of Micro-Scale Meteorological Models, [www.mi.uni-hamburg.de/Home.484.0.html](http://www.mi.uni-hamburg.de/Home.484.0.html)

<sup>5</sup> CODASC data base, (COncentration DATA for Street Canyons), Laboratory of Building and Environmental Aerodynamics, IfH Karlsruhe Institute of Technology, [www.codasc.de](http://www.codasc.de)

Table 3. Description of the MISKAM model

<b>Model equations</b>	
Model version	MISKAM 5.01
Flow model	Reynolds-averaged Navier-Stokes equation with turbulence closure
Turbulence model	Modified version of Kato-Launder $k$ - $\varepsilon$ (Kato and Launder, 1993; López, 2002)
Model constants	$C_\mu = 0.09$ , $C_{\varepsilon 1} = 1.44$ , $\sigma_k = 1$ , $\sigma_\varepsilon = 1.3$ , $\kappa_\mu = 0.4$
Wall treatment	Logarithmic wall function
Vegetation treatment	Porosity-based model
Dispersion model	Reynolds-averaged advective diffusion equation
Turbulent Schmidt number	0.74
<b>Numerical schemes</b>	
Order in time	1st order explicit
Advection terms	
– momentum equation	Upstream
– dispersion equation	MPDATA scheme (Smolarkiewicz and Grabowski, 1989)
Diffusive terms	ADI (Alternating Direction Implicit) method
<b>Computational grid</b>	
Grid type	Arakawa-C non-equidistant Cartesian grid (staggered grid), with buildings and topography blocked out from the grid
Variable definition	$u$ , $v$ , $w$ defined at the centre of the corresponding face of the cell, scalar quantities defined at the centre of the cell
<b>Boundary conditions</b>	
Flow variables	
Inlet velocity profile	Logarithmic profile with roughness length $z_0$ fitted to reference height $H_{ref}$ and velocity $u_{ref}$
Inlet turbulence profile	Generated from the assumption of equilibrium boundary layer
Ground & building surfaces	No-slip (with wall function)
Top boundary	Constant values of $u$ , $v$ , $w$ , $k$ , $\varepsilon$ taken from the top of the inlet profile
Lateral boundaries	No-flux
Outflow boundary	No-flux with pressure correction to ensure overall mass conservation
Dispersion variables	
Inflow boundary	$c = 0$
Lateral and outflow boundaries	No-flux
Source cells	Volume source strength $Q$ with optional vertical momentum $w$ prescribed
Vegetation cells	Leaf drag coefficient $c_D = 0.2$ and $LAD$ (leaf area density) prescribed

The computational domains and grids were created following the Best Practice Guideline of Franke *et al.* (2007) using an in-house preprocessor. In each junction, close investigation areas of  $1.5 \text{ km} \times 1.5 \text{ km}$  were defined (see black rectangles in Fig. 1), for which grids of uniform horizontal resolution were generated. Inflow and outflow zones of sufficient length were attached to these to prepare correct inflow conditions in the investigated area (Fig. 4).

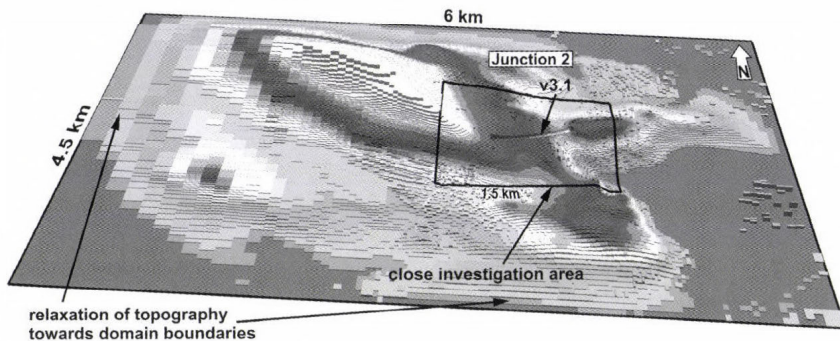


Fig. 4. View of the MISKAM model domain of Junction 2 showing the non-uniform grid with the highest grid resolution around the two tunnel portals and the relaxation of topography at the boundaries.

The domain height was 2 km to ensure a low blockage ratio of 3%. Terrain height sunk to zero at the boundaries. The cell number of each grid was above 5 million. The simulation time on a 3 GHz Intel Core2 computer was about one week for a case. Further details of the simulations are given in *Table 4*.

Table 4. Grid and simulation details. In each junction, simulations were run for every wind direction and every source, resulting in a high number of simulations

	Unit	Junction 1	Junction 2	Junction 3
No. of grid cells	–	246 × 255	206 × 321	252 × 273
– vertical direction	–	97	77	97
Highest resolution	m	5 × 7.5		
– vertical direction	m	1.5		
Max. cell growth ratio	–	1.2		
Cell number	million	5.526	5.244	5.225
Wind directions investigated	–	N, SE, S, WSW, W, WNW, NW	N, NE, S, W, NW	N, SE, S, W, NW
Leaf area density	m <sup>2</sup> m <sup>-3</sup>	0.5 (in forest areas)		
Vent. stack vertical velocity	m s <sup>-1</sup>	6		
No. of dispersion simulations	–	107	92	52

### 3.2. Source treatment and simulations on a simplified tunnel model

Traffic pollutants released in a one-directional motorway tunnel are exhausted usually through the forward tunnel portal in a low-speed jet. In the MISKAM simulations, as it is not allowed for the user to prescribe horizontal momentum, this jet was replaced by a point source without momentum located in a certain

distance in front of the tunnel portal. To justify the above simplification, several numerical simulations were performed using the more flexible FLUENT code. The FLUENT 6.3 simulations used a simple tunnel portal geometry shown in Fig. 5 on the left.

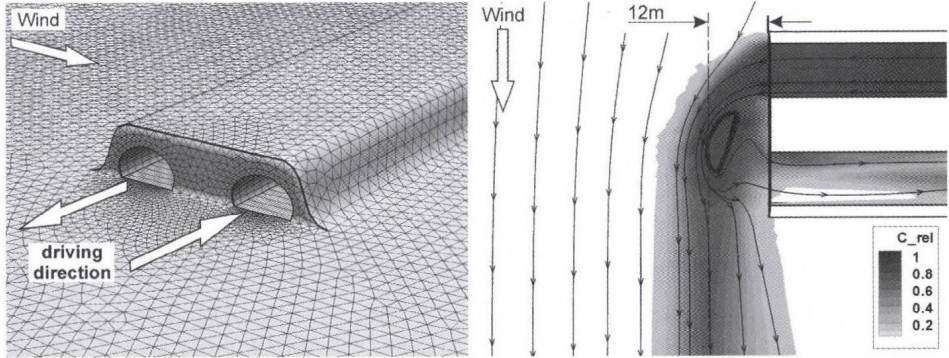


Fig. 5. Left: simplified tunnel geometry and grid for the preliminary investigation of flow around the portals using FLUENT with tunnel cross-section of 12 m  $\times$  6.5 m, portal height 10 m, tunnel axis distance 24 m. Right: simulation results in a horizontal cross-section at 3 m height with streamtraces and relative concentration contours. Tunnel outflow velocity is 3 m s<sup>-1</sup>. Note the plume displacement of 12 m as well as the unfavorable suction of polluted air into the other tunnel.

First, the flow conditions inside a one-directional tunnel were investigated. Vehicle traffic moving with 80 km h<sup>-1</sup> was substituted in the simulation by momentum sources determined from drag coefficient  $c_D$ , vehicle cross-section  $A_{veh}$ , and the traffic density. The piston effect of a single vehicle can be expressed according the Swiss standard (ASTRA, 2004) by the pressure difference caused by it:

$$0.5 \rho (u_{veh} - u_{air})^2 c_D A_{veh} A_{tunnel}^{-1}. \quad (1)$$

In the FLUENT simulation utilizing this assumption, at maximal traffic density and without the use of a longitudinal tunnel ventilation system, an average tunnel air velocity  $u_{air}$  of 1.8 m s<sup>-1</sup> was developed.

Following this simulation, the tunnel portal model was placed in an atmospheric boundary layer flow to observe the pollutant plume's displacement at several wind directions. The simulations utilized the RANS approach with standard  $k-\epsilon$  turbulence closure on a mesh consisting of 800,000 tetrahedral and polyhedral cells. External flow velocity was 3 m s<sup>-1</sup> at 100 m height, tunnel air velocity was also 3 m s<sup>-1</sup>. Simulation at cross-flow wind showed a plume displacement of about 12 m from the tunnel portal (Fig. 5, right). Remarkably, the other one-directional tunnel is sucking in a part of polluted air released by

the other tunnel. (This short-circuit is unfavorable and can be prevented by increasing the distance between the two portals, e.g., shifting the two portals away in longitudinal direction, or by building a separation wall between them.)

Based on the results mentioned, the pollutants sources in the MISKAM simulations were placed 10 m in front of the portals. To account for the high concentration gradients, the grid density in the portal region was increased to  $5\text{ m} \times 7.5\text{ m} \times 1.5\text{ m}$ .

### 3.3. Wind tunnel testing

Wind tunnel testing proved to be a sufficient physical modeling method of the real scale dispersion processes in the past (Cermak, 1984; Plate, 1999), and thus, it can serve as reference data source for the current CFD simulations.

As in most environmental wind tunnels, only the modeling of neutral conditions was possible in the current wind tunnel test campaign. The atmospheric boundary layer profile was modeled by a horizontal grid, spikes, and roughness elements (Fig. 6) and was checked by two-component hot-wire measurements (cross-wire sensor with DISA 55M CTA bridges). The profile measurement results are shown in Fig. 7.

The wind tunnel measurements were carried out on a modular 1:1000 scale model with a total area of  $28.5\text{ m}^2$  (largest extents about  $8\text{ m} \times 5\text{ m}$ ), resolving the topography, buildings, vegetation, and pollutant sources of the surroundings. From the modules, models of the three junctions at various wind directions and route alternatives could be constructed and investigated separately in the wind tunnel. The elevation at the model boundaries was relaxed to zero level using artificial slopes.

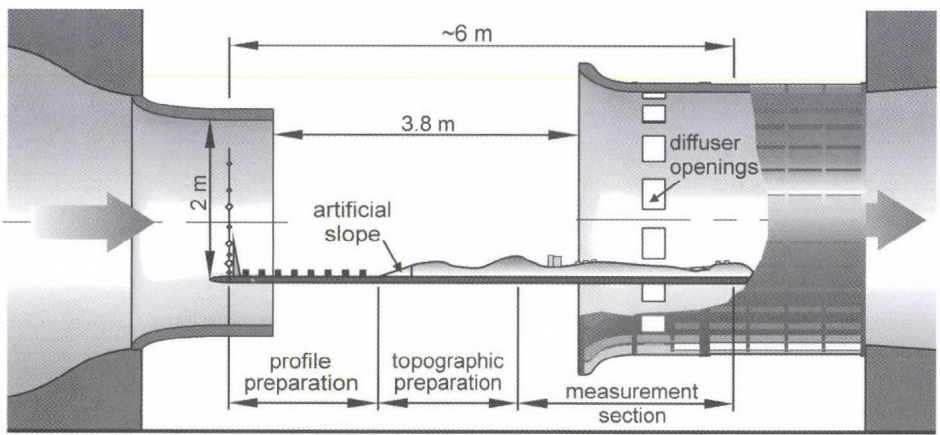


Fig. 6. Vertical cross section view of the model arranged in the test section of the Göttingen-type wind tunnel.

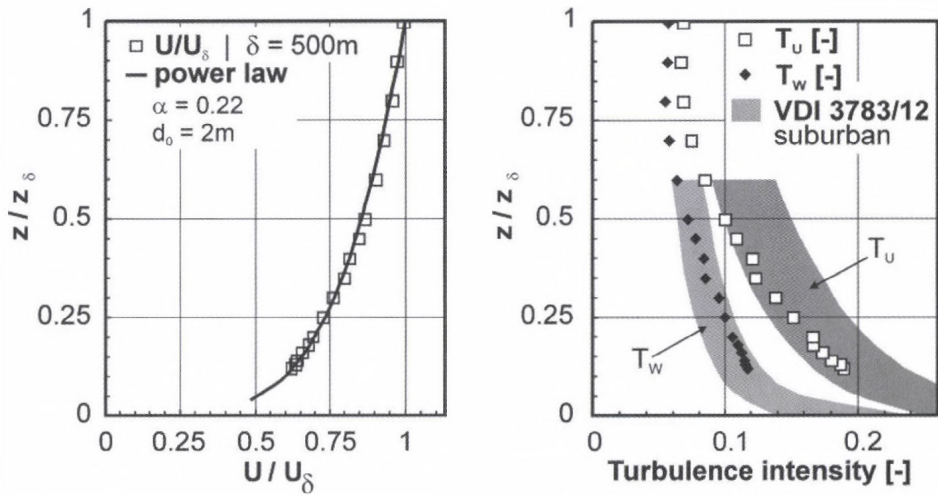


Fig. 7. Inlet profiles of mean velocity and turbulence measured by two-component CTA. The reference height  $\delta$  is 500 m at full scale.

Fifty sampling points were distributed on the model (see black dots in Fig. 1) near tunnel portals and road sections, and inside inhabited areas and locations of specific care, for example at school buildings. Unfortunately, detailed concentration field mapping along lines or arcs could not be fitted into the four-month timeframe of the wind tunnel tests.

Methane was used as tracer gas, and source strengths  $Q_i$  were controlled using digital mass flow controllers. Road segments were treated as line sources, and therefore, tracer was released from underfloor source units lying in line with the model's surface. The construction ensured homogeneous exhaust along the road following the line source construction principle of Meroney *et al.* (1996). The pollutants produced in the road tunnels were supposed to leave the tunnel at the portal in the direction of traffic and were modeled accordingly as point sources with a small horizontal momentum. Air samples were collected simultaneously by an automatic 24-channel sampling system built from stepmotor-driven sampling cylinders and magnetic valves, and they were analyzed by a flame ionization detector (FID) afterwards. The system was calibrated with gas samples of known concentration. Repeatability tests of the whole measurement system gave an average relative uncertainty of 9% over a range of  $10^2$ – $10^4$  ppm  $\text{CH}_4$  concentration.

To a further check of the concentration measurement system, a simple test case known from the literature was measured, consisting of a line source placed into a crosswind boundary layer flow. The measured concentration downwind the source was inside the limits given by the VDI guideline 3783/12 (VDI, 2004). This test also proved that the use of methane as tracer

gas, regardless of its different density is proper, if testing wind speed is high enough, and thus, buoyancy effects are suppressed.

Afterwards, the Reynolds number dependency of concentration results was checked on the terrain model by repeating concentration measurements at different wind speeds. It was found that above the mean flow velocity  $u_{ref}$  of  $3 \text{ m s}^{-1}$  (at  $H_{ref} = 50 \text{ mm}$  height), normalized concentrations

$$c^+ = cu_{ref} H_{ref}^2 Q^{-1} \quad (2)$$

remain constant, thus independent of the Reynolds number. In the final tests,  $u_{ref}$  was set to  $4.5 \text{ m s}^{-1}$ .

The horizontal momentum of polluted air inlet at the tunnel portals was determined by keeping the ratio of tunnel air momentum and incident wind momentum ( $\rho_Q u_Q^2 \rho_{air}^{-1} u_{ref}^{-2}$ ) constant in both full and model scale. This gave  $3 \text{ m s}^{-1}$  model scale tunnel air velocity for  $2.3 \text{ m s}^{-1}$  full scale tunnel air velocity.

In total, 126 sets of concentration measurements, each consisting of 10 to 22 sampling points, were performed. The wind tunnel's background concentration and calibration gas were sampled in each set. The influence of each individual source  $i$  (road segment, tunnel portal) on the concentration distribution was measured separately at each wind direction to determine the contribution of the different sources to the total concentration.

Full scale concentrations  $c_{FS}$  [ $\text{g m}^{-3}$ ] of  $\text{NO}_x$ ,  $\text{PM}_{10}$ , and  $\text{CO}$  at a specific wind direction were determined based on the similarity of normalized concentrations  $c_i^+$  in both model and full scale by taking into consideration the real traffic emissions  $Q_{i,FS}$  [ $\text{g s}^{-1}$ ] of the individual sources, and finally by adding the background concentrations  $c_{bg}$  from *Table 1*, as

$$c_{FS} = c_{hg} + u_{ref\,FS}^{-1} H_{ref\,FS}^{-2} \sum c_i^+ Q_{i,FS} \quad (3)$$

#### 4. Results and discussion

As the ratio of the emitted pollutant mass flow and the corresponding concentration limit value is far the highest for  $\text{NO}_x$  (among the pollutants mentioned above), the distribution maps of  $\text{NO}_x$  will be analyzed further in Section 4. Although the photochemical reactions, which lead to the formation of more dangerous  $\text{NO}_2$  and  $\text{O}_3$ , were not included in this study, annual mean values of  $\text{NO}_x$  can be correlated to those of  $\text{NO}_2$  based on long-term station observations, and thus, a prediction can be given also for annual  $\text{NO}_2$  concentrations.

#### 4.1. General observations

The flow field at the three junctions could be analyzed using velocity profiles, streamlines, and contour plots of the CFD results. An example is shown in Fig. 8.

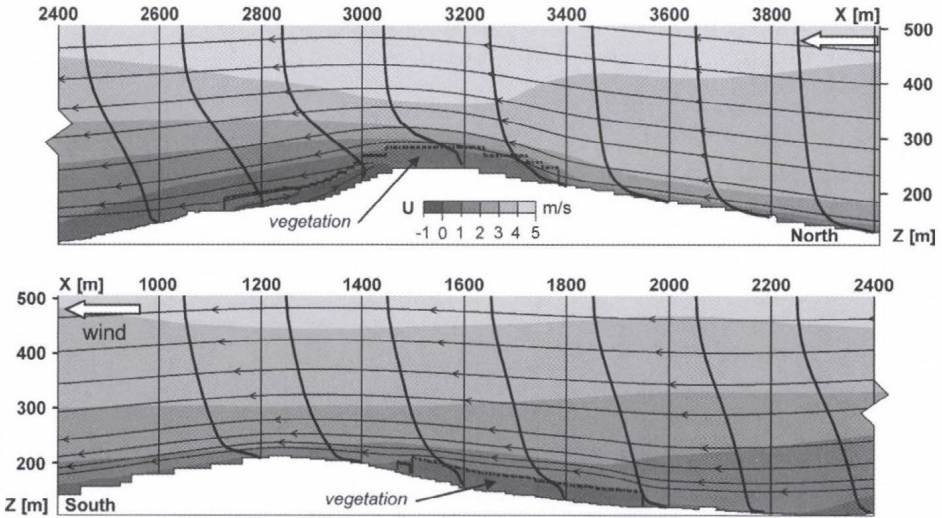


Fig. 8. North-south cross section of the flow over hills of Junction 3 for a north wind with streamlines and vertical profiles of the  $U$  velocity component. Boundaries of deciduous forests are shown with dotted lines. Note the speedup above the hills and the small separation region and backward flow on the lee side of the northern hill.

The most important factors affecting the flow field are listed in the following:

- (1) The influence of topography ranges from slight changes of wind direction and wind speed to the full three-dimensionality of flow. Speed-up could be observed above the hill ridges. Separation zones can develop behind steeper hills (see at Junction 3 in Fig. 8 and later in Fig. 12).
- (2) Building effects are only worth mentioning near the 10–15 storey block buildings of Junction 1, while at the other junctions detached houses of suburban towns act rather like roughness elements because the grid resolution is not sufficient to resolve the small flow structures around them (buildings accommodate only a few grid cells).
- (3) Vegetation zones are slowing down the flow and at the same time shifting the main flow upwards (Fig. 8).

Based on both wind tunnel measurements and CFD simulations we can draw the following conclusions about the concentration field:

- (1) In the case of road segments running on the surface, concentration limits are exceeded only in a narrow strip of about 50 m along the road.
- (2) On the other hand, the emission from tunnel portals can cause plumes of more than 100 m length above the hourly concentration limit ( $200 \mu\text{g m}^{-3}$ ), reaching even populated areas (Fig. 9).
- (3) The direction of the tunnel plumes is slightly modified by the topography; see, for example, at Junction 2 with a northeast wind direction (Fig. 9).

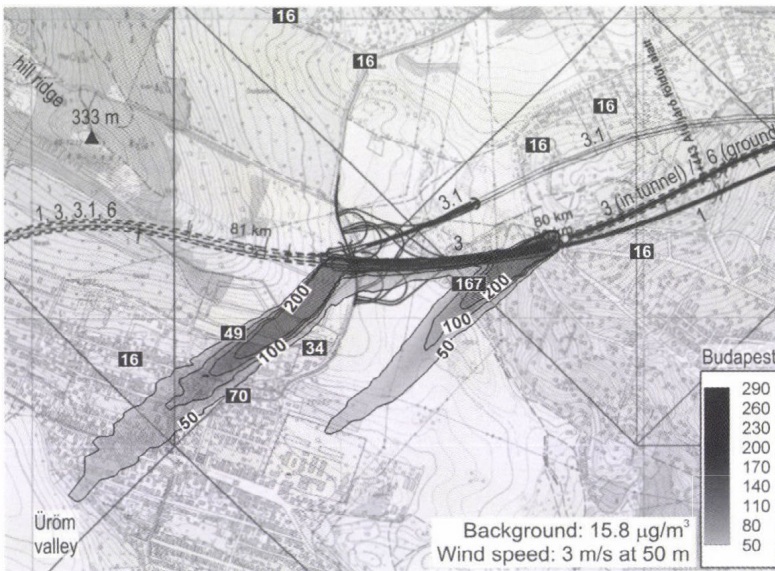


Fig. 9. Concentrations of NO<sub>x</sub> [ $\mu\text{g m}^{-3}$ ] at Junction 2, 3 m above the surface with a NE wind direction and a wind velocity of  $3 \text{ m s}^{-1}$ , in the case of route alternative 3 without ventilation stacks operating. White numbers: concentrations from wind tunnel measurement, contour plot; bold black numbers: simulation results. (The other route alternatives are drawn in the figure but are not in operation.)

- (4) In separation zones, upwind dispersion is possible due to the recirculating flow.
- (5) Pollution coming from viaducts has an almost negligible footprint at the surface due to the higher wind speed and the higher altitude of release (Fig. 12).

#### 4.2. Modeling of ventilation stacks

To account for the most prominent observation made in Section 4.1, the large pollutant plumes released from tunnel portals, which threaten the air quality of nearby settlements at low wind speeds and rush-hour traffic density, the design of the tunnel ventilation system was extended by ventilation stacks. These will be put into operation if the above mentioned conditions are met and will then exhaust the polluted tunnel air at more than 20 m height above ground. In this way, large concentrations at ground level in the vicinity of the portals can be avoided. In Fig. 10, the revised ventilation concept can be seen. The stacks are located near the tunnel portals.

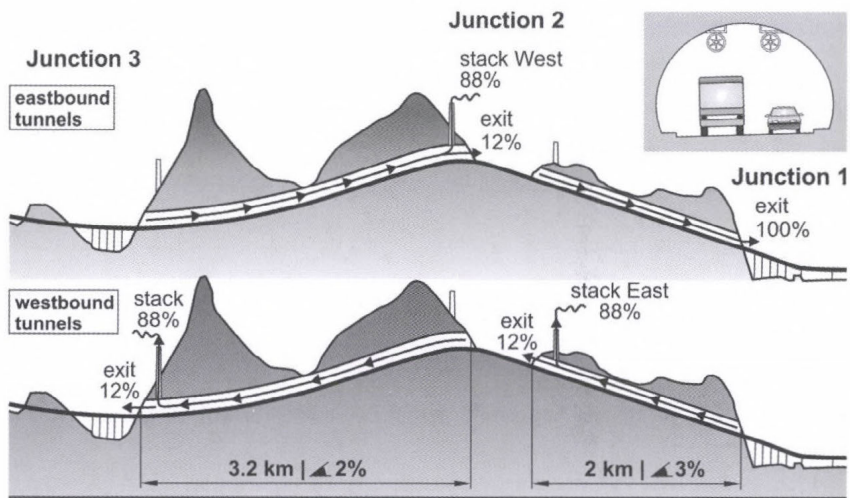


Fig. 10. Tunnel ventilation concept with stack locations. The ventilation of the eastbound and westbound one-directional tunnels is independent, and thus, shown separately. Elevation is scaled approximately by 10. Upper right corner: cross-section of a one-directional tunnel with axial ventilation fans.

The concept was checked in further MISKAM simulations. Stack heights range between 20–25 m, and vertical outflow velocity of the exhaust was set to  $6 \text{ m s}^{-1}$ . Based on the simulation results, if external wind speed is  $3 \text{ m s}^{-1}$  at 50 m height, at least 88% of the polluted tunnel air has to be exhausted through the stacks to avoid concentration limit exceedance near the portals. When comparing Figs. 9 and 11, the decrease of the area with concentrations above the hourly concentration limit ( $200 \mu\text{g m}^{-3}$ ) is obvious, while footprints of stack plumes on the surface are well below the limit. The plume of the west stack is also modified by the topography, more specifically by the NW oriented nearby hill ridge.

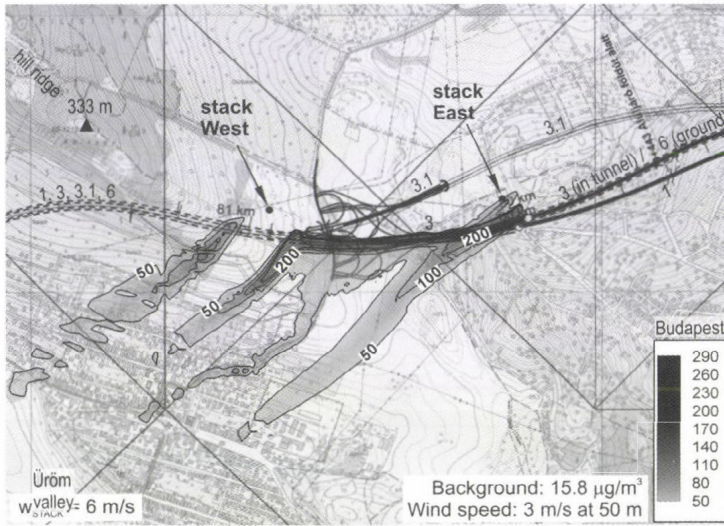


Fig. 11. Concentrations of  $\text{NO}_x$  [ $\mu\text{g m}^{-3}$ ] at Junction 2, 3 m above the surface with a NE wind direction and a wind velocity of  $3 \text{ m s}^{-1}$ , in case of route variant 3. Ventilation stacks are in operation, vertical West stack velocity is  $6 \text{ m s}^{-1}$ . Compare this figure to Fig. 9.

Detailed analysis of the flow and concentration fields showed that plume axes run at about 40 m height above ground (see Fig. 12). Surface concentrations below the stack plumes are significantly smaller than those at the tunnel portals, although they exhaust seven times more pollutant. Fig. 12 also demonstrates the ability of CFD models in resolving three-dimensional flows above complex terrain.

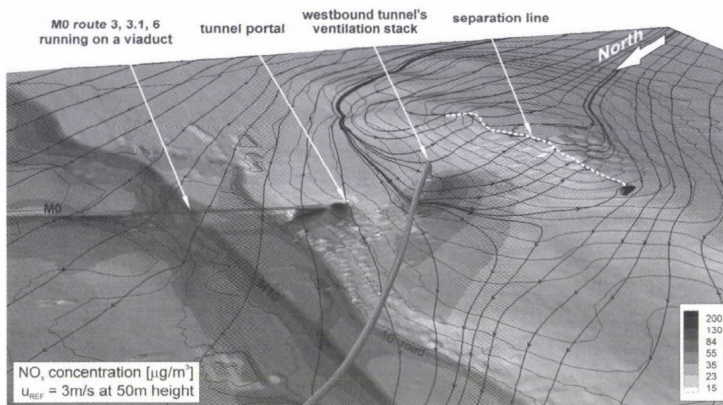


Fig. 12. MISKAM simulation of Junction 3 with a north wind direction and  $3 \text{ m s}^{-1}$  wind velocity at 50 m height. Tunnel ventilation stacks are in operation. Streamlines (thicker black lines) at 6 m height above ground show a separation behind the northern hill and the modification of the ventilation stack's plume centerline (dark grey rod). Thin black lines: topographic level curves; surface color: concentration (logarithmic scale).

To decrease the power consumption of the ventilation system, it is proposed to operate it only at lower wind speeds with full power. In case of higher wind speeds pollutant dilution is faster, thus, a larger portion of polluted tunnel air can be released through the portal without causing limit exceedances. Similarly, in periods with low traffic, further ventilation energy can be saved.

### 4.3. Comparison of experimental and numerical results

The comparison of experimental and numerical concentrations (in total 499 non-zero value pairs) in the left part of *Fig. 13*, shows acceptable agreement in general. However, some larger deviations were observed, which are partly due to limitations of the modeling methods. The deviations were analyzed point by point and the most typical causes found are listed in the following.

- (1) Known limitations of  $k-\varepsilon$  models: *Castro et al.* (2003) concluded from their Askervein Hill simulations that speed-up above the hilltop is underpredicted. Furthermore, being originally a steady-state simulation, the time-dependency, especially in recirculating zones, is not captured by the models. In our case this is not problematic, as we are interested in mean values only. Concerning the dispersion results, according to the validation tests in *Eichhorn and Balczó* (2008), MISKAM 5 predicts thinner and longer pollutant plumes from point sources than those measured in wind tunnel.
- (2) Minor geometrical differences between the wind tunnel and numerical model: Near the line sources very large concentration gradients can occur, meaning that even a small displacement of a sampling point in the physical and numerical model could cause errors of above 50%.
- (3) Different initial dilutions of the pollutant sources can again affect near-source measurements (passive scalar released in source grid cells in CFD vs. tracer gas released along a line from the surface of the wind tunnel model).
- (4) Different vegetation modeling: In the numerical model, the parameter expressing the vegetation density, known as leaf area density (*LAD*), was 0.5, an average value for deciduous forests taken from the literature. This corresponds according to *Balczó et al.* (2009) and *Gromke and Ruck* (2009) at the model scale of 1:1000 to a crown porosity of about 96–97% in the wind tunnel measurement. In the physical model, however, artificial grass of lower porosity was used for forest modeling (approximately 94%), leading to smaller wind velocities and higher displacement thicknesses in vegetation covered areas.
- (5) Coarse numerical grid resolution: Because of the staggered grid (without terrain-following coordinate system), slopes, especially in the

inflow and outflow zones, have higher roughness, influencing the near-surface balance of  $k$  and, in consequence, the dispersion.

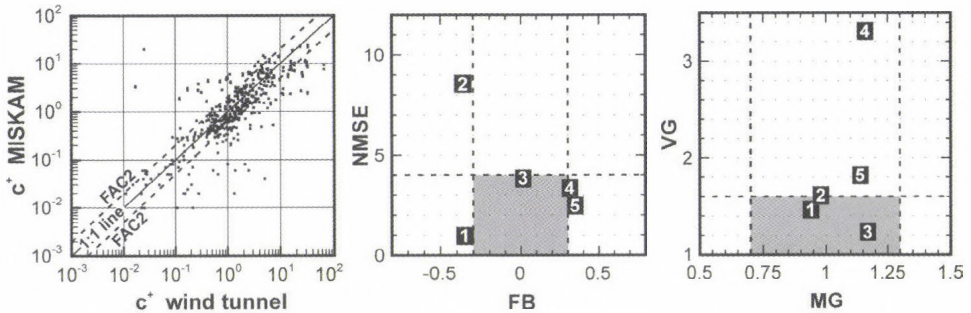


Fig. 13. Left: logarithmic scatter plot of measured and simulated concentrations  $c^+$ . The plot contains all non-zero value pairs which were measured respectively simulated in the 50 sampling point locations (see Fig. 1), in total about 499 points. Dashed lines show 50% and 200% of the measurements. Points between the two lines represent predictions within a factor of two of observations (FAC2).

Middle and right: Plots of linear and logarithmic validation metrics of normalized concentration  $c^+$  from different MISKAM simulations. Cases compared: (1) perpendicular flow in a street canyon with vegetation of *Balczó et al.* (2009); (2) simulation of the Mock Urban Setting Test (*Eichhorn and Balczó*, 2008) using MISKAM 5.02; (3) simulation of the Mock Urban Setting Test using MISKAM 6; (4) present simulation, all non-zero values; and (5) present simulation, all values  $> 0.5$ . The model acceptance range is marked grey.

#### 4.4. Validation metrics

To quantify the extent of deviations between results from numerical and physical modeling, statistic metrics after *Chang and Hanna* (2004) were calculated. The values can be seen in *Table 5*; many of them are within or at least close to the limits of acceptance proposed for state-of-the-art models. The larger positive value of the fractional bias (FB) shows that wind tunnel results are moderately underestimated by the simulation at large concentrations. However, this is not the case at medium and small concentrations, because geometric mean bias (MG), which is not dominated by the large concentration values, is very good. The worse value of geometric variance (VG) while at the same time the normal mean square error (NMSE) is clearly inside the limit, can be explained by the scattering of small concentration values due to the measurement error. After filtering  $c^+$  values smaller than 0.5, metrics of the remaining 336 data points improve significantly.

In *Fig. 13*, middle and right, one can see the metrics of concentrations from already published validation studies using the MISKAM code. Point 1 of the figure refers to a simulation in a street canyon with a building height to street width ratio of 1:1 and a street length to width ratio of 10:1, at perpendicular flow direction and with tree planting inside the canyon, described in detail in *Balczó et al.* (2009).

Table 5. Calculated statistic metrics for concentration (after Chang and Hanna, 2004)

Validation metric	Abbreviation	Limit	All non-zero values	Values <0.5 filtered	Classification
Correlation coefficient	R	0.8	0.608	0.722	Fair
Fractional bias	FB	$\pm 0.3$	0.313	0.347	Nearly good
Normalized mean square error	NMSE	0–4	3.35	2.47	Good
Geometric mean bias	MG	0.7–1.3	1.16	1.14	Good
Geometric variance	VG	0–1.6	3.31	1.82	Nearly good
Fraction of predictions within a factor of two of observations	FAC2	0.5	0.655	0.723	Good

Points 2 and 3 show test results from the Mock Urban Setting Test (Eichhorn and Balczó, 2008). The Mock Urban Setting Test (MUST) was a full-scale measurement campaign on a rectangular grid-like arrangement of 120 standard shipping containers in Utah as described by Yee and Biltoft (2004), wind tunnel tests of the same arrangement were carried out by Leidl *et al.*, (2007). MISKAM was used to simulate dispersion from a source between the containers at slanted  $-45^\circ$  flow. Tracer dispersion data was compared in 256 data points. This test case was run with the current and future MISKAM versions 5.02 (point 2 in Fig. 13) and 6 (point 3).

Point 4 refers to all non-zero  $c^+$  values of the current study, point 5 to all  $c^+$  values larger than 0.5. A comparison of these data with those mentioned above indicates clearly, that in case of practical applications and complex geometries like this investigation, the code performs less accurately, but an acceptable level of accuracy can be still achieved.

## 5. Conclusions

The current paper gives an overview about a larger microscale CFD and wind tunnel test campaign performed in a suburban area of complex terrain in the north of Budapest. Emission determination, mesoscale influences on local wind statistics, and background concentrations were also discussed.

The CFD simulations and accompanying wind tunnel measurements showed that open road sections cause limit exceedance along a narrow strip of some 50 m along the investigated motorway routes, while pollutant plumes from the tunnel portals can spread more hundred meters away. They also provided information on the necessary changes of the tunnel ventilation system. The effect of the proposed ventilation stacks on air quality was estimated by CFD. The  $\text{NO}_x$  concentration maps delivered by this investigation helped the authorities to select the final route, which is a slightly modified version of route alternative 3.1.

Numerical simulation using the RANS approach with  $k-\varepsilon$  closure proved to be a reliable tool to understand and predict flow and dispersion phenomena, resolving all main features of the three-dimensional flow, but deviations from the

experimental results signal that the use of wind tunnel or on-site reference data is still useful. These can provide valuable information for the evaluation and assessment of simulation results, as shown here with the application of statistic metrics.

**Acknowledgements**—Thanks are due to the Hungarian Meteorological Service, to department staff members *Tamás Réger*, *Viktor Szente*, *Zoltán Szucsán*, *Gábor Kalmár*, and finally to all participating students for their valuable contributions. The investigations presented in this paper were financed by the National Infrastructure Development Corporation of Hungary. This work is connected to the scientific program of the “Development of quality-oriented and harmonized R+D+I strategy and functional model at BME” project, which is supported by the New Széchenyi Plan (grant agreement no.: TAMOP-4.2.1/B-09/1/KMR-2010-0002). *Miklós Balogh*'s participation was also financed by his current project, which is supported by the European Union and co-financed by the European Social Fund (grant agreement no. TAMOP 4.2.1./B-09/1/KMR-2010-0003).

## References

- ASTRA, 2004: *Guideline for the ventilation of road tunnels*. ASTRA Bundesamt für Strassen/Swiss Federal Roads Office FEDRO, Bern.
- Ayotte, K., Hughes, D., 2004: Observations of boundary-layer wind-tunnel flow over isolated ridges of varying steepness and roughness. *Bound.-Lay. Meteorol.* 112, 525-556.
- Balczó, M., Gromke, C., Ruck, B., 2009: Numerical modeling of flow and pollutant dispersion in street canyons with tree planting. *Meteorol. Z.* 18, 197-206.
- Belcher, S.E., Hunt, J.C.R., 1998: Turbulent flow over hills and waves. *Annu. Rev. Fluid. Mech.* 30, 507-538.
- Berkowicz, R., 2000: A simple model for urban background pollution. *Environ. Monit. Assess.* 65, 259-267.
- Bettelini, M., Brandt, R., Riess, I., 2001: Environmental aspects of tunnel ventilation. *AITES-ITA 2001 World Tunnel Congress*, Milano, June 10-13, 2001.
- Bowen, A. J., 2003: Modelling of strong wind flows over complex terrain at small geometric scales. *J Wind. Eng. Ind. Aerod.* 91, 1859-1871.
- Brodeur, P., Masson, C., 2006: Numerical simulations of wind distributions over very complex terrain. *44th AIAA Aerospace Sciences Meeting and Exhibit*, 9–12 January 2006, Reno, Nevada AIAA 2006-1362.
- Castro, F.A., Palma, J. M. L. M., Silva Lopes, A., 2003: Simulation of the Askervein flow. Part 1: Reynolds averaged Navier-Stokes equations ( $k-\epsilon$  turbulence model). *Bound.-Lay. Meteorol* 107, 501-530.
- Cermak, J. E. 1984: Physical modelling of flow and dispersion over complex terrain. *Bound.-Lay. Meteorol.* 30, 261-292.
- Chang, J.C., Hanna, S. R., 2004: Air quality model performance evaluation. *Meteorol. Atmos. Phys.* 87, 167-196.
- Colberg, C. A., Tona, B., Stahel, W. A., Meier, M., Staehelin, J., 2005: Comparison of a road traffic emission model (HBEFA) with emissions derived from measurements in the Gubrist road tunnel, Switzerland. *Atmos. Environ.* 39, 4703-4714.
- Contini, D., Procino, L., Massini, M., Manfreda, G., 2003: Ground-level diffusion of pollutant emitted at the portal of a road tunnel model. *Proceedings of PHYSMOD 2003 International Workshop on Physical Modelling of Flow and Dispersion Phenomena*, Prato, Italy, 244-251.
- Cremades, L., 2000: Estimating the background air concentration excluding the contribution of an individual source. *Environ. Model. Assess.* 5, 119-124.
- Dixon, N., Tomlin, A., 2007: A Lagrangian stochastic model for predicting concentration fluctuations in urban areas. *Atmos. Environ.* 41, 8114-8127.
- Donnelly, R., Lyons, T., Flassak, T., 2009: Evaluation of results of a numerical simulation of dispersion in an idealised urban area for emergency response modelling. *Atmos. Environ.* 43, 4416-4423.

- Eichhorn, J., 2008: MISKAM Manual for version 5. giese-eichhorn environmental meteorological software, Wackernheim, Germany
- Eichhorn, J., Balczó, M., 2008: Flow and dispersal simulations of the Mock Urban Setting Test. The 12th Int. Conf. on Harmonization within Atmospheric Dispersion Modelling for Regulatory Purposes (HARMO12), Cavtat, Croatia, October 6-9, 2008. *Croatian Meteorol. J.* 43, 67-72.
- Eichhorn, J., Kniffka, A., 2010: The numerical flow model MISKAM: State of development and evaluation of the basic version. *Meteorol. Z.* 19, 81-90.
- Franke, J., Hellsten, A., Schlüenzen, H., Carissimo, B., 2007: *Best practice guideline for the CFD simulation of flows in the urban environment*. COST Office Brussels ISBN: 3-00-018312-4.
- Goricsán, I., Balczó, M., Rékert, T., Suda, J. M., 2004: Comparison of wind tunnel measurement and numerical simulation of dispersion of pollutants in urban environment. *International Conference on Urban Wind Engineering and Building Aerodynamics, von Karman Institute, Rhode-Saint-Genése, Belgium, May 5-7, 2004* D.6.1-D.6.10.
- Goricsán, I., Balczó, M., Czáder, K., Rákai, A., Tonkó, C., 2011: Simulation of flow in an idealised city using various CFD codes. *Int. J. Environ. Pollut.* 44, 359-367.
- Gromke, C., Ruck, B., 2009: On the impact of trees on dispersion processes of traffic emissions in street canyons. *Bound.-Lay. Meteorol.* 131, 19-34.
- Holmes, N., Morawska, L., 2006: A review of dispersion modelling and its application to the dispersion of particles: An overview of different dispersion models available. *Atmos. Environ.* 40, 5902-5928.
- Infras, 2004: *The Handbook of Emission Factors for Road Transport (HBEFA 2.1)*. www.hbefa.net, CD-ROM database.
- Jones, A. M., Yin, J., Harrison, R. M. 2008: The weekday-weekend difference and the estimation of the non-vehicle contributions to the urban increment of airborne particulate matter. *Atmos. Environ.* 42, 4467-4479.
- Kaimal, J., Finnigan, J., 1994: *Atmospheric Boundary Layer Flows*. Oxford University Press.
- Kato, M., Launder, B., 1993: The modelling of turbulent flow around stationary and vibrating square cylinders. *Ninth Symp. on Turbulent Shear Flows*, Kyoto, Japan, August 1993, 10.4.1-10.4.6.
- Ketzel, M., Berkowicz, R., Lohmeyer, A., 2000: Comparison of numerical street dispersion models with results from wind tunnel and field measurements. *Environ. Monit. Assess.* 65, 363-370.
- Ketzel, M., Louka, P., Sahm, P., Guilloteau, E., Sini, J. F., Moussiopoulos, N., 2002: Intercomparison of numerical urban dispersion models - Part II: Street canyon in Hannover, Germany. *Water Air Soil Pollution: Focus* 2, 603-613.
- Ketzel, M., Omstedt, G., Johansson, C., Düring, I., Pohjola, M., Oettl, D., Gidhagen, L., Wahlin, P., Lohmeyer, A., Haakana, M., Berkowicz, R., 2007: Estimation and validation of PM<sub>2.5</sub>/PM<sub>10</sub> exhaust and non-exhaust emission factors for practical street pollution modelling. *Atmos. Environ.* 41, 9370-9385.
- Kim, H. G., Patel, V. C., 2000: Test of turbulence models for wind flow over terrain with separation and recirculation. *Bound.-Lay. Meteorol.* 94, 5-21.
- Kristóf, G., Rácz, N., Balogh, M., 2009: Adaptation of pressure based CFD solvers for mesoscale atmospheric problems. *Bound.-Lay. Meteorol.* 131, 85-103.
- Leitl, B., Bezpalcova, K., Harms, F., 2007: Wind tunnel modelling of the MUST experiment. *The 11th International Conference on Harmonisation within Atmospheric Dispersion Modelling for Regulatory Purposes (HARMO11)*. Cambridge, UK, July 2-5. 435-439.
- Liu, H., Zhang, B., Sang, J., Cheng, A. Y. S., 2001: A laboratory simulation of plume dispersion in stratified atmospheres over complex terrain. *J. Wind Eng. Ind. Aerod.* 89, 1-15.
- Lohmeyer, A., Mueller, W. J., Baechlin, W., 2002: A comparison of street canyon concentration predictions by different modellers: final results now available from the Podbi-exercise. *Atmos. Environ.* 36, 157-158.
- Longley, I., Kelly, F., 2008: Systematic literature review to address air quality in and around traffic tunnels. *National Health and Medical Research Council*, Commonwealth of Australia.
- López, S. D., 2002: Numerische Modellierung turbulenter Umströmungen von Gebäuden. *PhD thesis, University of Bremen, Germany*.
- McBride, M., Reeves, A., Vanderheyden, M., Lea, C., Zhou, X., 2001: Use of advanced techniques to model the dispersion of chlorine in complex terrain. *Process. Sa. Environ.* 79, 89-102.
- Mensink, C., De Ridder, K., Deutsch, F., Lefebvre, F., Van de Vel, K., 2008: Examples of scale interactions in local, urban, and regional air quality modelling. *Atmos. Res.* 89, 351-357.

- Meroney, R.N., Pavageau, M., Rafailidis, S., Schatzmann, M., 1996: Study of line source characteristics for 2-D physical modelling of pollutant dispersion in street canyons. *J. Wind Eng. Ind. Aerod.* 62, 37-56.
- Moussiopoulos, N., Flassak, T., Knittel, G., 1988: A refined diagnostic wind model. *Environ. Softw.* 3, 85-94.
- Nadel, C., Vanderheyden, M. D., Lepage, M., Davies, A., Wan, P., Ginzburg, H., Schattaneck, G., 1994: Physical modelling of dispersion of a tunnel portal exhaust plume. *8th International Symposium on Aerodynamics & Ventilation of Vehicle Tunnels*, Liverpool, UK.
- Oettl, D., Sturm, P., Almbauer, R., Okamoto, S., Horiuchi, K., 2003: Dispersion from road tunnel portals: comparison of two different modelling approaches. *Atmos. Environ.* 37, 5165-5175.
- Olesen, H., Berkowicz, R., Ketzel, M., Løfstrøm, P., 2009: Validation of OML, AERMOD/PRIME and MISKAM using the Thompson wind-tunnel dataset for simple stack-building configurations. *Bound.-Lay. Meteorol.* 131, 73-83.
- Palma, J., Castro, F., Ribeiro, L., Rodrigues, A., Pinto, A., 2008: Linear and nonlinear models in wind resource assessment and wind turbine micro-siting in complex terrain. *J. Wind. Eng. Ind. Aerod.* 96, 2308-2326.
- Plate, E.J. (ed.), 1982: *Engineering Meteorology*. Elsevier.
- Plate, E. J., 1999: Methods of investigating urban wind fields – physical models. *Atmos. Environ.* 33, 3981-3989.
- Ries, K., Eichhorn, J., 2001: Simulation of effects of vegetation on the dispersion of pollutants in street canyons. *Meteorol. Z.* 10, 229-233.
- Rodrigues, C. A. V., 2005: Analysis of the atmospheric boundary layer flow over mountainous terrain. *Master's thesis, Von Karman Institute*.
- Sahm, P., Louka, P., Ketzel, M., Guilloteau, E., Sini, J. F., 2002: Intercomparison of numerical urban dispersion models – Part I: Street canyon and single building configurations. *Water Air Soil Poll: Focus* 2, 587-601.
- Silva Lopes, A., Palma, J., Castro, F., 2007: Simulation of the Askervein flow. Part 2: Large-eddy simulations. *Bound.-Lay. Meteorol.* 125, 85-108.
- Smolarkiewicz, P., Grabowski, W., 1989: The multidimensional positive definite advection transport algorithm: Nonoscillatory option. *J. Computat. Phys.* 86, 355–375.
- Snyder, W. H., 1990: Fluid modeling applied to atmospheric diffusion in complex terrain. *Atmos. Environ. Part A General Topics.* 24, 2071-2088.
- Stern, R., Yamartino, R. J., 2001: Development and first evaluation of Micro-Calgrid: a 3-D, urban-canopy-scale photochemical model. *Atmos. Environ.* 35, 149-165.
- Taylor, P. A., Teunissen, H. W., 1987: The Askervein Hill project: Overview and background data. *Bound.-Lay. Meteorol.* 39, 15-39.
- Tchepel, O., Borrego, C., 2010: Frequency analysis of air quality time series for traffic related pollutants. *J. Environ. Monitor.* 12, 544-550.
- Tchepel, O., Costa, A., Martins, H., Ferreira, J., Monteiro, A., Miranda, A., Borrego, C., 2010: Determination of background concentrations for air quality models using spectral analysis and filtering of monitoring data. *Atmos. Environ.* 44, 106-114.
- Vardoulakis, S., Fisher, B. E. A., Pericleous, K., Gonzalez-Flesca, N., 2003: Modelling air quality in street canyons: a review. *Atmos. Environ.* 37, 155-182.
- VDI, 2004: VDI 3783, Part 12: Environmental meteorology, Physical modelling of flow and dispersion processes in the atmospheric boundary layer. *Application of Wind Tunnels*. Beuth-Verlag, Germany.
- VDI, 2005: VDI 3783, Part 9: Environmental meteorology. Prognostic microscale windfield models: *Evaluation for Flow Around Buildings and Obstacles*. Beuth-Verlag, Berlin, Germany.
- Walmsley, J. L., Taylor, P. A., 1996: Boundary-layer flow over topography: Impacts of the Askervein study. *Bound.-Lay. Meteorol.* 78, 291-320.
- Wood, N., 2000: Wind flow over complex terrain: A historical perspective and the prospect for large-eddy modelling. *Bound.-Lay. Meteorol.* 96, 11-32.
- Xie, Z. T., Castro, I. P., 2009: Large-eddy simulation for flow and dispersion in urban streets. *Atmos. Environ.* 43, 2174-2185.
- Yee, E., Biltoft, C.A., 2004: Concentration fluctuation measurements in a plume dispersing through a regular array of obstacles. *Bound.-Lay. Meteorol.* 111, 363-415.

# IDŐJÁRÁS

Quarterly Journal of the Hungarian Meteorological Service  
Vol. 115, No. 3, July–September 2011, pp. 205–216

## Application of a new aridity index in Hungarian forestry practice

Ernő Führer<sup>1\*</sup>, László Horváth<sup>2</sup>, Anikó Jagodics<sup>1</sup>, Attila Machon<sup>2,3,4</sup>, and  
Ildikó Szabados<sup>5</sup>

<sup>1</sup>Hungarian Forest Research Institute,  
Papréti 17, 9400 Sopron, Hungary

<sup>2</sup>Hungarian Meteorological Service,  
P.O. Box 39, 1675 Budapest, Hungary; E-mail: horvath.l@met.hu

<sup>3</sup>Center for Environmental Science, Eötvös Loránd University,  
Pázmány P. sétány 1/A, 1117 Budapest, Hungary

<sup>4</sup>Institute of Botany and Ecophysiology, Szent István University,  
Páter K. utca 1, 2103 Gödöllő, Hungary

<sup>5</sup>Hungarian Forest Research Institute,  
Várkerület 30/a, 9600 Sárovar, Hungary

\*Corresponding author; E-mail: fuhrere@erti.hu

(Manuscript received in final form September 7, 2010)

**Abstract**—The ecophysiological observations and the investigations of the weather dependent vital processes of the forests have clearly proved that the water supply in the main growing–main water consumption period (from May to July) as well as in the critical months (July and August) have crucial influence on the growth, vitality, and organic matter production of the forest. Evapotranspiration rate is higher in these periods; and forest ecosystems are most sensitive to the extreme weather conditions this time. Relationship between meteorological parameters and girth-growth of trees (proportional with organic matter production) can be characterized by a simplified forestry aridity index (FAI) for Hungarian conditions:  $FAI = 100 T_{VII-VIII} / (P_{V-VII} + P_{VII-VIII})$ , where  $T_{VII-VIII}$  is the average temperature in July and August (°C),  $P_{V-VII}$  is the precipitation sum (mm) of the period from May to July, and  $P_{VII-VIII}$  is the precipitation sum (mm) of July and August. By this index, the average weather conditions of different climate categories applied in forestry practice can be described. FAI values representative for different species are beech: < 4.75; hornbeam–oak: 4.75–6.00; sessile oak and Turkey oak: 6.00–7.25; forest-steppe: > 7.25.

**Key-words:** forest ecosystem, climate change, productivity, forestry aridity index, forestry climate categories

## **1. Introduction**

The predicted climate change is one of the greatest challenges of the 21st century. In terms of Hungary's climate, warmer and drier weather circumstances will be expected (Láng *et al.*, 2007). Main reasons for the increasing aridity in air and soil would be the decrease and change of seasonal distribution of precipitation as well as the significant increase of air temperature (Führer, 2010; Führer and Járó, 1992; Várallyai, 2002, 2010; Várallyai and Farkas, 2008). All these changes have impact on the productivity of forests influencing not only the structure and species composition of forests but also, indirectly, the organic matter production (Führer, 1995). For these reasons, the investigation of the effect of the possible climate change on forestry practice is important not only from the point of view of change of spreading and vitality of species (Berki *et al.*, 2007, 2009; Mátyás, 2010; Mátyás *et al.*, 2009), and the increase of biotic and abiotic damages (Csóka *et al.*, 2007; Molnár and Lakatos, 2007). The detailed evaluation – from practical production biology approximation –, the climate effect on the growth properties of trees and stands will also be more and more necessary.

Aridity indices frequently used in agrometeorology are summarized in Dunkel (2009). Some of them take into account measured precipitation and temperature characteristics; others apply derived or complicated parameters as potential evapotranspiration, radiation balance, Bowen ratio, etc. The primary aim of this paper is to describe and specify the climatic-ecophysiological relationships and to propose a simple index based on meteorological parameters measured routinely and available all over the country.

## **2. Scientific background**

### **2.1. Seasonal variation of tree growth**

Regarding the annual tree growth, it is important to distinguish between the growing period and the vegetation period. On one hand, vegetation period is the season of the potential growth. In the temperate climate zone, this period ranges between the early and late frost (Linderholm, 2006). On the other hand, the growing period is a term when actual growing (shoot or thickness) or other physiological processes take place such as the formation of bud structure.

In Hungary, trunk thickness and growth-pattern observations have shown that more than 80% of organic material production takes place during the months from May to July in case of various tree species (Szőnyi, 1962; Halupa, 1967; Járó and Tátraaljai, 1984-85; Führer, 1994, 1995; Manninger, 2004). This means that in Hungary the low precipitation and high summer temperatures basically influence the intensity and magnitude of organic material production and they also have an impact on the ratio of spring and autumn tree rings.

Vegetation period out of main growing period and critical months only plays an important role when weather circumstances restrict the physiological processes leading to organic matter production. Such circumstances can be observed during the late May frost period or during April droughts.

## 2.2. Water supply and girth-growth of tree

Apart from the changing temperatures, the organic material production of trees is mostly influenced by the water supply. The growth of trees is restricted by the common water shortage in Hungary during warm months with high potential evapotranspiration rate. The annual water cycle of forests and the related organic matter production is based on three phases of water supply and water consumption, and three life cycles of growth (Führer, 1994, 1995, 2008, 2010; Führer and Járó, 2000; Járó, 1989). When evaluating the precipitation relations in different life-cycles, we have to take into consideration many dominating interdependent factors, both in time and space. These all may either strengthen or balance the effect of extreme weather circumstances.

From the point of view of water cycle, the winter season between November and April is the *storage period*, while regarding the growth it is the *dormant* and *initial growth* phase (Fig. 1). In this phase, most amount of precipitation, somewhat decreased by crown and litter interception infiltrates into the soil, and gradually fills it up. The physiological water consumption is negligible. During winter drought in storage period when precipitation deficit exceeds the 40% compared to regular years, the effect of water deficiency on the growth is difficult to define since transpiration process starts only later.

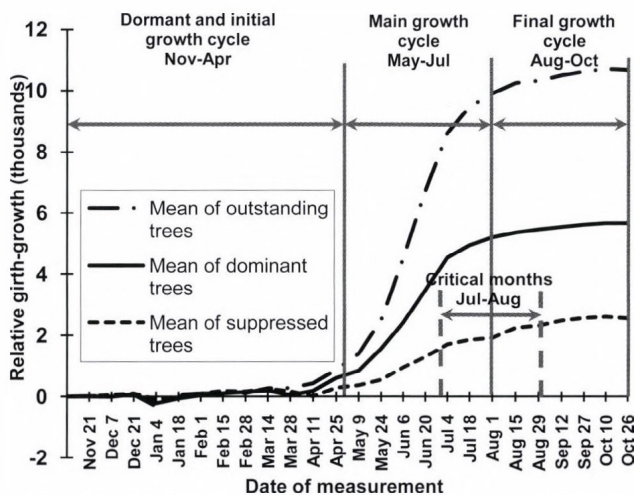


Fig. 1. Average annual girth-growth of a Brennbergbánya beech forest over five years in relative units (1988–1992) (Führer, 1994, 2010).

The period between May and July is called *main utilization phase* or *main growth cycle*. At this time, the precipitation decreased by crown and litter interception gets into only the upper layers of the soil. It is used later – together with the water left from the storage period – mostly for organic matter production and less for other physiological processes. In this cycle, 80% of the increment of the forest occurs, and this is why the extreme weather conditions, namely the effect of deficient precipitation can be more effective. This happens in case of increment decrease, i.e., in case of *partial aridity damage*.

The period between August and October is called *final growth phase*. At this time, the precipitation decreased by interception fills up only the upper layers of the soil recovering the amount of water used up during the main growth cycle; supplying the water demand of physiological processes apart from thickness growing (e.g., cropping). Low precipitation can only result in small increment decrease.

If significant deficit of precipitation in the main and final growth phase (May to October) is accompanied by extremely high temperatures in July and August (critical months), not only increment loss can be observed, but even organic matter production of trees can stop. This may happen because water is used for transpiration to keep the heat balance of trees during extreme circumstances. In extreme cases, the physiological debilitation of trees might result in decrease in trunk number of trees. This so-called total drought damage is mostly characteristic for hybrid poplars and spruces planted at marginal sites in Hungary.

### 3. Results

#### 3.1. Forestry aridity index (FAI)

The principle of the further development of forest management shall be the ecosystem based evaluation of ecological (site) factors of forest management regions. In this system, climate has become a dynamically changing site factor. The ecophysiological observations and the investigation of the physiological processes of forests depending on weather have clearly proved that water supply in the *main growth cycle – main utilization cycle* (May to July) and in the *critical months* (July and August) essentially influences the growth and organic matter production of the forests. In this period, evapotranspiration is most intensive, therefore, forest reacts sensitively to the extreme weather conditions.

To describe the relationship between weather conditions and thickness growth of tree stands, we propose a simplified forestry aridity index applicable for Hungarian conditions. The index is based on meteorological parameters, namely on precipitation and temperature that have been measured extensively all over Hungary with adequate precision, so adaptation and up-scaling for the whole country can be surely done. In the formula, based on monthly temperature

and precipitation averages, theoretical approximations of the aridity index for arable land proposed by Pálfi (2002, 2007, 2010) and the critical water supply index applied for dry forestry regions (Führer and Járó, 2000), appear together. Consequently, the *FAI* index takes into account the ratio of the average temperature of the critical months (July and August) and the precipitation sums in main growth cycle (May to July) plus the precipitation sums in the critical months (from July to August) (Führer, 2008, 2010):

$$FAI = 100 T_{VII-VIII} / (P_{V-VII} + P_{VII-VIII}), \quad (1)$$

where  $T_{VII-VIII}$  is the average temperature in July and August ( $^{\circ}\text{C}$ ),  $P_{V-VII}$  is the precipitation sum (mm) in the period from May to July, and  $P_{VII-VIII}$  is the precipitation sum (mm) in July and August.

In the future, we aim to refine the *FAI* values with developing more exact relationships, i.e., we have to apply some correction factors taking into account: (i) the weather circumstances in dormant season (from November to March), (ii) especially in April, when weather conditions may influence the start of vegetation, (iii) the correct weighting in the formula for the magnitude of the role of different months in organic matter production, (iv) the exposure and slope circumstances.

With the help of the *FAI* we are able to classify the average climate of a spot or even a region from forestry viewpoint. On the other hand, we can characterize the expansion area of certain tree species, and we are also able to measure the impact of extreme weather conditions.

It clearly follows from Eq. (1) that increasing *FAI* means warmer and dryer weather in the main growth cycle and in the critical months and vice versa; decreasing *FAI* indicates cooler and wetter climate.

### 3.2. Relation between *FAI* and tree growth

The adaptability of the forestry aridity index is tested by an experiment (Führer and Jagodics, 2009), where mass of organic material (dendromass) were measured above and below the ground of a beech, hornbeam-English oak, and Turkey oak ecosystem. The age of the investigated ecosystems is 50–70 years; the canopy density is between 95–100%. Stands are located on deep, brown forest soil, and the source of water is solely the precipitation infiltrating into the soil. The climate of stands differs. The total mass of organic matter of a stand at a given forest site is basically determined by the production capacity (ecological potential) of the site. Taking into account that production capacity strongly depends on the climate parameters, the mass of organic matter is less ( $191 \text{ tC ha}^{-1}$ ) where the forestry aridity index is higher ( $FAI=5.50$  as for Turkey oak) (Fig. 2). In contrast, in beech stand with cooler and wetter climate ( $FAI=4.45$ ) the mass of organic matter is high ( $292 \text{ tC ha}^{-1}$ ).

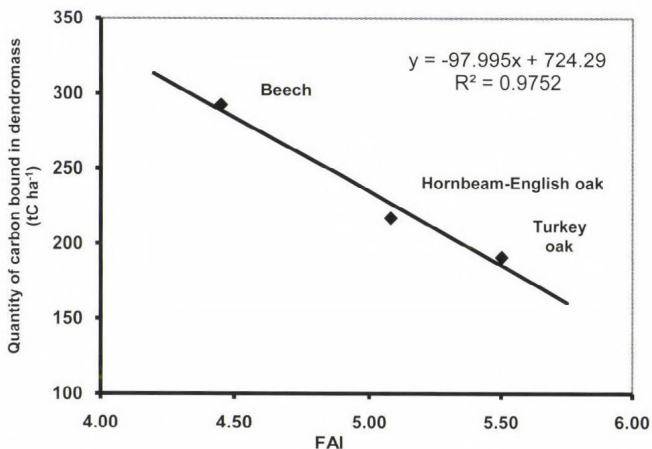


Fig. 2. Correlation between carbon bound in dendromass and *FAI* (Führer and Jagodics, 2009).

The applicability of *FAI* is also justified by another experiment evaluating the annual thickness (girth) growing of a hundred-year-old beech stand at Brennbergbánya research site. Increase of girth of trees was observed weekly by dendrometer bands located at stems of emergent, dominant, and suppressed trees. Basal area growth was calculated from girth-growth data. In Fig. 3 we can see that variation of annual *FAI* values from average was always inverse in the examined 9 years (1999–2007) compared to the difference from the average basal area growth of beech. This means that warmer and drier years (represented by higher *FAI*) resulted in less of growth increment (Fig. 4).

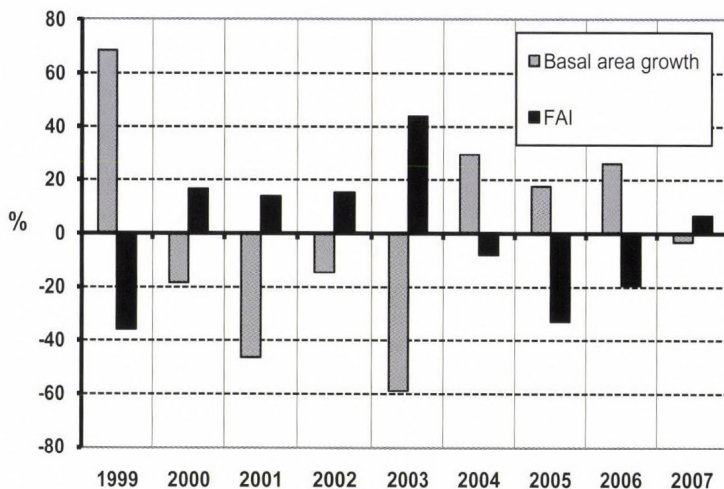


Fig. 3. Annual difference from average annual *FAI* values and basal area growth.

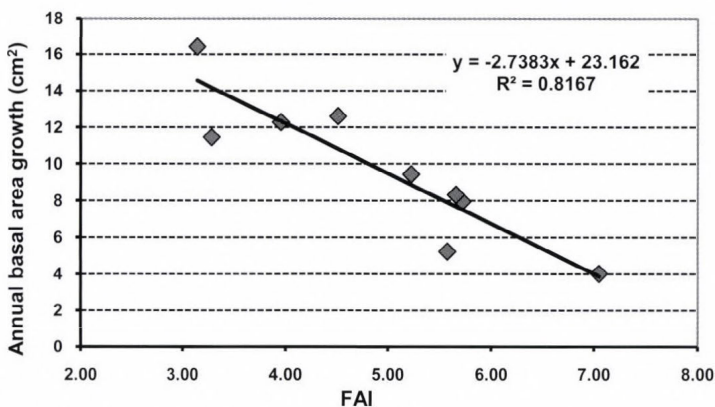


Fig. 4. Annual basal area growth as the function of *FAI*.

### 3.3. Calculation of *FAI* by means of meteorological data used at earlier forestry evaluations; characterization of forestry climate categories

Current forestry climate classification in Hungary is based on air humidity circumstances, since water-loss of trees (transpiration) is strongly determined among others by the relative humidity.

On the basis of agrometeorological investigations, daily relative humidity at 2 p.m. in July seemed to be the most suitable index, because humidity is the function of the temperature of the warmest summer month and more or less of the precipitation needed for evaporation. From data of 62 meteorological stations, between 1901 and 1950 we can draw the following conclusion (*Führer* and *Járó*, 2000); when the mean relative air humidity in July, 2 p.m. is higher than 58%, the natural plant community is beech. Between 53–58% and 48–53%, the plant community hornbeam-oak and sessile oak / Turkey oak, respectively. When air humidity is lower than 48%, the area is originally treeless (forest-steppe climate). Beside July, low relative humidity can also be observed in August; sometimes it is even lower than in July, therefore, mean humidity of critical months (July–August) would represent better the weather of climate categories according to our newest knowledge. Unfortunately, the exact characterization by air temperature and precipitation data – according to the climate categories – of annual periods essential in the physiological processes of trees has not been realized yet. So far, in forestry practice, the climate categories have been determined according to occurrence of test species (beech, hornbeam, sessile oak, and Turkey oak) in Hungary.

However, *FAI* index takes into account the temperature and precipitation characteristics of the period when organic matter production is directly influenced by these parameters. According to this criterion, we evaluated the data of meteorological stations in the important growth periods, which were earlier taken into consideration in the characterization of forestry regions.

Using data of 94 meteorological stations between 1901 and 1950 covering the whole area of the country, on the basis of the *Járó-type* evaluation (Führer and Járó, 2000), there are 11 stations in the beech climate, 16 in the hornbeam–oak climate, 43 in the sessile oak / Turkey oak, while 24 stations of them belong to the forest-steppe climate. On the basis of the mean of 50-year long measurement record (Table 1), we can conclude that:

Table 1. Meteorological features of forestry climate categories (Führer, 2010)

Meteorological parameters			Forestry climate categories			
			Beech	Hornbeam–oak	Sessile oak–Turkey oak	Forest-steppe
			(FAI <4.75)	(FAI: 4.75–6.00)	(FAI: 6.00–7.25)	(FAI >7.25)
Precipitation (mm)	annual	mean	752	663	598	546
		S.D.	31.0	55.4	43.4	29.0
	Nov–Apr	mean	297	267	248	233
		S.D.	25.9	36.5	26.1	18.7
	May–Jul	mean	259	218	192	174
		S.D.	12.5	15.0	11.3	6.6
	May–Oct	mean	455	395	350	313
		S.D.	22.0	25.5	22.7	13.0
	Jul–Aug	mean	167	139	118	101
		S.D.	8.6	12.8	8.9	5.4
Temperature (°C)	annual	mean	8.80	9.40	9.90	10.4
		S.D.	0.87	0.73	0.61	0.29
	Nov–Apr	mean	2.30	2.70	3.00	3.40
		S.D.	0.95	0.85	0.66	0.35
	May–Jul	mean	16.6	17.50	18.20	19.0
		S.D.	0.84	0.80	0.66	0.33
	May–Oct	mean	15.2	16.20	16.80	17.5
		S.D.	0.82	0.71	0.62	0.34
	Jul–Aug	mean	18.5	19.60	20.30	21.1
		S.D.	0.79	0.74	0.67	0.39
	<b>FAI</b>	<b>mean</b>	<b>4.36</b>	<b>5.51</b>	<b>6.56</b>	<b>7.65</b>
		S.D.	0.30	0.41	0.38	0.31

- (a) In the *beech climate*, where the climate marker species is beech, the sum of annual average precipitation reaches the 750 mm. During winter (in the storage period, from November to April), the average precipitation is nearly 300 mm; in the main growth phase (from May to July) it is 260 mm, whilst in the critical months it is 170 mm. The annual average temperature ranges between 8.5 and 9.0 °C, and during the warmest, critical months it is 18.5 °C.
- (b) In the *hornbeam–oak climate*, where the climate marker species is hornbeam, the annual average precipitation sum is higher than 660 mm,

and in the water storage period it is nearly 270 mm. In the main growth phase and in the critical months, it reaches 225 and 140 mm, respectively. These values are about 10–15% lower than in the beech climate. The annual average temperature is 9.4 °C, but in the critical months it is higher than 19.5 °C.

- (c) In the *sessile oak–Turkey oak* climate, where the climate marker species depending on the acidity of the soil is either the sessile oak (acidic site) or the Turkey oak (alkaline site), the annual average precipitation is around 600 mm, and in the water storage period it hardly reaches 250 mm. In the main growth cycle and in the critical months it is 190 and 120 mm, respectively. These values are about 10% lower than in the hornbeam–oak climate. The annual average temperature can reach 10 °C, and in the critical months it is higher than 20 °C.
- (d) The *forest-steppe* climate cannot be characterized by tree species since it is originally treeless area. The lowest annual average precipitation sum under 550 mm is found here. In the storage period it is 230 mm and in the main growth cycle it is 175 mm. In the critical months the value goes down to 100 mm. This climate is the warmest in Hungary, the annual average temperature is nearly 10.5 °C and the average temperature in the critical months is higher than 21.0 °C.
- (e) The average data of the climate categories significantly differ from each other at the confidence level of 90%.

Average value of forestry aridity index in the beech climate is nearly 4.4. Lowest value in Hungary can be derived at the meteorological station of Kékestető ( $FAI=3.3$ ), Hungary's highest peak (1005 m above sea level). The average  $FAI$  value at the stations in the hornbeam–oak climate is 5.5. The average  $FAI$  value in the sessile oak–Turkey oak climate nearly reaches 6.6. At stations of the forest-steppe climate, the average  $FAI$  value is higher than 7.6. The highest value ( $FAI=8.3$ ) was calculated for Csongrád town, in the warmest and lowest area of the Great Hungarian Plain.

Although the spatial distribution of considered meteorological stations only partially agrees with the distribution of marker stands representing various climate categories, we can still draw – on the basis of calculated mean  $FAI$  values and its deviation – the borders of different forestry climate categories with sufficient reliability, and we can also specify the classification of meteorological stations taking into consideration in our evaluation.

This means that in the *beech climate* zone the  $FAI$  index is 4.75 or below. *Hornbeam–oak climate* can be characterized by  $FAI$  value between 4.75 and 6.00, while we have *sessile oak–Turkey oak climate* between the values of 6.00 and 7.25. The *forest-steppe climate* can be found over higher  $FAI$  values.

#### 4. Application of forestry aridity index for future estimations

On the basis of different climate scenarios during the summer months, the average temperature in Hungary increases, while precipitation will be less in this period (Bartholy, 2006). The *FAI* number allows us to model the expected impact of climate change on the basis of different scenarios, in other words, how the area of the certain climate categories will change.

In a simple way when we increase the mean temperature of critical months in calculation of *FAI* index with parallel decrease of precipitation according to the scenarios, we get the *FAI* representing the expected climate category in the future. Based on 30-year average meteorological data for 1961–1990, we have determined the distribution of the forestry climate categories. The distribution of categories in Transdanubian region will substantially be modified by a moderate temperature increase (1.0 °C) in summer (Figs. 5 and 6). Taking into account higher temperature increase (1.7 °C) and lower precipitation (8.2%) in summer (Fig. 7), 90% of the beech climate will disappear and the territory of the hornbeam-oak climate will decrease by 50%. The area ratio of the Turkey oak climate will remain the same, but it will be moved to the area of the today's hornbeam-oak climate. Expectedly, the area of the forest-steppe climate will be 4 times larger, and it will occupy the area of the current Turkey oak climate and partly in some extent that of hornbeam-oak climate.

The practical impact of this new situation (the change of areas of climate categories) is significant. It basically modifies the future forestry strategy of the country and the principle of forestry management from the point of view both of ecology aspects (species selection) and cultivation technology (regeneration, nursing silvicultural treatment), as well as profitability.

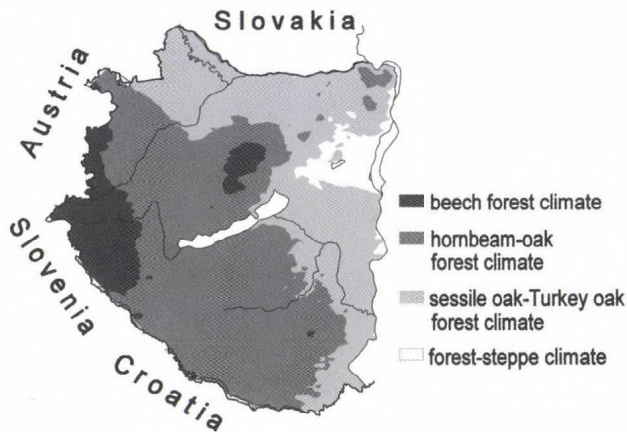


Fig. 5. Current distribution of climate categories in Transdanubian region according to today's weather conditions.

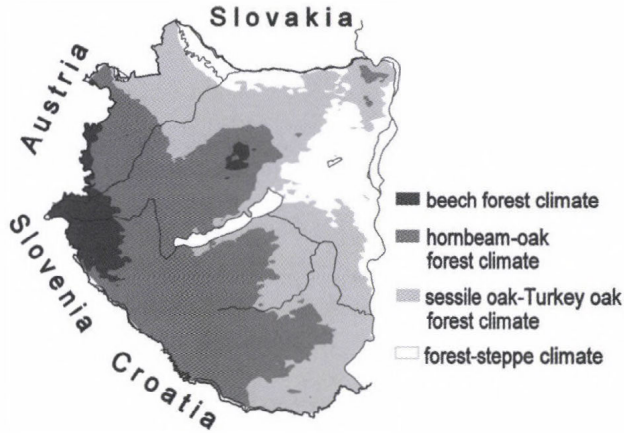


Fig. 6. Distribution of climate categories in Transdanubian region with a weak summer temperature (1.0 °C) increase scenario.

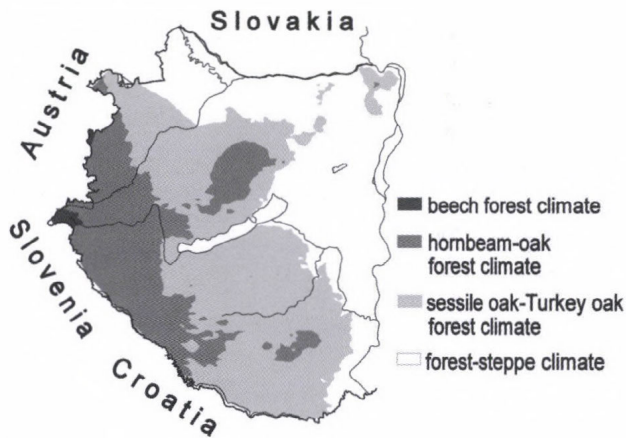


Fig. 7. Distribution of climate categories in Transdanubian region with a summer temperature increase of 1.7 °C and summer precipitation decrease of 8.2% scenario.

**Acknowledgements**—The authors acknowledge funding by a Hungarian research project NKTH–OTKA 80305 and 80335 CK.

### References

- Bartholy, J., 2006: The possible climate consequences of the global climate change in Hungary (in Hungarian). "AGRO-21" Füzetek 48, 12-18.
- Berki, I., Mórincz, N., Rasztoivits, E. and Vig, P., 2007: Determination of the drought tolerance limit of beech (in Hungarian). *Proceedings of the V. Erdő és klíma konferencia* (eds.: Cs. Mátyás, P. Vig). Nyugat-Magyarországi Egyetem, Sopron, 213-228.

- Berki, I., Rasztovits, E., Móricz, N. and Mátyás, Cs., 2009: Determination of the drought tolerance limit of beech forests and forecasting their future distribution in Hungary. *Cereal Research Communications* 37, 613-616.
- Csóka, Gy., Koltay, A., Hirka, A. and Janik, G., 2007: Influence of drought on health of sessile oak and beech stands in Hungary (in Hungarian). *Proceedings of the V. Erdő és klíma konferencia* (eds.: Cs. Mátyás, P. Vig). Nyugat-Magyarországi Egyetem, Sopron, 229-239.
- Dunkel, Z., 2009: Brief surveying and discussing of drought indices used in agricultural meteorology. *Időjárás* 113, 23-38.
- Führer, E., 1994: Precipitation measurements in beech, sessile oak and spruce ecosystems (in Hungarian). *Erdészeti Kutatások* 84, 11-35.
- Führer, E., 1995: The effect of weather on the productivity and health state of the forests (in Hungarian). *Erdészeti Lapok* 130, 176-178.
- Führer, E., 2008: Forest management (in Hungarian). In *Klimaváltozásról mindenkinek* (eds.: Zs. Harnos, M. Gaál, L. Hufnagel). Budapesti Corvinus Egyetem, Kertészettudományi Kar, Matematikai és Informatikai Tanszék, Budapest, 90-102.
- Führer, E., 2010: Tree growth and the climate (in Hungarian). "Klíma-21" *Füzetek* 61, 98-107.
- Führer, E. and Jagodics, A., 2009: Carbon stocks in the stands of climate indicator tree species (in Hungarian). "Klíma-21" *Füzetek* 57, 43-55.
- Führer, E. and Járó, Z., 1992: Auswirkungen der Klimaänderung auf die Waldbestände Ungarns. *Österreichische Forstzeitung* 9, 25-27.
- Führer, E. and Járó, Z., 2000: The effectiveness of drought and drainage water in the silviculture of the Great Plain I. (in Hungarian). *Erdészeti Tudományos Intézet Kiadványai* 12, 1-144.
- Halupa, L., 1967: Data to the investigation of the growing process of saline oak forests (in Hungarian). *Erdészeti Kutatások* 63, 95-108.
- Járó, Z., 1989: Water cycle in the forest (in Hungarian). *Az Erdő* 38, 352-355.
- Járó, Z. and Tátraaljai, E., 1984-85: Yearly growth of trees (in Hungarian). *Erdészeti Kutatások* 76-77, 221-234.
- Láng, I., Csete, L. and Jolánkai, M. (eds.), 2007: Global climate change: home impacts and answers (in Hungarian). *A VAHAVA jelentés*, Szaktudás Kiadó Ház, Budapest, p. 227.
- Linderholm, H.W., 2006: Growing season changes in the last century. *Agr. Forest Meteorol.* 137, 1-14.
- Manninger, M., 2004: Annual and periodic growth pattern of forest trees and its relation to ecological factors (in Hungarian). In *Proceedings of the IV. Erdő és klíma konferencia* (eds.: Cs. Mátyás, P. Vig). Nyugat-Magyarországi Egyetem, Sopron, 151-162.
- Mátyás, Cs., 2010: Forecasts needed for retreating forests. *Nature* 464 (7293), 1271.
- Mátyás, Cs., Nagy, L. and Ujvári-Jármay, É., 2009: Climatic stress and the genetically determined response of tree species at the aridity limit of distribution: analysis and predictions (in Hungarian). "Klíma-21" *Füzetek* 56, 57-65.
- Molnár, M. and Lakatos, F., 2007: Beech decline in Zala county: triggered by climate change? (in Hungarian). *Proceedings of the V. Erdő és klíma konferencia* (eds.: Cs. Mátyás, P. Vig). Nyugat-Magyarországi Egyetem, Sopron, 257-267.
- Pálfai, I., 2002: Drought zones of Hungary (in Hungarian). *Vízügyi Közlemények* 84, 323-357.
- Pálfai, I., 2007: Climate change and drought (in Hungarian). "Klíma-21" *Füzetek* 49, 59-65.
- Pálfai, I., 2010: The frequency of droughts in the Carpathian Basin in the last three hundred years (in Hungarian). "Klíma-21" *Füzetek* 59, 42-45.
- Szőnyi, L., 1962: Data to the girth growth of some tree species (in Hungarian). *Az Erdő* 11, 289-300.
- Várallyai, Gy., 2002: Climate change and soil processes. *Időjárás* 106, 113-124.
- Várallyai, Gy., 2010: Soil as water reservoir; soil aridification (in Hungarian). "Klíma-21" *Füzetek* 59, 3-25.
- Várallyai, Gy. and Farkas, Cs., 2008: Expected impacts of climate change on the soils in Hungary (in Hungarian). In *Klimaváltozás: környezet – kockázat – társadalom* (eds.: Zs. Harnos, L. Csete). Szaktudás Kiadó Ház, Budapest, 91-129.

## BOOK REVIEW

*Haszpra, László* (editor), 2011: **Atmospheric Greenhouse Gases: The Hungarian Perspective**. Springer, Dordrecht – Heidelberg – London – New York. 393 pages, with nearly 120 figures and 50 tables (ISBN 978-90-481-9949-5).

Human induced global climate change is one of the biggest challenges humankind faces today. Increasing amount of atmospheric greenhouse gases play a crucial role in the evolution of the climate. Without the understanding of the contributing processes, feedbacks, and interactions we cannot predict the future changes and develop effective mitigation/adaptation strategies. To decrease the uncertainty of the global studies, detailed regional studies are needed surveying the regional characteristics of the atmospheric greenhouse gas budget and the influencing factors. The book covers a coherent subset of the Hungarian climate change oriented research that is directly related to greenhouse gases.

The 16 chapters written by 44 Hungarian and foreign authors are grouped into four parts. The first part of the book covers the atmospheric trends and fluctuations of the major greenhouse gases as observed in Hungary. Here, first, the interested readers can get acquainted with the history and technical background of the Hungarian atmospheric greenhouse gas measurements. The following two chapters present the concentration trends, seasonal and diurnal variations, as well as the characteristic changes observed during the measurement period. For these studies impressive 17–30 years long data series were available.

The second and third parts of the book deal with the exchange of greenhouse gases between the biosphere (including the soil) and the atmosphere. The response of the biosphere is an important feedback in the climate system. In the case of carbon dioxide and methane it can act as both a net source and a net sink depending on climate. Biospheric nitrous oxide emission also depends on climate. In turn, the greenhouse gas budget of the biosphere influences the climate through the control on the atmospheric greenhouse effect.

The first of these two parts covers the measurements, while the other focuses on the mathematical modeling of the processes. Both parts follow the same structure. They start with an introductory chapter presenting the measurement/modeling methods, then they discuss the grasslands, the forests, and the arable lands in separate chapters. The part on modeling finishes with a summary chapter giving the overall biospheric greenhouse gas budget of Hungary.

Atmospheric greenhouse gases cannot be discussed without mentioning the anthropogenic contribution. The three chapters of the last part of the book present the effect of the anthropogenic perturbation of the biosphere, the contribution of the different industrial processes (energy production, waste

management, etc.) giving also a methodological introduction to the emission estimations. The authors also review the trends in the Hungarian greenhouse gas emissions.

This book of 393 pages calls the attention to the regional properties, which may modulate the European scale or global picture on the variation of atmospheric greenhouse gases. Although, the book is intended primarily for scientists studying the atmospheric and biospheric greenhouse gas budgets, most of the topics are general enough also for students studying geosciences, ecology, or environmental sciences to get an overview on a part of atmospheric greenhouse gas budget research.

*L. Bozó*

## INSTRUCTIONS TO AUTHORS OF *IDŐJÁRÁS*

The purpose of the journal is to publish papers in any field of meteorology and atmosphere related scientific areas. These may be

- research papers on new results of scientific investigations,
- critical review articles summarizing the current state of art of a certain topic,
- short contributions dealing with a particular question.

Some issues contain "News" and "Book review", therefore, such contributions are also welcome. The papers must be in American English and should be checked by a native speaker if necessary.

Authors are requested to send their manuscripts to

*Editor-in Chief of IDŐJÁRÁS*  
P.O. Box 38, H-1525 Budapest, Hungary  
E-mail: [journal.idojaras@met.hu](mailto:journal.idojaras@met.hu)

including all illustrations. MS Word format is preferred in electronic submission. Papers will then be reviewed normally by two independent referees, who remain unidentified for the author(s). The Editor-in-Chief will inform the author(s) whether or not the paper is acceptable for publication, and what modifications, if any, are necessary.

Please, follow the order given below when typing manuscripts.

*Title page:* should consist of the title, the name(s) of the author(s), their affiliation(s) including full postal and e-mail address(es). In case of more than one author, the corresponding author must be identified.

*Abstract:* should contain the purpose, the applied data and methods as well as the basic conclusion(s) of the paper.

*Key-words:* must be included (from 5 to 10) to help to classify the topic.

*Text:* has to be typed in single spacing on an A4 size paper using 14 pt Times New Roman font if possible. Use of S.I. units are expected, and the use of negative exponent is preferred to fractional sign. Mathematical formulae are expected to be as simple as possible and numbered in

parentheses at the right margin.

All publications cited in the text should be presented in the *list of references*, arranged in alphabetical order. For an article: name(s) of author(s) in Italics, year, title of article, name of journal, volume, number (the latter two in Italics) and pages. E.g., *Nathan, K.K.*, 1986: A note on the relationship between photo-synthetically active radiation and cloud amount. *Időjárás* 90, 10-13. For a book: name(s) of author(s), year, title of the book (all in Italics except the year), publisher and place of publication. E.g., *Junge, C.E.*, 1963: *Air Chemistry and Radioactivity*. Academic Press, New York and London. Reference in the text should contain the name(s) of the author(s) in Italics and year of publication. E.g., in the case of one author: *Miller* (1989); in the case of two authors: *Gamov* and *Cleveland* (1973); and if there are more than two authors: *Smith et al.* (1990). If the name of the author cannot be fitted into the text: (*Miller*, 1989); etc. When referring papers published in the same year by the same author, letters a, b, c, etc. should follow the year of publication.

*Tables* should be marked by Arabic numbers and printed in separate sheets with their numbers and legends given below them. Avoid too lengthy or complicated tables, or tables duplicating results given in other form in the manuscript (e.g., graphs).

*Figures* should also be marked with Arabic numbers and printed in black and white or color (under special arrangement) in separate sheets with their numbers and captions given below them. JPG, TIF, GIF, BMP or PNG formats should be used for electronic artwork submission.

*Reprints:* authors receive 30 reprints free of charge. Additional reprints may be ordered at the authors' expense when sending back the proofs to the Editorial Office.

*More information* for authors is available: [journal.idojaras@met.hu](mailto:journal.idojaras@met.hu)

Published by the Hungarian Meteorological Service

---

Budapest, Hungary

**INDEX 26 361**

**HU ISSN 0324-6329**

# IDOJÁRÁS

QUARTERLY JOURNAL  
OF THE HUNGARIAN METEOROLOGICAL SERVICE

## CONTENTS

- Attila Machon, László Horváth, Tamás Weidinger, Krisztina Pitér, Balázs Grosz, Zoltán Nagy and Ernő Führer:* Weather induced variability of nitrogen exchange between the atmosphere and a grassland in the Hungarian Great Plain..... 219
- Simone Orlandini, Marco Mancini, Grifoni Daniele, Francesca Orlando, Anna Dalla Marta and Valerio Capecci:* Integration of meteo-climatic and remote sensing information for the analysis of durum wheat quality in Val d'Orcia (Tuscany, Italy)..... 233
- Boryana Tsenova and Rumjana Mitzeva:* Comparative modeling study of the effect of parameterizations based on rime accretion rate and effective water content on the simulated charge density in thunderstorms ..... 247
- Jit Singh Mandeep, Anthony Cheng Chen Yee, Mardina Abdulah and Mohammad Tariqul Islam:* Tropospheric scintillation measurements in Ku-band satellite signals on Earth-space paths with low elevation angle..... 265
- Zsolt Bottyán:* Estimation of structural icing intensity and geometry of aircrafts during different conditions – a fixed-wing approach..... 275

\*\*\*\*\*

<http://www.met.hu/Journal-Idojaras.php>

# IDŐJÁRÁS

*Quarterly Journal of the Hungarian Meteorological Service*

*Editor-in-Chief*  
**LÁSZLÓ BOZÓ**

*Executive Editor*  
**MÁRTA T. PUSKÁS**

## EDITORIAL BOARD

- |                                       |   |
|---------------------------------------|---|
| AMBRÓZY, P. (Budapest, Hungary)       | MIKA, J. (Budapest, Hungary)                        |
| ANTAL, E. (Budapest, Hungary)         | MERSICH, I. (Budapest, Hungary)                     |
| BARTHOLY, J. (Budapest, Hungary)      | MÖLLER, D. (Berlin, Germany)                        |
| BATCHVAROVA, E. (Sofia, Bulgaria)     | NEUWIRTH, F. (Vienna, Austria)                      |
| BRIMBLECOMBE, P. (Norwich, U.K.)      | PINTO, J. (Res. Triangle Park, NC, U.S.A.)          |
| CZELNAI, R. (Dörgicse, Hungary)       | PRÁGER, T. (Budapest, Hungary)                      |
| DUNKEL, Z. (Budapest, Hungary)        | PROBÁLD, F. (Budapest, Hungary)                     |
| FISHER, B. (Reading, U.K.)            | RADNÓTI, G. (Reading, U.K.)                         |
| GELEYN, J.-Fr. (Toulouse, France)     | S. BURÁNSZKI, M. (Budapest, Hungary)                |
| GERESDI, I. (Pécs, Hungary)           | SIVERTSEN, T.H. (Risør, Norway)                     |
| GÖTZ, G. (Budapest, Hungary)          | SZALAI, S. (Budapest, Hungary)                      |
| HASZPRA, L. (Budapest, Hungary)       | SZEIDL, L. (Budapest, Hungary)                      |
| HORÁNYI, A. (Budapest, Hungary)       | SZUNYOGH, I. (College Station, TX, U.S.A.)          |
| HORVÁTH, Á. (Siófok, Hungary)         | TAR, K. (Debrecen, Hungary)                         |
| HORVÁTH, L. (Budapest, Hungary)       | TÄNCZER, T. (Budapest, Hungary)                     |
| HUNKÁR, M. (Keszthely, Hungary)       | TOTH, Z. (Camp Springs, MD, U.S.A.)                 |
| LASZLO, I. (Camp Springs, MD, U.S.A.) | VALI, G. (Laramie, WY, U.S.A.)                      |
| MAJOR, G. (Budapest, Hungary)         | VARGA-HASZONITS, Z. (Moson-<br>magyaróvár, Hungary) |
| MATYASOVSZKY, I. (Budapest, Hungary)  | WEIDINGER, T. (Budapest, Hungary)                   |
| MÉSZÁROS, E. (Veszprém, Hungary)      |   |

*Editorial Office: Kitaibel P.u. 1, H-1024 Budapest, Hungary*  
*P.O. Box 38, H-1525 Budapest, Hungary*  
*E-mail: journal.idojaras@met.hu*  
*Fax: (36-1) 346-4669*

---

**Indexed and abstracted in Science Citation Index Expanded™ and  
Journal Citation Reports/Science Edition  
Covered in the abstract and citation database SCOPUS®**

---

*Subscription by*  
*mail: IDŐJÁRÁS, P.O. Box 38, H-1525 Budapest, Hungary*  
*E-mail: journal.idojaras@met.hu*

# IDŐJÁRÁS

*Quarterly Journal of the Hungarian Meteorological Service*  
Vol. 115, No. 4, October–December 2011, pp. 219–232

## **Weather induced variability of nitrogen exchange between the atmosphere and a grassland in the Hungarian Great Plain**

**Attila Machon<sup>\*1,2,4</sup>, László Horváth<sup>1</sup>, Tamás Weidinger<sup>3</sup>,  
Krisztina Pintér<sup>4,5</sup>, Balázs Grosz<sup>3</sup>, Zoltán Nagy<sup>4,5</sup>, and Ernő Führer<sup>6</sup>**

<sup>1</sup>*Hungarian Meteorological Service,  
Gilice tér 39, H-1181 Budapest, Hungary*

<sup>2</sup>*Center for Environmental Science, Eötvös Loránd University,  
Pázmány P. sétány 1/A, H-1117 Budapest, Hungary*

<sup>3</sup>*Department of Meteorology, Eötvös Loránd University,  
Pázmány P. sétány 1/A, H-1117 Budapest, Hungary*

<sup>4</sup>*Institute of Botany and Ecophysiology, Szent István University,  
Páter Károly utca 1, H-2103 Gödöllő, Hungary*

<sup>5</sup>*Plant Ecology Research Group of Hungarian Academy of Sciences,  
Páter Károly utca 1, H-2103, Gödöllő, Hungary*

<sup>6</sup>*Hungarian Forest Research Institute,  
Papret 17, H-9400 Sopron, Hungary*

*\*Corresponding author; E-mail: machon@caesar.elte.hu*

*(Manuscript received in final form October 21, 2011)*

**Abstract**—The paper describes some of the preliminary results of the ecological research on nitrogen exchange in a grassland in central Hungary (Kiskunság National Park, Bugacpuszta). The changes in different climate parameters evidently affect not only N-deposition but also N-exchange and N-gas emissions through the processes of soil and plant metabolism. Measurements of nitrogen fluxes and basic meteorological parameters have been started above a semi-natural grassland ecosystem in 2002. Seasonal and long-term nitrogen exchange (both emission and deposition) is under climatic control. In the years of 2006 and 2007, the amount of the deposited N markedly decreased (by 27% and 15%, respectively) compared to the average of the earlier (2002–2004) years. The main source of the deposited N is NH<sub>3</sub>. The ratio of dry to wet deposition varies between 1.5 and 2.3. In the dry year of 2007, emissions of N<sub>2</sub>O were four times lower compared to the

average ( $90 \text{ mg N m}^{-2} \text{ yr}^{-1}$ ) of the earlier years caused by the changes in weather conditions including lower precipitation and  $1 \text{ }^{\circ}\text{C}$  higher annual average temperature. In the year with higher precipitation (2010),  $\text{N}_2\text{O}$  emissions increased again and reached  $180 \text{ mg N m}^{-2} \text{ yr}^{-1}$  when the annual rainfall was twice the normal rate. It should be noted that soil water filled pore space (WFPS) cannot explain all of the variations in  $\text{N}_2\text{O}$  fluxes. With increasing soil temperature,  $\text{NO}$  flux grows faster than  $\text{N}_2\text{O}$  up to  $20 \text{ }^{\circ}\text{C}$  until the role of other factors (e.g., water stress, nutrient supply, and other complex processes linked to heat stress) will determine the magnitude of metabolism. The relatively high soil  $\text{N}_2\text{O}$  flux under  $5 \text{ }^{\circ}\text{C}$  could come from the thawing period 2–3 months after wintertime which could result in high emission peaks for a few days with low soil temperature. It seems to be the case that soil temperature usually generates short term variability of trace gas exchange, whereas the magnitude of the biogenic emission is dominantly controlled by soil wetness, pH, and other site specific factors. The net N flux – excluding grazing, manure, farm management, etc. – ranged between  $9.5$  and  $13 \text{ kg N ha}^{-1} \text{ yr}^{-1}$ . Reduced  $\text{N}_2\text{O}$  emission presents a potential negative feedback to emission; on the other hand, vegetation can become a net  $\text{CO}_2$  source in extremely dry years such as 2003 and 2007 as a positive feedback to climate change.

*Key-words:* N-exchange, N-emission, N-deposition, climate perturbation, grassland, denitrification

## 1. Introduction

The climate in middle and southern Europe will likely be warmer, with drier summers; in some parts with shorter or mild and wetter winters, and more variable patterns of rainfall and temperature in the 21st century as predicted by *EEA* (2004). Grasslands are one of the most widespread vegetation types in Europe and, especially, in the Hungarian Great Plain, which also appear to be drifting to desertification. This is an important environmental problem, because grassland ecosystems are important in the cycle of nitrogen (N) and carbon (C) between the land surface and the atmosphere. Sensitivity of N balance of grasslands to climatic perturbations such as drought remains uncertain (*Schimel et al.*, 1996; *Reich et al.*, 2006).

Interactions between climate perturbations and changing dynamics of N-cycle of grasslands have received much less attention than the C-cycle and corresponding interactions in forests. Some studies were carried out for Hungarian grassland sites on how net ecosystem exchange (NEE) of carbon dioxide, respiration processes (*Balogh et al.*, 2005, 2008), or the greenhouse gas (GHG) flux will change as a consequence of climate change (*Nagy et al.*, 2005, 2007). The markers such as heat and drought extremes – which will become more frequent as a result of the climate perturbations – can also have an impact the nitrogen budget through trace gas soil fluxes as well as the carbon and water balance (*Pintér et al.*, 2008) due to soil functioning, and they may lead to reduced plant growth or changes in grassland species composition. Some European studies pointed out the effects of soil condition on  $\text{NO}$ ,  $\text{NO}_2$ , and  $\text{N}_2\text{O}$  emission from different soils (*Schindlbacher et al.*, 2004) or on  $\text{CH}_4$  uptake by sandy grassland

ecosystems (*van den Pol-van Dasselaar et al.*, 1998). Many aspects of the relation between N and C cycles (e.g., *Soussana and Hartwig*, 1996), estimation of the nitrogen and carbon fluxes (*Levy et al.*, 2007) and budgets (*Ammann et al.*, 2009; *Skiba et al.*, 2009) in grassland were also studied.

The changed weather condition – through the changes of soil conditions (e.g., soil temperature, humidity etc.) – greatly affects the soil processes like mineralization, decomposition, nitrification, and denitrification as the significant sources and controllers of atmospheric C and N trace gases (*Conrad*, 1996) and the sink of  $\text{NH}_4^+$  and  $\text{NO}_3^-$  substrates. Due to the processes above, the organic/inorganic N pool of soil or soil emission of NO,  $\text{N}_2\text{O}$ , as well as N uptake of plants are subject to change. These processes are linked with other stressors (e.g., heat stress, water deficiency, etc.) and may easily influence plant physiology, productivity or plant species composition.

The objective of this work is to investigate the nitrogen exchange between atmosphere and grassland and its dependence on climatic conditions, and focusing on links with reactive trace gas emissions and N-deposition, and on the possible feedbacks to soil-vegetation dynamics.

## 2. Materials and methods

Investigations were conducted at the *Bugacpuszta* nature reserve research site (46.69°N, 19.60°E, h = 110 m asl) in the Hungarian Great Plain. Measurements of nitrogen fluxes and basic micrometeorological parameters above a semi-natural ecosystem were started in 2002. This station also provides input data for modeling, validation, and calibration of models. The climate is continental with annual average temperature of 10.5 °C, and the average precipitation is about 530 mm year<sup>-1</sup>. The vegetation is semi-arid sandy grassland (*Cynodonti Festucetum pseudovinae*) where *Festuca pseudovina*, *Carex stenophylla*, *Salvia pratensis*, and *Cynodon dactylon* are the dominant plant species. The landscape is flat. The soil is a Chernozem-type sandy soil (*Machon et al.*, 2010) (sand : silt : clay = 82 : 7 : 11% is the average composition of the top 20 cm soil).

Soil emission of NO has been determined by dynamic chamber method as described in *Horváth et al.* (2006). Soil  $\text{N}_2\text{O}$  flux measurements were carried out bi-weekly (2002–2004), later weekly (2006–2010) by 8 parallel static soil chambers (*Clayton et al.*, 1994; *Christensen et al.*, 1996). Samples were taken at t = 0, 15, and 30 minutes after closure of chambers. Concentration changes (within 30 min) were determined by gas chromatography-mass spectrometry (GC-MS). According to statistical analysis, the non-systematic bulk error (CV: coefficient of variation) of sampling and analysis, estimated using parallel sampling, was always below 10%. In 2007, the detector was changed to electron capture (GC-ECD). Three-stage filter pack method was used for daily sampling of particles and gases followed by ion-chromatography (nitrate, nitric acid) and

spectrophotometry (indophenol-blue method for ammonium and ammonia) (EMEP, 1996). The minimum detection limit (MDL) is  $0.1 \mu\text{g N m}^{-3}$  for all components. The precision (bulk relative error) of sampling and measurements was around 10%. Dry deposition of nitrogen dioxide, ammonia, nitric acid vapour, nitrate, and ammonium particles were inferred using dry deposition velocities (Horváth *et al.*, 2005) measured above surfaces with the same characteristics as those of Bugacpuszta station. Fluxes of  $\text{NH}_3$ , within the atmosphere and the canopy (excluding soil emission) were also inferred this way. Wet depositions of nitrate and ammonium ions were calculated on the basis of daily precipitation sampling and concentration measurements of ammonium and nitrate ions by the analytical methods described in Machon *et al.* (2010). The calculated bulk error of precipitation sampling and concentration measurements was around 10%. Minimum detection limit was  $0.05 \text{ mg N L}^{-1}$  for both ions. Meteorological parameters like precipitation, air and soil temperature, and soil moisture were also observed.

### 3. Results and discussion

The studied sandy grassland soil has poor water supply with deep water table (6 m). In summer months, high ground surface temperatures can be observed ( $>30^\circ\text{C}$ ) and the upper layer of soil dries out. Nitrate leaching is estimated to be negligible. Suction cups applied below rooting zone did not collect measurable quantity of soil water. The soil N trace gas production depends strongly on soil biology, chemistry, and physics (Smith *et al.*, 2003). Denitrification is stimulated by hypoxia. In dry soils (down to water filled pore space (WFPS) of about 30%, see Fig. 1) this process is limited due to the unfavorable soil conditions for the anaerobic microbial communities (nitrous oxide production and subsequent emission rate are maximized at WFPS range of 40–50% (Horváth *et al.*, 2010)). In drier soils, in the well aerated zone, the nitrification is the dominant process producing  $\text{NO}$ .

During the summer, microbial productivity is elevated (mineralization, nitrification, immobilization, decomposition, etc.), but denitrification ( $\text{N}_2\text{O}$  production) is suppressed when the WFPS is low. In dormant period, despite the higher WFPS, the activity of microbial community decreases in parallel with soil temperature decrease, resulting in low  $\text{N}_2\text{O}$  production.

Changes in seasonality, distribution, and frequency of precipitation and the total amount of rainfall may have an impact greatly on the nitrogen exchange of this ecosystem, resulting in a switch between the  $\text{N}_2\text{O}$  and  $\text{NO}$  production (determined by soil processes). Both seasonal and long-term nitrogen exchanges of this ecosystem is, therefore, linked to the soil water content (due to rainfall regime) and soil temperature (Machon *et al.*, 2010). Fig. 1 shows that higher soil  $\text{NO}$  emissions were observed in comparison to  $\text{N}_2\text{O}$  in the dry soil in summer

seasons, especially in 2007. During summers, the WFPS ranged between 20–30% (with exception of 2010). In 2007, the average soil wetness was 19%, close to the optimum for NO production by nitrification processes. Nitrification processes were dominating this year and NO emission ( $70 \text{ mg N m}^{-2} \text{ yr}^{-1}$ ) was higher than N<sub>2</sub>O soil flux ( $15 \text{ mg N m}^{-2} \text{ yr}^{-1}$ ); later it significantly decreased compared to the earlier (2002–2004) years when average emission was  $90 \text{ mg N m}^{-2} \text{ yr}^{-1}$  (Flechard *et al.*, 2007). In recent years, similar significantly lower emissions of N<sub>2</sub>O were observed at different types of grasslands in Hungary (Horváth *et al.*, 2008), in comparison to 2002–2004, on the basis of weekly sampling. In 2010, N<sub>2</sub>O emissions ( $180 \text{ mg N m}^{-2} \text{ yr}^{-1}$ ) exceeded NO emissions ( $78 \text{ mg N m}^{-2} \text{ yr}^{-1}$ ) due to the unusually high precipitation and WFPS in summer months, favoring denitrification metabolisms.

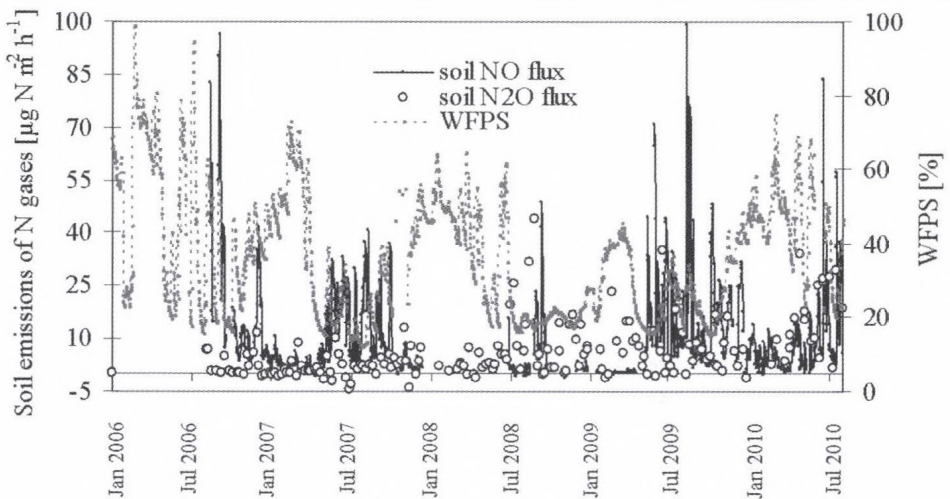


Fig. 1. Soil N gases emissions and linkage to soil humidity (WFPS) at Bugacpuszta station. (Due to instrument failure, there are only a few data points for soil NO flux in 2008.)

Trace gas emissions and N-deposition can be highly variable from season-to-season or year-to-year, but available parameters such as air and soil temperature, precipitation, and soil moisture more or less can explain this variability. Some uncertainty may arise from the complexity of soil and atmospheric processes and/or accuracy of measurements.

It can clearly be seen in *Table 1*, that emission of N<sub>2</sub>O decreases by a factor of 4 in 2006 and 2007 and increases by a factor of two in 2010 compared to the earlier (2002–2004) measurements at the same place. This phenomenon is explainable by soil microbial processes, as the rate of denitrification, etc., strongly depends on the varying weather conditions (e.g., water or heat stress). In 2009, the annual mean temperature was the same as in 2008, but this year was

drier. In contrast, substantial decrease was not observed in the measured flux. It can be explained partly by the fact that the sandy soil dried out within a short time after the rain events, and the effective time for denitrifying bacteria, preferring anaerobic condition, was shorter than in wet soils with higher water retaining capacity. On the other hand, in extremely wet soils emission of nitrous oxide is limited, and reduction leads to production of di-nitrogen (N<sub>2</sub>). The weather conditions (e.g., abiotic stress) prevent optimum soil condition for nitrous oxide production to be sustained for long periods during the study.

Table 1. Annual sum of climatic conditions and N-exchange [mg N m<sup>-2</sup> yr<sup>-1</sup>] between the surface and atmosphere at Bugacpuszta station

Measured parameters	2002–2004	2006	2007	2008	2009	2010
Precipitation [mm]	545	524	446	567	486	967
WFPS mean [%] (SD)		34.6 ± 11.7	33.6 ± 16.6	30.2 ± 13.9	27.9 ± 9.67	43 ± 12
T <sub>air</sub> , mean [°C]	10.1	10.1	11.1	11.0	11.2	11
T <sub>soil (5cm)</sub> , mean [°C] (SD)		10.2 ± 6.6	11.5 ± 4.5	11.1 ± 3.7	11.4 ± 3.7	10.9
Wet (NO <sub>3</sub> <sup>-</sup> and NH <sub>4</sub> <sup>+</sup> ) deposition (SD)	-470 ± 23 <sup>a</sup>	-338 ± 17	-420 ± 21	-520 ± 26	-450 ± 23	-578 ± 29
Dry HNO <sub>3</sub> deposition (SD)	-320 ± 32 <sup>a</sup>	-157 ± 16	-172 ± 17	-264 ± 26	-235 ± 24	-295 ± 30
Dry NH <sub>3</sub> deposition (SD)	-460 ± 23 <sup>a</sup>	-418 ± 21	-454 ± 23	-532 ± 27	-425 ± 21	-379 ± 19
Dry NO <sub>3</sub> <sup>-</sup> and NH <sub>4</sub> <sup>+</sup> deposition (SD)	-130 ± 7 <sup>a</sup>	-136 ± 7	-85 ± 4	-109 ± 5	-116 ± 6	-104 ± 5
Dry NO <sub>2</sub> deposition (SD)	-75 <sup>b</sup>	-75 ± 4	-45 ± 2	-80 ± 4	-79 ± 4	-95 ± 5
Soil N <sub>2</sub> O emission	80 <sup>c</sup>	18	15	56	63	180
Soil NO emission	119 <sup>d</sup>	160	79	119 <sup>d</sup>	118	78
Total deposition	-1.455	-1.124	-1.176	-1.505	-1.305	-1.451
<b>Sum of net N flux</b>	<b>-1.256</b>	<b>-946</b>	<b>-1.082</b>	<b>-1.330</b>	<b>-1.124</b>	<b>-1.193</b>

<sup>a</sup> Kugler et al., 2008

<sup>b</sup> Estimated from the average of 2006–2010

<sup>c</sup> Horváth et al., 2010

<sup>d</sup> No data for technical reason, calculated from the mean NO emission for 2006–2007 and 2009

Wet deposition of nitrate and ammonium together with the dry flux of ammonia and nitric acid vapor are responsible for the majority (80%) of the net N budget.

The sum of the atmospheric N-deposition (excluding deposited organic N) varied between 1.1 and 1.5 mg N m<sup>-2</sup> yr<sup>-1</sup>. It is noteworthy, that the precipitation amount nearly doubled in 2010 (see in *Table 1*), nevertheless, the wet deposition does not follow this pattern. Ratio of dry to wet deposition varied in the range of 1.5–2.3. According to the results (*Fig. 2*), in 2007 and 2009 the annual precipitation amount was significantly lower, and in 2010 it was two times higher than the long term mean. The deficit in the yearly precipitation mainly occurred in July in the vegetation period of 2006–2009 (see *Fig. 3*) resulting in less biomass production, because the drought and the main growing period coincided. At the same time, the lack of precipitation affects the N-cycle through missing wet deposited N, plant uptake, water stress, and other soil processes. In 2007, the annual mean temperature has increased by 1 °C associated with mild winter (soil frost occurred rarely) and less number of rain events were observed. In 2008, the amount of precipitation reached the regular level, but the annual mean temperature remained 1 °C higher as in 2007. The year of 2010 had extra amount of precipitation (it was one of the most wet of the last 100 years; <http://www.met.hu>) and differs from the long-term statistical averages (see in *Figs. 2 and 3*). For this reason, all the circumstances and conditions are different from the previous years.

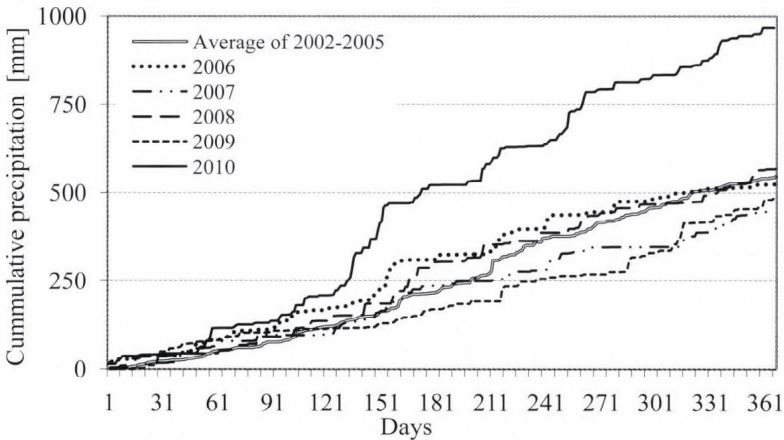


*Fig. 2.* Cumulative precipitation for the last decade at Bugacpuszta station.

N-compounds can easily be leached into the soil by rain, while canopy can retain dry deposited nitrogen through the N-uptake by stomatae or cuticles, which also depends on the meteorological conditions (*Horváth et al., 1999*). For this reason, in drier years less amount of deposited, reaches the topsoil layers

nitrogen and it can limit the mineral N-conversion to gases (through denitrification and nitrification processes). Reduced availability of soil mineral nitrogen may limit the plant uptake and probably impacts on the plant physiology and biomass production of different species; nevertheless, changes of plant species composition or coverage of plant functional group are not observed. Further research of N-linkage to the coenological experiment of grassland association is needed in the future.

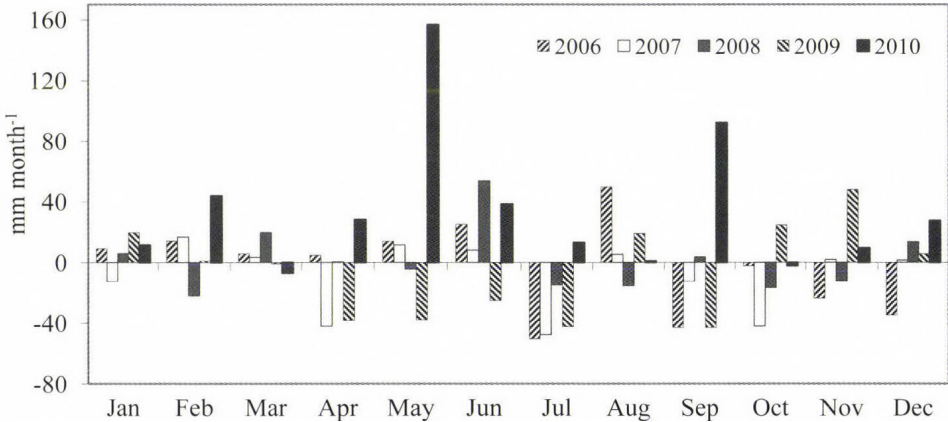
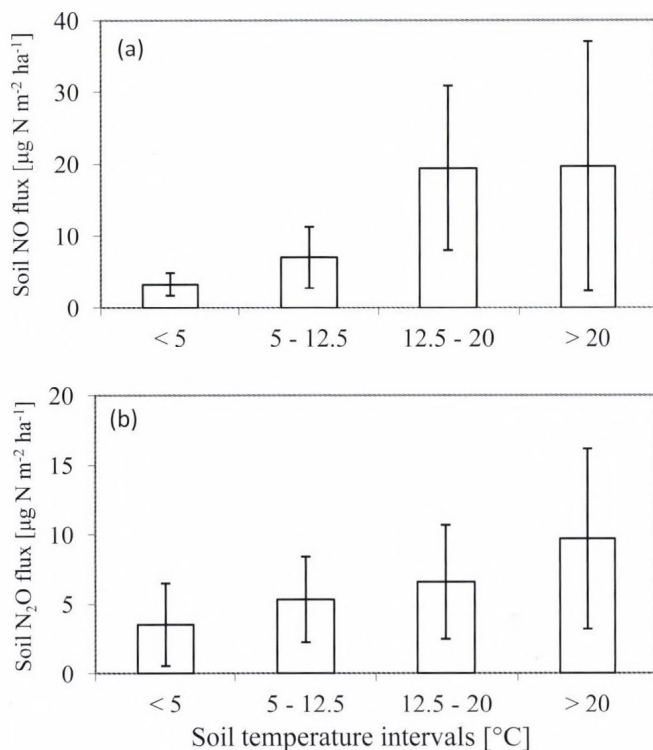


Fig. 3. Deviation of monthly precipitation of the studied years from the average of long term period (1986–2006) at Bugacpuszta station.

NO and N<sub>2</sub>O soil emissions as consequences of nitrification and denitrification are, like all biological processes, influenced by temperature and correlate with the soil temperature as many studies discussed before (Smith *et al.*, 1998; Gödde and Conrad, 1999; Horváth *et al.*, 2010), but sometimes the correlation remains poor or not readily understandable (Clayton *et al.*, 1997). With increasing soil temperature, the NO flux increases faster than N<sub>2</sub>O up to 20 °C; until the role of other factors (e.g., water stress, nutrient supply, and other complex processes linked to heat stress) will determine the rate of metabolism of soil microorganisms (see Fig. 4). The relatively high soil N<sub>2</sub>O flux under 5 °C could be the reason of thawing period after 2–3 month wintertime which resulting in high emission peaks for a few days even at low soil temperature (Priemé and Christensen, 2001; Müller *et al.*, 2002).

The optimal soil wetness for NO and N<sub>2</sub>O is ranged around 20–30% and 40–50%, respectively (see Fig. 5) for this sandy soil. The optimal WFPS content is reached only in 2010 for N<sub>2</sub>O. High water content (WFPS > 70%) was rarely observed, so the dependence of N-gas production on soil humidity is incomplete, but we expect (according to earlier studies) that emissions of both gases are continuously suppressed with higher WFPS content (Horváth *et al.*, 2010).

It should be noted that the soil water filled pore space can not explain all of the variations of  $N_2O$  fluxes (see *Fig. 4b*). It seems to be more likely, that soil temperature usually generate short-term variations of the trace gas exchange, whereas the magnitude of the biogenic emission is predominantly influenced by soil wetness, and other factors (*Meixner and Yang, 2004*).



*Fig. 4.* Variation of nitric oxide flux (a) and nitrous oxide flux (b) as a function of soil temperature at Bugacpuszta station.

On the other hand, *Kool et al. (2007, 2009a)* studied our soils by incubation technique using isotope tracers of oxygen and nitrogen, when O-exchange between water and intermediate forms of the N-transformations were measured. By this novel approach they showed that nitrifier denitrification (nitrite reduction by ammonia oxidizers) can be a contributor to the majority of  $N_2O$  production at Bugacpuszta site, thus,  $N_2O$  can be produced at lower water content – this phenomenon may explain the secondary higher emission on low (20–30%) WFPS – see in *Fig. 5b*. This biochemical pathway also demonstrates that pH may be the major factor determining nitrifier-induced  $N_2O$  production,

and the community of microorganisms may not be the key driver in different pathways of  $N_2O$  formation (Kool *et al.*, 2010). By this methodology it was also observed that water is effectively the main oxygen source (instead of  $O_2$  as it was assumed earlier) in  $N_2O$  formation and possibly in the formation of other nitrogen oxides in some European soil samples including Bugacpuszta. The oxygen isotopic measurement of  $N_2O$  showed that in Bugacpuszta the soil  $NH_4^+$  can be the nitrogen source (and it does not necessarily reflect that  $NO_3^-$  is functioning as a substrate) in  $N_2O$  formation though the nitrifier denitrification as an alternative pathway of metabolism of microorganisms (Kool *et al.*, 2009b). Further investigations are needed for better understanding the metabolism processes.

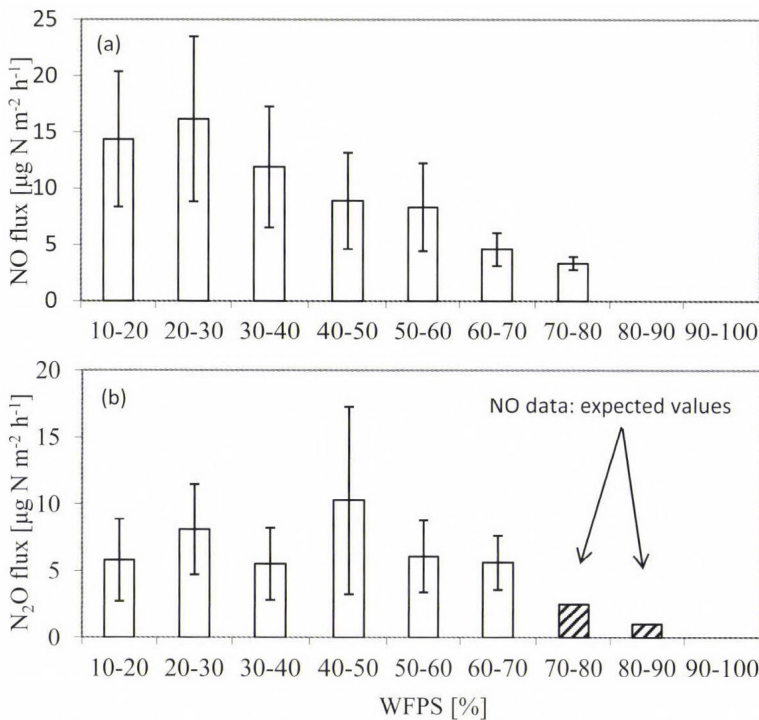


Fig. 5. Variation of nitric oxide flux (a) and nitrous oxide flux (b) as a function of water filled pore space at Bugacpuszta station.

The changes in N-exchange may impact on the carbon cycle as well as on plant uptake leading to opening up and desertification of the grassland, in spite of the fact that the studied ecosystem is evolved and more adapted to drought (in terms of NEE, etc.) than other grasslands (Pintér *et al.*, 2008).

#### 4. Conclusions

Weather perturbations can substantially modify both timing and magnitude of N-deposition and soil N-gas emission. In summertime, parallel with the precipitation deficit, less easily available nitrogen is deposited to the surface leaching to the rooting zone; thus, it can limit the mineral N uptake by plants or may affect the soil emission (through suppress of microbial processes) of N-gases during the main vegetation period.

Summarizing, many soil process (e.g., nitrification, denitrification, N-leaching) are strongly depend on soil temperature and precipitation as ecological drivers. The changes in these parameters influence directly the soil nitrogen gas emission rates, though the complex system of the relationships makes it difficult to explain all changes of NO and N<sub>2</sub>O formation. Though NO flux was higher than N<sub>2</sub>O flux, the soil emission was an order of magnitude lower than the atmospheric deposition (see *Table 1*).

The seasonal fluctuation of N<sub>2</sub>O and NO emission has been mainly influenced by precipitation. N<sub>2</sub>O emissions were not significant in the N-budget at this site in the last years. Reduced N<sub>2</sub>O emission (occurring through desertification due to perturbed climate conditions) means a potential negative feedback to the greenhouse effect. On the other hand, the vegetation can turn into being a net CO<sub>2</sub> source in extremely dry years like 2003 and 2007 (*Pintér et al.*, 2008; *Barcza et al.*, 2009) as a positive feedback for climate change. The ratio and strength of this two phenomena can not be neglected, since the area of temperate grass covered surface is large and will be increasing with increasing aridity of climate (and/or agricultural policy of Hungary). Extended periods of soil water deficit and high air and soil temperatures can affect a wide range of plant physiological functions. The plant communities will be frequently exposed to naturally induced droughts and should become open grassland in accordance with the value of the changing weather conditions.

Due to the forecasted potentially drying Hungarian climate, more frequent natural fires, as ecosystem function distractions, will occur in the dry sandy grassland (Hungarian Great Plain). The estimated nitrogen loss by fires equals to or even exceeds the amount of nitrogen from atmospheric deposition.

Based on the observed phenomena, it can be concluded that climate extremes are significant factors in soil organism functioning and dynamics of N-exchange and emissions. As a result, the N-content of the soil is continuously changing with the climatic anomalies (*Czóbel et al.*, 2008) due to the pool of NH<sub>4</sub><sup>+</sup> and NO<sub>3</sub><sup>-</sup> – which depends on the N-consumption and exchange of soil microbial community – affecting the plant N-uptake (demand), plant growth, etc. The living roots and bacteria are competitors for the same nutrients, so plants also induce effect on soil N-transformations. Further research relating to soil biochemistry in natural grasslands is also needed. Compared to the average of earlier years (13.8 kg N ha<sup>-1</sup>; *Kugler et al.*, 2008), less nitrogen deposited onto

the surface (11.2 and 11.7 kg N ha<sup>-1</sup>) in the driest period (2006 and 2007) and more nitrogen deposited (15.0 and 14.5 kg N ha<sup>-1</sup>) in the wetter years (2008 and 2010) during the study period. Wet deposition of nitrate and ammonium together with the dry flux of ammonia and nitric acid vapor is responsible for the majority (80%) of the net N-deposition flux. Seasonal and annual variation of N-gas emissions and N-deposition can be considerable, but precipitation, soil moisture, air and soil temperature, as easily measured parameters, can more or less explain this variability.

**Acknowledgements**—The authors are grateful for the permission of the Management of Kiskunság National Park to conduct the studies in the territory of the national park near Bugacpuszta. This work has been supported by the NitroEurope Framework EU 6th IP, by the National Research and Innovation Programs (NKFP/088/2004, NKFP6- 00028/2005 and NKFP6-00079/2005), COST Action 0804, and partly supported by the European Union and co-financed by the European Social Fund grant agreement (No. TAMOP 4.2.1/B-09/1/KMR-2010-0003).

## References

- Ammann, C., Spirig, C., Leifeld, J., and Neftel, A., 2009: Assessment of the nitrogen and carbon budget of two managed temperate grassland fields. *Agr. Ecosyst. Environ.* 133, 150–162.
- Balogh, J., Czöbel, Sz., Fóti, Sz., Nagy, Z., Szirmai, O., Péli, E. and Tuba, Z., 2005: The influence of drought on carbon balance in loess grassland. *Cereal Res. Commun.* 33, 149–152.
- Balogh, J., Biró, M. and Pintér, K., 2008: Root respiration in dry grassland. *Cereal Res. Commun.* 36, Supl. 355–358.
- Barcza, Z., Haszpra, L., Somogyi, Z., Hidy, D., Lovas, K., Churkina, G. and Horváth, L., 2009: Estimation of the biospheric carbon dioxide balance of Hungary using the BIOME-BGC model. *Időjárás* 113, 203–219.
- Clayton, H., Arah, J.R.M. and Smith, K.A., 1994: Measurement of nitrous oxide emissions from fertilized grassland using closed chambers. *J. Geophys. Res.* 99, 16599–16607.
- Clayton, H., McTaggart, I.P., Parker, J., Swan, L. and Smith, K.A., 1997: Nitrous oxide emission from fertilized grassland: A 2-year study of the effects of N fertilizer form and environmental conditions. *Biol. Fertil. Soils* 25, 252–260.
- Christensen, S., Ambus, P., Arah, J.R.M., Clayton, H., Galle, B., Griffith, D.W.T., Hargreaves, K.J., Klemetsson, L., Lind, A.-M., Maag, M., Scot, A., Skiba, U., Smith, K.A., Welling, M. and Wienhold, F.G., 1996: Nitrous oxide emission from an agricultural field: comparison between measurements by flux chamber and micro-meteorological techniques. *Atmos. Environ.* 30, 4183–4190.
- Conrad, R., 1996: Soil Microorganisms as controllers of atmospheric trace gases (H<sub>2</sub>, CO, CH<sub>4</sub>, OCS, N<sub>2</sub>O, and NO). *Microbiological Reviews* 60, 609–640.
- Czöbel, Sz., Balogh, J., Fóti, Sz. and Szirmai, O., 2008: Temporal changes in biomass and soil element contents under different manipulations of temperate grassland. *Cereal Res. Commun.* 36, 1963–1966.
- EEA (European Environment Agency), 2004: *Impacts of Europe's changing climate. An indicator-based assessment*. Luxembourg, Office for Official Publications of the European Communities — pp. 107, ISBN 92-9167-692-6.
- EMEP, 1996: Manual for sampling and chemical analysis. EMEP/CCC-Report 1/95, NILU, Kjeller, Norway.
- Flechard, C.R., Ambus, P., Skiba, U., Rees, R.M., Hensen, A., van Amstel, A., van den Pol-van Dasselaar, A., Soussana, J.-F., Jones, M., Clifton-Brown, J., Raschi, A., Horvath, L., Neftel, A., Jocher, M., Ammann, C., Leidfield, J., Fuhrer, J., Calanca, P.L., Thalman, E., Pilegaard, K., Di Marco, C., Campbell, C., Nemitz, E., Hargreaves, K.J., Levy, P., Ball, B.C., Jones, S., van de Bulk, W.C.M.,

- Groot, T., Blom, M., Domingues, R., Kasper, G., Allard, V., Ceshia, E., Cellier, P., Laville, P., Henault, C., Bizouard, F., Abdalla, M., Williams, M., Baronti, S., Berretti, F. and Grosz, B., 2007: Effects of climate and management intensity on nitrous oxide emissions in grassland systems across Europe. *Agr. Ecosyst. Environ.* 121, 135–152.
- Gödde, M. and Conrad, R., 1999: Immediate and adaptational temperature effects on nitric oxide production and nitrous oxide release from nitrification and denitrification in two soils. *Biol. Fertil. Soils* 30, 33–40.
- Horváth, L., Christensen, S., Führer, E., Kelecsényi, S., Mészáros, R., Nagy, Z. and Weidinger, T., 1999: A preliminary estimation of the nitrogen compounds exchange between the atmosphere and a Spruce forest. *Időjárás* 103, 1–18.
- Horváth, L., Asztalos, M., Führer, E., Mészáros, R. and Weidinger, T., 2005: Measurement of ammonia exchange over grassland in the Hungarian Great Plain. *Agr. Forest Meteorol.* 130, 282–298.
- Horváth, L., Führer, E. and Lajtha, K., 2006: Nitric oxide and nitrous oxide emission from Hungarian forest soils; linked with atmospheric N-deposition. *Atmos. Environ.* 40, 7786–7795.
- Horváth, L., Grosz, B., Machon, A., Balogh, J., Pintér, K. and Czóbel, Sz., 2008: Influence of soil type on N<sub>2</sub>O and CH<sub>4</sub> soil fluxes in Hungarian grasslands. *Community Ecol.* 9 (Suppl): 75–80.
- Horváth, L., Grosz, B., Machon, A., Tuba, Z., Nagy, Z., Czóbel, Sz., Balogh, J., Péli, E., Fóti, Sz., Weidinger, T., Pintér, K. and Führer, E., 2010: Estimation of nitrous oxide emission from Hungarian semi-arid sandy and loess grasslands; effect of grazing, irrigation and application of fertilizer. *Agr. Ecosyst. Environ.* 139, 255–263.
- Kool, D.M., Wrage, N., Oenema, O., Dolfing, J. and Van Groenigen, J.W., 2007: Oxygen exchange between (de)nitrification intermediates and H<sub>2</sub>O and its implications for source determination of NO<sub>3</sub><sup>-</sup> and N<sub>2</sub>O: a review. *Rapid Commun. Mass Spectrom.* 21, 3569–3578.
- Kool, D.M., Müller, C., Wrage, N., Oenema, O. and Van Groenigen, J.W., 2009a: Oxygen exchange between nitrogen oxides and H<sub>2</sub>O can occur during nitrifier pathways. *Soil Biol. Biochem.* 41, 1632–1641.
- Kool, D.M., Wrage, N., Oenema, O., Harris, D. and Van Groenigen, J.W., 2009b: The 18O signature of biogenic nitrous oxide is determined by O exchange with water. *Rapid Commun. Mass Spectrom.* 23, 104–108.
- Kool, D.M., Wrage, N., Zechmeister-Boltenstern, S., Pfeffer, M., Brus, D., Oenema, O., Van Groenigen, J.W., 2010: Nitrifier denitrification can be a source of N<sub>2</sub>O from soil: a revised approach to the dual isotope labelling method. NitroEurope Open Science Conference: Reactive Nitrogen and the European Greenhouse Gas Balance. February 3–4, 2010, Solothurn, Switzerland. Book of abstracts: pp. 12.
- Kugler, Sz., Horváth, L. and Machon, A., 2008: Estimation of nitrogen balance between the atmosphere and Lake Balaton and a semi natural grassland in Hungary. *Environ. Pollut.* 154, 498–503.
- Levy, P.E., Mobbs, D.C., Jones, S.K., Milne, R., Campbell, C. and Sutton, M.A., 2007: Simulation of fluxes of greenhouse gases from European grasslands using the DNDC model. *Agr. Ecosyst. Environ.* 121, 186–192.
- Machon, A., Horváth, L., Weidinger, T., Grosz, B., Pintér, K., Tuba, Z. and Führer, E., 2010: Estimation of net nitrogen flux between the atmosphere and a semi-natural grassland ecosystem in Hungary. *Eur. J. Soil Sci.* 61, 631–639.
- Meixner, F.X. and Yang, W.X., 2004: Biogenic emissions of nitric oxide and nitrous oxide from arid and semi-arid land. In *Dryland Ecohydrology*, (eds.: P. D'Odorico and A. Porporato.), pp. 23–46. Kluwer Academic Publishers B.V., Dordrecht, Netherlands.
- Müller, C., Martin, M., Stevens, R.J., Laughlin, R.J., Kamman, C., Ottow, J.C.G. and Jager, H.J., 2002: Processes leading to N<sub>2</sub>O emissions in grassland soil during freezing and thawing. *Soil Biol. Biochem.* 34, 1325–1331.
- Nagy, Z., Czóbel, Sz., Balogh, J., Horváth, L., Fóti, Sz., Pintér, K., Weidinger, T., Csintalan, Zs. and Tuba Z., 2005: Some preliminary results of the Hungarian grassland ecological research: carbon cycling and greenhouse gas balances under changing. *Cereal Res. Commun.* 33, 279–281.
- Nagy, Z., Pintér, K., Czóbel, Sz., Balogh, J., Horváth, L., Fóti, Sz., Barcza, Z., Weidinger, T., Csintalan, Zs., Dinh, N.Q., Grosz, B. and Tuba, Z., 2007: The carbon budget of semi-arid grassland in a wet and a dry year in Hungary. *Agr. Ecosyst. Environ.* 121, 21–29.

- Pintér, K., Barcza, Z., Balogh, J., Czóbel, Sz., Csintalan, Zs., Tuba, Z. and Nagy, Z., 2008: Interannual variability of grasslands' carbon balance dependson soil type. *Community Ecol.* 9 (Suppl.): 43–48.
- van den Pol-van Dasselaar, A., van Beusichem, M.L. and Onema, O., 1998: Effects of soil moisture content and temperature on methane uptake by grasslands on sandy soils. *Plant Soil* 204, 213–222.
- Priemé, A. and Christensen, S., 2001: Natural perturbations, drying-wetting and freezing-thawing cycles, and the emission of nitrous oxide, carbon dioxide and methane from farmed organic soils. *Soil Biol. Biochem.* 33, 2083–2091.
- Reich, P.B., Hobbie, S.E., Lee, T., Ellsworth, D.S., West, J.B., Tilman, D., Knops, J.M.H., Naeem, S. and Trost, J., 2006: Nitrogen limitation constrains sustainability of ecosystem response to CO<sub>2</sub>. *Nature* 440, 922–925.
- Schimel, D., Braswell, B., McKeown, R., Ojima, D., Parton, W. and Pulliam, W., 1996: Climate and Nitrogen controls on the geography and timescales of terrestrial biogeochemical cycling. *Global Biogeochem. Cycles* 10, 677–692.
- Schindlbacher, A., Zechmeister-Boltenstern, S. and Butterbach-Bahl, K., 2004: Effect of soil moisture and temperature on NO, NO<sub>2</sub>, and N<sub>2</sub>O emissions from European soils. *J. Geophys. Res.* 109, D17302.
- Skiba, U., Drewer, J., Tang, Y.S., van Dijk, N., Helfter, C., Nemitz, E., Famulari, D., Cape, J.N., Jones, S.K., Twigg, M., Pihlatie, M., Vesala, T., Larsen, K.S., Carter, M.S., Ambus, P., Ibrom, A., Beier, C., Hensen, A., Frumau, A., Erisman, J.W., Brüggemann N., Gasche, R., Butterbach-Bahl, K., Neftel, A., Spirig, C., Horvath, L., Freibauer, A., Cellier, P., Laville, P., Loubet, B., Magliulo, E., Bertolini, T., Seufert, G., Andersson, M., Manca, G., Laurila, T., Aurela, M., Lohila, A., Zechmeister-Boltenstern, S., Kitzler, B., Schauffler, G., Siemens, J., Kindler, R., Flechard, C. and Sutton, M.A., 2009: Biosphere–atmosphere exchange of reactive nitrogen and greenhouse gases at the NitroEurope core flux measurement sites: Measurement strategy and first data sets. *Agr. Ecosyst. Environ.* 133, 139–149.
- Smith, K.A., Thomson, P.E., Layton, H., McTaggart, I.P. and Conen, F., 1998: Effects of temperature, water content and nitrogen fertilization on emission of nitrous oxide by soils. *Atmos. Environ.* 32, 3301–3309.
- Smith, K.A., Ball, T., Conen, F., Dobbie, K.E., Massheder, J. and Rey, A., 2003: Exchange of greenhouse gases between soil and atmosphere: interactions of soil physical factors and biological processes. *European Journal of Soil Science* 54, 779–791.
- Soussana, J.F. and Hartwig, U.A., 1996: The effects of elevated CO<sub>2</sub> on symbiotic N<sub>2</sub> fixation: A link between carbon and nitrogen cycles in grassland ecosystems. *Plant Soil* 187, 321–332.

Internet sources:

[http://www.met.hu/eghajlat/visszatekinto/elmult\\_evszazad/](http://www.met.hu/eghajlat/visszatekinto/elmult_evszazad/)

# IDŐJÁRÁS

*Quarterly Journal of the Hungarian Meteorological Service  
Vol. 115, No. 4, October–December 2011, pp. 233–245*

## **Integration of meteo-climatic and remote sensing information for the analysis of durum wheat quality in Val d'Orcia (Tuscany, Italy)**

**Simone Orlandini<sup>\*1</sup>, Marco Mancini<sup>1</sup>, Grifoni Daniele<sup>2</sup>,  
Francesca Orlando<sup>1</sup>, Anna Dalla Marta<sup>1</sup>, and Valerio Capecchi<sup>2</sup>**

<sup>1</sup>*Department of Plant, Soil and Environmental Science,  
University of Florence  
Piazzale delle Cascine 18, 50144 Florence, Italy*

<sup>2</sup>*CNR–Institute of Biometeorology,  
Via Caproni 8, 50145 Florence, Italy*

*\*Corresponding author; E-mail: [simone.orlandini@unifi.it](mailto:simone.orlandini@unifi.it)*

*(Manuscript received in final form May 13, 2011)*

**Abstract**—Climatic and weather conditions largely affect agricultural activities, modifying plant responses and determining the quantity and quality of products. In this respect, the aim of this research was to analyze the quality of winter durum wheat (*Triticum turgidum* L. var. *durum*) in terms of protein content (%) and test weight through the combined use of meteorological information from ground stations and remote sensing. Meteorological conditions were described using both temperature and precipitation from ground weather stations and the North Atlantic Oscillation (NAO) index. The spectral index used for monitoring the crop was the Normalized Difference Vegetation Index (NDVI). The analysis was carried out for the period 1999–2009 in Tuscany, Central Italy.

Air temperature of the period from February to June was positively correlated with grain protein concentration, while test weight showed negative correlations to temperature in March and May and for all multi-monthly periods starting from March onward. Grain protein concentration appeared as negatively correlated with precipitation cumulated during the entire period from November to June, while no significant effect was observed in test weight. With regard to the NAO, higher correlations to protein content were found for the monthly values of November and February, but more significant results were obtained by aggregating NAO index on a multi-monthly basis when November and February were included. On the other hand, the correlations were negative between the winter NAO index and the specific weight mainly in February and for the period from February to March. Finally, NDVI starting from mid May showed to be negatively related to protein content and positively to test weight. These results demonstrated that precipitation and air temperature over the production area represent

two crucial variables affecting growth and development of winter durum wheat. On the other hand, the use of large-scale meteorological information and specific spectral indices showed a great possibility in the perspective of a local quality forecast system setup.

*Key-words:* Triticum durum, protein content, specific weight, meteorological information, Normalized Difference Vegetation Index (NDVI), North Atlantic Oscillation index (NAO)

## 1. Introduction

Cereals are a key product of Italian agriculture, both in terms of direct annual consumption and of the food processing industry's demand. In 2009, Italian wheat production was 6.3 million tons, making it the second most-produced cereal after maize (7.9 million tons; *EUROSTAT*, 2010). In particular, winter durum wheat (*Triticum turgidum* L. var. *durum*) represents approximately 40% of cultivated wheat of area of production (*EUROSTAT*, 2010). In fact, winter durum wheat provides the raw material for the pasta industry, and a progressively higher amount is also required for the production of special breads, typical products of the southern part of the country. For these reasons, the effect of weather patterns on winter durum wheat is of primary interest. Due to the water shortage and climatic adversities characterizing the cultivation areas, the qualitative and quantitative planning of production is very uncertain and represents an important challenge (*MIPAAF*, 2009).

Most of winter durum wheat in Italy is sown in November and harvested at the beginning of July of the following year. The stem elongation phase starts in April, when the average temperature is 10–12 °C, while ripening starts when the average temperature reaches 18–20 °C. Shooting, grain filling, and grain ripening are the most important development phases that determine the final quality of the grains, so that weather conditions during these periods are crucial for determining the characteristics of production (*Paredes-Lopez et al.*, 1985; *Ciaffi et al.*, 1996).

Several studies confirmed that meteorological factors strongly affect wheat cultivation, by modifying plant responses and determining the final yield and the quality of production.

In general, meteorological variables such as temperature (*Benzian and Lane*, 1986; *Smith and Gooding*, 1999; *Daniel and Triboi*, 2000), sunshine (*Spiertz*, 1977), and rainfall (*Hopkins*, 1968; *Faridi and Finley*, 1989; *Bassett et al.*, 1989; *Powlson et al.*, 1992) during grain filling can largely affect the specific weight, the protein content and its composition of wheat grains, as well as the final yield. In UK, the specific weight of wheat grains was correlated negatively with summer precipitation and positively with cumulative sunshine (*Kettlewell et al.*, 2003; *Atkinson et al.*, 2008).

In Australia, the cumulated precipitation during the period from May to September is negatively associated with grain protein content (*Correll et al.*,

1994), while rising temperature after anthesis may increase the grain nitrogen concentration (Kolderup, 1975; Sofield *et al.*, 1977). While spring temperature exceeding 30 °C may increase the protein content (Pan *et al.*, 2006), heat stress can cause a reduction of kernel weight and diameter (Labuschagne *et al.*, 2009).

The use of large-scale climatic variables has also been investigated in order to forecast agricultural yields and product quality in several regions of the world (Atkinson *et al.*, 2005). Among these variables and indices that identify the large-scale distribution of air pressure and temperature over defined geographical areas, the Sea Surface Temperature (SST), the El Nino Southern Oscillation (ENSO), and the North Atlantic Oscillation (NAO) are the most studied due to their significant impact on the climate of important production regions worldwide. In Spain, Gimeno *et al.* (2002) found that the yields of many crops (lemon, orange, tangerine, wheat, rye, and olive) were affected by the variations of ENSO and NAO, while in Italy, the effect of NAO, together with 500 hPa geopotential height and SST were related to the quality of wine and durum wheat (Grifoni *et al.*, 2006; Dalla Marta *et al.*, 2010). Many studies demonstrated a relationship between the wheat grain quality (Hagberg falling number, specific weight, and protein concentration) and the winter NAO in the UK (Kettlewell *et al.*, 1999; Wanner *et al.*, 2001; Hurrell *et al.*, 2003; Atkinson *et al.*, 2005; Atkinson *et al.*, 2008). According to Kettlewell *et al.* (2003), the winter NAO has an effect on cumulated precipitation during summer in England and Wales and, consequently, on wheat quality, while Colman (1997) suggested an association between SST and NAO in the UK.

Beside the use of meteorological information and numerical model outputs, numerous studies have related to various vegetation indices, of which the normalized difference vegetation index (NDVI) is the most widespread, with crop vigour and biomass (Filella and Penuelas, 1994; Broge and Lebanco, 2001). Optical remote sensing data have also been used to predict quantitative performances of crops, such as grain yield (Labus *et al.*, 2002; Singh *et al.*, 2002) and biomass production (Filella and Penuelas, 1994; Broge and Lebanco, 2001). In particular, NOAA-AVHRR NDVI data were related to wheat yield over Italy (Rossini and Benedetti, 1993) and used for wheat yield estimation over North Africa (Maselli and Rembold, 2001). Other studies integrated the remote sensing data with crop simulation models for the assessment of crop yield at a regional scale (Moriondo *et al.*, 2007).

On the other hand, there are a few reports on forecasting grain quality, such as protein content, from optical remote sensing data (Hansen *et al.*, 2002; Basnet *et al.*, 2003; Liu *et al.*, 2006).

The main objective of this paper is to analyze the effectiveness of the combined use of large-scale meteorological information and remote sensing imagery, freely available on internet, in analyzing and predicting the winter durum wheat quality in Tuscany (Central Italy).

## 2. Materials and methods

The research was carried in Val d'Orcia, a large region of central Italy (Tuscany), where winter durum wheat is considered an important quality production, and about 15% of the total cultivated surface is allotted to this crop. The study area is characterized by a typical Mediterranean climate, mainly affected by the Azores and Russian anticyclones and by Mediterranean depressions, with a mean annual temperature of about 13.6 °C and a cumulated precipitation of 715 mm, mostly distributed during winter and autumn.

The characteristics of winter durum wheat taken into consideration were the protein content and test weight, mainly related to the production of good quality pasta, to the economics of grain transport, and to milling characteristics.

Data of grain protein content (%) and test weight (kg hl<sup>-1</sup>) were supplied by the Consorzio Agrario di Siena for the period 1999–2009. Wheat varieties used for this study had similar characteristics and, during the period analyzed, nitrogen fertilization and crop management remained constant. In particular, the fertilization applied was the standard one for the study area with 160 kg ha<sup>-1</sup> of nitrogen applied in three times and 90 kg ha<sup>-1</sup> of P<sub>2</sub>O<sub>5</sub> applied before sowing. The soil was clay loam.

Air temperature and precipitation (years 1999–2009) were supplied as the mean of five ground stations, in order to most accurately represent the mean meteorological conditions of the production area.

Moreover, the NAO index was used. The NAO is a large-scale mode of natural climate variability that has an important impact on the weather and climate of the North Atlantic region and surrounding continents, especially Europe. The NAO can be described as a temporal fluctuation of the zonal wind strength across the Atlantic Ocean due to pressure variations in both the subtropical anticyclone belt and the subpolar low near Iceland. It is particularly important in winter (December–March), when it exerts a strong control over the climate of the Northern Hemisphere showing a significant relationship with storm track, temperature, and precipitation (Hurrell and van Loon, 1997). The strength of the NAO is described by the NAO index. It is traditionally defined as the normalized pressure difference between a station in the Azores and one in Iceland. An extended version of the index can be obtained for the winter half of the year by using a station in the southwestern part of the Iberian Peninsula (Hurrell, 1995). Jones *et al.* (1997) used early instrumental data to extend the NAO index calculated from Gibraltar and Iceland back to 1823. In this study, we used this last version of the index (<http://www.cru.uea.ac.uk/>). The NAO index varies from year to year, but also exhibits a tendency to remain in one phase (positive or negative) for intervals lasting several years.

The NDVI was calculated using satellite data derived from the AVHRR sensor. The imagery, downloaded from the website “Free vegetation products” (<http://www.free.vgt.vito.be>) for the period from November 1988 to June 2009,

were acquired by the satellite SPOT (Satellite Pour l'Observation de la Terre). The spatial resolution was about  $1 \text{ km} \times 1 \text{ km}$  and time resolution was ten days.

All the considered variables were correlated to wheat protein content and specific weight on a monthly and multi-monthly basis, and all possible combinations were investigated in order to identify the periods during which each variable or index is mainly able to affect or predict the final quality.

Moreover, stepwise multiple regressions between winter durum wheat quality data and the best single descriptors were applied in order to identify the best predictive model (SPSS 15.0).

### 3. Results and discussion

Individual, monthly air temperature levels were not significantly correlated with protein content, however, persistent positive correlations were observed from February to June with the highest values for April followed by May and June, respectively. The multi-monthly analysis showed significant positive correlations between protein content and air temperature observed from spring to early summer (*Fig. 1*). Concerning specific weight, negative correlations were significant in March and May and for all multi-monthly periods including March (*Fig. 2*).

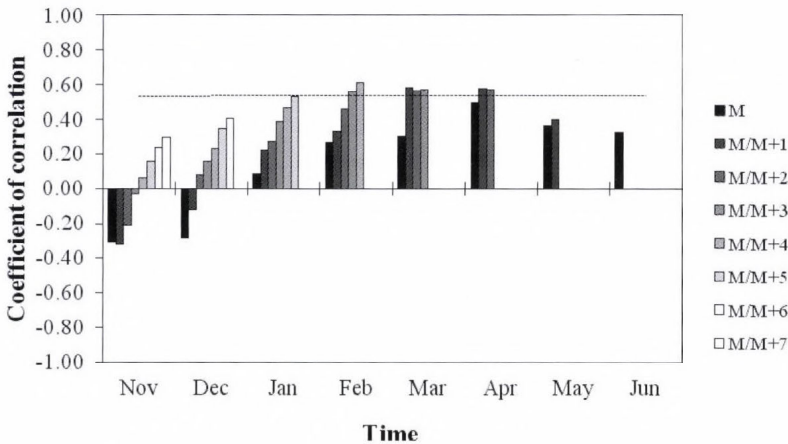


*Fig. 1.* Coefficient of correlation between protein content at the harvest and air temperature of the preceding single months in x axis ( $M$ ) and of the multi-monthly periods starting from each month ( $M$ ) and ending in one of the following months ( $M+1, \dots, M+n$ ). Dotted line represents the critical values of  $r$  for statistical significance at  $P \leq 0.05$ .

The positive effect of temperature, mainly spring-summer temperature on protein concentration is well known (*Benzian and Lane, 1986; Gooding and*

Davies, 1977; Motzo *et al.*, 2007). The duration of grain filling in wheat is strongly affected by temperature during this phase (Wheeler *et al.*, 1996) and smaller grains are often resulted from high temperature conditions because, even if the rate of grain growth is increased, this does not compensate for the reduced duration of grain growth. This effect of high temperature penalizes the accumulation of total carbohydrate, thus increasing the relative protein content and decreasing the test weight because of the final grain size and shape; and hence, the degree of dilution of accumulated nitrogen is closely related to the length of time the crop stays green after flowering (Spiertz, 1977; Smith and Gooding, 1999).

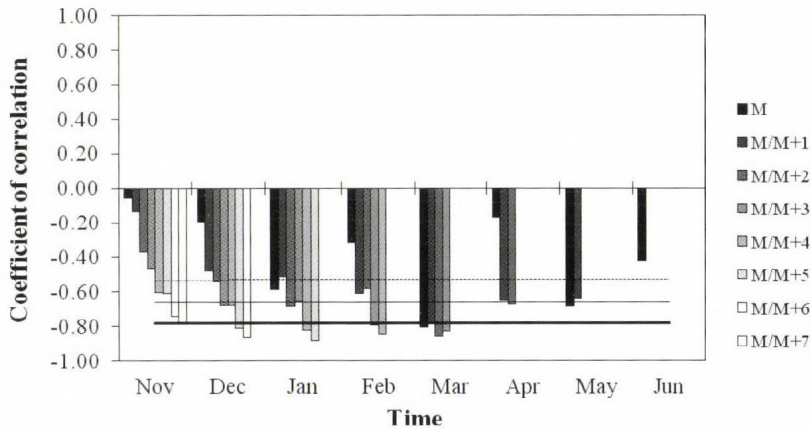


Fig. 2. Coefficient of correlation between specific weight at the harvest and air temperature of the preceding single months listed in x axis ( $M$ ) and of the multi-monthly periods starting from each month ( $M$ ) and ending in one of the following months ( $M+1, \dots, M+n$ ). Dotted line, thin and marked solid lines represent the critical values of  $r$  for statistical significance at  $P \leq 0.05$ ,  $P \leq 0.01$ , and  $P \leq 0.001$ , respectively.

Monthly precipitation was negatively correlated with protein concentration for the entire period from November to May. The higher and significant correlations were observed for November and April. The multi-monthly analysis showed a more complex situation, where significant negative correlations were mainly observed for periods including November (all the periods starting from November up to the end of the growing season) and April (Fig. 3). No significant correlation was found between rainfall and specific weight (data not shown), although other studies, carried on in the UK on wheat, showed a negative effect of precipitation during grain filling, mainly due to the alternate wetting and drying causing wrinkling of the grain surface (Kettlewell *et al.*, 2003; Atkinson *et al.*, 2008).

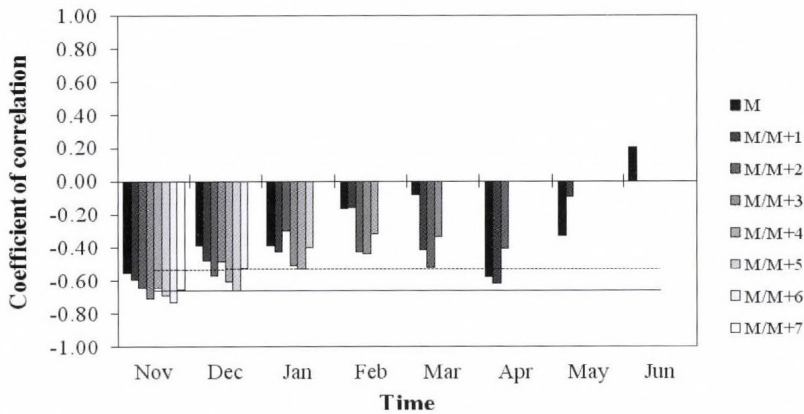


Fig. 3. Coefficient of correlation between protein content at the harvest and cumulated rainfall of the preceding single months listed in x axis ( $M$ ) and of the multi-monthly periods starting from each month ( $M$ ) and ending in one of the following months ( $M+1, \dots, M+n$ ). Dotted and solid lines represent the critical values of  $r$  for statistical significance at  $P \leq 0.05$  and  $P \leq 0.01$ , respectively

Rainfall and soil water availability reduces protein content because they enhance dilution of early nitrogen reserves by vegetative proliferation; it increases leaching and other forms of soil nitrogen losses and it may augment soil moisture reserves so that leaf life is extended during grain growth, favouring carbohydrate assimilation and translocation more than that of nitrogen; thus, a yield increase corresponds to a reduction in protein concentration (Schlehuber and Trucher, 1959; Hopkins, 1968; Taylor and Gilmour, 1971; Smith and Gooding, 1999; Oweis *et al.*, 1999).

As far as the NAO is concerned, winter durum wheat quality was positively correlated with the index several months, in particular during the winter period. Higher correlations on a monthly basis were found for November and February, and more significant results were obtained by aggregating the NAO index on a multi-monthly basis when November and February were included (Fig. 4). On the contrary, the correlations were negative between the winter NAO index and specific weight, mainly the index of February and for the period January–March (Fig. 5).

This result can be explained by the winter NAO index defining a specific atmospheric synoptical configuration over the Atlantic Ocean, affecting winter precipitation and winter and early spring temperatures over the Mediterranean sea and consequently over the study area (Hurrell and van Loon, 1997; Bartolini *et al.*, 2009). Winter durum wheat protein and specific weight were slightly stronger correlated with the NAO index than with cumulated precipitation and temperature, respectively, probably because the NAO index is able to better describe the environmental conditions (being a consequence of atmospheric circulation) rather than a single meteorological variable.

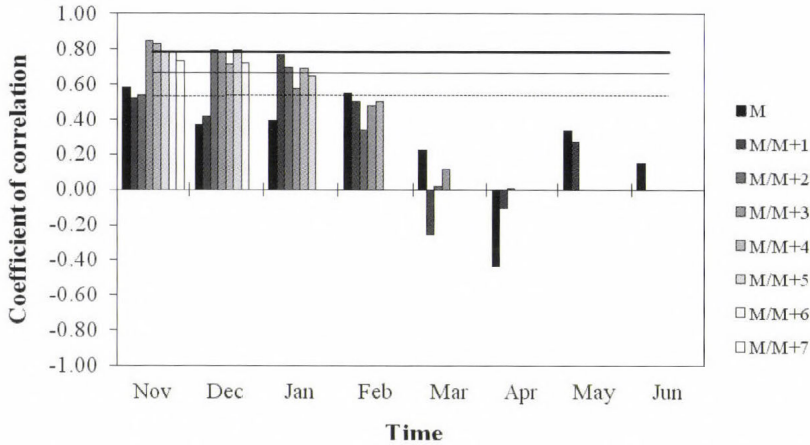


Fig. 4. Coefficient of correlation between protein content at the harvest and the NAO Index of the preceding single months listed in x axis ( $M$ ) and of the multi-monthly periods starting from each month ( $M$ ) and ending in one of the following months ( $M+1, \dots, M+n$ ). Dotted line, thin and marked solid lines represent the critical values of  $r$  for statistical significance at  $P \leq 0.05$ ,  $P \leq 0.01$ , and  $P \leq 0.001$ , respectively.

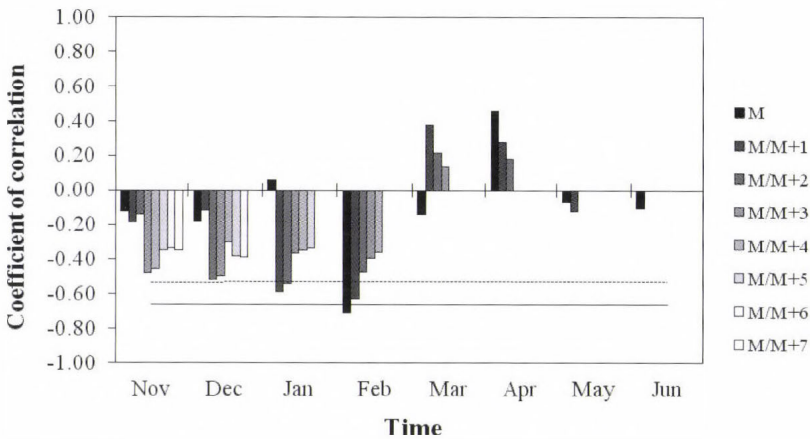


Fig. 5. Coefficient of correlation between specific weight at the harvest and the NAO Index of the preceding single months listed in x axis ( $M$ ) and of the multi-monthly periods starting from each month ( $M$ ) and ending in one of the following months ( $M+1, \dots, M+n$ ). Dotted and solid lines represent the critical values of  $r$  for statistical significance at  $P \leq 0.05$  and  $P \leq 0.01$ , respectively.

NDVI was significantly correlated with durum wheat quality parameters, negatively with protein content and positively with specific weight, starting from mid May to the end of the season (Tables 1 and 2).

Table 1. Coefficient of correlation ( $r$ ) between wheat protein content at harvest and NDVI for decadal and multi-decadal periods. The number after the month indicates the decade considered. Critical values of  $r$  for statistical significance are:  $r \geq 0.576$ ,  $P \leq 0.05^*$ ;  $r \geq 0.708$ ,  $P \leq 0.01^{**}$

<b>Apr3</b>	<b>Apr3–May1</b>	<b>Apr3–May2</b>	<b>Apr3–May3</b>	<b>Apr3–Jun1</b>	<b>Apr3–Jun2</b>	<b>Apr3–Jun3</b>
0.132	0.108	0.023	-0.303	-0.432	-0.665*	-0.685*
<b>May1</b>	<b>May1–May2</b>	<b>May1–May3</b>	<b>May1–Jun1</b>	<b>May1–Jun2</b>	<b>May1–Jun3</b>	
0.017	-0.106	-0.515	-0.646*	-0.726**	-0.735**	
<b>May2</b>	<b>May2–May3</b>	<b>May2–Jun1</b>	<b>May2–Jun2</b>	<b>May2–Jun3</b>		
-0.190	-0.428	-0.700*	-0.768**	-0.775**		
<b>May3</b>	<b>May3–Jun1</b>	<b>May3–Jun2</b>	<b>May3–Jun3</b>			
-0.787**	-0.425	-0.440	-0.443			
<b>Jun1</b>	<b>Jun1–Jun2</b>	<b>Jun1–Jun3</b>				
-0.606*	-0.766**	-0.774**				
<b>Jun2</b>	<b>Jun2–Jun3</b>					
-0.783**	-0.772**					
<b>Jun3</b>						
-0.667*						

Table 2. Coefficient of correlation ( $r$ ) between wheat specific weight at harvest and NDVI for decadal and multi-decadal periods. The number after the month indicates the decade considered. Critical values of  $r$  for statistical significance are:  $r \geq 0.576$ ,  $P \leq 0.05^*$ ;  $r \geq 0.708$ ,  $P \leq 0.01^{**}$ ;  $r \geq 0.823$ ,  $P \leq 0.001^{***}$

<b>Apr3</b>	<b>Apr3–May1</b>	<b>Apr3–May2</b>	<b>Apr3–May3</b>	<b>Apr3–Jun1</b>	<b>Apr3–Jun2</b>	<b>Apr3–Jun3</b>
0.184	0.312	0.417	0.689*	0.722**	0.771**	0.731**
<b>May1</b>	<b>May1–May2</b>	<b>May1–May3</b>	<b>May1–Jun1</b>	<b>May1–Jun2</b>	<b>May1–Jun3</b>	
0.350	0.576*	0.836***	0.717**	0.744**	0.708**	
<b>May2</b>	<b>May2–May3</b>	<b>May2–Jun1</b>	<b>May2–Jun2</b>	<b>May2–Jun3</b>		
0.501	0.693*	0.665*	0.713**	0.686*		
<b>May3</b>	<b>May3–Jun1</b>	<b>May3–Jun2</b>	<b>May3–Jun3</b>			
0.845***	0.782**	0.735**	0.695*			
<b>Jun1</b>	<b>Jun1–Jun2</b>	<b>Jun1–Jun3</b>				
0.376	0.593*	0.584*				
<b>Jun2</b>	<b>Jun2–Jun3</b>					
0.700*	0.633*					
<b>Jun3</b>						
0.466						

Protein concentration is often closely related to wheat yield, that is the parameter most widely monitored and predicted by the use of NDVI. Typically, wheat is fertilized during seeding to meet a specific yield and/or protein concentration potential based on available information on soil fertility, water holding capacity, and expected growing season rainfall (*Selles and Zentner, 1998*). If growing conditions are more favorable than anticipated, strong early growth of the crop will deplete soil nutrients leaving little for the critical grain filling period in wheat. This can often result in a high yield but lower protein concentration than desired. Thus, there is a common inverse relationship between wheat yield and protein concentration (*Siman, 1974*). For the same reason, a positive correlation was found between NDVI and specific weight.

The final step of this study was to evaluate the effect of all the considered variables as a whole by means of a stepwise linear multiple regression analysis. The model, based on an automatic procedure of variable inclusion/exclusion was tested by using the multi-monthly periods for which the best correlation coefficients were obtained for each single variable previously analyzed. In particular, for protein content the variables used were February–June air temperature, November–May precipitation, November–February NAO, and NDVI of the third decade of May. For the specific weight, the variables used were February NAO, January–June temperature, and NDVI of the third decade of May. In the first case, within the stepwise regression results, the simplest model was obtained using NAO index ( $R^2=0.822$ ), while the addition of temperature gave the best-fit model and resulted in an  $R^2$  of 0.905. Precipitation and NDVI were excluded, since their addition to the model failed to improve its performance. Concerning specific weight, the simplest and best-fit model was obtained using temperature data ( $R^2=0.781$ ), while the other variables considered were excluded.

#### 4. Conclusions

This paper investigates relations between climatic and weather conditions, information derived from remote sensing data and the quality of winter durum wheat cultivated in Val d'Orcia. The results demonstrated that precipitation and temperature over the production area represent two crucial variables, which drive the vegetative and productive responses of wheat. On the other hand, the use of large-scale meteorological information showed a great possibility. In fact, the correlation existing between the NAO index, partially determining the distribution of temperature and precipitation over the study area, and winter durum wheat protein content, seems to provide a great deal of information which is capable of summarizing the effect of climate on the qualitative characteristics. This assumption was confirmed by the multiple regression model that selected the NAO index and temperature as the best predictors of the final grain quality. On the other hand, also the analysis of NDVI showed its crucial

importance for predicting the final quality. In fact, already starting from May, about one month before the harvest, this index was strongly correlated to both quality characteristics considered. Moreover, indices derived from remote sensing have the advantage to well represent the spatial variability of the observed parameters.

For analyzing the effect of climate on winter durum wheat quality on the long term, the application of crop growth simulation models is desirable in order to create datasets that are unaffected by particular trends due to technological development or variety improvement. Then, the use of high resolution satellite imagery has to be analyzed for the monitoring of the crop at farm level.

Significant future applications of this knowledge are possible by the development of specific forecast tools. In fact, the analysis of such meteorological variables during specific times could be used to forecast the winter durum wheat quality of the following production with a certain level of accuracy. Moreover, the possibility of using meteorological information freely available on internet can reduce costs and spatial and temporal representativeness limitations related to weather monitoring in loco.

The importance of the above described studies is mostly related to the potential development of a winter durum wheat local quality forecast system in order to provide cereal growers, technicians and pasta producers with useful information on the potential quality of the following production. The integration of these results with operational climatic seasonal forecasts may, in fact, represent the basis of a provisional quality system to support the winter durum wheat production sector.

**Acknowledgments**—The authors wish to thank *Fondazione Monte dei Paschi di Siena* and *Consorzio Agrario di Siena*, for their support to this research, and *Federico Guasconi* for his help in data processing.

## References

- Atkinson, M.D., Kettlewell, P.S., Poulton, P.R. and Hollins, P.D., 2008: Grain quality in the Broadbalk wheat experiment and the winter North Atlantic Oscillation. *J. Agric. Sci.* 146, 541–549.
- Atkinson, M.D., Kettlewell, P.S., Hollins, P.D., Stephenson, D.B., and Hardwick, N.V., 2005: Summer climate mediates UK wheat quality response to winter North Atlantic Oscillation. *Agr. Forest Meteorol.* 130, 27–37.
- Bartolini, E., Claps, P. and D’Odorico, P., 2009: Interannual variability of winter precipitation in the European Alps: relations with the North Atlantic Oscillation. *Hydrol. Earth Syst. Sci.* 13, 17–25.
- Basnet, B., Apan, A., Kelly, R., Jensen, T., Strong, W. and Butler, D., 2003: Relating satellite imagery with grain protein content of grain crops. *Proceedings of the Spatial Sciences Conference*, Canberra, Australia (CD-ROM), 22–27.
- Bassett, L.M., Allen, R.E. and Rubenthaler, G.L., 1989: Genotype × environment interactions on soft white winter wheat quality. *Agron J.* 81, 955–960.
- Benjian, B. and Lane, P.W., 1986: Protein concentration of grain in relation to some weather and soil factors during 17 years of English winter-wheat experiments. *J. Sci. Food Agric.* 37, 435–444.

- Broge, N.H. and Lebane, E., 2001: Comparing prediction power and stability of broadband and hyperspectral vegetation indices for estimation of green leaf area index and canopy chlorophyll density. *Remote Sens. Environ.* 76, 156–172.
- Ciaffi, M., Tozzi, L., Borghi, B., Corbellini, M. and Lafiandra, D., 1996: Effect of heat shock during grain filling on the gluten protein composition of bread wheat. *J. Cereal Sci.* 24, 91–100.
- Colman, A., 1997: Prediction of summer central England temperature from preceding North Atlantic winter sea surface temperature. *Int. J. Climatol.* 17, 1285–1300.
- Correll, R., Butler, J., Spouncer, L. and Wrigley, C., 1994: The relationship between grain-protein content of wheat and barley and temperatures during grain filling. *Aus. J. Plant Physiol.* 21, 869–873.
- Dalla Marta, A., Grifoni, D., Mancini, M., Zipoli, G. and Orlandini, S., 2010: The influence of climate on durum wheat quality in Tuscany, Central Italy. *Int. J. Biometeorol.* DOI: 10.1007/s00484-010-0310-8.
- Daniel, C. and Triboui, E.J., 2000: Effects of temperature and nitrogen nutrition on the grain composition of winter wheat: effects on gliadin content and composition. *J. Cereal Sci.* 32, 45–56.
- Faridi, H. and Finley, J.W., 1989: Improved wheat for baking. *CRC Crit. Rev. Food Sci. and Nutr.* 28, 175–209.
- Filella, I. and Peñuelas, J., 1994: The red edge position and shape as indicators of plant chlorophyll content, biomass and hydric status. *Int. J. Remote Sens.* 15, 1459–1470.
- Gimeno, L., Ribera, P., Iglesias, R., de la Torre, L., Garcia, R. and Hernandez, E., 2002: Identification of empirical relationships between indices of ENSO and NAO and agricultural yields in Spain. *Clim. Res.* 21, 165–172.
- Gooding, M.J. and Davies, W.P., 1997: Wheat production and utilization: systems, quality and the environment. CAB International, Wallingford, UK.
- Grifoni, D., Mancini, M., Maracchi, G., Orlandini, S. and Zipoli, G., 2006: Analysis of Italian wine quality using freely available meteorological information. *Am. J. Enol. Vitic.* 57, 339–346.
- Hansen, P., Jørgensen, J.R. and Thomsen, A., 2002: Predicting grain yield and protein content in winter wheat and spring barley using repeated canopy reflectance measurements and partial least squares regression. *J. Agric. Sci.* 139, 307–318.
- Hopkins, J.W., 1968: Protein content of western Canadian hard red spring wheat in relation to some environmental factors. *Agr. Meteorol.* 5, 411–431.
- Hurrell, J.W., 1995: Decadal trends in the North Atlantic Oscillation and relationships to regional temperature and precipitation. *Science* 269, 676–679.
- Hurrell, J.W. and van Loon, H., 1997: Decadal variations in climate associated with the North Atlantic Oscillation. *Climatic Change* 36, 301–326.
- Hurrell, J.W., Kushnir, Y., Ottersen, G. and Visbeck, M., 2003: An Overview of the North Atlantic Oscillation. In *The North Atlantic Oscillation: Climate Significance and Environmental Impact* (eds.: J.W. Hurrell, Y. Kushnir, G. Ottersen, and M. Visbeck). Geophysical Monograph Series 134, 1–36.
- Jones, P.D., Jonsson, T. and Wheeler, D., 1997: Extension to the North Atlantic Oscillation using early instrumental pressure observations from Gibraltar and South-West Iceland. *Int. J. Climatol.* 17, 1433–1450.
- Jones, P.D., Osborn, T.J. and Briffa, K.R., 1997: Estimating sampling errors in large-scale temperature averages. *J. Climate* 10, 2548–2568.
- Kettlewell, P.S., Sothorn, R.B. and Koukkari, W.L.J., 1999: U.K. wheat quality and economic value are dependent on the North Atlantic Oscillation. *J. Cereal Sci.* 29, 205–209.
- Kettlewell, P.S., Stephenson, D.B., Atkinson, M.D. and Hollins, P.D., 2003: Summer rainfall and wheat grain quality: relationships with the North Atlantic Oscillation. *Weather* 58, 155–164.
- Kolderup, F., 1975: Effects of temperature, photoperiod and light quantity on protein production in wheat grains. *J. Sci. Food and Agric.* 26, 583–592.
- Labus, M.P., Nielsen, G.A., Lawrence, R., Engel, R. and Long, D.S., 2002: Wheat yield estimates using multi-temporal NDVI satellite imagery. *Int. J. Remote Sens.* 23, 4169–4180.
- Labuschagne, M.T., Elago, O. and Koen, E.J., 2009: The influence of temperature extremes on some quality and starch characteristics in bread, biscuit and durum wheat. *J. Cereal Sci.* 49, 184–189.

- Liu, L., Wang, J., Bao, Y., Huang, W., Ma, Z. and Zhao C., 2006: Predicting winter wheat condition, grain yield and protein content using multi-temporal EnviSat-ASAR and Landsat TM satellite images. *Int. J. Remote Sens.* 27, 737–753.
- Maselli, F. and Rembold, F., 2001: Analysis of GAC NDVI data for cropland identification and yield forecasting in Mediterranean African countries. *Photogramm. Eng. Rem. S.* 67, 593–602.
- Moriondo, M., Maselli, F. and Bindi, M., 2007: A simple model of regional wheat yield based on NDVI data. *Eur. J. Agron.* 26, 266–274.
- Motzo, R., Fois, S. and Giunta, F., 2007: Protein content and gluten quality of durum wheat (*Triticum turgidum* subsp. *durum*) as affected by sowing date. *J. Sci. Food Agric.* 87, 1480–1488.
- Oweis, T., Pala, M. and Ryan, J., 1999: Management alternatives for improved durum wheat production under supplemental irrigation in Syria. *Eur. J. Agron.* 11, 255–266.
- Pan, J., Zhu, Y., Cao, W., Dai, T. and Jiang, D., 2006: Predicting the protein content of grain in winter wheat with meteorological and genotypic factors. *Plant Prod. Sci.* 9, 323–333.
- Paredes-Lopez, O., Corravioubas-Alvarez, M. and Barquin-Carmona, J., 1985: Influence of nitrogen fertilization on the physicochemical and functional properties of bread wheats. *Cereal Chem.* 62, 427–432.
- Powelson, D.S., Hart, P.B.S., Poulton, P.R., Johnston, A.E. and Jenkinson, D.S., 1992: Influence of soil type, crop management and weather on the recovery of 15N-labelled fertilizer applied to winter wheat in spring. *J. Agric. Sci.* 118, 83–100.
- Rossini, P. and Benedetti, R., 1993: On the use of NDVI profiles as a tool for agricultural statistics: the case study of wheat yield estimate and forecast in Emilia Romagna. *Remote Sens. Environ.* 45, 311–326.
- Schlehuber, A.M. and Tucker, B.B., 1959: Factors affecting the protein content of wheat. *Cereal Sci. Today* 4, 240–242.
- Selles, F. and Zentner, R.P., 1998: Environmental factors affecting wheat protein. In *Proceedings of the Wheat Protein Symposium on Production and Marketing* (eds.: D.B. Fowler, W.E. Geddes, A.M. Johnston, and K.R. Preston). University of Saskatchewan, Saskatoon, Canada, 139–1150.
- Siman, G., 1974: Nitrogen status in growing cereals. *PhD Thesis of The Royal Agricultural College of Sweden*, Uppsala.
- Singh, R., Semwal, D.P., Rai, A. and Chhikara, R.S., 2002: Small area estimation of crop yield using remote sensing satellite data. *Int. J. Remote Sens.* 23, 49–56.
- Smith, G.P. and Gooding, M.J., 1999: Models of wheat grain quality considering climate, cultivar and nitrogen effects. *Agr. Foest. Meteorol.* 94, 159–170.
- Sofield, I., Evans, L.T., Cook, M.G. and Wardlaw, I.F., 1977: Factors influencing the rate and duration of grain filling in wheat. *Aust. J. Plant Physiol.* 4, 785–797.
- Spiertz, J.H.J., 1977: The influence of temperature and light intensity on grain growth in relation to the carbohydrate and nitrogen economy of the wheat plant. *Neth. J. Agr. Sci.* 25, 182–197.
- Taylor, A.C. and Gilmour, A.R., 1971: Wheat protein prediction from climatic factors in southern New South Wales. *Aust. J. Exp. Agr. Anim. Husbandry* 11, 546–549.
- Wanner, H., Bronnimann, S., Casty, C., Gyalistras, D., Luterbacher, J., Schmutz, C., Stephenson, D.B. and Xoplaki, E., 2001: North Atlantic Oscillation – Concepts and studies. *Surv. Geophys.* 22, 321–381.
- Wheeler, T.R., Hong T.D., Ellis R.H., Batts G.R., Morison J.I.L. and Hadley P., 1996: The duration and rate of grain growth, and harvest index, of wheat (*Triticum aestivum* L.) in response to temperature and CO<sub>2</sub>. *J. Exp. Bot.* 298, 623–630.

#### Internet sources:

- EUROSTAT (Statistical Office of the European Commission), 2010:  
<http://epp.eurostat.ec.europa.eu/portal/page/portal/eurostat/home/>
- MIPAAF (Ministero delle Politiche Agricole Alimentari e Forestali), 2009:  
<http://www.politicheagricole.it/default.html>



# IDŐJÁRÁS

*Quarterly Journal of the Hungarian Meteorological Service*  
Vol. 115, No. 4, October–December 2011, pp. 247–263

## **Comparative modeling study of the effect of parameterizations based on rime accretion rate and effective water content on the simulated charge density in thunderstorms**

**Boryana Tsenova<sup>1\*</sup> and Rumjana Mitzeva<sup>2</sup>**

<sup>1</sup> *National Institute of Meteorology and Hydrology,  
Bulgarian Academy of Sciences,  
66 Tsarigradsko chaussee, 1784 Sofia, Bulgaria*

<sup>2</sup> *Department of Meteorology and Geophysics, Faculty of Physics,  
University of Sofia,  
5 James Bourchier Blvd, 1164 Sofia, Bulgaria  
E-mail: rumypm@phys.uni-sofia.bg*

\* *Corresponding author; E-mail: boryana.tsenova@meteo.bg*

*(Manuscript received in final form May 3, 2011)*

**Abstract**—A new parameterization for non-inductive charging based on the laboratory studies of *Takahashi* (1978) is proposed that includes the effect of rime accretion rate on the charge transfer. Numerical simulations of two idealized cloud cases are performed to test the effect of parameterizations used in the model on the cloud charge structure. The parameterizations are based on two different sets of well known laboratory experiments applying two different manners of determination of separated charge as a function of the effective water content or the rime accretion rate. Results show that using parameterizations based on the data of *Saunders et al.* (1991) the total charge density is larger in comparison to cases when *Takahashi* based parameterizations are used. Additionally, the different manner of charge determination (as a function of the effective water content or the rime accretion rate) leads to more considerable differences in the cloud charge structure when *Saunders* parameterizations are used, comparing to the cases when *Takahashi* parameterizations are used.

*Key-words:* non-inductive charging, parameterization, rime accretion rate, effective water content

## 1. Introduction

It is accepted that thunderstorm electrification is mainly due to non-inductive charging during interactions between ice cloud particles. The non-inductive mechanism of charging is the mechanism known to be capable of generating an electric field of  $\sim 100$  kV/m in a few minutes. It results from charge separation (independently of external electric fields) during rebounding collision between riming graupel and ice crystals in the presence of supercooled cloud droplets. Many experimental studies (*Takahashi*, 1978; *Jayarathne et al.*, 1983; *Saunders et al.*, 1991; *Takahashi and Miyawaki*, 2002; *Saunders et al.*, 2004, and others) were directed to reveal the factors controlling the sign and magnitude of the separated charge. Based on laboratory experiments, it was specified that the sign and the magnitude of the charge transfer during a collision between a riming target simulating a graupel particle and an ice crystal depends on cloud temperature and cloud effective water content determined by the ability of the graupel to capture supercooled water droplets. However, dependencies are different for the various experiments and there is no consensus which laboratory results are more reliable in representing charging in real clouds. Recently, it was assumed (*Pereyra et al.*, 2000; *Saunders et al.*, 2006) that the marked difference in the charge sign reversal lines in the laboratory experiments is due to the type of the laboratory clouds (one-cloud chamber or two-cloud chamber), and that the different results should be used for charge separation in different cloud regions. In numerical models, thunderstorm electrification is calculated using different parameterizations based on the laboratory experiments. Based on their laboratory results, *Saunders et al.* (1991) proposed empirical equations for the sign and magnitude of the separated charge as a function of the effective water content and the temperature. In *Tsenova and Mitzeva* (2009), equations for *Takahashi* (1978) laboratory data are proposed to determine the separated charge depending on the cloud temperature and effective water content, to avoid the use of the look-up table data (which is computationally more time-expensive) used in all numerical model studies before.

Based on laboratory measurements and physical considerations *Brooks et al.* (1997) suggested that the rime accretion rate (*RAR*) which includes the effect of the relative velocity of interacting particles on the separated charge, is more appropriate to be used for the determination of the charge transfer than the effective water content. They proposed modifications of the equations in *Saunders et al.* (1991) for the separated charge to be presented as a function of cloud temperature and rime accretion rate.

In the present study, following the idea in *Brooks et al.* (1997) we propose modification of the equations in *Tsenova and Mitzeva* (2009) for the charge transfer obtained in *Takahashi* (1978) as a function of the rime accretion rate. Besides introducing a new parameterization of non-inductive charging that uses these equations, the present work is directed to test the difference in the charge

structures as a result of the different parameterizations (based on *Saunders et al.* (1991) or *Takahashi* (1978) laboratory results, or determining the separated charge as a function of the effective water content or the rime accretion rate). Numerical simulations of two cloud cases are carried out with a 1.5-D cloud model. Many authors have performed similar studies with 3-D cloud models (*Helsdon et al.*, 2001; *Mansell et al.*, 2005; *Barthe et al.*, 2007, and others) and their results are certainly more representative for real clouds. However, we believe that such a basic numerical study performed with a 1.5-D cloud model, which is appropriate to simulate the cloud core, would be helpful for a better understanding of the effect of the used scheme for non-inductive charging on thundercloud electrification. It has to be stressed that as it is shown in *Mitzeva et al.* (2009), model-simulated charge structures during growth stages of thunderstorms depend significantly on the particular model used. Thus, using 1.5-D cloud model we do not intend to make conclusions regarding which of the parameterizations are better suited to the realistic simulation of the electrical charging in real clouds.

## **2. Parameterization of non-inductive charging**

The revised equations presented here take into account the dependence of the charge transfer on the relative velocity between interacting particles, which was 8 m/s during the laboratory experiments in *Takahashi* (1978). The equations are presented in two forms, involving  $EW$  (effective water content) or  $RAR$  (rime action rate); the factor 8 normalizes the results of Takahashi obtained at 8 m/s.

For  $T > -10$  °C:

- $\left( EW \times \frac{V}{8} \right) \leq 1.6 \text{ g}/(\text{m}^2\text{s})$ :

$$\begin{aligned}
 q_T = & 146.981 \left( EW \times \frac{V}{8} \right) - 116.37 \left( EW \times \frac{V}{8} \right)^2 + 29.762 \left( EW \times \frac{V}{8} \right)^3 \\
 & - 0.03T^3 \left( EW \times \frac{V}{8} \right) - 2.581T - 0.0209T^3 \left( EW \times \frac{V}{8} \right)^3 + 0.356T^3 \left( EW \times \frac{V}{8} \right)^2, \quad (1a) \\
 & + 0.15T^2 + 2.918T \left( EW \times \frac{V}{8} \right)^3 - 4.215T \left( EW \times \frac{V}{8} \right) - 8.5059
 \end{aligned}$$

- $RAR \leq 12.8 \text{ g}/(\text{m}^2\text{s})$ :

$$\begin{aligned}
 q_T = & 18.37RAR - 1.82RAR^2 + 0.06RAR^3 \\
 & - 0.004T^3RAR - 2.581T - 0.0004T^3RAR^3 + 0.006T^3RAR^2, \quad (1b) \\
 & + 0.15.T^2 + 0.006TRAR^3 - 0.53TRAR - 8.5059
 \end{aligned}$$

- $\left(EW \times \frac{V}{8}\right) > 1.6 \text{ g}/(\text{m}^2\text{s})$ :

$$\begin{aligned}
 q_T = & 4.17952T - 0.00452T^2 \left(EW \times \frac{V}{8}\right)^2 + 0.91617 \left(EW \times \frac{V}{8}\right)^2 \\
 & - 1.33266T \left(EW \times \frac{V}{8}\right) - 7.46539 \left(EW \times \frac{V}{8}\right) + 0.10968T \left(EW \times \frac{V}{8}\right)^2, \quad (2a) \\
 & + 0.00057T^2 \left(EW \times \frac{V}{8}\right)^3 - 0.03504 \left(EW \times \frac{V}{8}\right)^3 + 50.84454
 \end{aligned}$$

- $RAR > 12.8 \text{ g}/(\text{m}^2\text{s})$ :

$$\begin{aligned}
 q_T = & 4.17952T - 0.00007T^2 RAR^2 + 0.01RAR^2 \\
 & - 0.17TRAR - 0.93RAR + 0.002TRAR^2, \quad (2b) \\
 & + 0.000001T^2 RAR^3 - 0.00007RAR^3 + 50.84454
 \end{aligned}$$

For  $T \leq -10^\circ\text{C}$ :

- $\left(EW \times \frac{V}{8}\right) \leq 0.4 \text{ g}/(\text{m}^2\text{s})$ :

$$\begin{aligned}
 q_T = & -3.3515T + 95.957T \left(EW \times \frac{V}{8}\right)^2 + 511.8315 \left(EW \times \frac{V}{8}\right) \\
 & + 17.4482T^2 \left(EW \times \frac{V}{8}\right)^3 - 0.0007T^3 + 20.5702T \left(EW \times \frac{V}{8}\right) \\
 & + 0.1656T^2 \left(EW \times \frac{V}{8}\right) + 0.4954T^3 \left(EW \times \frac{V}{8}\right)^3 - 0.0975T^3 \left(EW \times \frac{V}{8}\right)^2, \quad (3a) \\
 & + 67.4565T \left(EW \times \frac{V}{8}\right)^3 - 0.1066T^2 - 24.5715
 \end{aligned}$$

- $RAR \leq 3.2 \text{ g}/(\text{m}^2\text{s})$ :

$$\begin{aligned}
 q_T = & -3.3515T + 1.5TRAR^2 + 63.98RAR \\
 & + 0.03T^2 RAR^3 - 0.0007T^3 + 2.57TRAR \\
 & + 0.02T^2 RAR + 0.001T^3 RAR^3 - 0.002T^3 RAR^2, \quad (3b) \\
 & + 0.13TRAR^3 - 0.1066T^2 - 24.5715
 \end{aligned}$$

- $0.4 \text{ g}/(\text{m}^2\text{s}) < \left(EW \times \frac{V}{8}\right) \leq 3.2 \text{ g}/(\text{m}^2\text{s})$ :

$$\begin{aligned}
 q_T = & -1.5676 T \left(EW \times \frac{V}{8}\right) + 0.2484 T \left(EW \times \frac{V}{8}\right)^3 + 0.0112 T^3 \\
 & + 19.1993 T + 0.8051 T^2 + 5.97 \left(EW \times \frac{V}{8}\right)^3 - 83.3911 \left(EW \times \frac{V}{8}\right), \quad (4a) \\
 & + 15.3636 \left(EW \times \frac{V}{8}\right)^2 + 167.9278
 \end{aligned}$$

- $3.2 \text{ g}/(\text{m}^2\text{s}) < RAR \leq 25.6 \text{ g}/(\text{m}^2\text{s})$ :

$$\begin{aligned}
 q_T = & -0.2TRAR + 0.0005TRAR^3 + 0.0112T^3 \\
 & + 19.1993T + 0.8051T^2 + 0.01RAR^3 - 10.42RAR, \quad (4b) \\
 & + 0.24RAR^2 + 167.9278
 \end{aligned}$$

- $\left(EW \times \frac{V}{8}\right) > 3.2 \text{ g}/(\text{m}^2\text{s})$ :

$$\begin{aligned}
 q_T = & 4.212661T - 0.83119T \left(EW \times \frac{V}{8}\right) + 0.067005T \left(EW \times \frac{V}{8}\right)^2, \quad (5a) \\
 & + 0.004245T^2 \left(EW \times \frac{V}{8}\right) + 40.96417
 \end{aligned}$$

- $RAR > 25.6 \text{ g}/(\text{m}^2\text{s})$ :

$$\begin{aligned}
 q_T = & 4.212661T - 0.1TRAR + 0.001TRAR^2 \\
 & + 0.0005T^2RAR + 40.96417, \quad (5b)
 \end{aligned}$$

where  $q_T$  is the separated charge in fC,

$T$  is the in-cloud temperature in  $^{\circ}\text{C}$ ,

$EW$  is the effective water content in  $\text{g}/\text{m}^3$ ,

$V$  is the relative velocity between the interacting particles, and

$RAR$  is the rime accretion rate in  $\text{g}/(\text{m}^2\text{s})$ .

*Fig. 1* shows the sign of charge transfer to a riming target during ice crystal collisions at 8 m/s as a function of rime accretion rate and temperature calculated by the Eqs. (1b)–(5b) corresponding to laboratory results (Takahashi, 1978; Takahashi and Miyawaki, 2002).

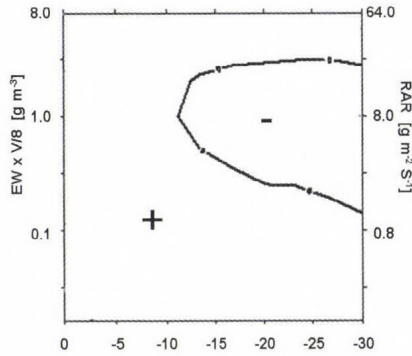


Fig. 1. Sign of the charge transfer to a riming target during ice crystal collisions at 8 m/s obtained by Eqs. (1b)–(5b) corresponding to laboratory results in *Takahashi (1978)* and *Takahashi and Miyawaki (2002)*, as a function of in-cloud temperature (x axis) and rime accretion rate:  $RAR = EW \times V$ .

In *Fig. 2* one can see the sign of the charge transfer in  $EW/T$  (left panel of *Fig. 2*) and  $RAR/T$  (right panel of *Fig. 2*) diagrams according to *Saunders et al. (1991)* and *Brooks et al. (1997; SKM and BSMP, respectively)* and *Takahashi (1978)* (TAK and TRAR, respectively) laboratory results. In  $EW/T$  diagram (*Fig. 2*, left panel) the charge sign reversal lines are obtained using the two parameterizations denoted here with SKM and TAK. The SKM parameterization is based on equations presented in *Saunders et al. (1991)* for the non-inductive charge transfer as a function of cloud temperature and effective water content,  $EW$ . The TAK parameterization consists of the empirical equations proposed in *Tsenova and Mitzewa (2009)* to calculate the charge values of *Takahashi (1978)* at different cloud temperatures and effective water contents.

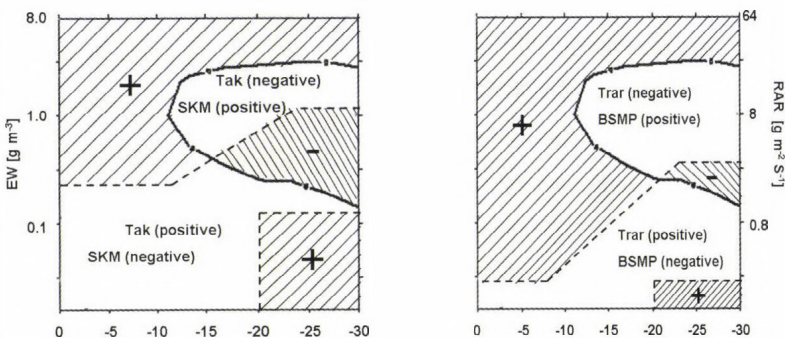


Fig. 2. Charge transfer sign in  $EW/T$  (left panel) and  $RAR/T$  (right panel) diagrams according to *Saunders et al., (1991; SKM and BSMP, respectively)* and *Takahashi (1978; TAK and TRAR respectively)* laboratory results, as a function of in-cloud temperature (x axis). Hatching indicates the regions where the charge sign is identical based on both parameterizations, while on non-hatched regions the charge sign is different based on both parameterizations.

From *Fig. 2* one can see the regions where the charge sign is identical based on both parameterizations which are hatched, and the regions where the charge sign is different based on both parameterizations which are not hatched. At low values of  $EW$ , the charge transfer according to SKM parameterization is negative, except for the positive charging at temperatures lower than  $-20\text{ }^{\circ}\text{C}$  (corresponding to the “positive anomaly” in *Saunders et al. (1991)*), while, according to TAK the charge transfer is positive. Conversely, at intermediate and high values of  $EW$  and  $T$ , according to SKM parameterization, the charge is positive, while according to TAK, it is negative. In  $RAR/T$  diagram (*Fig. 2*, right panel), the charge sign reversal lines are obtained using the BSMP and TRAR parameterizations. The BSMP parameterization is represented by a set of the revised equations presented in *Brooks et al., (1997)* for the non-inductive charge transfer taking into account the effect of rime accretion rate and temperature on the charge transfer to the target during ice crystal collisions at 3 m/s. The anomalous zones are also included (at low  $EW$ ), presented in *Saunders et al. (1991)*, but not considered in *Brooks et al. (1997)*. The TRAR parameterization is the set of the Eqs. (1b) – (5b). In the  $RAR/T$  diagram, the positively charged region according to both parameterizations BSMP and TRAR is larger than the positively charged region according to SKM and TAK in  $EW/T$  diagram. Conversely, the negatively charged region according to both parameterizations BSMP and TRAR is narrowed compared to the negatively charged region according to SKM and TAK. At low temperatures, the differences between the values of RAR, at which the charge sign reverses from negative to positive according to BSMP and TRAR, are more pronounced than these differences between the values of  $EW$  according to SKM and TAK. The reason is the different relative velocities, 3 m/s and 8 m/s at which the laboratory experiments were conducted, respectively in *Saunders et al. (1991)* and *Takahashi (1978)*.

### 3. Numerical simulations and results

Simulations are performed to test the difference in cloud charge structure obtained with parameterizations of non-inductive charging that depends on the effective water content on one hand, and on the rime accretion rate on the other hand. For this purpose, laboratory results of *Takahashi (1978)* and of *Saunders et al. (1991)* are used to study if the inclusion of the effect of the relative velocity on the charge transfer (by means of the rime accretion rate) affects the charge structure in the same direction using the two main parameterization schemes of non-inductive charge, *Takahashi's* and SKM.

The model used for the simulations is the same as in *Brooks et al. (1997)* and *Tsenova and Mitzeva (2009)*. During the simulations, the charge transfer  $Q$  (in fC) to a riming target per ice crystal separation event is calculated by

$$Q = B d^a V^b q, \quad (6)$$

where  $d$  is the crystal size (m),  $V$  is the relative velocity between graupel and ice crystals (m/s), and  $q$  (fC) is determined from empirically derived equations linking  $q$  with  $T$  and  $EW$  or  $RAR$  (for TAK/SKM and TRAR/BSMP parameterizations, respectively). The constants  $B$ ,  $a$  and  $b$  are tabulated in *Saunders et al.* (1991). The values of  $a$ ,  $b$ ,  $B_S$  (for *Saunders et al.* (1991) charge values obtained with  $V=3$  m/s and  $d=110$   $\mu\text{m}$ ), and  $B_T$  (for *Takahashi* (1978) charge values obtained with  $V=8$  m/s and  $d=100$   $\mu\text{m}$ ) are shown in *Table 1*. To generalize, the following parameterizations for the non-inductive charging (*Fig. 2*) are tested:

- (1) SKM: equations presented in *Saunders et al.* (1991) for the separated charge  $q_S$ , and

$$Q = B_S d^a V^b q_S(T, EW). \quad (7)$$

- (2) BSMP: equations presented in *Brooks et al.*, (1997) for the separated charge  $q_S$  and

$$Q = B_S d^a V^b q_S(T, RAR). \quad (8)$$

- (3) TAK: equations presented in *Tsenova and Mitzeva* (2009), for the separated charge  $q_T$  during *Takahashi's* experiment, and

$$Q = B_T d^a V^b q_T(T, EW). \quad (9)$$

- (4) TRAR: equations presented here for the separated charge  $q_T$  during *Takahashi's* experiment, and

$$Q = B_T d^a V^b q_T(T, RAR). \quad (10)$$

In the model, convective clouds are composed of an active cloud mass representing the updraught region of convective clouds and a non-active cloud mass representing the environment surrounding the cloud updraught. The active cloud mass is modeled by successive spherical thermals ascending above cloud base, while the non-active cloud mass is modeled by previously risen thermals that have stopped at the level where their velocity is zero. The

model uses bulk microphysical parameterizations with five classes of water substances — water vapor, cloud water, rain, cloud ice, and precipitating ice (graupel). The cloud droplets are formed by condensation; raindrops are formed by autoconversion of the cloud droplets and grow by collision and coalescence with cloud drops (*Kessler*, 1969). Ice crystals originate from activation of ice nuclei in supercooled cloud droplets, their concentration is given by *Fletcher* (1962). Homogeneous freezing occurs below  $-40\text{ }^{\circ}\text{C}$ . Graupel are formed by the freezing of rain drops (*Bigg*, 1953), contact nucleation of ice crystals and rain droplets (*Cotton*, 1972), and conversion of ice crystals (*Hsie et al.*, 1980). Ice crystals grow by deposition and riming. Graupel grows by deposition and coalescence with cloud and rain drops. Evaporation of rain drops and melting of graupel during their descent (*Farley and Orville*, 1986) as well as recycling is included. Cloud drops and ice crystals are assumed to be monodisperse and have negligible fall velocities, therefore, they move upward with the air. Particle size distributions for the precipitation species (rain drops and graupel) are parameterized using inverse exponential distributions of the general form. Precipitation fallout is calculated in the same manner as in *Cotton* (1972), and it comprises the portion of raindrops and graupel that have terminal velocities greater than the updraught speed.

*Table 1.* Values of the constants  $B_s$  (for *Saunders et al.* (1991) laboratory charge values),  $B_T$  (for *Takahashi* (1978) laboratory charge values),  $a$  and  $b$

Charge sign	Crystal size ( $\mu\text{m}$ )	$a$	$b$	$B_s$	$B_T$
+Q	<155	3.76	2.5	$4.9 \times 10^{13}$	$6.1 \times 10^{12}$
+Q	155–452	1.9	2.5	$4 \times 10^6$	$5 \times 10^5$
+Q	>452	0.44	2.5	52.8	6.5
-Q	<253	2.54	2.8	$5.24 \times 10^8$	$4.3 \times 10^7$
-Q	>253	0.5	2.8	24	2

The recycling of precipitating particles is possible in the model through the incorporation of the mass of raindrops and graupel falling out from the upper ascending successive thermals. In the model, ice crystals and graupel in ascending thermals, together with larger falling graupel, are the electric charge carriers in the cloud model.

Two different cloud cases were simulated: C1 and C2. Some of their microphysical and dynamical properties can be seen in *Table 2*. From the table it is visible that the two simulated cases have similar maximum values of the water/ice species contents. However, the maximum updraft velocity in C2 is almost twice as large as the maximum updraft velocity in C1. The maximum mean terminal velocity of graupel particles in C2 is larger than that of C1

(9.5 m/s and 8.17 m/s, respectively) and it is achieved higher in the cloud (at 9.4 km above cloud base compared to 2.8 km above cloud base in C1).

*Table 2.* Microphysical and dynamical properties of the simulated cloud cases C1 and C2: CB – cloud base height (km), CWCmax – maximum cloud water content ( $\text{g/m}^3$ ), CICmax – maximum cloud ice content ( $\text{g/m}^3$ ), GCmax - maximum graupel content ( $\text{g/m}^3$ ), Wmax – maximum updraft velocity (m/s), Vmax - maximum graupel mean fall velocity (m/s); the height and the model time of their achievement are indicated

	CB	CWCmax	CICmax	GCmax	Wmax	Vmax
C1	3.9 ( $\sim 1^\circ\text{C}$ )	1.3 11 min, 2.1 km	1.1 21.5 min, 5 km	0.2 18.5 min, 2.8 km	17.4 23.5 min, 6.9 km	8.17 18.5 min, 2.8 km
C2	2.9 ( $\sim 11^\circ\text{C}$ )	1.42 12 min, 3 km	0.9 12.5 min, 6.3 km	0.2 14.5 min, 3.4 km	29.74 18.5 min, 7.7 km	9.5 19 min, 9.4 km

*Fig. 3* shows the total charge density, the density of the charge carried by ice crystals, and the density of the charge carried by graupel particles in one of the thermals (chosen in a way to represent the most active charging in the C1 cloud), which ascended between the 12th and 24th minutes of the model time (MT), obtained by the different parameterizations SKM, BSMP, TAK, and TRAR. The charge densities are presented as a function of cloud temperature. With the four parameterizations, the obtained charge distribution consists of a negative charge below and a positive one above. However, the temperature interval with negative total charge density is the smallest with the TRAR parameterization (at  $T_a > -21^\circ\text{C}$ ) and the largest with the BSMP parameterization (at  $T_a > -31^\circ\text{C}$ ). The largest negative total charge density is simulated with the SKM parameterization ( $\sim -6 \text{ nC/m}^3$ ). In the upper part of the thermal, the charge obtained with the four parameterizations is positive, reaching the highest positive charge density with the SKM parameterization – above  $6 \text{ nC/m}^3$ . Using parameterizations based on Takahashi’s laboratory experiments (TAK and TRAR), the ice crystals are carriers of positive charge in this thermal, while the graupel particles carry negative charge, because the cloud conditions are similar to the conditions of negative charge in the *EW/T* and *RAR/T* diagrams in *Fig. 2*. Using parameterizations based on *Saunders et al.*, (1991) (SKM and BSMP), at higher temperatures the ice crystals are negatively charged, which is well pronounced when the BSMP parameterization is used (the crystal charge density is negative at  $T_a > -30^\circ\text{C}$ , where it reaches values above  $-1 \text{ nC/m}^3$ ), as in this region *RAR* is above  $3.3 \text{ g/m}^2\text{s}$ . In a very narrow temperature region, ice crystals are negatively charged with a weak negative charge density ( $\sim 0.1 \text{ nC/m}^3$ ) when the SKM parameterization is used, due to the fact that *EW* is not high enough to maintain the positive charge of graupel in the *EW/T* diagram in *Fig. 2*.

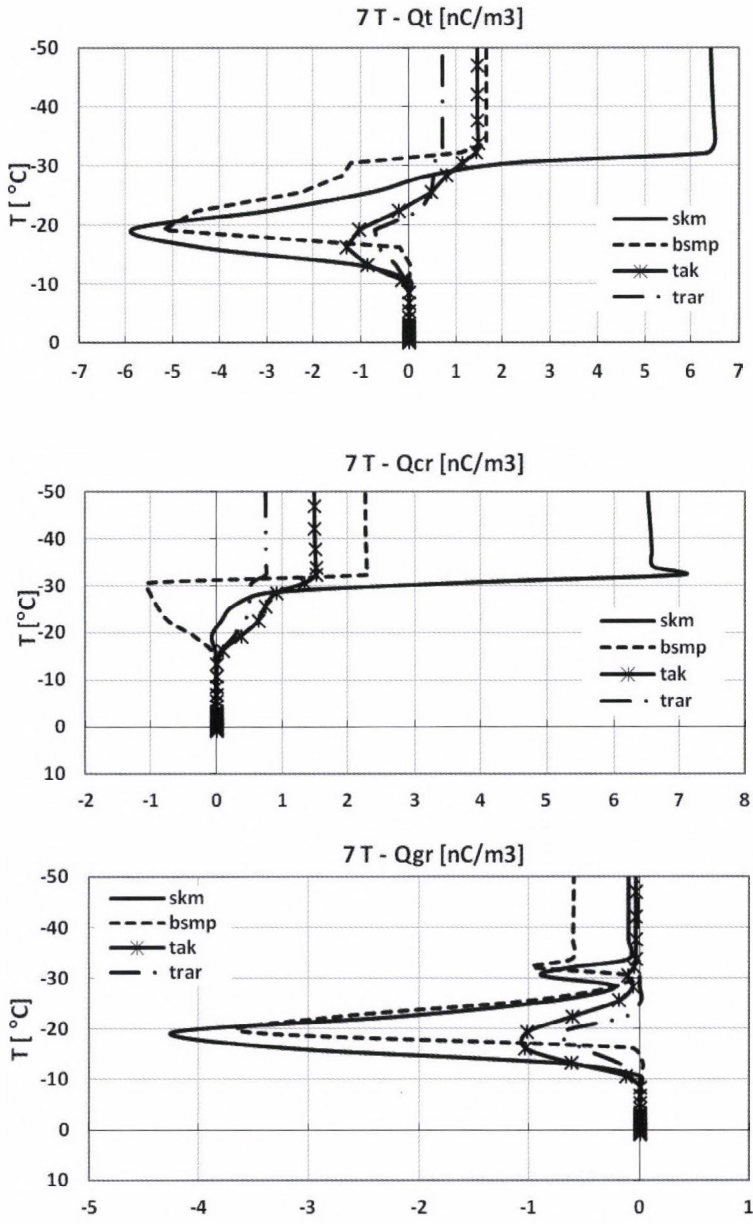


Fig. 3. C1 case: Total charge density ( $Q_t$ ), the density of the charge carried by the ice crystals ( $Q_{cr}$ ) and the density of the charge carried by graupel particles ( $Q_{gr}$ ) in the 7th thermal, which ascended between the 12th and 24th minutes of the model time obtained by the different parameterizations SKM, BSMP, TAK, and TRAR. The charge densities in  $\text{nC}/\text{m}^3$  are presented as a function of the cloud temperature.

Fig. 4 shows the total charge density as a function of the height above the cloud base  $Z$  (km) and the model time  $MT$  (min) obtained with TAK, TRAR, SKM, and BSMP parameterizations. Using Takahashi based parameterizations (TAK and TRAR), the cloud charge structure consists of a normal dipole (a negatively charged region at the lower part of the cloud and a positively charged one above it) until 22 min  $MT$ . When TRAR (the  $RAR$  based parameterization) is used, a lower positively charged region appears, which leads to the formation of a normal tripolar structure. Using the results of Saunders, between 14 and 16 min  $MT$  an inverted tripolar structure forms – a positive charge between two negative ones below and above it. The cloud charge structure obtained with BSMP ( $RAR$  based parameterization) is an inverted tripole during almost the whole simulation. However, considering the maximum values of the total charge density obtained with the different parameterizations, as well the maximum values of the charge carried by ice crystals and graupel particles shown in Table 3, one can see that the maximum negative total charge density using all parameterizations is around  $-15^{\circ}\text{C}$ , while the maximum positive total charge density is at temperatures lower than  $-30^{\circ}\text{C}$ .

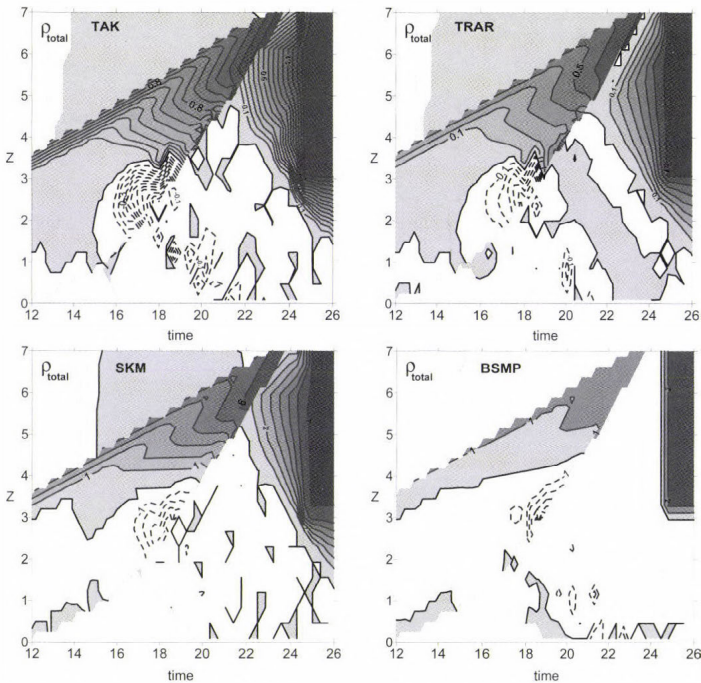


Fig. 4. C1 case: Total charge density as a function of  $Z$  (km) – height above the cloud base, and the model time (min) obtained with TAK, TRAR, SKM, and BSMP parameterizations (dark background with bold isolines indicates positive charge; bright background with dashed isolines indicates negative charge). Information on maximum values of positive and negative total charge densities, as well the height and the model time of their achievements can be seen in Table 3.

Table 3. C1 case: Maximum values of the negative (min) and positive (max) total charge density in  $\text{nC/m}^3$ , and of the charge density “carried” by ice crystals (Qcr) and graupel particles (Qgr) obtained with TAK, TRAR, SKM, and BSMP parameterizations

	TAK	TRAR	SKM	BSMP
Qt	-1.28/1.48	-0.7/0.7	-5.85/6.5	-5.2/2.2
min/max	18 min/21.5 min 2.4 km/4.9 km	18.5 min/ 24.5 min 2.8 km/7.6 km	18.5 min/21.5 min 2.8 km/4.9 km	18.5 min/24.5 min 2.8 km/4.9 km
Qcr	~0/1.52	~0/0.7	~0/7.1	-1.04/2.28
min/max	12.5 min/21 min 1.5 km/4.6 km	11 min/21.5 min 1.7 km/4.9 km	18.5 min/21 min 2.8 km/4.6 km	20.5 min/21 min 4.3 km/4.6 km
Qgr	-1.03/~0	-0.7/~0	-4.23/~0	-3.54/~0
min/max	18 min/13 min 2.4 km/2.8 km	18.5 min/19.5 min 2.8 km/3.6 km	18.5 min/16 min 2.8 km/2.2 km	18.5 min/17.5 min 2.8 km/2.0 km

Fig. 5 shows the total charge density, the density of the charge carried by the ice crystals, and the density of the charge carried by graupel particles in one of the thermals in simulated C2 cloud obtained by the different parameterizations SKM, BSMP, TAK, and TRAR. The chosen thermal (as representing the most active charging in the cloud) ascended between 8 and 21 min MT. As mentioned above, the C2 cloud case has microphysical properties close to C1, at least regarding the maximum values of the water/ice species. However, the updraft velocity in C2 is almost twice as high as in C1. In C2, there are graupel particles in a wider region compared to C1, especially at lower temperatures, while in C1, there are no graupel above the level  $-40^\circ\text{C}$ . However, the total charge density in C2 is considerably lower than that of C1 using all parameterizations. The analysis of microphysical properties showed that the conditions in the larger part of C2 are close to those near the reversal lines in  $EW/T$  and  $RAR/T$  diagrams, thus, the charge density does not have the possibility to accumulate to higher values. This can be seen in Fig. 5. The total charge density alternates between positive and negative values when all parameterizations are used. It is the most “stable” when TAK is used. In this case  $Qt$  is negative at  $T_a > -15^\circ\text{C}$ , and positive above this level. When the TRAR parameterization is used, the total charge density is similar to the one obtained with TAK, but close to the cloud top  $Qt < 0$  with TRAR. Similar, even more pronounced negative total charge at the cloud top is obtained with SKM and BSMP. This negative charge at high cloud level is carried by graupel that come from lower levels where they have been charged negatively during their interactions with ice crystals.

From Fig. 6 it is visible that between 12 and 20 min MT using the TAK parameterization, the cloud is a normal dipole, while using TRAR, SKM, and BSMP gives an inverted tripole. This can be confirmed by Table 4, where the achievements of the maximum negative charge densities is later and higher in the cloud compared to the achievements of maximum positive charge densities

when TRAR, SKM, and BSMP parameterizations are used, which suggests inverted charge structures. After 20 min MT, the charge structure obtained with all parameterizations is a normal dipole.

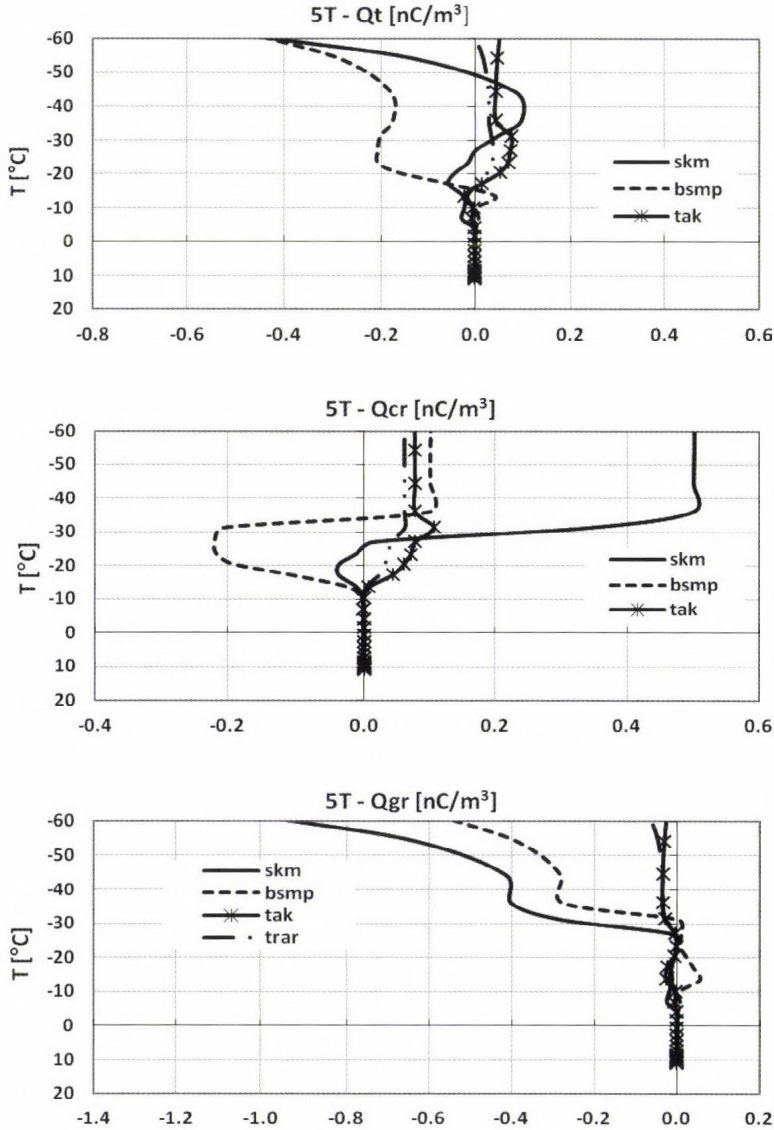


Fig. 5. C2 case: Total charge density (Qt), the density of the charge carried by the ice crystals (Qcr), and the density of the charge carried by graupel particles (Qgr) in the 5th thermal, which ascended between 8th and 21th minutes of the model time obtained by the different parameterizations SKM, BSMP, TAK, and TRAR. The charge densities in  $\text{nC/m}^3$  are presented as a function of the cloud temperature.

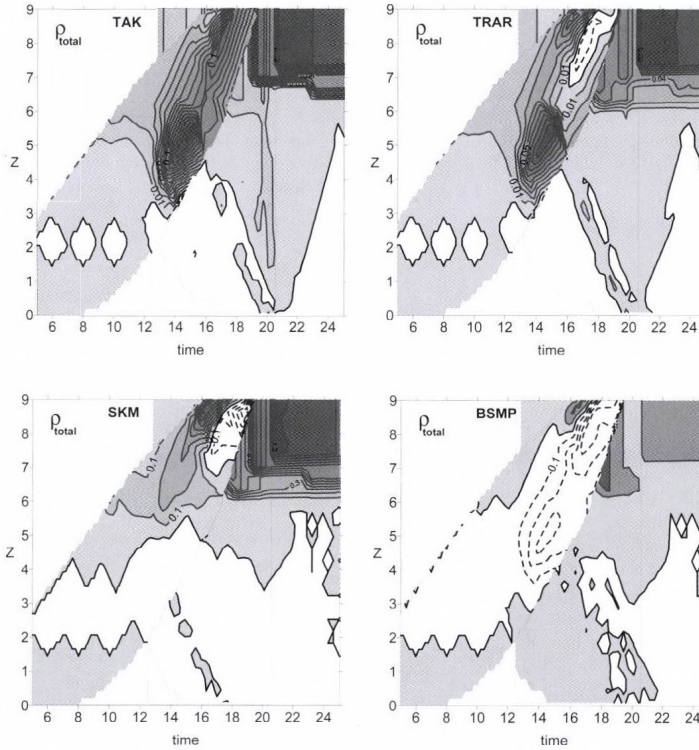


Fig. 6. C2 case: Total charge density as a function of  $Z$  [km] – height above the cloud base, and the model time obtained with TAK, TRAR, SKM, and BSMP parameterizations (dark background with bold isolines – positive charge; bright background with dashed isolines – negative charge). Information on maximum values of positive and negative total charge densities, as well the height and the model time of their achievements can be seen in Table 4.

Table 4. C2 case: Maximum values of the negative (min) and positive (max) total charge density in  $\text{nC}/\text{m}^3$ , and of the charge density “carried” ice crystals ( $Q_{\text{cr}}$ ) and graupel particles ( $Q_{\text{gr}}$ ) obtained with TAK, TRAR, SKM, and BSMP parameterizations

	TAK	TRAR	SKM	BSMP
$Q_t$	-0.02/0.16	-0.02/0.1	-0.7/0.9	-0.6/0.3
min/max	14.5 min/15 min 3.4 km/5.5 km	17 min/ 15 min 8 km/5.5 km	19.5 min/16.5 min 9.4 km/8.8 km	19.5 min/17 min 9.4 km/9.1 km
$Q_{\text{cr}}$	-0.02/0.2	~0/0.4	-0.09/0.9	-0.4/0.3
min/max	13.5 min/15 min 2.6 km/5.5 km	14 min/15 min 3 km/5.5 km	13.5 min/13.5 min 4.3 km/5.8 km	15 min/13.5 min 5.5 km/5.8 km
$Q_{\text{gr}}$	-0.03/0.05	-0.07/~0	-1.2/0.1	-0.7/0.06
min/max	17.5 min/13.5 min 6.1 km/5.8 km	19.5 min/12 min 9.4 km/3.0 km	19.5 min/13.5 min 9.4 km/7.2 km	19.5 min/15 min 9.4 km/5.5 km

#### 4. Conclusions

In the present study a new parameterization of *Takahashi* (1978) laboratory data for non-inductive charging is proposed. This parameterization represents the separated charge as a function of the rime accretion rate, which takes into account the relative velocity between the interactive ice particles additionally to the effective water content and the temperature in the cloud. Numerical simulations using a 1.5-D model (suitable to simulate thundercloud core during growth stage) are performed for two different cloud cases, where the cloud electrification is parameterized based on the two sets of laboratory experiments *Takahashi* (1978) and *Saunders et al.* (1991), as the charge is calculated by means of the effective water content, as well as by means of the rime accretion rate. Results show that using parameterizations based on the data of *Saunders et al.* (1991) (SKM and BSMP), the total charge density is larger than the total charge density simulated with parameterizations based on the data of *Takahashi* (TAK and TRAR). Additionally, the different manner for representing the charge (as a function of the effective water content or the rime accretion rate) leads to more considerable differences in cloud charge structure when the parameterizations of *Saunders et al.* are used, comparing to the cases when parameterizations of *Takahashi* are used, due to different relative velocities during the two laboratory experiments.

As mentioned above, the present work is directed to give a better understanding of the effect of the scheme used for non-inductive charging on thundercloud electrification, without intending to make conclusions regarding which of the parameterizations are better suited to the realistic simulation of electrical charging in real clouds. Moreover, in *Saunders et al.* (2006) it was suggested that equations for their laboratory data should be used for simulations of the non-inductive charge transfer, when the interacting particles have had time to come to a steady growth state in their environment, while equations for laboratory data of *Takashi* may apply for simulations of charging in cloud regions where slow-growing ice crystals in a low-supersaturated environment are entrained into a region of high supersaturation. This case may be relevant to regions of clouds where entrainment has reduced the cloud supersaturation, and subsequent mixing of particles from regions with different saturation values will lead to transient growth that may influence the charge sign during crystal/graupel collisions. Thus, numerical simulations with a 3-D cloud model, where parameterization for non-inductive charging based on *Saunders et al.* (1991) (SKM or BSMP) is used for calculating the charging between interacting ice particles moving with the updraft, and parameterization for non-inductive charging based on the *Takahashi* (1978; TAK or TRAR) is used for calculating the charging between particles that interact at the regions between the updraft and downdraft are necessary for more adequate simulations of thunderstorm electrification.

## References

- Barthe, C., Pinty, J.P., 2007: Simulation of electrified storms with comparison of the charge structure and lightning efficiency. *J. Geophys. Res.* 112, D19204.
- Bigg, E.K., 1953: The supercooling of water. *Proc. R. Soc., London, Ser. B* 66, 688–694.
- Brooks, M., Saunders, C.P.R., Mitzeva, R.P., Peck, S.L., 1997: The effect on thunderstorm charging of the rate of rime accretion by graupel. *J. Atmos. Res.* 43, 277–295.
- Cotton, W., 1972: Numerical simulation of precipitation development in super-cooled cumuli — part II. *Mon. Weather Rev.* 100, 764–784.
- Farley, R.D., Orville, H.D., 1986: Numerical modelling of hailstones and hailstone growth. I.: preliminary model verification and sensitivity tests. *J. Appl. Meteorol.* 25, 2014–2036.
- Fletcher, N.H., 1962: *The Physics of Rainclouds*. Camb. Univ. Press.
- Helsdon, J.H., Wojcik, W.A., Farley, R.D., 2001: An examination of thunderstorm-charging mechanisms using a two dimensional storm electrification model. *J. Geophys. Res.* 106, 1165–1192.
- Hsie, E., Farley, R.D., Orville, H., 1980: Numerical simulation of ice-phase convective cloud seeding. *J. Appl. Meteorol.* 19, 950–977.
- Jayarathne, E.R., Saunders, C.P.R., Hallett, J., 1983: Laboratory studies of the charging of soft-hail during ice crystal interactions. *Q. J. Roy. Meteorol. Soc.* 109, 609–630.
- Kessler, E., 1969: On the Distribution and Continuity of Water Substance in Atmospheric circulations. *Meteorol. Monogr. Boston*, 10, No 32.
- Mansell, E.R., MacGorman, D.R., Ziegler, C.L., 2005: Charge structure and lightning sensitivity in simulated multicell thunderstorm. *J. Geophys. Res.* 110, D12101.
- Mitzeva, R., Tsenova, B., Albrecht, R., Petersen, W., 2009: A study of charge structure sensitivity in simulated thunderstorms. *Atmos. Res.* 91, 299–309.
- Pereyra, R.G., Avila, E.E., Castellano, N.E., Saunders, C.P.R., 2000: A laboratory study of graupel charging. *J. Geophys. Res.* 105, 20803–20812.
- Saunders, C.P.R., Keith, W.D., Mitzeva, R.P., 1991: The effect of liquid water on thunderstorm charging. *J. Geophys. Res.* 96, 11007–11017.
- Saunders, C.P.R., Bax-Norman, H., Avila, E. E. and Castellano, N. E., 2004: A laboratory study of the influence of ice crystal growth conditions on subsequent charge transfer in thunderstorm electrification. *Q. J. Roy. Meteorol. Soc.*, 130, 1395–1406.
- Saunders, C.P.R., Bax-Norman, H., Emersic, C., Avila, E.E., Castellano, N.E., 2006: Laboratory studies of the effect of cloud conditions on graupel/crystal charge transfer in thunderstorm electrification. *Q. J. Roy. Meteorol. Soc.* 132, 2655–2676.
- Takahashi, T., 1978: Riming electrification as a charge generation mechanism in thunderstorms. *J. Atmos. Sci.* 35, 1536–1548.
- Takahashi, T., and Miyawaki, K., 2002: Reexamination of riming electrification in a wind tunnel. *J. Atmos. Sci.* 59, 1018–1024.
- Tsenova, B.D., Mitzeva, R.P., 2009: New parameterization of non-inductive charge transfer based on previous laboratory experiments. *Atmos. Res.* 91, 79–86.



## **Tropospheric scintillation measurements in Ku-band satellite signals on Earth-space paths with low elevation angle**

**Jit Singh Mandeep<sup>1,2\*</sup>, Anthony Cheng Chen Yee<sup>1</sup>,  
Mardina Abdullah<sup>1,2</sup>, and Mohammad Tariqul Islam<sup>2</sup>**

<sup>1</sup>*Department of Electrical, Electronic & Systems Engineering,  
Faculty of Engineering & Built Environment,  
University Kebangsaan Malaysia,  
43600 UKM, Bangi, Selangor Darul Ehsan, Malaysia*

<sup>2</sup>*Institute of Space Science,  
Faculty of Engineering & Built Environment,  
University Kebangsaan Malaysia,  
43600 UKM, Bangi, Selangor Darul Ehsan, Malaysia  
E-mail; mardina@eng.ukm.my, tariqul@ukm.my*

*\*Corresponding author E-mail; mandeep@eng.ukm.my*

*(Manuscript received in final form April 26, 2011)*

**Abstract**—This paper discusses the tropospheric scintillation of a KU-band satellite antenna, which installed at the University Sains Malaysia (USM), Malaysia, on an elevation angle of 40.1°, at frequency of 12.255 GHz. Tropospheric scintillation in this context means rapid fluctuation of radiowave signals occurring during data transmission due to the turbulence at the atmosphere when the signal propagates. It occurs every day and tends to affect the quality of the communication link, especially for the link that utilizes frequency band higher than 10 GHz. The paper compares the measured tropospheric scintillation data with gamma and normal (Gaussian) distributions for short-term and long-term scintillation distributions. The findings show that for short-term scintillations, the probability density function (PDF) will tend to follow gamma distribution and for long-term scintillation, the PDF will follow normal distribution. The results are very useful to develop a new tropospheric scintillation model for Malaysia and for other areas with similar climate.

*Key-words:* tropospheric scintillation, satellite communication, Ku-band satellite signals, probability density function

## 1. Introduction

Tropospheric scintillation can be defined as rapid fluctuation of the amplitude or phase of a radiowave caused by changes of refractive index at the altitude. It is caused by the humidity and temperature of the atmosphere. The effects of tropospheric scintillation are seasonal and vary from day to day with the local climate (*Mandeep and Yun Yang Ng, 2010*). The scintillations effect is needed to take into the link budget design of millimeter-wave communication system, as it will bring huge impact to the quality of the signal. For low-margin systems operating at high frequency (Ku-band and above) and low elevation angle (*Mandeep and Yun Yang Ng, 2010*), signal degradation caused by scintillation can be more dominant compared to rain attenuation (*Mandeep et al., 2010*). For this reason, accurate scintillation models are needed to achieve satisfactory signal quality for daily satellite communication usage.

To predict the signal fade and enhancement, there is a need to determine the short-term (several minutes) and long-term scintillation pattern (4 months) throughout the year. Short-term and long-term fluctuations are to be calculated based on the collected data. Objective of this paper is to verify the mathematic model that fits to the short-term and long-term scintillation patterns in Malaysia. Probability density functions (PDF) of short-term (several minutes) and long-term 4 months scintillations will be compared with gamma and normal distributions to verify which distribution fits to the tropospheric scintillation in Malaysia.

## 2. Methodology

For this data analysis, we obtain the signal parameter from a 12.255 GHz Superbird C beacon at elevation angle of 40.1 using a sampling rate of 1 minute. The beacon is located at the USM campus at Parit Buntar, Malaysia (5.170°N, 100.4°E). The data for this analysis is taken from January 1, 2009 to December 31, 2009. Apart from the satellite signal, weather informations such as humidity, temperature, air pressure, rain rate etc. are taken down using the same sampling rate for further analysis purpose. *Table 1* shows the ground station configuration for the Superbird C beacon.

*Table 1.* Satellite specification

Ground station location	5.170N, 100.40E
Beacon frequency	12.255 GHz
Elevation angle	40.10
Polarisation	Horizontal
Antenna configuration	Offset parabolic
Antenna Diameter	2.4 m
Satellite position	1440 E
Antenna height	57 m above sea level

The term “scintillation” means fast fluctuations of signal amplitude and phase, caused by atmospheric turbulence. This effect is due to turbulent irregularities in temperature, humidity, and pressure, which translate into small-scale variations in refractive index. An electromagnetic wave passing through this medium will then encounter various refraction and scattering effects, which will result in a multipath effect.

It is known that over relatively short time periods, where the meteorological conditions are fairly constant, scintillation amplitudes, in dB, follow a Gaussian distribution around the mean signal level which is zero. This is why they can be characterized by standard deviation  $\sigma$ , which is commonly referred to as scintillation intensity. For long time periods, the distribution of scintillation amplitude deviates significantly from a Gaussian probability density function (pdf, especially in the tails) (*Kassianides and Otung, 2003*).

Scintillation is defined in terms of the received log-amplitude signal,  $\chi$  (in dB) that is related to the signal amplitude,  $A$ , the mean signal amplitude,  $\langle A \rangle$ , and the (zero-mean) fluctuating signal component  $\Delta A = A - \langle A \rangle$ , by

$$\chi = 20 \log_{10} \left( 1 + \frac{\Delta A}{A} \right). \tag{1}$$

Scintillation occurs continually in both rainy and clear sky conditions (*Mandeep, 2009*). Precaution is needed to take when rain occurs, since the amplitude-level of signal fluctuation is accompanied by the rain attenuation and needed to be removed to avoid inconsistency in data analysis. The measured data is inspected for any inconsistencies. The procedure to extract reliable scintillation statistics comprises both manual and automatic steps. Rain periods have been removed using rain gauge data. Visual inspection is performed in all data sequences to eliminate spurious and invalid data. All the valid measurements have been passed through a high-pass filter with a cutoff frequency ( $f_c$ ) of 0.025 Hz, which allows isolating the fast variations caused by scintillation from other slowly varying signal components (*Otung et al., 1998*). To examine the effect on scintillation statistics of the cutoff frequency, used for data filtering, 14 different values of ( $f_c$ ) between 2 and 500 mHz were used. For each scintillation data set (obtained using a particular value of  $f_c$ ), a goodness-of-fit test were performed to determine whether the 1 minute distribution of the scintillation amplitude followed a Gaussian pdf. The value of  $f_c$  must be carefully set. If  $f_c$  is too low, then non-scintillation effects are inadvertently included in the signal fades and enhancements about the mean level. On the other hand, if  $f_c$  is too high, then legitimate contributions to scintillation at Fourier components lower than the set value of  $f_c$  are excluded. Scintillation variance, that represents the best way to characterize scintillation intensity, has

been calculated as the square of the standard deviation of the signal amplitude (dB) over periods of 1 minute (*Otung et al.*, 1998).

The gamma distribution is a two-parameter continuous probability distribution. It has a scale parameter  $\theta$  and a shape parameter  $k$ , where the mean and the variance are  $k\theta$  and the  $k\theta^2$ . The probability density function of random variable,  $x$ , which is gamma-distributed with  $\theta$  and  $k$ , can be formulated as (*ITU-R P. 618-10*, 2009):

$$x^{k-1} \frac{\exp(-x/\theta)}{\Gamma(k)\theta^k}, \tag{2}$$

The normal distribution or Gaussian distribution is a continuous probability distribution that variates with mean,  $\mu$  and variance,  $\sigma^2$ , that can be obtain using conventional statistic formula. The probability density function of the variable  $x$  that follows normal distribution is (*Marzano and d'Auria*, 1998)

$$f(x) = \frac{1}{\sqrt{2\pi\sigma^2}} e^{-\frac{(x-\mu)^2}{2\sigma^2}}. \tag{3}$$

### 3. Results and discussion

Malaysia has an equatorial climate, producing a warm and wet weather due to its proximity to the equator. The temperature is maintained at around 25–28 °C, and the humidity is high all over the year with values between 72.2 and 82.3%. There are two monsoon winds that influence the rainfall in the different intervals of the year in Malaysia. The southwest monsoon usually occurs between May and September, bringing rainfall to the western side of Malaysia. On the other hand, the northeast monsoon starts from November and lasts till March, bringing heavy rainfall to areas on the east side of Peninsular Malaysia (*Mandeep*, 2009). Since these two monsoons will increase the rain rate in Malaysia, it tends to have affect on the tropospheric scintillation probability distribution. *Table 2* shows the averaged temperature and humidity for each month in 2009.

A suggestion of the departure of the probability density function of a random variable from symmetry about the mean is given by its skewness  $S = \mu_3 / (\mu_1)^3$ , where  $\mu_1$  is the first moment about the mean (or standard deviation) and  $\mu_3$  is the third moment about the mean. *Table 3* shows the values of standard deviation and skewness calculated for each month of 2009. All measured results report a negative skewness of scintillation amplitude distribution.

Table 2. Monthly temperature and humidity for year 2009

Month	Temperature (°C)	Humidity (%)
Jan	25.32	75.29
Feb	26.07	77.89
Mar	25.95	80.21
Apr	26.47	79.94
May	26.92	78.30
Jun	27.94	72.21
Jul	27.14	74.45
Aug	25.77	82.08
Sep	26.09	79.76
Oct	26.39	79.43
Nov	25.60	82.37
Dec	25.00	82.22

Table 3. Standard deviation and skewness of the probability density function for 2009

Month	Standard deviation (dB)	Skewness
Jan	0.20	-0.023
Feb	0.23	-0.060
Mar	0.09	-0.009
Apr	0.10	-0.020
May	0.15	-0.070
Jun	0.12	-0.015
Jul	0.11	-0.034
Aug	0.14	-0.040
Sep	0.18	-0.070
Oct	0.20	-0.005
Nov	0.14	-0.027
Dec	0.21	-0.120

The scintillation standard deviation shows some variations on a long-term basis (i.e., from several weeks), which are not Gaussian-distributed. This can be expressed as

$$p(\sigma) = \frac{1}{\sigma_1 \sigma \ln 10 \sqrt{2\pi}} e^{-\frac{(\log \sigma - m_1)^2}{2\sigma_1^2}}, \quad (4)$$

where  $m_1$  is the mean value of  $\log \sigma$ ,  
 $\sigma_1$  is the standard deviation of  $\log \sigma$ .

### 3.1 Short term scintillation analysis

In this paper, short term scintillation is taken as scintillation that occurs in an interval of 20 minutes in a day and accumulated into a month. With a sampling rate of 1 minute, for each set of data, scintillation data are processed and the PDF are plotted into graphs. The graph is then compared with the respective gamma and normal distributions.

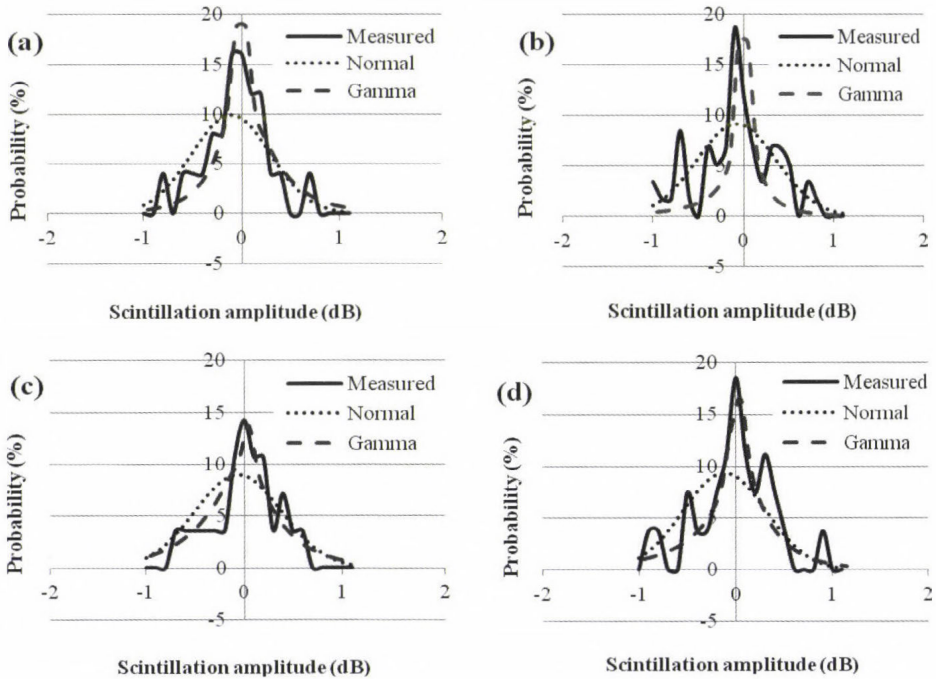


Fig. 1. Short-term scintillation for (a) January, (b) May, (c) September, and (d) December 2009.

Figs. 1(a) – (d) shows the short-term scintillation for every quarter of the year 2009. Each of the graphs represents a set of amplitude scintillation data in an interval of 20 minutes for each day and accumulated over a month. Due to the low sampling rate, the measured PDF for short-term scintillation looks a bit spiky. Regardless from the spiky graphs, the short-term scintillation data are similar to the gamma distribution function. Throughout the whole year, short-term scintillation is following gamma distribution without being affected by the monsoon season. The measured data have sharper edge on steeper curve and the 0 dB. These characteristics are similar to gamma distribution. Normal distribution is not suitable to predict short-term scintillation as the curves tend to be wider.

### 3.2 Long-term scintillation analysis

For long-term scintillation, the scintillation data is processed on a quarterly basis. In each quarter of the year, tropospheric scintillation data for every month will be averaged, and the PDFs are plotted into a graph. The graphs will be then compared to normal and gamma distributions for that particular time interval.

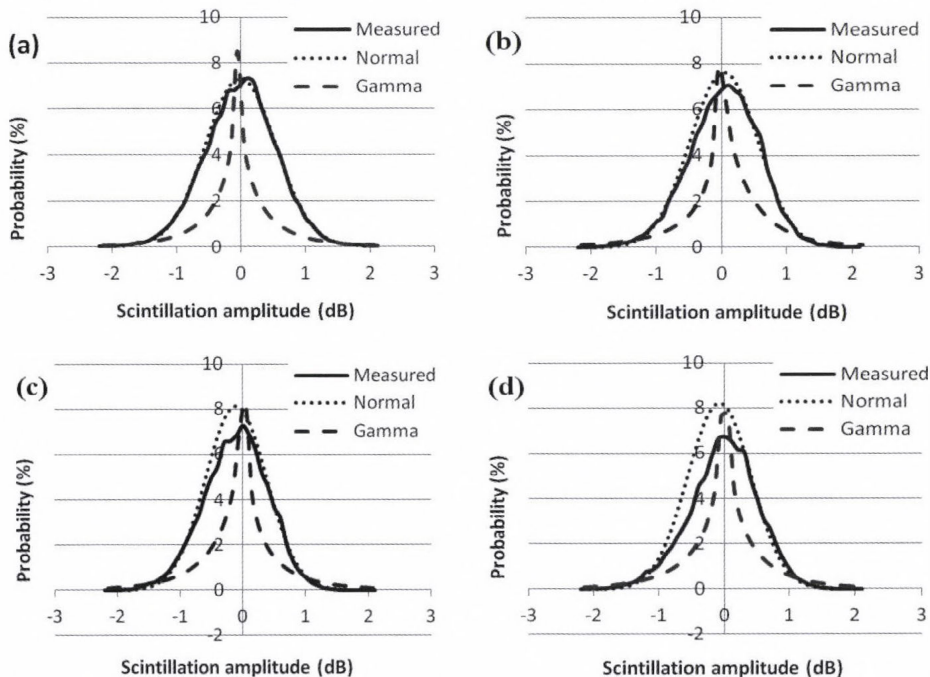


Fig. 2. Long-term scintillation for the (a) first quarter of 2009 (January 1 – March 31), (b) second quarter of 2009 (April 1 – June 30), (c) third quarter of 2009 (July 1 – September 30), and (d) fourth quarter of 2009 (October 1 – December 31).

Scintillation data for monthly period is mentioned as it will be averaged. Scintillation intensity is stationary on a time-scale of up to one month. The monthly tropospheric scintillation data were calculated based on

$$p(x) = \int_0^{\infty} p(\sigma_x) p(x/\sigma_x) d\sigma_x, \quad (5)$$

where  $\sigma_x$  is the standard deviation,  $\sigma_x^2$  is the variance of the signal level, and

$$p(x/\sigma_x) = \frac{1}{\sigma_x \sqrt{2\pi}} \exp \left[ -\left( \frac{x^2}{2\sigma_x^2} \right) \right]. \quad (6)$$

Figs. 2 (a)–(d) show scintillation data on quarterly basis for 2009. As it is shown in the graphs, for long-term scintillations, the distribution fits more to the normal distribution than gamma distribution. The measured scintillation PDF gives a bell-curve shape that identical to normal distribution. Gamma distribution has sharper edge at 0dB and it differs from the measured data; therefore, it is not likely to be used to predict long-term tropospheric scintillation. Overall, the measured data fit exceptionally close to the normal distribution, especially in the first two quarters of the year.

From Table 2 we can observe, that there are increases in humidity from August to December. The last two quarters of the year vary more to normal distribution, and it may be caused by the increases of humidity due to the monsoon season.

Fig. 3 shows the tropospheric scintillation probability density function of year 2010. From the graph we can see, that throughout the year, the scintillation pattern follows the normal distribution. The measured scintillation amplitude has wider bell shape as in normal distribution and differs from gamma distribution in term of the curve shape.

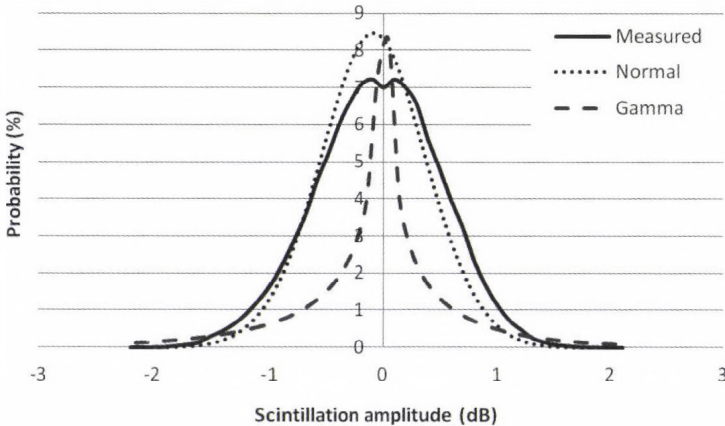


Fig. 3. Probability density function of measured data compared with normal and Gaussian distributions for 2010.

#### 4. Conclusion

From the graphs presented in this paper, we can see, that short-term scintillation follows the gamma distribution closely while, on the other hand, long-term distribution follows the normal distribution. It is essential to verify the pattern of tropospheric scintillations in Malaysia before developing a new tropospheric scintillation model. For short-term scintillations, gamma distribution gives a more similar curve where the edge is sharper at the 0 dB level, so it is suitable to

predict the short-term scintillations. For long-term scintillations, normal distribution fits better to the scintillation pattern compared to the gamma distribution. Long-term scintillation has wider curve at both ends and less sharp edge at 0dB level, which is similar to the normal distribution.

**Acknowledgements**—The authors would like to acknowledge the University Kebangsaan Malaysia, University Sains Malaysia, MOSTI grant Science Fund (01-01-92-SF0670), UKM-GGPM-ICT-108-2010, UKM-DLP-2011-003 and the Association of Radio Industry Business (ARIB) of Japan for providing the instruments used for collecting the data.

## References

- ITU-R P. 618-10, 2009: *Propagation Data and Prediction Methods Required for the Design of Earth-Space Telecommunication systems*. ITU Radiocomm. Bureau, Geneva, 6 pp.
- Kassianides, C.N. and Otung, I.E. 2003: Dynamic model of tropospheric scintillation on earth-space paths. *IEE Proc.-Microw Antenna Propg.*, 150, 97–104.
- Mandeep, J.S., 2009: Rain attenuation statistics over a terrestrial link at 32.6 GHz at Malaysia. *IET Micro., Anten. & Prop.* 3, 1086–1093.
- Mandeep, J.S., 2009: Slant path rain attenuation comparison of prediction models for satellite applications in Malaysia. *J. Geophys. Res.-Atmos.* 114, D17108. doi:10.1029/2009JD011852.
- Mandeep, J.S., and Yun Yang Ng, 2010: Satellite beacon experiment for studying atmospheric dynamics. *J. Inf. Millim. Tera. Wav.* 31, 988–994.
- Mandeep, J.S., Ng, Y.Y., Abdullah, H., and Abdullah, M., 2010: The study of rain specific attenuation for the prediction of satellite propagation in Malaysia. *J. Inf. Millim. Tera. Wav.* 3, 681–689.
- Marzano, F.S. and d'Auria, G., 1998: Model-based prediction of amplitude scintillation variance due to clear-air tropospheric turbulence on Earth-satellite microwave links. *IEEE Trans. Antennas Propag.* 46, 1506–1518.
- Otung, I.E., Al-Nuaimi, M.O., Evans, B.G., 1998: Extracting scintillations from satellite beacon propagation data. *IEEE Trans. Antennas Propag.* 46, 1580–1581.



# IDŐJÁRÁS

*Quarterly Journal of the Hungarian Meteorological Service  
Vol. 115, No. 4, October–December 2011, pp. 275–288*

## **Estimation of structural icing intensity and geometry of aircrafts during different conditions – a fixed-wing approach**

**Zsolt Bottyán**

*Aviation Weather Laboratory, Department of Air Traffic Controller  
and Pilots' Training, Zrínyi Miklós National Defence University,  
P.O. Box 1, H-5008 Szolnok, Hungary  
E-mail: bottyan.zsolt@zmne.hu*

*(Manuscript received in final form May 8, 2011)*

**Abstract**—The estimation of aircraft structural icing characteristics is a very important procedure as the accreted ice layer may cause some dangerous effects for aircraft such as lift force degradation, increasing of drag force, and malfunction of control surfaces and sensors. The intensity and geometry of ice contamination on the surface of an aircraft depend on meteorological (cloud droplet size distribution, liquid water content, ambient temperature), aerodynamical (airspeed), and geometrical (size and shape of the aircraft) conditions, too. In this paper a 2D similar ice accumulation model is shown which is based on a cylindrical approximation of airfoil and the thermodynamics of icing processes. Applying this model, the intensity and geometry of accreted ice layer can be accessed on the wing of a popular fixed-wing aircraft Cessna-185 Skywagon in a special cold-pool-like weather situation. On the basis of our calculation it is clear, that the severity of icing phenomena strongly depends not only on the meteorological but also on aerodynamical conditions. On the other hand, this method can be adapted for an operational structural airframe icing severity forecasting.

*Key-words:* aviation meteorology, aircraft structural icing, icing severity, liquid water content, Cessna-185 Skywagon

### **1. Introduction**

The airframe (structural) icing occurs when an aircraft flies mainly under IFR (instrument flight rules) condition (generally in cloud), the ambient static temperature is below zero, and supercooled water droplets impinge and freeze on the aircraft's unprotected surface. The ice accretions cause many dangerous problems during the flight such as reduced lift and increased drag forces,

significantly decreased angle of attack, strong vibrations and structural imbalances of aircrafts, malfunction of control surfaces and air pressure sensors, reduced visibility, and improper radio communication (Bragg *et al.*, 2005). On the other hand, there are some differences between the structural icing of fixed-wing aircrafts and rotorcrafts (helicopters), e.g., the different icing problem of helicopters along their rotor blades (Gent *et al.*, 1987; Gent *et al.*, 2000). On the basis of these facts, a reliable estimation of expected ice accretion during the proposed flight is very useful and important information for the pilots (Jeck, 1998; Fuchs and Lütkebohmert, 2001; Lankford, 2001; Fuchs, 2003).

Forecasting of airframe (structural) icing of aircrafts is a very complex procedure since the magnitude of the ice accretion on the aircrafts' surfaces highly depends on ambient meteorological and aerodynamical conditions and on aircraft's geometry, too. The rate and amount of structural ice accretion curiously depend on the followings (Gent *et al.*, 2000; Lankford, 2001; Bragg *et al.*, 2005):

- static ambient temperature of airflow around the aircraft,
- static air pressure at the level of flight,
- liquid water content (*LWC*) of cloud,
- cloud droplet size distribution,
- true airspeed (*TAS*) of aircraft, and
- shape and size of aircraft structures with the special regard to wings.

It is clear that the surfaces with high rate of ice accretion are located near the leading edge of wings and tail. They are relatively narrow and their positions are usually opposite the freestream. For that very reason, the ice accretion models have to approach the wing geometry well. In many 2D ice accumulation models a suitable cylinder is applied to describe the ice accretion characteristics along its surface because the cloud droplet trajectory calculation in the airflow around the cylinder is a relatively simple procedure (List, 1977; Lozowski *et al.*, 1983a; Makkonen, 1981; Launiainen and Lyyra, 1986; Finstad *et al.*, 1988; Makkonen and Stallabrass, 1987; Mazin *et al.*, 2001).

In our work we apply a 2D ice accretion non-rotating cylinder model based on the methods of Lozowski *et al.* (1983a) estimating the rate and geometrical characteristics of ice contamination on a small popular aircraft such as Cessna-185 Skywagon under different aerodynamic and meteorological conditions.

## **2. The ice accretion model**

The applied ice accretion model is based on the quasi-stationary heat balance equation for a freezing surface which is assumed to define the thermodynamics of icing phenomena, first described by Ludlam (1951) and Messinger (1953). The local collection efficiency calculation used by Langmuir and Blodgett

(1946), *Lozowski et al.* (1983a), *Finstad et al.* (1988) and the ice growth estimation along the cylinder surface is described by *Lozowski et al.* (1983a).

Assume a non-rotating horizontal cylinder with a diameter of  $D_c$  located in a uniform airstream with the velocity of  $U$  (freestream velocity). The streaming air under cloudy circumstances contains supercooled droplets with the concentration of  $W$ . Supposing that the airstream and droplets are in thermodynamic and mechanical equilibrium, the temperature of airstream  $T_a$  equals the droplet temperature. Apparently, the velocity of supercooled droplets far from the cylinder is also  $U$ .

In order to calculate the local impingement of water droplets, we divided the upwind surface of the cylinder into angular sectors of  $5^\circ$  and centered the angles  $\theta_i = 5i^\circ$ ,  $i = 1, 2, \dots, 18$ . The applied droplet size characteristics are also discretized by establishing 9 diameter categories with  $5 \mu\text{m}$  wide intervals centered the diameters  $D_j = 5j \mu\text{m}$ ,  $j = 1, 2, \dots, 9$ . We assume that the droplets have the same size (central diameter) in each category. On the basis of assumptions mentioned above the local droplet collision efficiency can be calculated for all angular sectors and droplet size categories as follows:

$$\beta_i = \sum_j f_j \beta_{ij}, \quad (1)$$

where  $f_j$  is the fraction of total water mass flux in the airflow, containing droplets in the  $j$ th diameter category. After that, the liquid water mass flux impinging all sectors along the upstream face of the cylinder can be expressed as:

$$R_{wi} = \beta_i U W. \quad (2)$$

The quasi-stationary heat balance equation for a freezing surface is given by

$$Q_c + Q_e + Q_v + Q_k + Q_f + Q_w + Q_i + Q_r + Q_w^* + Q_f^* = 0, \quad (3)$$

where

- $Q_c$  is the sensible heat flux between freezing surface and airstream;
- $Q_e$  is the latent heat flux of evaporation;
- $Q_v$  is the viscous aerodynamic heating due to airstream;
- $Q_k$  is the flux of kinetic energy of impinged droplets on the icing surface;
- $Q_f$  is the latent heat flux of accretion due to freezing of impinging water;
- $Q_w$  is the sensible heat flux required to warm the freezing water droplets;
- $Q_i$  is the heat flux between the iced and the underlying surface;

- $Q_r$  is the long-wave radiative heat flux;
- $Q_w^*$  is the sensible heat flux required to heat the runback and shedding part of impinging water (similar to  $Q_w$ );
- $Q_f^*$  is like  $Q_f$  but for runback water only.

If the physical and aerodynamic conditions allow the existence of any unfrozen water on the icing surface (wet-growth ice accretion), the mass of it in any angular sectors is supposed to be moved to the next downstream sector by airstream. On the other hand, we also assume the runback water will be shed into the airstream at  $\theta = 90^\circ$ . The items in Eq. (3) are formularized as follows:

$$Q_c = h(T_a - T_s), \quad (4)$$

where  $h$  is the heat transfer coefficient,  $T_a$  and  $T_s$  are the temperatures of airstream and icing surface, respectively. The calculation of  $h$  is based on the results of *Achenbach* (1977), and we applied the rough cylinder case (because the icing process produces a rough cylinder surface).

The evaporation heat flux term is given by

$$Q_e = h \left( \frac{Pr}{Sc} \right)^{0.63} \frac{\varepsilon l_v}{pc_p} (e_a - e_s), \quad (5)$$

where  $Pr$  and  $Sc$  are the Prandtl and Schmidt numbers,  $\varepsilon$  is the ratio of the molecular weights of water vapor and dry air,  $p$  is the static pressure of air in the freestream,  $c_p$  is the specific heat capacity of dry air at a constant pressure,  $l_v$  is the latent heat of vaporization, and finally,  $e_a$  and  $e_s$  are the saturation water vapor pressures of moist air at  $T_a$  and  $T_s$ . If the accretion is dry, the latent heat of sublimation  $l_s$  has to be applied.

The viscous heating can be given by

$$Q_v = \frac{hr_c U^2}{2c_p}, \quad (6)$$

where  $r_c$  is the local recovery factor along the cylinder surface described by *Seban* (1960). This term explains the adiabatic heating due to the air compressibility at higher velocities and the frictional heating in the boundary layer. This factor is very important when the Mach number of airstream is higher than 0.3 (in this case the compressibility of air will be higher than 5%).

The kinetic energy flux of droplets can be calculated by

$$Q_k = \frac{1}{2} R_w U^2, \quad (7)$$

where  $R_w$  is the droplet mass flux and  $R_w = \beta W U$ .

During the freezing of impinging supercooled water the latent heat flux is

$$Q_f = n R_w l_{fs}, \quad (8)$$

where  $l_{fs}$  is the latent heat of freezing at  $T_s$  and  $n$  is the fraction of accreted mass of impinging water. It is obvious, that if  $T_s < 273.15$  K then  $n = 1$  (dry-growth icing) and in the case of  $T_s = 273.15$  K,  $n < 1$  (wet-growth icing and there are some runback water along the icy surface of the cylinder).

The sensible heat flux is required to warm the impinging droplets to the equilibrium temperature  $T_s$ , and it is given by

$$Q_w = R_w \bar{c}_w (T_a - T_s), \quad (9)$$

where  $\bar{c}_w$  is the average specific heat of water between  $T_a$  and  $T_s$ . Its value is a constant in this model.

The linear approximation of radiative heat flux between the droplets and accreted surface can be written by

$$Q_r = \sigma (\varepsilon_a T_a^4 - \varepsilon_s T_s^4) = a (T_a - T_s), \quad (10)$$

where  $\varepsilon_a$  and  $\varepsilon_s$  are the radiative emissivity of air and surface, respectively,  $\sigma$  is the Stefan-Boltzmann constant, and  $a$  is a coefficient.

The amount of existing runback water (unfrozen part of impinged droplets in a given sector) also plays an important role in the heat exchange between the sectors. We suppose, that there are not any parallel flows to the cylinder axis, and the leaving part of runback water (with the steady-state temperature of the given sector) influences the next sector's heat balance only. Obviously the amount of entering runback water adjusts the steady-state temperature in the given sector thus the heat flux in connection with it is described by

$$Q_w^* = R_w^* \bar{c}_w (T_s^* - T_s), \quad (11)$$

where  $R_w^*$  is the mass flux of runback water entering the given sector,  $T_s^*$  is the

temperature of runback water. It is obvious the  $T_s^*$  equals 0 °C if there are any runback water (because the steady-state condition). Evidently there is not any runback water into the first sector and the entering part of runback water from the first sector to the second one is the half of the amount of total outflow runback water from the first sector (it is based on the cylinder geometry). The latent heat flux of freezing the runback water is given by

$$Q_f^* = nR_w^* l_{fs}. \quad (12)$$

In our model the  $Q_i$  heat flux was omitted and taken into account by Eqs. (4)–(12). In this case, Eq. (3) is a non-linear differential equation which can be solved by numerically within each sector. The two unknowns in Eq. (3) are  $T_s$  and  $n$ . The solving procedure of Eq. (3) is described by *Gent et al.* (2000) and *Saeed* (2000).

After the calculation of impinging water flux ( $R_{wi}$ ), runback water flux ( $R_{wi}^*$ ), and freezing faction ( $n_i$ ), we can determine the icing flux ( $R_i$ ) in all sectors:

$$R_i = n_i (R_{wi} + R_{wi}^*). \quad (13)$$

The calculation of the ice growth is given by

$$h_i = \frac{2R_i \delta t / \rho_i}{1 + \left(1 + \frac{4R_i \delta t}{\rho_i D_c}\right)^{0.5}}, \quad (14)$$

where  $h_i$  means the local thickness of accretion,  $\delta t$  is the accretion time, and  $\rho_i$  is the ice density (*Lozowski et al.*, 1983a). The application of this ice growing approach is limited in time because we have to assume that the ice accretion phenomena does not significantly influence the environment of airstream and the heat exchange around the surface. However, this approach can be applied to estimate the ice accretion rate if we use a short time interval ( $\delta t$ ). Experimental results of wind tunnels have confirmed the applicability of Eq. (14) if the time interval is not longer than 5–7 minutes (*Lozowski et al.*, 1983b). On the other hand, the shapes of accreted ice contamination grew during the wind tunnel experiments are very similar to those calculated by the applied ice growth model. These experiments were executed under conditions such as (–5 °C)–(–15 °C) temperature, 30.5–122 m s<sup>–1</sup> airspeed, 0.13–1.27 g m<sup>–3</sup> LWC, and 1–10 minutes time intervals, respectively (*Lozowski et al.*, 1983b).

### 3. Methods

The ice accretion model described in Section 2 can be used to estimate the amount, rate and, geometry of ice contamination not only along a given cylinder but also along a surface that has the similar curvature (for example, a fixed-wing aircraft airfoil). For the real icing calculation, we applied the twice leading edge radius of the airfoil as cylinder diameter (Tsao and Anderson, 2005). Our examined fixed-wing aircraft was the popular Cessna-185 Skywagon (Fig. 1).



Fig. 1. The examined fixed-wing aircraft: Cessna-185 Skywagon.

The cross section of its wing airfoil (coded by NACA0012) with the  $0^\circ$  angle of attack (AOA) and the corresponding cylinder can be seen in Fig. 2. The difference of curvature between the leading edge segment of airfoil and the cylinder is neglectable, so this approximation can be a good choice in our model.

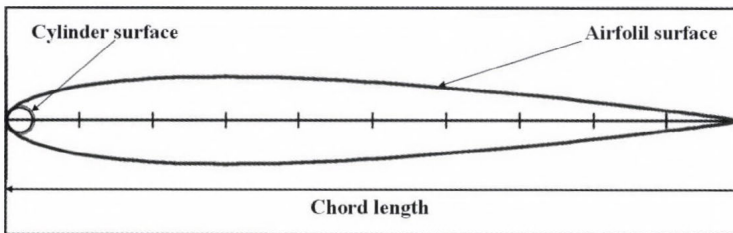


Fig. 2. The cross section of an airfoil and a corresponding cylinder which has the same curvature along the leading edge zone.

The calculation of corresponding cylinder diameter in the case of a given airfoil is based on the method of Abbott and von Doenhoff (1959):

$$D_c = 2kc, \quad (15)$$

where  $k$  is the leading edge radius and the  $c$  is the chord length. The data of examined aircraft can be found in *Table 1* (Lambert, 1994). As it can be seen, the chord length varies between 1.14 m (wingtip) and 1.63 m (root), so we used 1.385 m as an averaged value, because this number represents the middle segment of wing far enough from the fuselage. Thus, the used leading edge radius of the NACA0012 airfoil was 0.017. Applying Eq. (15) we received the corresponding cylinder diameter value of 0.04709 m. The speed limits of the Cessna-185 aircrafts are  $25 \text{ m s}^{-1}$  and  $80 \text{ m s}^{-1}$ , thus, we examined this *TAS* interval in our work (*Table 1*).

*Table 1.* Some important parameters of the examined fixed-wing aircraft Cessna -185 Skywagon II

Aircraft	Cessna -185 Skywagon II
Wingspan (m)	10.92
Airfoil type	NACA0012
Chord length (m)	1.14 – 1.63
Stall speed ( $\text{m s}^{-1}$ )	25
Maximum speed ( $\text{m s}^{-1}$ )	80
Maximum ceiling (m)	5455

In order to produce real physical (meteorological) background for our examination (as far as possible), we analyzed AIREP icing data between January 1, 2006 and December 31, 2010 over the middle part of Hungary using the atmospheric sounding data of Budapest during this period. There were many icing situations on different air pressure levels, temperatures, and microphysical conditions, and we selected a typical severe icing event of January 14, 2006 which was in connection with thick low level stratiform clouds under a strong inversion layer (cold-pool-like weather situation over the Carpathian Basin) (*Table 2*).

*Table 2.* AIREP reports during icing situations of January 14, 2006. The icing phenomenon is signed by bold underlined setting

Date and time	AIREP text
12:57:26 UTC, January 14, 2006	<b><u>SEV ICING</u></b> BTN GRD AND 2000FT ON 31R FINAL BY B737
15:28:58 UTC January 14, 2006	<b><u>SEV ICING</u></b> BTN GRD AND 5000FT ON 13R FINAL BY B737
18:56:52 UTC January 14, 2006	<b><u>SEV ICING</u></b> BTN 5000FT AND GROUND ON FINAL 13R

As it can be seen, the icing zones were located between the ground and 2000 ft (600 m) and later 5000 ft (1500 m) on January 14, 2006 (*Fig. 3*). We have to note that severe icing for a Boeing-737 does not mean the same icing severity occurrence for other aircrafts!

Based on the mentioned data, our examined air temperature values were  $-3\text{ }^{\circ}\text{C}$ ,  $-5\text{ }^{\circ}\text{C}$ , and  $-7\text{ }^{\circ}\text{C}$ , and air pressure values 1010, 970, and 890 hPa, respectively (Fig. 3).

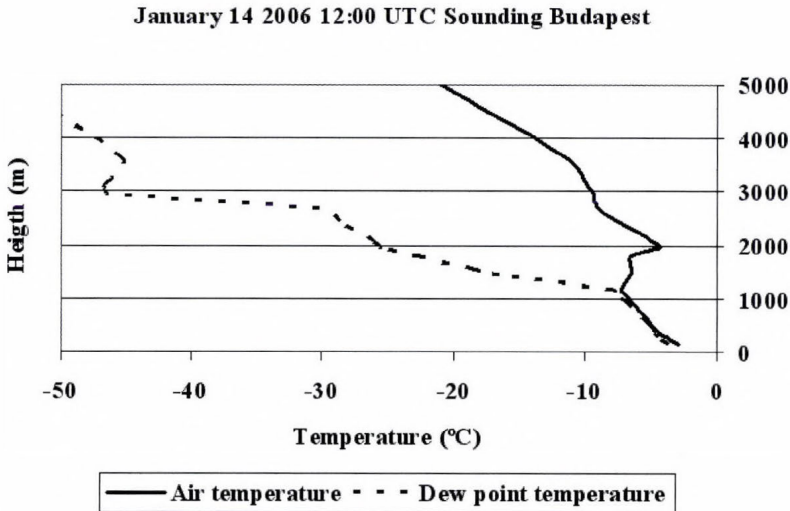


Fig. 3. Vertical air temperature and dew point temperature profiles of January 14, 2006 during AIREP based icing phenomena.

Taking into account the given cloud structure in which the icing was detected by some aircrafts on the mentioned day, we supposed a typical cloud water droplet size distribution ( $\Gamma$ -distribution, *Geresdi*, 2004) with  $20\text{ }\mu\text{m}$  median volume diameter (*MVD*), and we also assumed that this distribution was constant in the cloud. On the other hand, the used (presumed) liquid water content (*LWC*) values were  $0.2\text{ g kg}^{-1}$  and  $0.5\text{ g kg}^{-1}$  in our calculation. The applied values of cloud droplet size distribution and *LWC* in the thick low stratus are in tune with the measurements of *Kunkel* (1971), the work of *Jeck* (2002), and the numerical simulation of *Geresdi* and *Rasmussen* (2005).

We also supposed a 5 minutes hypothetical flight time of our aircraft under selected meteorological condition, because this time interval is not longer than used in the experimentally tested ice accretion model (*Lozowski et al.*, 1983b).

#### 4. Results and discussion

First of all, we calculated the ice accumulation and its rate along the airfoil (cylinder) surface under the given meteorological conditions at 12 UTC on January 14, 2006 over Budapest. Our results – regarding the ice growth intensity values – are in *Table 3*. The *TAS* (true airspeed of aircraft) as well as the *U*

(freestream velocity) were  $60 \text{ m s}^{-1}$  and the applied icing severity categories were the international standards by Jeck (1998), which are similar to ICAO ones. In spite of the same icing intensity category (moderate), it can be seen that the maximum icing growth intensity values vary between  $0.436$  and  $1.249 \text{ mm min}^{-1}$ . The largest value is three times higher than the smallest one, so the moderate marking of icing severity is not always enough to sign this phenomenon exactly. Obviously the higher values can be found at higher  $LWC$ , because the amounts of impinging droplets are proportional to  $LWC$  values.

Table 3. The calculated maximum ice growth intensity and severity under different meteorological conditions at 12 UTC on January 14, 2006 over Budapest

Temperature (°C)	Pressure (hPa)	LWC (g kg <sup>-1</sup> )	Ice growth intensity (mm min <sup>-1</sup> )	Icing severity
-3	1010	0.0002	0.51	Moderate
-3	1010	0.0005	1.25	Moderate
-5	970	0.0002	0.44	Moderate
-5	970	0.0005	1.20	Moderate
-7	890	0.0002	0.44	Moderate
-7	890	0.0005	1.17	Moderate

Supposing that the  $LWC$  was a constant value of  $0.0005 \text{ g kg}^{-1}$ , the aircraft flew at the  $970 \text{ hPa}$  pressure level, and the ambient temperature was  $-5 \text{ °C}$  we were able to estimate the icing intensities with different  $TAS$  values, too.

Our results can be seen in Table 4. Under conditions from  $30 \text{ m s}^{-1}$  to  $60 \text{ m s}^{-1}$   $TAS$  values, the maximum icing rate is moderate, but if the aircraft reaches  $70 \text{ m s}^{-1}$   $TAS$  value the icing rate is severe! We examined the  $TAS$  values when the icing rate changes from moderate to severe and from light to moderate. In the examined case the moderate/severe limit  $TAS$  value is  $64 \text{ m s}^{-1}$ , and the light/moderate one is  $28 \text{ m s}^{-1}$ . Allowing for Cessna-185 speed limits (Table 1), we can establish light ( $25\text{--}27 \text{ m s}^{-1}$ ), moderate ( $28\text{--}63 \text{ m s}^{-1}$ ) or severe ( $64\text{--}80 \text{ m s}^{-1}$ ) icing situations as a function of speed of flight during the same meteorological conditions! The thickness of accreted ice layer varies between  $1.75 \text{ mm}$  and  $8.25 \text{ mm}$  after 5 minutes flight time, thus, the amount of ice layer may reach the dangerous thickness (near maximum  $TAS$ ) during a short time period (within 15 minutes).

However, the estimated ice growth intensity is not enough to predict the exact icing risk potential for a given aircraft, because the spatial distribution of the ice layer has a crucial effect in the disturbance of airflow around the wing (Bragg et al., 2005). While the icing process is dry-growth ( $n=1$ ), the geometry of accreted ice layer mainly elliptical with its maximum ice growth at the leading edge, supposing  $0^\circ$  AOA (at the stagnation point or leading edge) (Lozowski, 1983a; Tsao and Anderson, 2005). On the other hand, if the icing process is already wet-growth, the unfrozen part of the collided droplets begin to

move from the leading edge along the airfoil's surface and it may freeze at the farther part of the wing causing the dangerous horn-shaped ice accretion instead of the elliptical one (Fig. 4).

Table 4. Icing severity conditions of Cessna-185 aircraft as a function of TAS under given constant meteorological conditions ( $T_a = -5\text{ }^\circ\text{C}$ ;  $p = 970\text{ hPa}$ ;  $LWC = 0.0005\text{ g kg}^{-1}$ )

TAS ( $\text{m s}^{-1}$ )	Icing growth intensity ( $\text{mm min}^{-1}$ )	Thickness of ice layer after 5 minutes flight (mm)	Icing severity
25	0.35	1.75	Light
30	0.48	2.41	Moderate
40	0.72	3.60	Moderate
50	0.95	4.76	Moderate
60	1.18	5.92	Moderate
70	1.41	7.07	Severe
80	1.65	8.25	Severe

The fundamental problems of an aircraft which has a similar horn-shaped ice contamination on its wing during flight are the extremely high drag force and mainly the loss of lift force because of the appearance of strongly turbulent airflow behind the big ice horns (between the ice horn and the airflow trajectory reattachment zone) (Fig. 4). This lift force degradation may reach the 30–40% of the clear (non-contaminated) value (Cooper et al., 1984; Bragg et al., 2005).

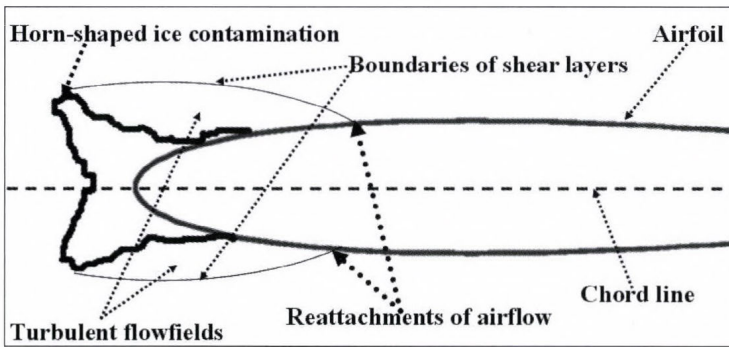
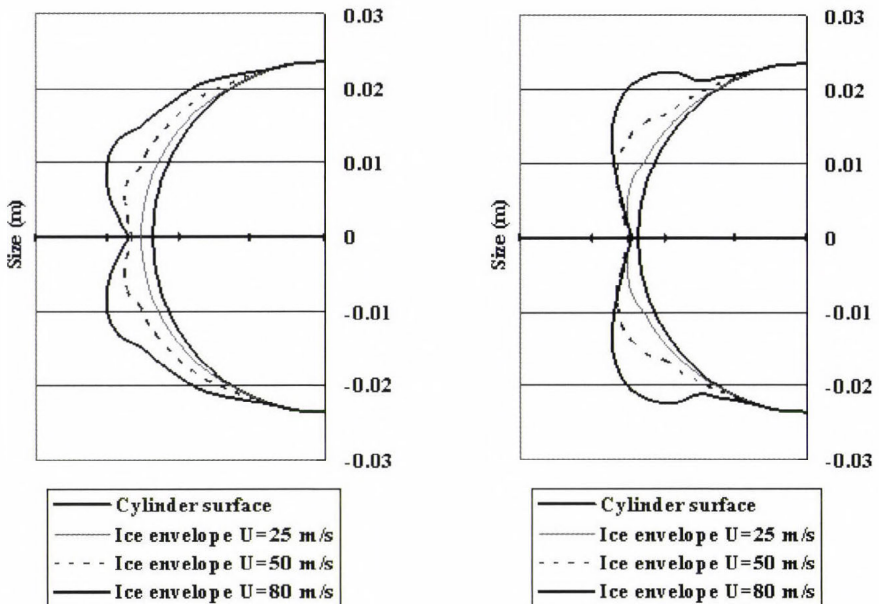


Fig. 4. The geometry of horn-shaped ice contamination and its effect on the airflow around NACA0012 airfoil.

It is clear that the correct estimation of accreted ice layer under different meteorological conditions requires the prediction of geometry of contaminated surface, too. In our work, we described a 2D estimation of the structural icing geometry of a given type of aircraft under measured ( $T_a, p$ ) and supposed ( $LWC, U$ , and droplet size distribution) ambient conditions as it can be seen in Fig. 5.

There are some important notes associated with the two calculated cases:

- At higher air temperature ( $T_a = -3\text{ }^\circ\text{C}$ , near  $0\text{ }^\circ\text{C}$ ), the ice envelopes have horn-like shape and this form is more significant at higher speed ( $TAS(U) = 50$  and  $80\text{ m s}^{-1}$ ). It is caused by the large amount of runback water (wet-growth icing) moving along the airfoil surface and freezing farther from the stagnation point (leading edge) (*Fig. 5*, right).
- At maximum airspeed ( $TAS(U) = 80\text{ m s}^{-1}$ ), we can see the horn-shaped ice contamination around the cylinder (airfoil) in both cases, but the distance of the location of maximum accretion from the stagnation point and the maximum of accreted ice thickness are different. When  $T_a = -7\text{ }^\circ\text{C}$  (*Fig. 5*, left), the amount of runback water is smaller, thus, the ice horn is also thinner and its position is closer to the stagnation point (leading edge) than in the other case ( $T_a = -3\text{ }^\circ\text{C}$ ).
- When the airspeed is close to the minimum value of Cessna-185 ( $TAS = 25\text{ m s}^{-1}$ ), the ice accretion geometry has the elliptical form in both cases, because the icing is dry-growth yet. It is clear that this shape causes less significant anomalies in airflow around the wing than the horn-iced one (*Fig. 5*, right and left).



*Fig. 5.* The 2D geometry of computed accreted ice layers on the surface of the given cylinder (airfoil) after 5 minutes flight time. Left:  $T_a = -7\text{ }^\circ\text{C}$ ;  $p = 890\text{ hPa}$ ;  $LWC = 0.0005\text{ g kg}^{-1}$ ; Right:  $T_a = -3\text{ }^\circ\text{C}$ ;  $p = 1010\text{ hPa}$ ;  $LWC = 0.0005\text{ g kg}^{-1}$ .

As long as the geometrical effects are initially constants, the environmental parameters may vary along wide ranges during the flight. It follows that the provision of a responsible quasi real-time prediction in the matters of rate, amount, and geometry of airframe ice accretion requires the good knowledge of meteorological (cloud microphysical) conditions and flight plan (airspeed, duration, and 3D route of flight), together. On the other hand, the necessary high resolution values of signed meteorological variables can be produced by a meso-scale numerical weather model such as WRF with a corresponding parameterization or a coupled microphysical model (Skamarock *et al.*, 2005; Geresdi *et al.*, 2001; Rasmussen and Geresdi, 2005).

Finally, we have to note that further additional studies are necessary to generate the corresponding high resolution meteorological fields of the mentioned ambient physical variables for operational use of our ice accretion model.

## 5. Summary

On the basis of the described model and our results, we are able to estimate the concrete icing rate and geometry on the wings of a given fixed-wing aircraft during a relatively short time period. There is also a good advantage to calculate the correct limits of the icing severities regarding to given meteorological, aerodynamical and geometrical conditions (aircraft-dependent estimations).

Applying the calculated geometry (shape) of the accreted ice layer, we are able to predict the most dangerous horn-iced phenomena and its probable location within the cloud.

The effectively accreted ice characteristics highly depend on flight time as well. Knowing the flight environment, we may derive a maximum flight time for a given fixed-wing aircraft during this situation without any dangerous icing (flight path optimization).

Moreover, the embedding of a similar ice accretion model (such as described one) into an operative forecasting procedure can level up the usage and reliability of icing predictions and may lead to higher level of flight safety.

*Acknowledgements*—The author thanks István Geresdi and Ferenc Wantuch for useful suggestions and comments on work, Péter Szalóky and Péter Kardos for providing AIRMET data set.

## References

- Abbott, I. H. and von Doenhoff, A.E., 1959: *Theor. Wing Sections*. Dover, New York.
- Achenbach, E., 1977: The effect of surface roughness on the heat transfer from circular cylinders to the cross flow of air. *Int. J. Heat Mass Transfer* 20, 359-369.
- Bragg, M.B., Broeren, A.P. and Blumenthal, L.A., 2005: Iced-airfoil aerodynamics. *Prog. Aerospace Sci.* 41, 323-362.

- Cooper, W.A., Sand, W.R., Politovich, M.K. and Veal, D.L., 1984: Effects of Icing on Performance of a Research Aircraft. *J. Aircraft* 21, 708-715.
- Finstad, J.K., Lozowski, E.P. and Gates, E.M., 1988: A computational investigation of water droplet trajectories. *J. Atmos. Ocean. Tech.* 5, 160-170.
- Fuchs, W., 2003: Forecast of aircraft icing by use of boundary layer model products: First experiences. *Proceedings of The 13<sup>th</sup> International Offshore and Polar Engineering Conference*. Honolulu, USA, 423-428.
- Fuchs, W. and Lütkebohmert, M., 2001: Aircraft icing forecast. *Proceedings of The 11<sup>th</sup> International Offshore and Polar Engineering Conference*. Stavanger, Norway, 686-689.
- Gent, R.W., Markiewicz, R.H. and Cansdale, J.T., 1987: Further studies of helicopter rotor ice accretion and protection. *Vertica* 11, 473-492.
- Gent, R.W., Dart, N.P. and Cansdale, J.T., 2000: Aircraft icing. *Phil. Trans. Roy. Soc. London. A* 358, 2873-2911.
- Geresdi, I., 2004: *Cloudphysics* (in Hungarian). Dialóg Campus Kiadó. Budapest – Pécs.
- Geresdi, I. and Rasmussen, R.M., 2005: Freezing drizzle formation in stably Stratified layer clouds: The role of giant nuclei and aerosol particle size distribution and solubility. *J. Atmos. Sci.* 62, 2037-2067.
- Geresdi, I. Rasmussen, R.M., Thompson, G., Manning, K., and Karplus, E., 2001: Freezing drizzle formation in stably stratified layer clouds: The role of radiative cooling of cloud droplets, cloud condensation nuclei, and ice initiation. *J. Atmos. Sci.* 59, 837-860.
- Jeck, R., 1998: A workable, aircraft-specific icing severity scheme. Appendix A. *Preprints of AIAA-98-0094. 36<sup>th</sup> Aerospace Sciences Meeting and Exhibit*. Reno, USA, 1-12.
- Jeck, R., 2002: Icing Design Envelopes (14 CFR Parts 25 and 29, Appendix C) Converted to a Distance-Based Format. *Final Report of U.S. Department of Transportation Federal Aviation Administration Office of Aviation Research*. Washington, USA, 1-48.
- Kunkel, B.A., 1971: Fog drop-size distributions measured with a laser hologram camera. *J. Appl. Meteorol.* 10, 482-486.
- Lambert, M. (ed.), 1994: *Jane's All theWorld's Aircrafts*. Jane's Publishing Co., London, UK.
- Langmuir, I. and Blodgett, K.B., 1946: A mathematical investigation of water droplet trajectories. *Collected Works of Irving Langmuir*. 10. Pergamon Press, 348-393.
- Lankford, T.T., 2001: *Aviation Weather Handbook*. McGraw-Hill, New York.
- Launiainen, J. and Lyyra, M., 1986: Icing on a non-rotating cylinder under conditions of high liquid water content in the air: II. Heat transfer and rate of ice growth. *J. Glaciol.* 32, 12-19.
- List, R., 1977: Ice accretions on structures. *J. Glaciol.* 19, 451-465.
- Lozowski, E.P., Stallabrass, J.R., and Hearty, P.F., 1983a: The icing of an unheated nonrotating cylinder. Part I: A simulation model. *J. Clim. Appl. Meteorol.* 22, 2053-2062.
- Lozowski, E.P., Stallabrass, J.R., and Hearty, P.F., 1983b: The icing of an unheated nonrotating cylinder. Part II: Icing wind tunnel experiments. *J. Clim. Appl. Meteorol.* 22, 2063-2074.
- Ludlam, F.H., 1951: The heat economy of a rimed cylinder. *Q. J. Roy. Meteor. Soc.* 77, 663-666.
- Makkonen, L., 1981: Estimating intensity of atmospheric ice accretion on stationary structures. *J. Appl. Meteorol.* 20, 595-600.
- Makkonen, L. and Stallabrass, J.R., 1987: Experiments on the cloud droplet collision efficiency of cylinders. *J. Clim. Appl. Meteorol.* 26, 1406-1411.
- Mazin, I.P., Korolev, A.V., Heymsfield, A., Isaac, G.A. and Cober, S.G., 2001: Thermodynamics of icing cylinder for measurements of liquid water content in supercooled clouds. *J. Atmos. Ocean. Tech.* 18, 543-558.
- Messinger, B.L., 1953: Equilibrium temperature of an unheated icing surface as a function of airspeed. *J. Aeronaut. Sci.* 20, 29-41.
- Rasmussen, R.M., and Geresdi, I. 2005: Freezing drizzle formation in stably stratified layer clouds. Part II: The role of giant nuclei and aerosol particle size distribution and solubility. *J. Atmos. Sci.* 62, 2037-2057.
- Saeed, F., 2000: State-of-the-art aircraft icing and anti-icing simulation. *ARA J.* 25-27, 106-113.
- Seban, R.A., 1960: The influence of free stream turbulence on the local heat transfer from cylinders. *J. Heat Trans.* 82, 101-107.

- Skamarock, W.C., Klemp, J.B., Dudhia, J., Gill, D.O., Barker, D.M., Wang, W. and Powers, J.G., 2005: A Description of the Advanced Research WRF Version 2. NCAR Technical. Note, Boulder, USA, 1-88.*
- Tsao J-C., and Anderson, D.N., 2005: Additional study of water droplet median volume diameter (MVD) effects on ice shape. NASA/CR-2005-213853 report, 1-11.*



# IDŐJÁRÁS

VOLUME 115 \* 2011

## EDITORIAL BOARD

- |                                       |   |
|---------------------------------------|---|
| AMBRÓZY, P. (Budapest, Hungary)       | MIKA, J. (Budapest, Hungary)                      |
| ANTAL, E. (Budapest, Hungary)         | MERSICH, I. (Budapest, Hungary)                   |
| BARTHOLY, J. (Budapest, Hungary)      | MÖLLER, D. (Berlin, Germany)                      |
| BATCHVAROVA, E. (Sofia, Bulgaria)     | NEUWIRTH, F. (Vienna, Austria)                    |
| BRIMBLECOMBE, P. (Norwich, U.K.)      | PINTO, J. (Res. Triangle Park, NC, U.S.A.)        |
| CZELNAI, R. (Dörgicse, Hungary)       | PRÁGER, T. (Budapest, Hungary)                    |
| DUNKEL, Z. (Budapest, Hungary)        | PROBÁLD, F. (Budapest, Hungary)                   |
| FISHER, B. (Reading, U.K.)            | RADNÓTI, G. (Budapest, Hungary)                   |
| GELEYN, J.-Fr. (Toulouse, France)     | S. BURÁNSZKI, M. (Budapest, Hungary)              |
| GERESDI, I. (Pécs, Hungary)           | SIVERTSEN, T.H. (Risør, Norway)                   |
| GÖTZ, G. (Budapest, Hungary)          | SZALAI, S. (Budapest, Hungary)                    |
| HASZPRA, L. (Budapest, Hungary)       | SZEIDL, L. (Budapest, Hungary)                    |
| HORÁNYI, A. (Budapest, Hungary)       | SZUNYOGH, I. (College Station, TX, U.S.A.)        |
| HORVÁTH, Á. (Siófok, Hungary)         | TAR, K. (Debrecen, Hungary)                       |
| HORVÁTH, L. (Budapest, Hungary)       | TÄNCZER, T. (Budapest, Hungary)                   |
| HUNKÁR, M. (Keszthely, Hungary)       | TOTH, Z. (Camp Springs, MD, U.S.A.)               |
| LASZLO, I. (Camp Springs, MD, U.S.A.) | VALI, G. (Laramie, WY, U.S.A.)                    |
| MAJOR, G. (Budapest, Hungary)         | VARGA-HASZONITS, Z.<br>(Mosonmagyaróvár, Hungary) |
| MATYASOVSKY, I. (Budapest, Hungary)   | WEIDINGER, T. (Budapest, Hungary)                 |
| MÉSZÁROS, E. (Veszprém, Hungary)      |   |

*Editor-in-Chief*  
**LÁSZLÓ BOZÓ**

*Executive Editor*  
**MARGIT ANTAL, MÁRTA T. PUSKÁS**

**BUDAPEST, HUNGARY**

## AUTHOR INDEX

Abdullah, M. (Selangor D. Ehsan, Malaysia) .....	265
Balczó, M. (Budapest, Hungary).....	179
Balogh, M. (Budapest, Hungary) .....	179
Bihari, Z. (Budapest, Hungary).....	1, 99
Bissolli, P. (Offenbach, Germany).....	31
Bankanza, J.C.M. (Prague, Czech Republic) ..	51
Bottyán, Zs. (Szolnok, Hungary).....	275
Bozó, L. (Budapest, Hungary).....	217
Capecchi, V. (Florence, Italy).....	233
Dalla Marta, A. (Florence, Italy).....	233
Enzsölné Gerencsér, E. (Mosonmagyaróvár, Hungary).....	167
Farda A. (Prague, Czech Republic).....	71
Führer, E. (Sopron, Hungary).....	205, 219
Goricsán, I. (Budapest, Hungary).....	179
Grifoni, D. (Florence, Italy) .....	233
Grosz, B. (Gödöllő, Hungary).....	219
Hlasny, T. (Zvolen, Slovakia) .....	71
Hogewind, F. (Karlsruhe, Germany).....	31
Horváth, L. (Budapest, Hungary).....	205, 219
Huth, R. (Prague, Czech Republic) .....	87
Jagodics, A. (Sopron, Hungary).....	205
Lajos, T. (Budapest, Hungary).....	179
Lakatos, M. (Budapest, Hungary) .....	1, 99
Lantos, Zs. (Mosonmagyaróvár, Hungary) ..	167
Machon, A. (Budapest, Hungary) .....	205, 219
Mancini, M. (Florence, Italy).....	233
Mandep, J.S. (Selangor D. Ehsan, Malaysia) ..	265
Mészáros, E. (Veszprém, Hungary).....	121
Mitzeva, R. (Sofia, Bulgaria).....	247
Möller, D. (Berlin, Germany).....	123
Nagel, T. (Karlsruhe, Germany).....	179
Nagy, Z. (Gödöllő, Hungary).....	219
Orlandini, S. (Florence, Italy).....	233
Orlando, F. (Florence, Italy).....	233
Pintér, K. (Gödöllő, Hungary).....	219
Sitkova, Z. (Zvolen, Slovakia).....	71
Skalak, P. (Praha, Czech Republic) .....	71
Štěpánek, P. (Prague, Czech Republic) ....	71, 87
Suda, J.M. (Budapest, Hungary).....	179
Szabados, I. (Sárvár, Hungary).....	205
Szabó-Takács, B. (Pécs, Hungary) .....	147
Szalai, S. (Budapest, Hungary).....	1
Szentimrey, T. (Budapest, Hungary) .....	1, 99
Tariqu, M. (Selangor D. Ehsan, Malaysia).....	265
Tsenova, B. (Sofia, Bulgaria) .....	247
Ustrnul, Z. (Krakow, Poland) .....	111
Valeriu, P.C. (Iasi, Romania).....	13
Varga, Z. (Mosonmagyaróvár, Hungary) ....	167
Varga-Haszonits, Z. (Mosonmagyaróvár, Hungary).....	167
Vízy, L. (Košice, Slovakia) .....	71
Weidinger, T. (Budapest, Hungary).....	219
Wypych, A. (Krakow, Poland) .....	111
Yee, A.C.C. (Selangor D. Ehsan, Malaysia) .....	265
Zahradníček, P. (Brno, Czech Republic) .....	87

## TABLE OF CONTENTS

### I. Papers

<i>Balczó, M., Balogh, M., Goricsán, I., Nagel, T., Suda, J.M. and Lajos, T.:</i> Air quality around motorway tunnels in complex terrain – computational fluid dynamics modeling and comparison to wind tunnel data .....	179
<i>Bankanza, J.C.M.:</i> Time variation of the effect of geographical factors on spatial distribution of summer precipitation over the Czech Republic .....	51
<i>Bottyán, Zs.:</i> Estimation of structural icing intensity and geometry of aircrafts during different conditions – a fixed-wing approach .....	275
<i>Enzsölné Gerencsér, E., Lantos, Zs., Varga-Haszonits, Z. and Varga, Z.:</i> Determination of winter barley yield by the aim of multiplicative successive approximation .....	167
<i>Führer, E., Horváth, L., Jagodics, A., Machon, A. and Szabados, I.:</i> Application of a new aridity index in Hungarian forestry practice .....	205
<i>Hogewind, F. and Bissolli, P.:</i> Operational maps of monthly mean temperature for WMO Region VI (Europe and Middle East).....	31
<i>Lakatos, M., Szentimrey, T. and Bihari, Z.:</i> Application of gridded daily data series for calculation of extreme temperature and precipitation indices in Hungary.....	99
<i>Machon, A., Horváth, L., Weidinger, T., Pintér, K., Grosz, B., Nagy, Z., and Führer, E.:</i> Weather induced variability of N-exchange between the atmosphere and a grassland in the Hungarian Great Plain.....	219

<i>Mandeep, J.S., Yee, A.C.C., Abdullah, M. and Tariqul, M.:</i> Tropospheric scintillation measurement in Ku-Band on Earth-Space paths with low elevation angle.....	265	dimensional kinematic model .....	147
<i>Möller, D.:</i> Atmospheric chemistry – Bridging the chemical air composition with the climate .....	123	<i>Szentimrey, T., Bihari, Z., Lakatos, M. and Szalai, S.:</i> Mathematical, methodological questions concerning the spatial interpolation of climate elements.....	1
<i>Orlandini, S., Mancini, M., Grifoni, D., Orlando, F., Dalla Marta, A. and Capecci, V.:</i> Integration of meteorological and remote sensing information for the analysis of durum wheat quality in Val d'Orcia (Tuscany, Italy) .....	233	<i>Tsenova, B. and Mitzeva, R.:</i> Comparative modelling study of the effect of parameterizations based on rime accretion rate and on effective water content on simulated charge density in thunderstorms .....	247
<i>Štěpánek, P., Zahradníček, P. and Huth, R.:</i> Interpolation techniques used for data quality control and calculation of technical series: an example of a Central European daily time series .....	87	<i>Valeriu, P.C.:</i> Aspects regarding the uncertainty of spatial statistical models of climate parameters .....	13
<i>Szabó-Takács, B.:</i> Numerical simulation of the cycle of aerosol particles in stratocumulus clouds with a two-		<i>Vizi, L., Hlásny, T., Farda, A., Štěpánek, P., Skalák, P. and Sitková, Z.:</i> Geostatistical modeling of high resolution climate change scenario data .....	71
		<i>Wypych, A. and Ustrnul, Z.:</i> Spatial differentiation of the climatic water balance in Poland.....	111

## II. Book review

*Haszpra, L. (ed.):* Atmospheric Greenhouse Gases: The Hungarian Perspective. (*L. Bozó*)

## III. News

Farewell to the Executive Editor, Margit Antal (*E. Mészáros*)

## SUBJECT INDEX

<b>A</b>		- chemistry	123
aerosol		- greenhouse gases	217
- particles	147	aviation meteorology	275
- regeneration	147	<b>B</b>	
- scavenging	147	background concentration	179
accretion of rime	247	barley yield	167
air		biogeochemistry	123
- pollution	123	Bulgaria	247
- quality	179	<b>C</b>	
aircraft		CECILIA project	87, 71, 99
- Cessna -185 Skywagon	275	Central Europe	87
- structural icing	275	Cessna -185 Skywagon	275
ALADIN Climate/CZ regional climatic model		charge density	247
87, 71		charging, non-inductive	247
analysis, spatial	111	chemistry	
annual precipitation totals	71, 51	- atmospheric	123
annual temperature, mean	71	- sustainable	123
anthroposphere	123	climate	
aridity index	205	- change	205, 167, 123, 219
atmospheric			

- chemical climate 123
- extreme indices 99
- forestry categories 205
- maps 31
- of Hungary 99
- parameters 13
- perturbation 219
- positive feedback 219
- climatic water balance 111
- climatology
  - statistical 1, 99
  - time series 87, 51
- cloud
  - droplet formation 147
  - physics 147
  - rime accretion 247
- collision coalescence 147
- complex terrain 179
- computational fluid dynamics 179
- concentration in background 179
- condensational growth 147
- continentality index 31
- Czech Republic 87, 51

## D

- data
  - homogenization 1, 99
  - interpolation 99
  - quality control 87
  - series 87, 71, 1, 99, 51
- denitrification 219
- drift kriging 71, 1
- drop formation 147

## E

- ecosystem
  - forest 205
  - grassland 219
- effect of climate change 167, 219
- effective water content 247
- environmental variables 51
- error
  - georeference 13
  - propagation 13
- Europe 31
- evapotranspiration, potential 111
- evolution 123
- external drift kriging 71
- extrapolation 13
- extreme climate indices 99

## F

- filling missing values 87
- fluxes of nitrogen 219
- forest ecosystem 205

- forestry climate categories 205

## G

- geographic influence 51
- geostatistical techniques 71, 1, 51
- Germany 31
- GIS 111, 1
- grassland 219
- greenhouse gases 123, 217, 219

## H

- heterogeneous regions 13
- homogenization 1, 99
- human evolution 123
- Hungary 71, 99, 205, 179, 167, 217, 219

## I

- ice accumulation model 275
- icing
  - severity on aircraft 275
  - structural 275
- index
  - aridity 205
  - climatic water balance 111
  - continentality 31
  - extreme climate 99
  - forestry aridity 205
  - landscape 51
  - normalized difference vegetation index 233
  - North Atlantic oscillation 233
- interpolation 99
  - geostatistical 1
  - meteorological 1
  - methods 111
  - radial basis function 31
  - optimal 71
  - spatial 1, 99, 31
  - techniques 87
- Italy 233

## K

- kriging 87, 71, 1
  - external drift 71
- Ku-band satellite signals 265

## L

- linear regression 31
- liquid water content in clouds 275

## M

- Malaysia 265
- measurement, wind tunnel 179
- meteorological information 233
- microphysics 147

MISH method	1		
missing values	87		
model			
- ALADIN Climate/CZ	87, 71		
- ice accumulation	275		
- dispersion around motorway tunnels	179		
- mathematical statistical	1		
- microscale	179		
- multiplicative successive	167		
- non-inductive charging in clouds	247		
- non-stationary	71		
- precipitation	51		
- regional climatic	71		
- spatial statistical	13, 31, 51		
- two-dimensional kinematic	147		
model validation	179		
multi-dimensional linear regression	31		
multiplicative successive model	167		
multivariate regression	51		
<b>N</b>			
network			
- rain gauge stations	13		
nitrogen			
- exchange	219		
- emission	219		
- deposition	219		
non-stationary modeling	71		
<b>O</b>			
optimal interpolation	87, 71		
outliers	13		
<b>P</b>			
parameterization			
- of rime accretion	247		
particles	147		
Poland	111		
potential evapotranspiration	111		
precipitation	13, 111		
- annual totals	71, 51, 205		
- extreme indices	99		
- models	51		
- summer	51		
probability density function	265		
productivity	205		
propagation of errors	13		
protein content	233		
<b>R</b>			
regression			
- multi-dimensional linear	31		
- multivariate	51		
remote sensing	233		
representativeness	13		
rime accretion rate	247		
Romania	13		
<b>S</b>			
satellite			
- communication	265		
- Ku-band signals	265		
scavenging of aerosols	147		
scintillations in Ku-band signals	265		
simulation, CFD	179		
Slovakia	87, 71		
spatial			
- analysis	111		
- interpolation	1, 99, 31		
specific weight	233		
statistical			
- climatology	1, 99		
- downscaling methods	87		
- model	13, 1, 51		
summer precipitation	51		
sustainable chemistry	123		
<b>T</b>			
temperature			
- extreme indices	99		
- mean annual	71		
- monthly mean	31		
temporal variability	51		
thunderstorms	247		
time series	87, 1, 99, 51		
tropospheric scintillation	265		
tunnel portal	179		
<b>U</b>			
uncertainty	13		
<b>V</b>			
validation of air quality model	179		
variability, temporal	51		
<b>W</b>			
water			
- balance, climatic	111		
- content in clouds	275, 247		
- liquid water content	275		
- supply	167		
weight, specific	233		
wheat ( <i>Triticum durum</i> )	233		
wind tunnel measurement	179		
winter barley	167		
WMO RA VI Region	31		
<b>Y</b>			
yield model	167		
yield of winter barley	167		



## INSTRUCTIONS TO AUTHORS OF *IDŐJÁRÁS*

The purpose of the journal is to publish papers in any field of meteorology and atmosphere related scientific areas. These may be

- research papers on new results of scientific investigations,
- critical review articles summarizing the current state of art of a certain topic,
- short contributions dealing with a particular question.

Some issues contain "News" and "Book review", therefore, such contributions are also welcome. The papers must be in American English and should be checked by a native speaker if necessary.

Authors are requested to send their manuscripts to

*Editor-in Chief of IDŐJÁRÁS*  
P.O. Box 38, H-1525 Budapest,  
Hungary  
E-mail: journal.idojaras@met.hu

including all illustrations. MS Word format is preferred in electronic submission. Papers will then be reviewed normally by two independent referees, who remain unidentified for the author(s). The Editor-in-Chief will inform the author(s) whether or not the paper is acceptable for publication, and what modifications, if any, are necessary.

Please, follow the order given below when typing manuscripts.

*Title page:* should consist of the title, the name(s) of the author(s), their affiliation(s) including full postal and e-mail address(es). In case of more than one author, the corresponding author must be identified.

*Abstract:* should contain the purpose, the applied data and methods as well as the basic conclusion(s) of the paper.

*Key-words:* must be included (from 5 to 10) to help to classify the topic.

*Text:* has to be typed in single spacing on an A4 size paper using 14 pt Times New Roman font if possible. Use of S.I. units are expected, and the use of negative exponent is preferred to fractional sign. Mathematical formulae are expected to be as simple as possible and numbered in parentheses at the right margin.

All publications cited in the text should be presented in the *list of references*, arranged in alphabetical order. For an article: name(s) of author(s) in Italics, year, title of article, name of journal, volume, number (the latter two in Italics) and pages. E.g., *Nathan, K.K.*, 1986: A note on the relationship between photosynthetically active radiation and cloud amount. *Időjárás* 90, 10-13. For a book: name(s) of author(s), year, title of the book (all in Italics except the year), publisher and place of publication. E.g., *Junge, C.E.*, 1963: *Air Chemistry and Radioactivity*. Academic Press, New York and London. Reference in the text should contain the name(s) of the author(s) in Italics and year of publication. E.g., in the case of one author: *Miller* (1989); in the case of two authors: *Gamov and Cleveland* (1973); and if there are more than two authors: *Smith et al.* (1990). If the name of the author cannot be fitted into the text: (*Miller*, 1989); etc. When referring papers published in the same year by the same author, letters a, b, c, etc. should follow the year of publication.

*Tables* should be marked by Arabic numbers and printed in separate sheets with their numbers and legends given below them. Avoid too lengthy or complicated tables, or tables duplicating results given in other form in the manuscript (e.g., graphs).

*Figures* should also be marked with Arabic numbers and printed in black and white or color (under special arrangement) in separate sheets with their numbers and captions given below them. JPG, TIF, GIF, BMP or PNG formats should be used for electronic artwork submission.

*Reprints:* authors receive 30 reprints free of charge. Additional reprints may be ordered at the authors' expense when sending back the proofs to the Editorial Office.

*More information* for authors is available: journal.idojaras@met.hu

Published by the Hungarian Meteorological Service

---

Budapest, Hungary

**INDEX 26 361**

**HU ISSN 0324-6329**